Department of Civil Engineering
University of Strathclyde

Numerical modelling of soft soils improved with stone columns

by

Daniela Kamrat-Pietraszewska

A Thesis presented for the Degree of Doctor of Philosophy

2011

Signed:
Date:

If we knew what it was we were doing,

It would not be called research, would it?

Albert Einstein

Acknowledgement

First and foremost, I would like to thank my supervisor Dr Minna Karstunen for her guidance and time spent to make this project happen. Without her support and the freedom she gave me, I would not have been able to complete this thesis in its present form. I would like to extend thanks to my former and present co-supervisors, Dr Marcelo Sánchez and Dr Mike Kenny, for their assistance.

I am also indebted to Dr Martino Leoni of Wechselwirkung Studio Italiano Snc. (former University of Stuttgart, Germany), whose constant interest and support allowed me to pursue research in constitutive modelling.

The research presented in this thesis was funded by a scholarship from the Faculty of Engineering at the University of Strathclyde. The funding is gratefully acknowledged. The work was also sponsored by the Marie Curie Research Training Network on Advanced Modelling of Ground Improvement on Soft Soils (AMGISS) and Industry-Academia Partnerships and Pathways Project Modelling Installation Effects in Geotechnical Engineering (GEO-INSTALL) (Contracts MRTN-CT-2004-512120 and PIAG-GA-2009-230638). The funding and collaboration of all parties is gratefully acknowledged. I would also like to thank Keller Foundation (UK) for making the site investigation data from Bishopton available.

Thanks are extended to my past and present colleagues at Department of Civil Engineering for the exchange of thoughts, friendly chats during the course of my research and constant help during those gruelling days of writing up. In random order: Marcin, Marco, Gráinne, Heather, Caroline, Antoine, Stella, Patrick, Siva,

Andrzej, Harald, Marti, Urs, Anna…- thank you. With special thanks to Gráinne and Heather for daunting task of reading and correcting the manuscript.

Finally, I would like to extend my greatest thanks to my Mother, Grandmother and Husband, who are my life's energy source and pillars of strength.

Abstract

Natural soft soils are very complex materials and geological processes greatly influence their stress-strain behaviour. Natural soft soils exhibit anisotropy and interparticle bonding, and their stress-strain response is time-dependent. Taking account of those soil characteristics is paramount for realistic and accurate predictions of soft soil behaviour. Geotechnical properties of natural soft soils can be improved with various techniques, such as stone columns. Stone columns are mainly used for settlement and consolidation time reduction, however underneath an embankment stone columns also enhance the slope stability. Despite the wide range of applications of stone columns, current design methods of stone columns are for the greater part based on simple assumptions and do not account for the complex soil-column interaction. Numerical methods are still fighting for their place in industrial design. They could be used, as a complementary solution to well-known empirical design procedures, for gaining a better understanding of the behaviour of soil improved with stone columns and for the optimisation of existing design procedures. Behaviour of a stone column foundation is largely governed by the surrounding soil, its compressibility characteristics and the stress-strain-strength response. The models commonly used by civil engineering practitioners predict often inaccurate and over-conservative stress-strain response, as characteristics of soft soils are ignored and the complexity of the soil-column interaction is neglected.

The novelty of this research lies in accounting for the complex features of natural soft soil behaviour, such as non-linearity, anisotropy, destructuration and viscosity, in soil modelling. Following that, the work enables optimisation of the

design of stone column foundations by reducing the risk of unexpected ground movements. Three-dimensional numerical studies on the effect of mechanical and physical properties of stone columns and the impact of soft soil layer thickness are carried out by application of advanced constitutive models to represent the soft soil mass. Additionally, the research aimed for the development of an advanced constitutive model which takes account of all important characteristics of soft soil, leading to more realistic predictions of soft soil behaviour. Next, the influence of anisotropy, apparent interparticle bonding and viscosity on predicted stress-strain response of the stone column foundation constructed on soft soil was studied via a three-dimensional benchmark problem and the application of advanced constitutive models.

Glasgow, March 2011

Daniela Kamrat-Pietraszewska

Contents

List of figures

List of tables

1

INTRODUCTION

As the amount of population in congested urban area increases, so does the proportion of structures which must be constructed on poor soils, such as flood plains, coastal regions or seismic areas. Moreover, construction on sites with favourable ground conditions is severely limited by economical, social and other constraints. Consequently, ground improvement methods, such as stone columns, are necessary for safe and economical geotechnical design and construction.

Recent advances in geomechanics have resulted in a better understanding of the characteristics of natural soft soils, such as anisotropy, destructuration and viscosity. Consequently, these soft soil features can be now represented in numerical modelling. Current design methods for stone columns are for the most part semi-empirical or based on simple elastic or plastic solutions, which ignored the non-linearity of the materials considered. Numerical techniques, such as finite element (FE) analyses, can be used as an alternative or complementary solution to the

traditional design methods. Using FE analyses enables a representation of both the geometry of the engineering problem and the complex response of the natural soft soil-stone columns system to be modelled. In this thesis, stone columns are used as a support for two types of foundations: an embankment and a raft footing. These problems, as with many other engineering projects, are three-dimensional problems and as such, are modelled by conducting three-dimensional FE analyses.

1.1 Aims and objectives

The aims of this thesis are to:

- confidently use the most advanced soil modelling expertise to simulate the stress-strain-strength behaviour of stone column foundations, used to reinforce soft soil, in three-dimensional FE analyses;
- gain an improved understanding of the behaviour of normally consolidated or slightly over-consolidated soft clays improved with stone columns;
- optimise stone column design for practical geotechnical applications.

The objectives of this research are to:

- represent the nature of soft soil deposits by advanced constitutive models in order to gain a full understanding of the stress-strain behaviour of this complex material;
- study and understand the behaviour of the soft soil improved with stone columns, considering both floating and end-bearing columns;

- assess the influence of the mechanical properties of the column material on the settlement response of the stone column foundation underneath an embankment, investigating factors such as the angles of friction, dilatancy and stiffness,
- investigate the impact of the arrangement of the columns, such as diameter, spacing and length, on the stress-strain behaviour of the soft soil deposit improved with floating stone columns;
- assess the influence of the thickness of the soft soil deposit on the settlement response of stone column-soil mass;
- give recommendations on stone column design and its optimisation, based on the results of a parametric study, in order to improve existing over-conservative engineering practice;
- develop and implement in a commercial FE code a new enhanced advanced constitutive model, in an attempt to capture the effect of rate-dependent behaviour of soft soils on the behaviour of the geo-material (columns-soil system);
- assess the influence of soft soil characteristics, such as anisotropy, destructuration and viscosity, of the predicted behaviour of a soft clay deposit improved with floating stone columns underneath an embankment,
- demonstrate the feasibility of the settlement and consolidation time reduction of a stone column foundation via a detailed three-dimensional FE analyses.

It should be noted that every numerical analysis is an approximation of the real engineering problem. At first the geometry model is simplified, then the soil profile

along with the soil properties are idealised. Next, the soil behaviour is described by a chosen constitutive model. Subsequently, the construction sequence is modified to reflect the most important actions which took place on site. Following that, the phenomena considered most relevant are simplified along with some assumptions and restrictions.

1.2 Layout of the thesis

The work presented in this thesis is divided into the following chapters:

Chapter 2 gives a general overview on soft soil characteristics along with some recent developments in the field of constitutive modelling. Natural soft clays exhibit some features, such as anisotropy, interparticle bonding and destructuration. Furthermore, the behaviour is rate-dependent. These are the main features of soft soil response considered in *Chapter 2*. First, a brief description of typical soft soil characteristics is presented, followed by the current developments related to state-of-the-art constitutive models. The models chosen for the numerical simulations of the soft soil and stone column material are discussed in detail. The constitutive models used should have wide application in engineering practice. As such, the authors of the models selected for the subsequent simulations, have tried to limit the complexity of their formulations to a minimum.

Chapter 3 presents a brief summary of the concept and application of stone columns in geotechnical engineering. Moreover, the limitations and possible pit-falls during the installation of granular columns are discussed. This is followed by a review of

some of the most common design methods. An overview of previous studies, both experimental and numerical, is also provided.

Chapter 4 considers a benchmark problem of stone columns installed underneath an embankment. The numerical simulations are performed using a three-dimensional FE code to analyse the controlling factors of stone column design on the stress-strain behaviour of the soil-column system. The aim is to understand the complex behaviour of stone columns installed beneath an embankment. For the numerical analyses, the advanced constitutive model S-CLAY1S is used to represent the soft soil deposit. This elasto-plastic model is able to account for plastic anisotropy, interparticle bonding and the destructuration process. Both physical and mechanical properties of the stone columns are considered, varying factors such as stiffness and angles of friction and dilatancy of the granular material, and length and arrangement of the columns. Additionally, the influence of the thickness of the soft deposit on the numerical predictions is also investigated. The findings from the parametric studies are used to give some guidance on an optimised design of the stone column foundation constructed in a soft soil deposit.

Chapter 5 presents an enhanced advanced constitutive model developed to capture the real stress-strain behaviour of the soft soil. The new ACM-S model is a time-dependent advanced constitutive model, which accounts for plastic anisotropy and erasure of interparticle bonds. This model has been based on the Anisotropic Creep Model (ACM) by Leoni *et al.* (2008). Although the model requires the values for two additional soil constants and one additional state variable in comparison to the ACM model, it is demonstrated that these parameters can be determined from standard laboratory tests, ensuring its wide application in engineering practice. The

formulation is described in detail, followed by validation of the assumptions of the model in simple laboratory tests reproduced numerically, and in a boundary value problem using a two-dimensional FE code. The comparison between the predictions using the ACM-S model and the measured test results highlights that a model which considers destructuration can significantly increase the quality of predictions when compared to the ACM model, thus extending the applicability of the model to time-dependent behaviour of structured soft clays.

Chapter 6 studies the influence of constitutive models on the numerical predictions using three-dimensional finite element analyses of floating stone columns installed in a soft natural soil deposit. For the calculations, several constitutive models are used to simulate the behaviour of the soft soil deposit. The aim is to understand and demonstrate the difference between the alternative modelling approaches, and to study the influence of anisotropy, destructuration and time-dependency (and their combinations) of the soft deposit improved with the stone columns on the stress-strain response. The importance of soft soil features and the reproduction of the complex behaviour of soft soil improved with stone columns in a FE analysis is emphasised. Additionally, the influence of the ratio between the secondary compression index C_α and the compression index C_c and the impact of the applied modelling approach on the numerical predictions are studied. Moreover, the impact of the selection of the over-consolidation ratio on the numerical predictions of the surface settlements and the excess pore water pressures evolution are discussed.

Chapter 7 investigates the interaction of the stone columns underneath a raft foundation at a site in Bishopton (Scotland). The differential and total settlements are the greatest concerns in engineering design, however other factors, such as the stress

distribution and the consolidation process, are also considered in this study. The aim is to understand the complex behaviour of stone columns installed beneath a raft foundation, and to demonstrate the feasibility of stone columns in the reduction of settlements and the time required for full dissipation of the excess pore water pressures in the particular case study presented. Three-dimensional simulations of floating stone columns installed beneath the raft footing are carried out by means of the advanced constitutive model S-CLAY1 used to represent the soft soil deposit behaviour. Given the extremely limited geotechnical data and poor quality sampling on this particular site, a preliminary study investigating the influence of the over-consolidation ratio determined from in-situ and laboratory testing is carried out.

Chapter 8 summarises the main conclusions reached in the previous chapters and gives recommendations for further research.

1.3 Publications

This thesis has led to the preparation and publication of two journal papers and seven conference papers. The journal papers stemming from this current research are listed below:

1. Kamrat-Pietraszewska D., Leoni M. & Karstunen M. *Accounting for viscosity, anisotropy and destructuration in natural soft soils,* Computers and Geotechnics (submitted).

2. McCabe B., Kamrat-Pietraszewska D. & Egan D. *Ground heave induced by the installation of stone columns in clay soils*, ICE Geotechnical Engineering (submitted).

A list of the conference papers as a result of the current research is given below:

1. Kamrat-Pietraszewska D., Krenn H., Sivasithamparam N. & Karstunen M., *The influence of anisotropy and destructuration on a circular footing,* Proceedings of the Second British Geotechnical Association, International Conference on Foundations, ICOF 2008, Dundee, IHS BRE Press, 1527-1536.

2. Gäb M., Schweiger H. F., Kamrat-Pietraszewska D. & Karstunen M., *Numerical analysis of a floating stone columns foundation using different constitutive models,* Proceedings of the Second International Workshop on Geotechnics of Soft Soils, Geotechnics of Soft Soils: Focus on Ground Improvement, Glasgow, 2008, Taylor & Francis Group137-142.

3. Kamrat-Pietraszewska D., Buggy F., Leoni M. & Karstunen M., *Numerical modelling of an embankment on PVD-improved soft alluvium- Limerick Southern Ring Road Phase II*, Proceedings of Joint Symposium Concrete Research in Ireland and Bridge and Infrastructure Research in Ireland 2008, NUI Galway, Galileo Editions, 443-452.

4. Kamrat-Pietraszewska D. & Karstunen M., *The behaviour of stone column supported embankment constructed on soft soil*, Proceedings of the First International Symposium on Computational Geomechanics COMGEO, Juan-les Pins, France 2009, *IC2E* International Centre for Computational Engineering, ISBN: 976-960-98750-0-4 (CD ROM), 829-841.

5. Kamrat-Pietraszewska D. & Karstunen M., *Modelling embankments on floating stone columns*, Proceedings of the Seventh European Conference on Numerical Methods in Geotechnical Engineering NUMGE, Trondheim, Norway 2010, Taylor & Francis Group, 851-856.

6. Sivasithamparam N., Kamrat-Pietraszewska D. & Karstunen M., *An anisotropic model for structured clays*, Proceedings of the Seventh European Conference on Numerical Methods in Geotechnical Engineering NUMGE, Trondheim, Norway 2010, Taylor & Francis Group, 21-26.

7. Kamrat-Pietraszewska D. & Karstunen M., *A numerical study of feasibility of using floating stone columns under low-rise buildings,* Proceedings of the Second International Symposium on Computational Geomechanics COMGEO, Dubrovnik, Croatia 2011, *IC2E* International Centre for Computational Engineering (accepted for publication).

2

CONSTITUTIVE MODELLING

An overview on soft soil characteristics along with some recent developments in the field of constitutive modelling are given in this chapter. Natural soft clays exhibit some features, such as anisotropy, interparticle bonding and destructuration, and their behaviour is rate-dependent. Therefore the behaviour related to those characteristics is presented here.

Next, seven constitutive models, related to the analyses presented in this thesis, are discussed:

- Modified Cam Clay (Roscoe & Burland, 1968),
- Soft Soil Model (Brinkgreve, 2002),
- Hardening Soil Model (Schanz, 1998),
- S-CLAY1 (Wheeler *et al.,* 2003),
- S-CLAY1S (Koskinen *et al,* 2002, Karstunen *et al.,* 2005),
- Soft Soil Creep Model (Brinkgreve, 2002),

- Anisotropic Creep Model (Leoni *et al*., 2008).

The first three models are isotropic models. They are followed with a discussion of the anisotropic extensions of the Modified Cam Clay model (S-CLAY1 and S-CLAY1S). Lastly, the Soft Soil Creep and Anisotropic Creep models describe the viscous effects and creep behaviour of soft soils; the former is an isotropic and the latter is an anisotropic constitutive model.

The constitutive models described in this chapter demonstrate the variety of different constitutive models for natural soft soil, along with some recent improvements and developments in that field. All of the models have the potential for wide application in engineering practice as the authors have tried to limit the complexity of their formulations to a minimum.

2.1 Background

It is estimated that by 2050 two thirds of the Earth's population will live in cities (Oliver, 2010), therefore there is an acute need for constructing new engineering structures. However, construction on sites with favourable ground conditions is severely limited by economical, social and other constraints. Thus, nowadays structures are often constructed on poor quality soft soils, such as in river valleys or coastal regions. Consequently, various ground improvement techniques, such as stone columns, are often used in order to provide satisfactory foundation performance. There are a number of geological processes influencing the stress-strain behaviour of natural soft soils and taking account of the complexity of soft soil

behaviour is of great importance for the accurate predictions of the soft soil's mechanical response.

The stress-strain behaviour of the soil may be studied by laboratory tests and its complexity can be taken into account by constitutive modelling. Most practising engineers model soft soil using the liner-elastic perfectly plastic Mohr-Coulomb or the elasto-plastic Modified Cam Clay models, (Roscoe & Burland, 1968). These models take account of simplified soil behaviour and the assumption of an isotropic stress history, (which is rarely the case for natural clay), may lead to a poor prediction of the mechanical response. This is due to the lack of the fundamental features of a natural clay incorporated within these models, such as anisotropy, destructuration and rate-dependency. This is particularly true for the modelling of soil improved with stone columns as those systems largely rely on the lateral resistance of the hosting ground material. Hence, a realistic modelling of the stress-strain behaviour of the surrounding soil is of great importance.

Almost all soils and rocks are anisotropic in terms of strength and stiffness. Anisotropy arises from the shape of clay pellets, sedimentation and subsequent loading history, see Casagrange & Carrillo (1944). Casagrande & Carillo (1944) distinguished two types of anisotropy: induced and inherent (also called geometrical). Induced anisotropy takes its name from the rearrangement of the initial fabric and changes at the interparticle contacts due to strains generated by loading of the soil layer, (Wheeler *et al.*, 2003). Inherent anisotropy is due to a combination of particle placement during deposition or formation. One can also distinguish a third type of anisotropy, the so-called initial anisotropy, which is a combination of both induced and inherent anisotropy. It is the description of the anisotropy possessed by

an in situ soil element, which is subject to a particular stress history and a subsequent set of applied stresses, (Zdravkovic & Potts, 1999).

The yield characteristic of the natural soil can also be an indication of the anisotropy of the material. Graham *et al.* (1983B) investigated the stress paths and yielding of the Winnipeg Clay (Canada) during triaxial tests and concluded that anisotropy may be demonstrated via an inclined yield surface in the non-dimensional stress plane, see Figure 2.1. Diaz-Rodriguez *et al.* (1992) compared data from Mexico City Clay with several other natural soils and illustrated that elliptical yield surfaces in the *p'-q* plane exhibited symmetry to the K_0- line (the stress path for one-dimensional straining). The mean effective stress and the deviatoric stress are represented as *p'* and *q,* respectively.

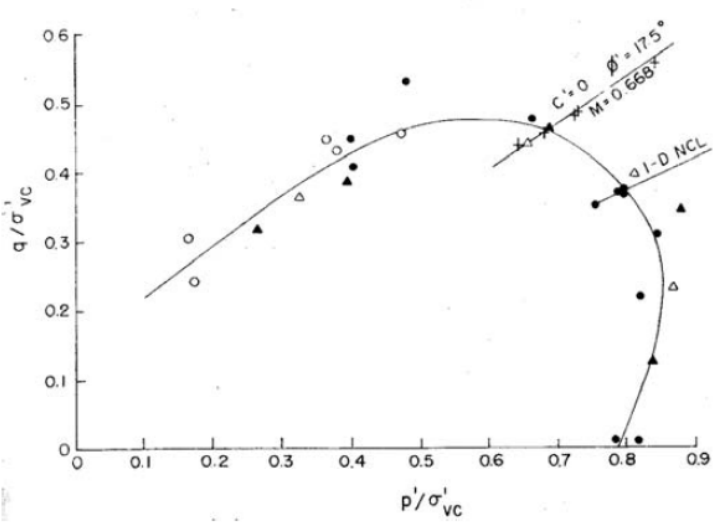

Figure 2.1: Stress paths and yielding of Winnipeg Clay in non-dimensional plane (Graham *et al*., 1983B).

Due to the one-dimensional strain history, soft soils are generally cross-anisotropic, this means that the long axes of the clay particles are perpendicular to the vertical stress direction in the ground during deposition, (Casagrande & Carrillo, 1944). It has been demonstrated by Yu & Axelsson (1994) that clay particles, deposited under the force of gravity and compressed by the deposition of further particles, orientate themselves in such a way. Therefore, the material properties are often identical in all horizontal directions in the ground, but differ in the vertical direction (the material exhibits a vertical axis of symmetry). Nevertheless, a soil with non cross-anisotropic behaviour can be found due to certain tectonic and geomorphological processes, such as tilting, moving ice sheets, erosion or crustal movements. In such cases the soil stresses or stress histories vary in different horizontal directions and this may influence the anisotropy of the fabric.

Fabric can be defined as the geometrical arrangement of soil particles, the interparticle contacts and the spatial arrangements of pore spaces. The soil fabric reflects the geological history of the soil and it influences the mechanical behaviour, (Collins & McGown, 1974). The state of the soil and the fabric are largely affected by the environment in which deposition and subsequent geological events take place. An anisotropic fabric leads to anisotropic soil behaviour with respect to strength. Such behaviour may be exhibited even if the initial stress state is isotropic. Anisotropic arrangement of the soil particles influences the elastic and plastic response of the natural soil, to loading for different stress paths.

Structure, described as the combination of the natural soil fabric and interparticle bonding, has been discussed since the 1970s (Mitchell, 1976). Interparticle bonding (defined as the interparticle forces which are not purely

frictional in nature), can be destroyed during the rearrangement of fabric caused by plastic straining, as found by Lambe & Whitman (1969) and Cotecchia & Chandler (1997). Leroueil & Hight (2003) expanded the proposed earlier definition of structure by adding the process of lithification, defined as the destructuration of porosity through compaction and cementation. In addition to that, Leroueil *et al.* (1985) and Burland (1990) explained that soil structure could arise from clay mineralogy, the depositional environment and post-depositional processes, such as erosion, thixotropic hardening, leaching, weathering, etc. After deposition soil may be subjected to a number of subsequent processes, which in turn will influence the soil properties. Structure in an intact state may be degraded by factors, such as weathering, chemical and/or mechanical degradation. Destructuration is a term which describes the progressive loss of structure (bonding) in natural soils due to plastic straining, (Leroueil *et al.*, 1979). Mechanical destructuration is the result of volumetric and/or shearing deformation and may lead to the highly sensitive response of some soils, such as Canadian or Scandinavian quick clays. It has been proven that bonded soils have a stiffer elastic response than unbonded materials, see Graham & Li (1985). Additionally, they exhibit a greater peak strength than an equivalent unbonded soil, see Leroueil & Vaughan (1990). Bonded soils exhibit higher yield stresses than unbonded materials. This phenomenon can be clearly explained by examining the behaviour of an unbonded and bonded material during a one-dimensional compression test, Figure 2.2. A reconstituted sample would follow the intrinsic compression line with gradient λ_i, whereas a natural soil would follow the line with a lower gradient until it reaches the yield stress. The natural soil would have a very high value of λ at the onset of yielding and the compression curve

would then gradually converge to the intrinsic compression line as bonding is gradually destroyed.

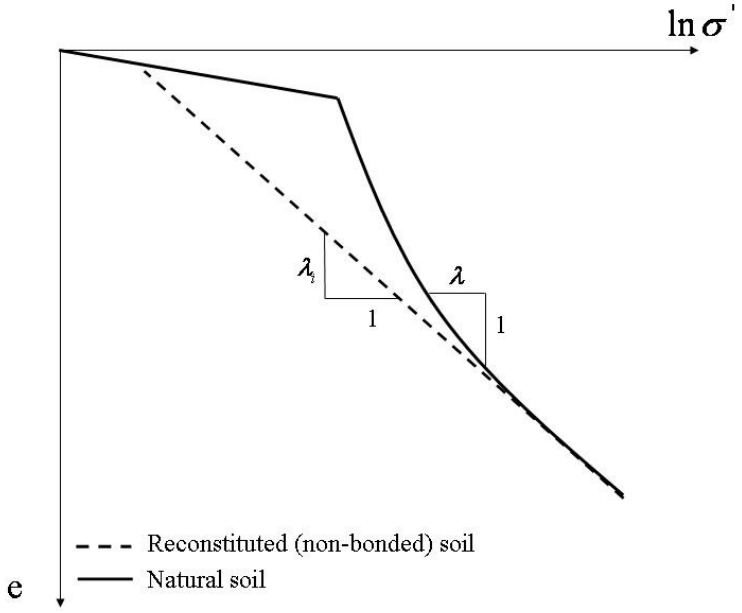

Figure 2.2: Natural and reconstituted soil during oedometric loading.

There is not necessarily a solid link between the soil particles (particularly with clays), but rather interparticle bonding is the consequence of several phenomena, such as compression, cementation and thixotropy, as concluded by Leroueil & Hight (2003).

The loading response of saturated clays is time-dependent due to the consolidation process. First, when a fully saturated clay is loaded in a fast undrained manner, excess pore water pressures are created and dissipation takes a long time as a result of low hydraulic conductivity and long drainage paths. Ultimately, the excess

pore water pressures will fully dissipate and then the consolidation process will be finished.

Consolidation is hence a time-dependent process as the water needs to drain through the pore system. The time-dependent response can be divided into two parts: primary consolidation and secondary compression (so-called creep). During primary consolidation the load, which is initially carried by the excess pore water pressure, is transferred to the soil skeleton. Throughout this process secondary compression takes place under constant effective stress. If effective stresses are held constant over a long period of time, substantial creep strains may be observed in natural soils. Creep itself is dependent on the rate of straining, which influences the yield stresses and the undrained shear strength.

For practical applications one usually assumes that for most normally consolidated clays within a stress range of 10..1 000 kPa the secondary compression index C_α and the compression index C_c are approximately constant, see Fang (1991). However, laboratory and field data for a wide range of natural soils show that the secondary compression index C_α may decrease/increase or remain constant over a significant period of time, see Mesri & Godlewski (1977 & 1979), Mesri & Castro (1987), Mesri *et al.* (1994) or Mesri (2001). For the sake of simplicity, it is often assumed that the magnitudes of C_α and C_c are directly linked, and that the value of C_α / C_c together with the end-of-primary consolidation (EOP) $e - \log \sigma_v^{'}$ curve characterise the secondary compression behaviour of soil, as stated by Mesri & Castro (1987). Creep of soft soils is of great importance, as continuous settlement

can impose damage of the structure if not considered accordingly in the design, (Bjerrum, 1967; Graham *et al.*, 1983B; Leroueil *et al.*, 1985).

2.2 Isotropic constitutive models

In this section, three isotropic constitutive models, the Modified Cam Clay, the Soft Soil and the Hardening Soil models are briefly described. All of these constitutive models are used in calculations presented in this thesis either to represent the soft soil deposit or to account for the behaviour of the stone column material.

2.2.1 Modified Cam Clay

The Modified Cam Clay (MCC) model was introduced by Roscoe & Burland (1968) based on the idea of the Cam Clay Model (Roscoe *et al.*, 1958). This is probably the most widely used hardening elasto-plastic model, by practicing engineers for the numerical simulations of soft normally or lightly over-consolidated soils. The relative simplicity of the formulation leads to many modelling applications, however one should remember its major weaknesses, such as the lack of anisotropy, bonding effects, destructuration or time-dependence, which result in the lower accuracy of the numerical predictions than those given by more advanced constitutive models.

The MCC model is based on the Cam Clay formulation presented by Roscoe *et al.* (1958) and uses the Critical State Concept where the state of a soil can be

characterised by three parameters: the effective mean stress p', the deviatoric shear stress q and the specific volume v:

$$p' = \frac{1}{3}\left(\sigma_1' + 2\sigma_3'\right) \tag{2.1}$$

$$q' = \sigma_1' - \sigma_3' \tag{2.2}$$

$$\nu = N - \lambda \ln p' = \nu_s - \kappa \ln p' \tag{2.3}$$

where: σ_1' and σ_3' are the principal effective stresses, and N, λ and κ are the characteristic properties of a particular soil sample as discussed in the following. The slope of the normal compression line and the critical state line (CSL) in $\nu - \ln p'$ space is defined as λ, while the slope of the swelling line in $\nu - \ln p'$ space is indicated as κ and both values are assumed to be characteristics of the particular soil. The slopes λ and κ can be defined as shown in Figure 2.3 and are related to the compression index C_c and the swelling index C_s as measured in the oedometer test by the following equations:

$$\lambda = \frac{C_c}{\ln 10} \tag{2.4}$$

$$\kappa \approx \frac{2C_s}{\ln 10} \tag{2.5}$$

The characteristic property of a soil sample N, the specific volume along the normal compression line at a unit pressure, is dependant on the units of measurement. Parameter ν_s depends on the loading history of a soil and it is different for each swelling line. The specific volume ν is related to the void ratio e via the relationship:

$$v = 1 + e \tag{2.6}$$

The Modified Cam Clay model overcomes some problems of the original Cam Clay model by adopting an ellipse as the yield surface. The shape of the MCC yield surface, without a singularity corner on the yield surface, excludes potential problems in numerical implementation. The elliptical yield surface is assumed to be centred on the mean effective stress axis, see Figure 2.4. As defined by the plasticity theory, the possible stress states of soil are either on or inside the yield surface. If the stress point remains inside the yield surface, the behaviour is elastic. However, if the stress point is on the surface of the yield surface irreversible plastic strains occur.

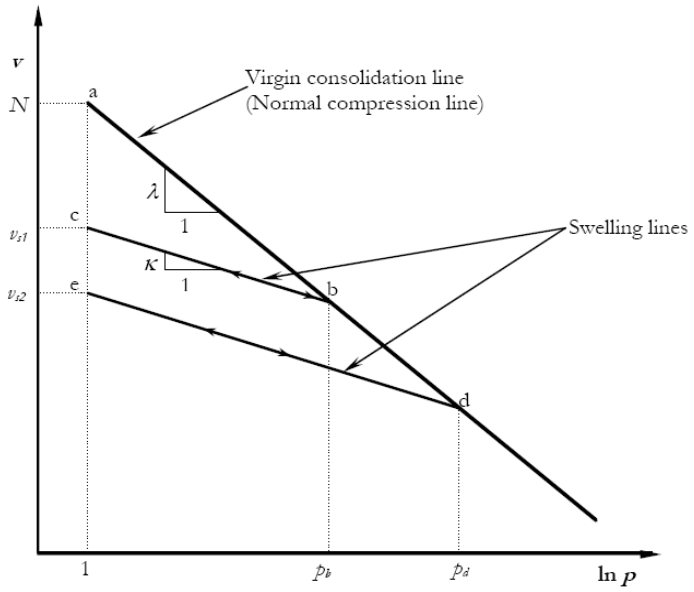

Figure 2.3: Soil sample under isotropic compression in relation to specific volume.

The yield surface *f* of the Modified Cam Clay model is defined as:

$$f = q^2 - M^2 p'(p'_m - p') = 0 \tag{2.7}$$

where: $p_m^{'}$ is the state parameter defined initially through the vertical pre-consolidation pressure $\sigma_p^{'}$ and describes the size of the yield surface in the $p'-q$ stress space. M is the slope of the critical state line (CSL) in $p'-q$ space and can be determined from the critical state soil friction angle $\varphi_{cr}^{'}$ for triaxial compression, see *Eq. (2.8).*

$$M = \frac{6\sin\varphi_{cr}^{'}}{3-\sin\varphi_{cr}^{'}} \tag{2.8}$$

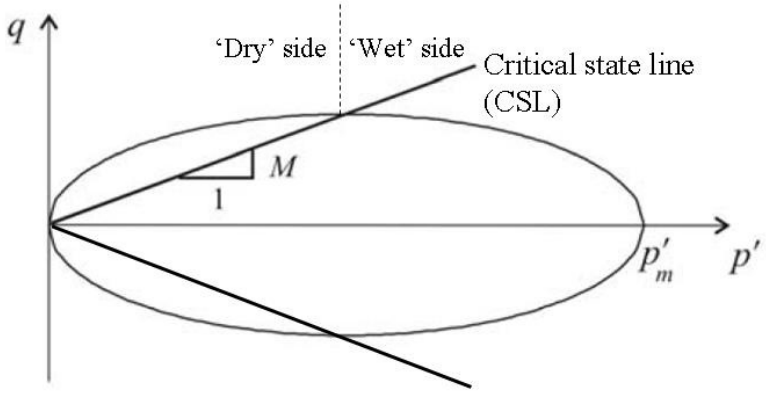

Figure 2.4: MCC yield surface in the $p'-q$ (triaxial) stress space.

The model uses a Drucker-Prager failure criterion with an associated flow rule. Ongoing plastic deviatoric strains without plastic volumetric strains can be found as the stress path reaches the yield surface on the CSL. Due to the sole dependence of the hardening law on the plastic volumetric strains, the size of the yield surface does not change on reaching the critical state. The soil continues to shear when the ultimate strength is mobilised, despite the lack of changes in the mean stress p', deviator stress q or plastic volumetric strains ε_v^p.

The incremental strain is composed of elastic $d\varepsilon^e$ and plastic parts $d\varepsilon^p$ following the normal convention of plasticity:

$$d\varepsilon = d\varepsilon^e + d\varepsilon^p \tag{2.9}$$

Moreover, the strains consist of volumetric ε_v and deviatoric ε_d components.

The change in the size of the yield surface (hardening/softening) $p_m^{'}$ is isotropic, and is related to plastic volumetric strains, as follows:

$$dp_m^{'} = \frac{(1+e)\,p_m^{'}}{\lambda - \kappa} d\varepsilon_v^p \tag{2.10}$$

where: e is the void ratio.

Hardening accompanied by compression occurs when yielding is observed on the 'wet' side, which is to the right of the point at which the CSL-line intersects the yield surface, see Figure 2.4. If, however, yielding is on the 'dry' side, softening behaviour along with dilatancy occurs and the yield surface reduces in size until the critical state is reached.

The current vertical effective stress $\sigma_v^{'}$ and pre-consolidation pressure $\sigma_p^{'}$ may describe the current state of the soil using the over-consolidation ratio OCR:

$$OCR = \frac{\sigma_p^{'}}{\sigma_v^{'}} \tag{2.11}$$

Over-consolidation of the material can be also expressed as the difference between the pre-consolidation pressure $\sigma_p^{'}$ and the current vertical effective stress $\sigma_v^{'}$, and defined as the pre-overburden pressure POP:

$$POP = \sigma_p^{'} - \sigma_v^{'} \tag{2.12}$$

MCC is a very useful modelling tool in the numerical analysis of boundary value problems, in particular when stress reversals and stress rotations are not present, (Gens & Potts, 1987). A major drawback of this model is the over-prediction of K_0- values and the under-prediction of the corresponding stress ratio $\eta_{K_0} = \frac{q}{p'}$ when compared to experimental results. This is due to both the isotropic elliptical yield surface and the associated flow rule, see Potts & Zdravković (1999). Furthermore, over-predictions in the axial strain values during drained shearing compared with experimental observations have also been reported, (Davies & Newson, 1993). Moreover, the model is applicable for soils with an isotropic stress history, which is rarely the case for natural clays due to the one-dimensional strain history of clays. Additionally, most often the loading imposed on soil deposits is not isotropic. Both the plastic surface and the plastic potential in the deviatoric plane are circular which results in a circular-shaped failure surface in the deviatoric plane. This shape of the failure surface does not represent very well the failure conditions of soils. Due to the form of the hardening law (which allows for changes in size but not in the orientation of the yield surface) and the lack of a destrucuration law or time-dependent rule, MCC describes an ideal soil which does not take into account the characteristics of soft natural deposits.

2.2.2 Soft Soil Model

The Soft Soil Model (Brinkgreve, 2002) was inspired by the Modified Cam Clay formulation. The model assumes two components of the yield surface: a volumetric

hardening cap yield surface and a Mohr-Coulomb failure yield surface, see Figure 2.5. The yield surface of the Soft Soil model (SS) defines the boundary for irreversible strains in primary compression and the failure surface is fixed. It can expand as a function of plastic volumetric strains.

The yield surface is determined by the following equation:

$$f = p^{eq} - p_p^{eq} \tag{2.13}$$

where: p_p^{eq} is the equivalent pre-consolidation stress and p^{eq} is the equivalent stress state and is related to the actual stress state.

The equivalent stress states are defined as:

$$p_p^{eq} = p_{p0}^{eq} \exp\left(\frac{d\varepsilon_v^p}{\lambda^* - \kappa^*} \right) \tag{2.14}$$

and

$$p^{eq} = \frac{q^2}{M^{*2}\left(p' + c' \cot\varphi'\right)} + \left(p' + c' \cot\varphi'\right) \tag{2.15}$$

where M^* in the Soft Soil model governs the aspect ratio of the yield surface, which defines the ratio of the horizontal to the vertical effective stresses in one-dimensional compression within the normally consolidated range and subsequently, the coefficient of the lateral earth pressure K_0^{NC}. It should be noted that the parameter M^* in the SS model is different from the parameter M used in the Modified Cam Clay model. In the Soft Soil model failure via the Mohr-Coulomb formulation may not be necessarily related to the critical state, unless a dilatancy angle ψ' is equal to zero. The parameter M^* is solely used for the definition of the shape of the yield

surface, not as a failure criterion. Because of it, in practice there is no 'dry' side in the SS model.

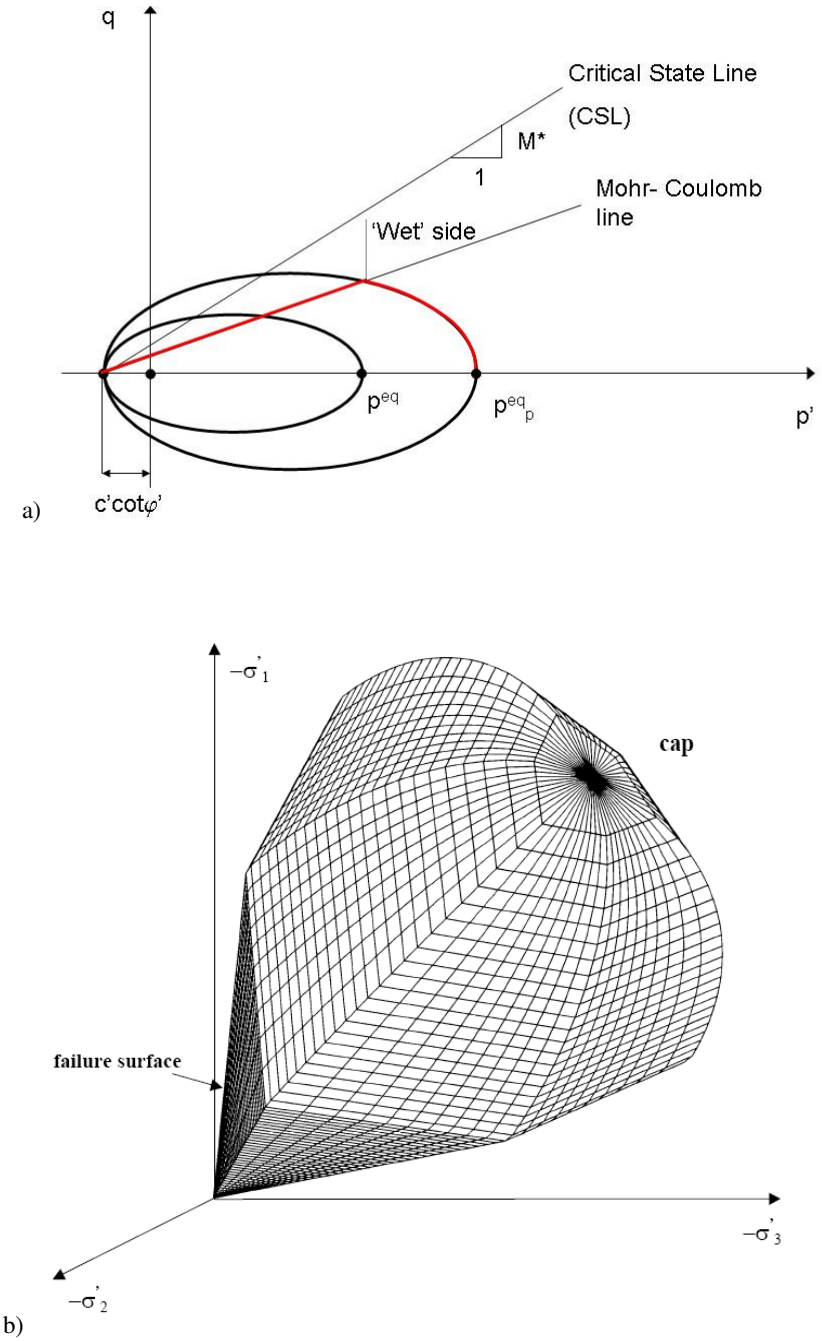

Figure 2.5: The yield surface of the SS model in:
a) triaxial stress space and b) principal stress space (Brinkgreve, 2002).

The model assumes a logarithmic relationship between volumetric strain ε_v and the equivalent effective stress p':

$$\varepsilon_v = \varepsilon_{v0} = -\lambda^* \ln\left(\frac{p'}{\sigma'_p}\right) \tag{2.16}$$

where: λ^* and κ^* are the modified compression and swelling indices respectively, and they differ from the conventional compression and swelling indices accordingly:

$$\lambda^* = \frac{\lambda}{(1+e)} = \frac{C_C}{2.3(1+e)} \tag{2.17}$$

$$\kappa^* = \frac{\kappa}{(1+e)} \approx \frac{2C_S}{2.3(1+e)} \tag{2.18}$$

The ratio between the modified indices λ^*/κ^* is equal to the ratio of λ/κ. *Eq. (2.18)* indicates that there is no direct relation between the modified swelling index κ^* and the one-dimensional swelling index C_S. That is due to the change in K_0 during one-dimensional unloading.

The Soft Soil model is very useful for normally consolidated clays and peat during primary loading as long as the time aspects are of secondary importance, see Husein *et al*. (2001). One major improvement, if compared with the MCC model, is the realistic predictions of the stress paths for one-dimensional compression.

Just like MCC, the SS model is isotropic. However, as natural soft soils are anisotropic and exhibit some apparent bonding, and the damage to existing interparticle bonds influences the stress-strain behaviour, constitutive models used for a realistic representation of a soft soil deposit should consider these soil characteristics. It is also worth noting that in the Soft Soil model there is no 'dry'

side, so the behaviour of a highly over-consolidated soils would be similar to that predicted by the Mohr-Coulomb model.

2.2.3 Hardening Soil Model

The Hardening Soil (HS) model was introduced by Schanz (1998) and was then further developed by Schanz *et al.* (1999). HS is commonly used by geotechnical engineers for the numerical modelling of uncemented sands and over-consolidated clays. Similar to the SS model, failure in HS is described by the Mohr-Coulomb criterion, and material dilatancy is included. The HS model is based on a double hardening model (Vermeer, 1978) to simulate triaxial tests in a more accurate way by accounting for the stress dependency of the soil stiffness modulus, which leads to an increase in stiffness with pressure.

The Hardening Soil model incorporates a multi-surface yield criterion combining a shear hardening surface on the so-called 'dry' side (cone) and a volumetric hardening elliptic cap surface with an associated flow rule on the 'wet' side. The deviatoric hardening surface expands with deviatoric strains and rotates anticlockwise until the failure condition is reached. The elastic region in the HS model is defined by both a cone and an additional cap. The cap surface is defined as:

$$f = \frac{\tilde{q}}{\alpha^2} + \left(p' + c' \cot \varphi'\right)^2 \quad - \quad \left(\sigma'_p + c' \cot \varphi'\right)^2 \tag{2.19}$$

where: $\tilde{q}$ is a special stress measure for deviatoric stresses ($\sigma'_1 + \sigma'_2(\delta - 1) - \delta\sigma'_3$), with $\delta = (3 + \sin\varphi')/(3 - \sin\varphi')$), α is an auxiliary parameter related to K_0^{NC}, p' is

the mean effective stress, c' is the effective cohesion and φ' is the effective angle of friction.

In order to model the irreversible strains due to primary deviatoric loading, shear hardening is included within the HS formulation. To account for the irreversible plastic strains (straining) due to primary compression during oedometer loading and isotropic loading, isotropic compression hardening is also incorporated in the HS model. The relationship between the deviatoric stress and the axial strain during primary triaxial loading is defined as illustrated in Figure 2.6.

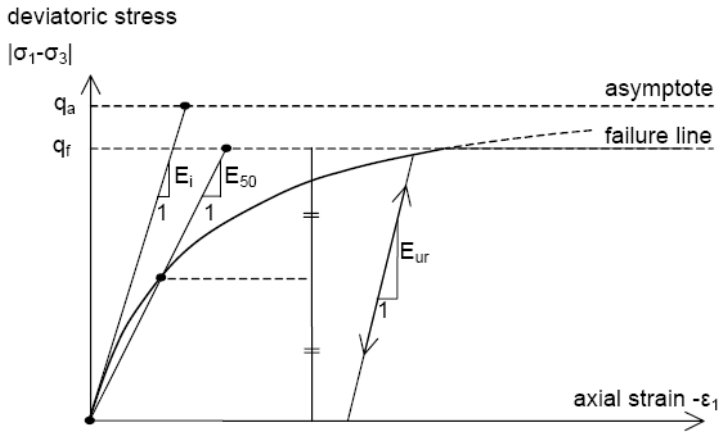

Figure 2.6: Deviatoric stress-axial strain relationship for the HS model (Brinkgreve 2002).

During primary shear, the stiffness of the soil is related to the power law as follows:

$$E_{50} = E_{50}^{ref}\left(\frac{c\cdot\cos\varphi - \sigma_3^{'}\cdot\sin\varphi}{c\cdot\cos\varphi + p_{ref}\cdot\sin\varphi}\right)^{m} \tag{2.20}$$

where: E_{50}^{ref} is the reference stiffness modulus corresponding to the reference stress p_{ref}, $\sigma_3^{'}$ is the minor principal stress and m defines the curvature of the $q-\varepsilon_1$ line

and depends on the nature of the soil considered. Brinkgreve (1994) recommends for soft soils a value of m equal to 1.

During an unloading-reloading path the soil stiffness can be described as:

$$E_{ur} = E_{ur}^{ref}\left(\frac{c\cdot\cos\varphi - \sigma_3^{'}\cdot\sin\varphi}{c\cdot\cos\varphi + p_{ref}\cdot\sin\varphi}\right)^{m} \tag{2.21}$$

where: E_{ur}^{ref} is the reference unloading-reloading stiffness modulus corresponding to the reference stress p_{ref} and $\sigma_3^{'}$ is the minor principal stress.

For the one-dimensional compression of soft soils (when m=1) the reference oedometer stiffness modulus E_{oed}^{ref} can be related to the modified compression index λ^{*}, and thus to λ:

$$E_{oed} = E_{oed}^{ref}\left(\frac{\sigma}{p^{ref}}\right)^{m} \tag{2.22}$$

$$E_{oed}^{ref} = \frac{p^{ref}}{\lambda^{*}} \tag{2.23}$$

The reference unloading-reloading stiffness modulus E_{ur}^{ref} can be related to the modified swelling index κ^{*} as follows:

$$E_{ur}^{ref} \approx \frac{2p^{ref}}{\kappa^{*}} \tag{2.24}$$

The Hardening Soil model is widely used for modelling granular materials and it also gives better predictions for normally and over-consolidated clays and dense and loose sands than the simple Mohr-Coulomb model. However, it is not suitable for simulating the behaviour of stiff heavily over-consolidated clays, see Brinkgreve (2002). HS accounts for stress dependency of the stiffness modulus and is considered

very useful in the case of deep and shallow excavations, and further extension of the model by Benz (2007) enables small strain stiffness to be accounted for.

2.3 Anisotropic constitutive models

In this section a short overview of developments in the constitutive modelling of anisotropic soils is given, followed by a brief description of the S-CLAY1 model (Wheeler *et al.*, 2003), which is the basis of most of the advanced constitutive models used in this thesis.

2.3.1 Modelling anisotropy

Evidence of the anisotropy of natural clays has been given by many researchers, see for example Tavenas & Leroueil (1977), Graham *et al*. (1983B) or Diaz- Rodriguez *et al.* (1995). Tavenas & Leroueil (1977) suggested that the yield surface of natural clays is inclined in the $t' - s'$ plane (where t' and s' are the shear stress and the mean effective stress in plane strain respectively) and that the expansion of the yield curve with time is due to creep. They proposed a time-dependent conceptual model to account for the initial anisotropy via an inclined ellipsoidal yield surface. The centre of the ellipse is orientated around a stress path following the K_0-line. In parallel, Sekiguchi & Ohta (1977) introduced their time-dependent model for normally consolidated clays, which allowed for stress induced anisotropy of the material. A major drawback of this model is the singularity corner on the yield surface, which

causes some problems during numerical implementation. Furthermore, the model is not able to represent the evolution of anisotropy.

Later, several elasto-plastic constitutive models were proposed, which account for changes in anisotropy as a result of plastic volumetric strains only, see Dafalias (1986), Davies & Newson (1993) and Whittle & Kavvadas (1994). A kinematic (translational) hardening law instead of a rotational hardening law was proposed by Di Prisco *et al.* (1993). The model proposed by Dafalias (1986 & 1987) is relatively simple in its formulation and is based on Modified Cam Clay, but the rotation of the yield surface is based on only plastic volumetric strains. This is physically unfounded and creates problems in relation to model predictions under some stress path directions (Karstunen & Wheeler, 2002 and Wheeler *et al.*, 2003). The lack of the dependence of the rotational hardening on plastic shear strains precludes the yield surface from further rotation in the critical state. This leads to the dependence of the final degree of anisotropy on the initial amount of anisotropy and on the stress path followed to reach the critical state. The mathematical form of the anisotropic yield surface (Figure 2.7) of the Dafalias (1986) model is such that it has a horizontal tangent where the yield surface intersects the critical state line (*M*-line), and it is identical to that proposed independently by Korhonen & Lojander (1987) based on experimental evidence.

Very similar in formulation but with a different aspect ratio of the sheared ellipse is a model proposed by Banerjee & Yousif (1986). This model assumes a rotational hardening law, which allows for a change of the yield surface inclination solely due to plastic volumetric strains, so it has the same problem as the Dafalias (1986) model. In the model developed by Davies & Newson (1993) a rotational

hardening law was incorporated within this model along with a non-associated flow rule.

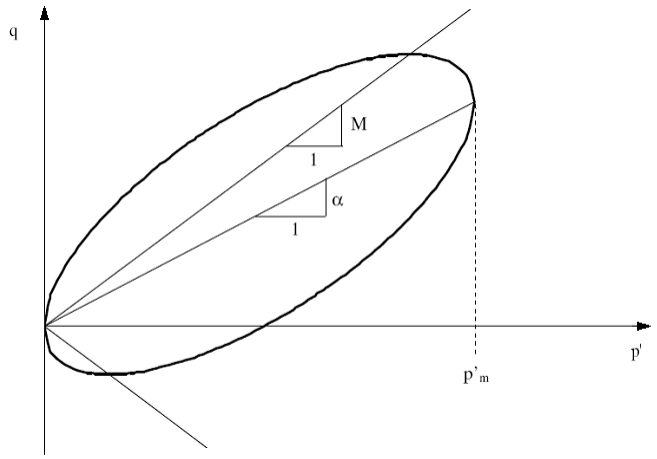

Figure 2.7: The yield surface proposed by Dafalias (1987).

The major drawback of their rotational hardening law is the lack of the rotation of yield surface during loading at a constant value of stress ratio η. This means that if an anisotropic soil is loaded along an isotropic stress path, the anisotropy will not change.

A link between the evolution and erasure of the fabric due to both plastic volumetric and shear strains was proposed by Whittle & Kavvadas (1994), Pestana & Whittle (1999) and Wheeler *et al.* (2003). Pestana & Whittle (1999) formulated a hierarchical constitutive model MIT-E3 for uncemented materials (such as sands) and stiff clays. This rather complicated model is able to predict unloading and reloading cycles by adopting bounding surface plasticity, see Figure 2.8. The originally isotropic yield surface is inclined with the consolidation direction which enables the rotation of the ellipse. To satisfy K_0 and critical state conditions the

authors used a non-associated flow rule, which slows down the analysis, as the resulting stiffness matrix is non-symmetric. The predictions of the model for soil behaviour under an embankment are in agreement with the investigations of Zdravkovic *et al.* (2002). However, as the model requires fifteen input parameters, which are difficult to obtain via standard laboratory tests, the formulation is used mainly for research and not by geotechnical practitioners. This problem does not apply to the model proposed by Wheeler *et al.* (2003), which was briefly presented in *Section 2.3.2*.

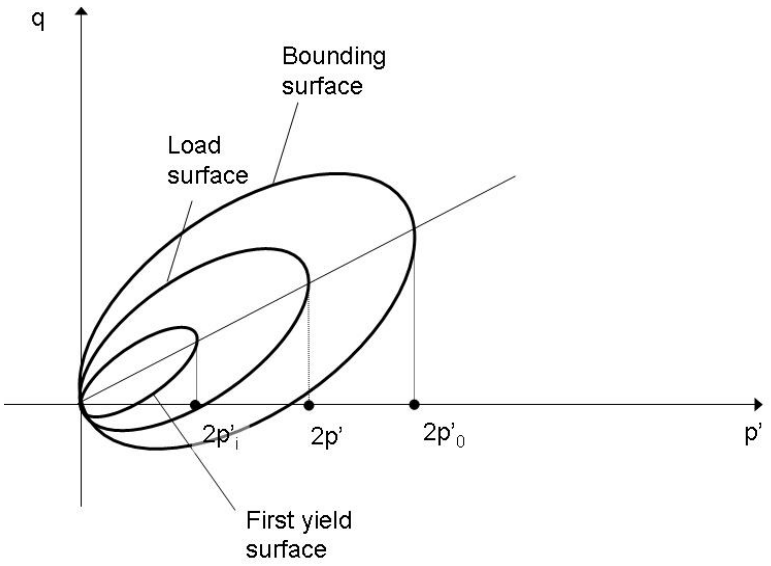

Figure 2.8: MIT-E3 yield surfaces proposed by Pestana & Whittle (1999).

An alternative way to represent anisotropy was proposed by Zienkiewicz & Pande (1977) for rocks using the so-called multilaminate framework. The idea has been extended to clays by Pande & Sharma (1983) and Pietruszczak & Pande (1987). Within the multilaminate framework a number of contact planes is associated with

each stress point and an integration rule defines the orientation of the contact planes. A local stress-strain relationship is formulated on each contact plane. The global strains are determined by numerical integration of the plastic strains from each sampling plane and the global elastic strain. However, a major drawback of this approach is that a global equivalent of the yield surface does not exist. Moreover, the state parameters have to be stored for each sampling plane, and hence the computational effort is significantly increased in comparison to the standard critical state models, as integration over all sampling planes for each individual stress point is required.

2.3.2 S-CLAY1

Wheeler *et al.* (2003) proposed an anisotropic extension of the Modified Cam Clay Model, the so-called S-CLAY1 model, which stemmed from the previously introduced work of Wheeler (1997) and Näätänen *et al.* (1999). High accuracy of the stress-strain predictions is assured via the incorporation of a rotating inclined yield surface, which has been proven to model data on natural soft soils (Wheeler *et al.* 2003).

The formulation in the general stress space will be presented below as it is required for the incorporation of full anisotropy instead of fixed cross-anisotropy in finite element modelling. Next, the description of the model parameters, including additional soil constants and initial state variables, and some brief advice regarding their determination are given.

The inclined yield surface can be visualised as in Figure 2.9 in triaxial and principal stress space and expressed in three-dimensional form as:

$$f = \frac{3}{2}[\{\underline{\sigma}_d^{'} - p'\underline{\alpha}_d\}^T\{\underline{\sigma}_d^{'} - p'\underline{\alpha}_d\}] - [M^2 - \frac{3}{2}\{\underline{\alpha}_d\}^T\{\underline{\alpha}_d\}](p_m^{'} - p')p' = 0 \tag{2.25}$$

where: $\underline{\sigma}_d$ is the deviatoric stress tensor, $\underline{\alpha}_d$ is the deviatoric fabric tensor and M is the stress ratio at critical state. The deviatoric stress tensor $\underline{\sigma}_d$ is defined as follows:

$$\underline{\sigma}_d^{'} = \begin{bmatrix} \sigma_x^{'} - p' \\ \sigma_y^{'} - p' \\ \sigma_z^{'} - p' \\ \sqrt{2}\tau_{xy} \\ \sqrt{2}\tau_{yz} \\ \sqrt{2}\tau_{zx} \end{bmatrix} = \begin{bmatrix} \frac{1}{3}(2\sigma_x^{'} - \sigma_y^{'} - \sigma_z^{'}) \\ \frac{1}{3}(-\sigma_x^{'} + 2\sigma_y^{'} - \sigma_z^{'}) \\ \frac{1}{3}(-\sigma_x^{'} - \sigma_y^{'} + 2\sigma_z^{'}) \\ \sqrt{2}\tau_{xy} \\ \sqrt{2}\tau_{yz} \\ \sqrt{2}\tau_{zx} \end{bmatrix} \tag{2.26}$$

The deviatoric fabric tensor $\underline{\alpha}_d$ is then analogous to the deviatoric stress tensor defined as below:

$$\underline{\alpha}_d = \begin{bmatrix} \frac{1}{3}(2\alpha_x - \alpha_y - \alpha_z) \\ \frac{1}{3}(-\alpha_x + 2\alpha_y - \alpha_z) \\ \frac{1}{3}(-\alpha_x - \alpha_y + 2\alpha_z) \\ \sqrt{2}\alpha_{xy} \\ \sqrt{2}\alpha_{yz} \\ \sqrt{2}\alpha_{zx} \end{bmatrix} = \begin{bmatrix} \alpha_x - 1 \\ \alpha_y - 1 \\ \alpha_z - 1 \\ \sqrt{2}\alpha_{xy} \\ \sqrt{2}\alpha_{yz} \\ \sqrt{2}\alpha_{zx} \end{bmatrix} \tag{2.27}$$

where the components of the tensor are defined as:

$$\frac{1}{3}(\alpha_x + \alpha_y + \alpha_z) = 1 \tag{2.28}$$

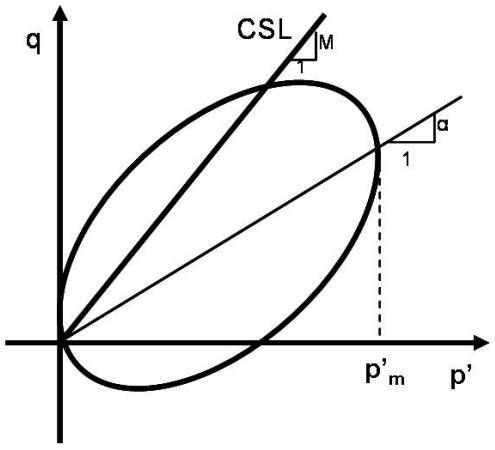

a)

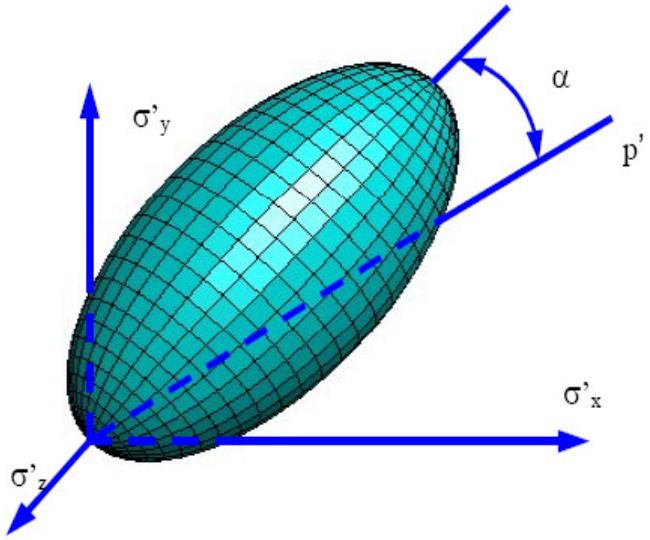

b)

Figure 2.9: S-CLAY1 yield surface in: a) triaxial stress space and b) principal stress space.

The scalar anisotropy parameter in simplified triaxial stress space can then be defined as:

$$\alpha^2 = \frac{3}{2}\{\underline{\alpha}_d\}^T\{\underline{\alpha}_d\} \tag{2.29}$$

Two hardening parameters, $p_m^{'}$ and $\underline{\alpha}_d$, define the size and orientation of the yield surface, respectively. The deviatoric fabric tensor $\underline{\alpha}_d$ indicates the degree of the plastic anisotropy of the soil and once the value of $\underline{\alpha}_d$ is equal to zero, the yield surface reduces to the yield surface of the MCC model. However, one should remember that for soils with a K_0 stress history the initial value of α is greater than zero.

In the S-CLAY1 model the elastic strains are defined in the same manner as in MCC, which means that the anisotropy is only considered for plastic straining.

Elastic volumetric strains are defined as follows:

$$d\varepsilon_v^e = \frac{\kappa dp^{'}}{vp^{'}} \tag{2.30}$$

And the deviatoric component of elastic strain is described as:

$$d\varepsilon_d^e = \frac{dq^{'}}{3G^{'}} \tag{2.31}$$

where: Poisson's ratio $\nu^{'}$ is constant and the shear modulus $G^{'}$ is defined as $G' = \frac{3(1-2\nu^{'})vp^{'}}{2(1+\nu^{'})\kappa}$.

In the S-CLAY1 model two hardening laws have been incorporated in order to account for the change in size and orientation (inclination) of the yield surface due to plastic straining.

Changes in the size of the yield surface $p_m^{'}$ in the S-CLAY1 model, as in MCC, is related solely to the plastic volumetric strains following the hardening law:

$$dp_m^{'} = \frac{vp_m^{'} d\varepsilon_v^p}{\lambda - \kappa} \tag{2.32}$$

where: λ is the slope of the normal compression line obtained from $v - \ln p'$ curve for stress paths at a constant stress ratio η where no change in anisotropy is assumed ($\alpha = const.$).

The amount of anisotropy in the soil material is not fixed and is altered during plastic straining, resulting in the development or erasure of fabric anisotropy. During this process, the orientation (inclination) of the yield surface changes and this can be defined by the plastic volumetric and deviatoric strains using the so-called rotational hardening law as follows:

$$d\underline{\alpha}_d = \omega\left[\left(\frac{3}{4}\underline{\eta} - \underline{\alpha}_d\right)\left\langle d\varepsilon_v^p \right\rangle + \omega_d\left(\frac{1}{3}\underline{\eta} - \underline{\alpha}_d\right)(d\varepsilon_d^p)\right] \tag{2.33}$$

where: $\underline{\eta} = \underline{\sigma}_d / p'$, $d\varepsilon_d^p$ is the plastic deviatoric strain increment, ω and ω_d determines the absolute and relative effectiveness of the rotational hardening of the yield surface, respectively. Wheeler *et al.* (2003) defined the target values of the inclination of the yield surface for the deviatoric and volumetric plastic strains as $\frac{1}{3}\underline{\eta}$ and $\frac{3}{4}\underline{\eta}$, respectively based on experimental evidence obtained for soft Otaniemi clay from Finland.

Similar to MCC, an associated flow rule has been employed in the S-CLAY1 model, which can be defined as follows:

$$\frac{d\varepsilon_d^p}{d\varepsilon_v^p} = \frac{2(\eta - \alpha)}{M^2 - \eta^2} \tag{2.34}$$

Determination of additional state variable and soil constants

In addition to the MCC model, S-CLAY1 requires two soil constants, namely ω and ω_d. Moreover, the components of the fabric tensor $\underline{\alpha}_d$ (or state variable α in triaxial stress state) have to be assigned values (α_0 for the triaxial stress space, respectively). This section will focus on the determination of these input parameters.

Assuming that the y-axis coincides with the vertical axis in the ground, for an initially cross-anisotropic soil, it is assumed that:

$$\alpha_x = \alpha_z \ , \ \alpha_{xy} = \alpha_{yz} = \alpha_{xz} = 0 \tag{2.35}$$

where: y-axis is the vertical axis in the ground. Following that, the components of the deviatoric fabric tensor (*Eq. (2.28)*) are reduced to:

$$\alpha_y = 3 - 2\alpha_x \tag{2.36}$$

Thus, the deviatoric fabric tensor $\underline{\alpha}_d$ can be expressed in terms of α_x:

$$\underline{\alpha}_d = \begin{bmatrix} \alpha_x - 1 \\ 2(1-\alpha_x) \\ \alpha_x - 1 \\ 0 \\ 0 \\ 0 \end{bmatrix} \tag{2.37}$$

Components of *Eq. (2.29)* are defined using *Eqs. (2.35 & 2.36)*:

$$\alpha_x = 1 - \tfrac{\alpha}{3} \tag{2.38}$$

As conventionally it is assumed that in triaxial loading $q = \sigma_1^{'} - \sigma_3^{'} = \sigma_y^{'} - \sigma_x^{'}$ is positive, a positive value of α is taken for the sake of consistency. Then the scalar parameter for cross-anisotropic and for K_0 consolidated soils is expressed as:

$$\underline{\alpha}_{d,0} = \begin{bmatrix} \frac{-\alpha}{3} \\ \frac{-2\alpha}{3} \\ \frac{-\alpha}{3} \\ 0 \\ 0 \\ 0 \end{bmatrix} = \begin{bmatrix} \frac{-\alpha_{K_0}}{3} \\ \frac{-2\alpha_{K_0}}{3} \\ \frac{-\alpha_{K_0}}{3} \\ 0 \\ 0 \\ 0 \end{bmatrix} \tag{2.39}$$

The initial value of the yield surface inclination α_0 can be estimated by assuming a unique α value corresponding to one-dimensional straining as a result of loading at a specific stress ratio η. One-dimensional straining can be defined as:

$$\frac{d\varepsilon_d}{d\varepsilon_v} = \frac{2}{3} \tag{2.40}$$

Assuming relatively small elastic strains (compared to plastic strains), one can approximate that:

$$\frac{d\varepsilon_d^p}{d\varepsilon_v^p} \approx \frac{2}{3} \tag{2.41}$$

Following the assumption about the associated flow rule, the initial value of the yield surface inclination α_0 for normally consolidated soil can be defined as:

$$\alpha_0 \approx \frac{\eta_{K_0}^2 + 3\eta_{K_0} - M^2}{3} \tag{2.42}$$

Applying Jaky's formula for estimating the coefficient of earth pressure at rest ($K_0 = (1 - \sin\varphi_{cv}^{'})$), the stress ratio η_{K_0} for normally consolidated soils can be defined as:

$$\eta_{K_0} = \frac{3(1 - K_0^{NC})}{(1 + 2K_0^{NC})} \tag{2.43}$$

Eqs. (2.42 & 2.43) suggest that the inclination of the yield surface is dependent on the critical state friction angle φ'_{cv} of the clay. However, in the case of heavily over-consolidated soils which are subjected to unloading, a change of the inclination and the size of the yield surface may take place (as a result of crossing over the yield surface along the unloading stress path and subsequent rotation towards the isotopic state). The procedure used for the determination of the initial value of α has been formed by applying the assumption that the soil considered is not heavily over-consolidated and that the orientation of the yield surface has not be influenced by any elastic unloading of the material to a lightly over-consolidated state. Moreover, the theoretical background on the initial anisotropy is valid if the soil layers are horizontal, which is not always the case (i.e. in the case of slopes). However, if inclined soil layers have been built up as a result of river or wind erosion, the background regarding the initial anisotropy will be valid.

A simple method of estimating the relative effectiveness of plastic deviatoric and volumetric strains in the rotation of the yield surface ω_d has been presented by Wheeler *et al.* (1999). By setting the components of $d\underline{\alpha}_d$ to zero in *Eq. (2.33)* one can see that only one specific value of the parameter ω_d will bring the yield surface to the required inclination $\alpha = \alpha_{K_0}$ during continuous loading at $\eta = \eta_{K_0}$:

$$\omega_d = \frac{3(4M^2 - 4\eta_{K_0}^2 - 3\eta_{K_0})}{8(\eta_{K_0}^2 - M^2 + 2\eta_{K_0})} \tag{2.44}$$

The rate at which the yield surface rotates towards its target value is defined via the parameter ω. However, no direct method of this parameter exists and to determine ω, a laboratory test which involves a significant rotation of the yield

surface (such as isotropic loading of a soil with a one- dimensional strain history or undrained shearing in triaxial extension) would be ideal for that purpose. Then, one can obtain ω by comparing the test results with model simulations for different values of ω. If such experimental tests are not available, ω can be determined using conclusions from the parametric studies conducted by Zentar *et al.* (2002), where the stress-strain behaviour of several Scandinavian clays was studied using triaxial tests. An empirical relation was proposed as a result of those studies in the form of: $10/\lambda \langle \omega \langle 20/\lambda$, where λ is the slope of the normal compression line obtained from the $v - \ln p'$ curve. Nevertheless, it has been demonstrated via numerical simulations of triaxial tests with different stress paths that predictions are not greatly influenced by the value of ω, (Wheeler *et al.*, 2003). In fact, Wheeler *et al.* (2003) suggested that within the range of ω studied by Zentar *et al.* (2002) an isotropic stress state three times larger than the yield stress must be applied to a soil sample before fabric anisotropy is entirely erased.

S-CLAY1 is a hierarchical model; if anisotropy is not considered, S-CLAY1 can be reduced to the MCC model by setting the rotational hardening parameter ω and the parameter describing the inclination of the yield surface (α) to zero.

The formulation of the S-CLAY1 model has a number of advantages over the isotropic MCC model and other constitutive models. First and foremost, this user-friendly model is relatively simple and all input parameters can be obtained via laboratory tests or have real physical meaning. The complexity of the model has been kept to a minimum, which allows geotechnical engineers to use it for practical applications. Keeping that in mind, this advanced model accounts for plastic anisotropy (and more importantly, the development and erasure of anisotropy with

plastic straining), and is in agreement with experimental evidence on the orientation of the yield surfaces of soft soils (Wheeler *et al.*, 2003). Therefore, improvement of the yield stresses along certain stress paths has been made compared to Modified Cam Clay, see Wheeler *et al.* (2003) and Karstunen & Koskinen (2004). The model also automatically gives a very good prediction of the coefficient of the lateral earth pressure K_0^{NC}. Moreover, as the orientation of the yield surface at critical state is independent of the stress path, the predicted level of anisotropy at the critical state is also independent of any initial anisotropy and of the loading history. This is a great improvement with respect to some constitutive models where the change in the inclination of the yield surface has been related solely to the plastic volumetric strains, such as those proposed by Banerjee & Yousif (1986) or Davies & Newson (1993). Because an associated flow rule is assumed, the stiffness matrix is symmetric which speeds up the computational effort, compared to for example the model by Pestana & Whittle (1999). In the version of the S-CLAY1 model used in this thesis, the failure at critical state is presented with a Drucker-Prager cone, imposing that the critical state stress ratio in triaxial compression M_C is equal to the critical state stress ratio in triaxial extension M_E. Due to the effects of anisotropy, the predicted undrained shear strength in extension is much lower than in compression, and hence this is an improvement compared to the MCC model. As discussed by Wheeler et al. (2003), it is also possible to incorporate with the cone a Lode angle-dependency for the formulation.

The S-CLAY1 model has been extended to the S-CLAY1S model which also accounts for interparticle bonding and destructuration processes (Koskinen *et al.*,

2002; Karstunen *et al.*, 2005). Details on the S-CLAY1S model are given in *Section 2.4.2.*

2.4 Constitutive models with anisotropy and destructuration

This section presents a brief overview of the developments in the constitutive modelling of interparticle bonding and destructuration and gives a short description of the S-CLAY1S model (Koskinen *et al.*, 2002 and Karstunen *et al.*, 2005) which is used in the current research to represent the soft soil deposits in a number of simulations.

2.4.1 Modelling interparticle bonding and destructuration

The presence of interparticle bonding, its implications and the process of destructuration have been described by many researchers since the early 1930s, see Casagrande (1932). Through many years of research, the influence of the structure of the material on the stress-strain behaviour of a natural soil sample has been established, see Bjerrum (1967) or Clayton *et al.* (1972) among others.

Gens & Nova (1993) proposed an isotropic elasto-plastic critical state model, which accounts for the effects of initial bonding and destructuration. They

incorporated two yield surfaces within this model; the first of them is the yield surface describing the natural material and the second, the so-called intrinsic yield surface, which describes the behaviour of the unbonded material. The latter, has got the same shape and orientation as the natural yield surface, but it is different in size, see Figure 2.10. The ratio between the sizes of these two yield surfaces determines the amount of bonding within the material. The degree of bonding can also be determined as the difference in void ratio for the bonded and the unbounded soil at the same stress level.

The change in the size of the natural yield surface is governed by two mechanisms: the conventional hardening (or softening) and the destructuration phenomena. All interparticle bonds are destroyed when the size of the natural yield surface becomes equal to the size of the intrinsic yield surface. Additionally, it has been assumed that the bonds are destroyed irrespective of the direction of plastic straining. The increase in the size of the intrinsic yield surface is associated with plastic volumetric strains via a volumetric hardening law, similarly to the MCC model; this also influences the size of the natural yield surface. The second hardening law, the so-called destructurational law, is incorporated within this model and it relates the reduction of the bonding effect to both plastic volumetric and shear strains. The major drawback of the model by Gens & Nova (1993) is the lack of anisotropy (often found in clay deposits) as the hardening is assumed to be only isotropic.

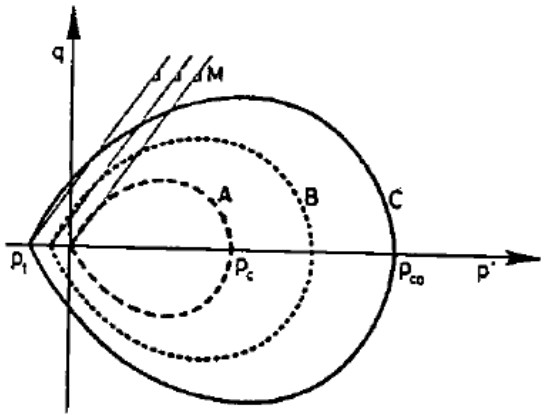

Figure 2.10: Yield surfaces for various degrees of bonding (Gens & Nova, 1993).

Rouainia & Muir Wood (2000) introduced kinematic yield surfaces into constitutive modelling, following the idea by Mróz *at el.* (1979) and Al-Tabbaa & Muir Wood (1989). They proposed a 'bubble' model, an extension of the Modified Cam Clay using boundary surface plasticity. The bonding effect leads to 'some' anisotropy of the yield surface of natural materials for large strains but it disappears once destructuration is finished. This is in contrast with the experimental evidence by Koskinen *et al*. (2002), where it was found that the change or evolution of the clay fabric orientation continues regardless whether or not interparticle bonding is present.

Another 'bubble' model was proposed by Kavvadas & Amarosi (2000). This formulation used the intrinsic yield surface idea as presented by Gens & Nova and the movement of a 'bubble' inside the yield surface is similar to the model by Rouainia & Muir Wood (2000). The model accounts for anisotropy, bonding effects and volumetric and deviatoric destructuration, nevertheless it requires eleven soil

constants and five additional initial values for state parameters. This may limit its use in practical geotechnical applications, as only experienced engineers would be able to use this model correctly and with engineering confidence.

An isotropic model, which accounts for bonding and destructuration as an extension of the Modified Cam Clay model was proposed by Liu & Carter (2000) and (2002). They introduced only a single yield surface, similar to the MCC one, which results in a simple formulation. Even so, the assumption that only plastic volumetric strains have an effect on destructuration which may lead to an incorrect solution, as the effect of plastic shear strains are neglected, which is counter-intuitive.

A bounding plasticity model, which in addition to this accounts for anisotropy, was proposed by Gajo & Muir Wood (2001). They proposed a further development of the destructurational law, by formulating the yield surface and hardening law in normalised stress space. This model is capable of modelling isotropic hardening, anisotropy, destructuration and also small strain stiffness.

Based on 3-SKM, introduced by Stallebrass & Taylor (1997), and following the kinematic yield surfaces approach, another formulation was proposed by Baudet & Stallebrass (2004). This model incorporates three surfaces, kinematic hardening and the influence of plastic volumetric and plastic shear strains on the rate of destructuration process is assumed to be equal. Applied within this formulation the destructurational law is similar to that presented in the Rouainia & Muir Wood (2000) model. The model itself has proven to be reasonably successful in the representation of the small strain non-linearity, however it does not account for the anisotropy of the natural soil. Moreover, the model proposed by Baudet &

Stallebrass (2004) has not been implemented into FE commercial code, which limits its applicability amongst geotechnical practitioners.

Along with elasto-plastic bonding models, the multilaminate framework has been extended to account for the destructuration process. The models proposed by Cudny (2003) and Galavi (2007), which account for both anisotropy and destructuration, have been proven to give the correct stress-strain response of soil during numerical simulations during element tests. The Galavi (2007) model, which has been compared with experimental data, accounts for anisotropic strength and anisotropic structure via a structure tensor and furthermore the novel application of the non-local approach has enabled the simulation of strain softening. However, Galavi (2007) has not verified numerical predictions of his model in any boundary value problem. More importantly, drawbacks of the multilaminate approach have not been overcome, such as the high computational cost required.

2.4.2 S-CLAY1S

Interparticle bonding and the destructuration process is highly important when considering the stress-strain behaviour of natural soft soils, as already discussed. As an alternative to the approaches proposed by Stallenbrass & Taylor (1997) or Gajo & Muir Wood (2001), the S-CLAY1S model was proposed by Koskinen *et al.* (2002) and Karstunen *et al.* (2005). This model is an extension of the anisotropic S-CLAY1 model and in order to account for bonding and destructuration, the idea proposed by Gens & Nova (1993) was used.

Experimental data on two Finnish soft soils (POKO clay and Vanttila clay) indicate that the slope of the normal compression line λ for natural clays depends on the stress ratio η of the stress path, see Figure 2.11 and Koskinen & Karstunen (2004). Koskinen & Karstunen (2004) concluded that the direction of the stress path influences the rate at which the destructuration process takes place. As a result of the damage to the interparticle bonds, the compression curve of the natural soil will converge towards the intrinsic compression curve. Therefore, it is recommended that the intrinsic λ_i and the apparent (natural) λ of the slope of the normal compression line be distinguished, and the selection of an appropriate λ value requires some thought.

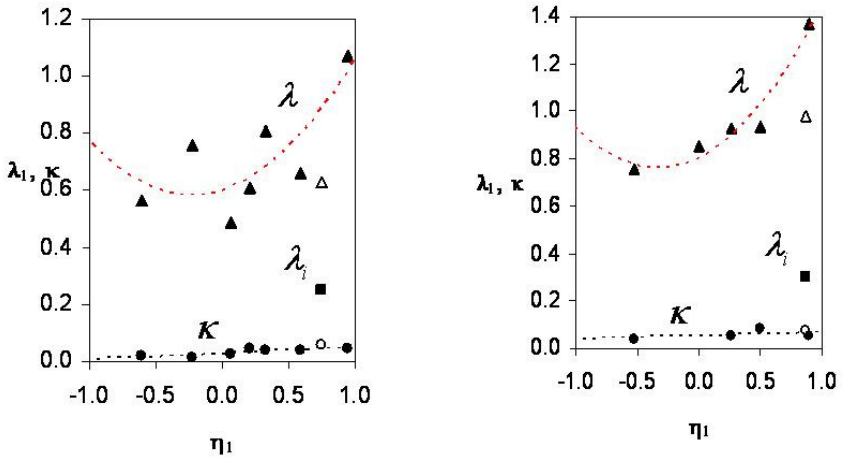

a) b)

Figure 2.11: Influence of the stress ratio on the apparent and intrinsic compression index: a) POKO clay and b) Vanttila clay (after Koskinen & Karstunen, 2004).

The S-CLAY1S model (Koskinen *et al.*, 2002 and Karstunen *et al.*, 2005) improves the predictions for highly structured soils, such as sensitive soils. The

model incorporates two yield surfaces, see Figure 2.12. The first of them is the yield surface describing the natural soil behaviour and it is the same as in the S-CLAY1 model. The second yield surface, named the intrinsic yield surface and indicated in Figure 2.12 in red, enables the interparticle bonding and erasure of those bonds to be represented.

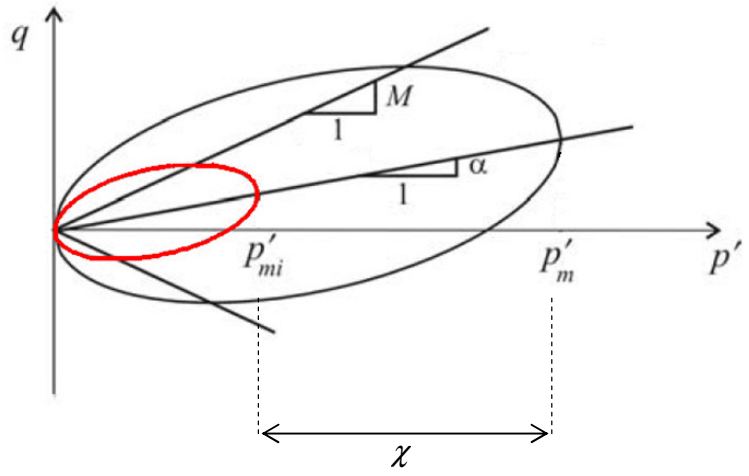

Figure 2.12: Natural and intrinsic yield surfaces, S-CLAY1S model.

The intrinsic yield surface describes an equivalent unbonded material with the same void ratio and fabric as the natural soil. It is of the same shape and orientation as the natural one, however it is smaller in size. In fact, the size of the intrinsic yield surface p'_{mi} is related to the size of the natural yield surface p'_m via the so-called bonding parameter χ:

$$p'_m = (1+\chi)p'_{mi} \tag{2.45}$$

The bonding parameter χ describes the amount of bonding enclosed in the soil material.

The increment of plastic volumetric strains in the S-CLAY1S model is a result of two components and can be described as follows:

$$d\varepsilon_v^p = \frac{(\lambda_i - \kappa)dp'_m}{vp'_m} + \frac{(\lambda_i - \kappa)(-d\chi)}{v(1+\chi)} \tag{2.46}$$

The first of the components is related to the increase in size of the natural yield surface (and is identical to the plastic volumetric strain predicted by S-CLAY1) and the second component represents the additional plastic volumetric strain due to destructuration.

In order to derive the ratio of the plastic volumetric and deviatoric strains, the S-CLAY1S model assumes, similar to S-CLAY1, an associated flow rule. Moreover, the elastic behaviour is assumed to be the same as in S-CLAY1 and MCC. It is assumed in the S-CLAY1S model that the elastic strains do not cause damage between the interparticle bonds and that the elastic properties are not influenced by the destructuration process. As the S-CLAY1 and S-CLAY1S model have been developed with normally or lightly over-consolidated soils in mind, the assumption about the dominance of plastic strains in practical geotechnical problems seems to be valid.

The behaviour of soil described by S-CLAY1S is governed by three hardening laws. The first of them, related to the rotation (orientation) of the yield surface is the same as in the S-CLAY1 model. The second hardening law, which describes the change in size of the yield surface, is very similar to the volumetric hardening law applied in S-CLAY1. However, in the case of the S-CLAY1S model the hardening law applies to the change in size of the intrinsic yield surface dp'_{mi} instead of the size of the natural yield surface:

$$dp'_{mi} = \frac{vp'_{mi} d\varepsilon_v^p}{\lambda_i - \kappa} \tag{2.47}$$

And hence an intrinsic value of λ_i has to be adopted.

The third hardening law, a so-called destructuration law, describes the process of the degradation of the interparticle bonds with plastic straining and can be presented as follows:

$$d\chi = \xi\left[(0-\chi)\left|d\varepsilon_v^p\right| + \xi_d (0-\chi)\left|d\varepsilon_d^p\right|\right] = -\xi\chi\left[\left|d\varepsilon_v^p\right| + \xi_d \left|d\varepsilon_d^p\right|\right] \tag{2.48}$$

where: ξ and ξ_d are two additional soil constants. The parameter ξ controls the absolute rate of destructuration and the parameter ξ_d controls the relative effectiveness of plastic deviatoric strains and plastic volumetric strains in destroying the bonding between particles. Both plastic volumetric and deviatoric strains take part in the degradation of the interparticle bonds and tend to reduce the bonding parameter χ towards a value of zero. *Eq. (2.48)* has the same form as that proposed by Gens & Nova (1993) and that adopted by for example Rouiainia & Muir Wood (2000).

When destructuration is complete, the natural yield surface coincides with the intrinsic one. It has been proven that the incorporation of the process of degradation of the interparticle bonds enables softening to be modelled as a result of destructuration, see Karstunen & Koskinen (2004) or Koskinen & Karstunen (2006).

Determination of additional state variable and soil constants

In addition to the S-CLAY1 model, S-CLAY1S requires three soil constants: ξ, ξ_D and λ_I. Moreover, the initial value for an additional state variable χ has to be determined. This section focuses on the determination of these input parameters.

The initial amount of bonding χ_0, the so-called bonding parameter, can be estimated based on the sensitivity of the soil S_t, measured for example by fall cone tests. As the sensitivity of the soil is defined as the ratio between the strength of the natural soil sample to the strength of a corresponding remoulded sample, the initial amount of bonding can be assumed as follows:

$$\chi_0 = S_t - 1 \tag{2.49}$$

Additionally, χ_0 can be also estimated from oedometer tests on intact soil samples as a $\sigma_p^{'} / \sigma_{pi}^{'}$ ratio determined from the $e - \log \sigma_v^{'}$ plot, see Figure 2.13. The incorporation of destructuration in S-CLAY1S resulted in improved predictions of volumetric strains when compared with the S-CLAY1 model, see Koskinen *et al.* (2002).

In order to determine the parameters ξ and ξ_d simulation tests with several different values of stress ratio η should be conducted, and the parameters calibrated by matching the post-yield compression curves, as outlined by Koskinen *et al.* (2002). The first, parameter ξ can be obtained by performing a drained triaxial test with very low values of the stress ratio η, in which the influence of the shear strains is very small and the value of ξ_d has a negligible effect. Once the parameter ξ has been selected, a drained triaxial test with a very high value of the stress ratio η

should be performed in order to obtain ξ_d. A number of numerical tests have been performed on Finnish clays, which have indicated that typical values of ξ and ξ_d range from 9..10 and 0.2..0.3, respectively (see Koskinen *et al.*, 2002). Research on the Scottish Bothkennar clay has indicated similar values of parameters ξ and ξ_d, using the optimisation procedure performed by Zentar *et al.* (2002) ($\xi = 8$ and $\xi_d = 0.3$) and McGinty (2006) ($\xi = 9$ and $\xi_d = 0.4$).

The intrinsic value of the post-yield compression index λ_i can be defined using oedometer tests on reconstituted soil samples. Alternatively, the value of λ_i may also be determined from oedometer tests on natural samples taken to high stress levels.

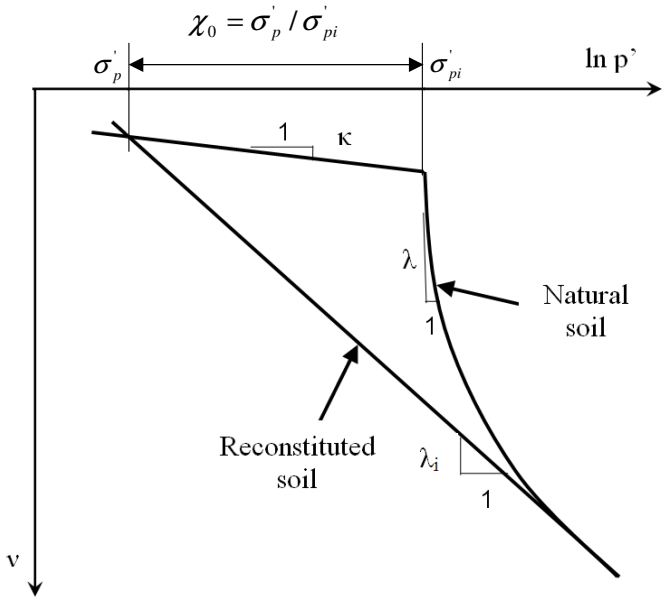

Figure 2.13: The behaviour of natural and reconstituted soil under one-dimensional loading and estimation of the initial interparticle bonding from oedometer tests.

As the two models (S-CLAY1 and S-CLAY1S) have been based on MCC and their complexity has been kept to a minimum, it is possible to reduce the advanced S-

CLAY1 type model into the isotropic MCC model without any changes to the formulation. By setting the initial amount of bonding in S-CLAY1S to zero, the model reduces to the anisotropic S-CLAY1 model (provided that the λ value inputted corresponds to a natural clay). Furthermore, by setting a few more model parameters to zero, the isotropic MCC will be recovered.

2.5 Time-dependent constitutive models

This section provides a short overview of the developments in time-dependent constitutive modelling and gives a brief description of two models, the Soft Soil Creep model (Brinkgreve, 2002) and the Anisotropic Creep Model (Leoni *et al.* 2008), which are applied in this thesis to represent the soft soil deposits in selected simulations.

2.5.1 Modelling time-dependency and viscosity

The observed rate dependent behaviour of soils is due to the inherent viscous characteristics of the soil skeleton and as such, this process is inevitable in every type of soil. However in some soils this phenomenon is more pronounced. This issue is of high importance, particularly in the case of normally consolidated soils, such as clays, clayey silts or peats.

At the beginning of the 1950s the overstress theory was formulated, and first of all a one-dimensional constitutive model was introduced by Malvern (1951). Later , this model was extended into three-dimensions by Perzyna (1966) and this gave the

foundation for many time-dependent formulations, either based on the Cam Clay model or on MCC, such as Adachi & Okano (1974), Sekiguchi & Ohta (1977), Nova (1984) and others. In the Perzyna (1966) approach, time-dependent behaviour in the elastic region is ignored. The model incorporates two yield surfaces: a static yield surface (similar to the surface used in time-independent plasticity) and a dynamic yield surface, which is bigger in size than the static one and is dependent on the loading. The viscoplastic regime is defined by these two yield surfaces, (Liingaard *et al*., 2004). The overstress is referred to as the distance between the static and dynamic yield surfaces. A change in the stress state generates the viscoplastic strain and the total predicted strain consists of two components: the elastic and the viscoplastic part.

The approach proposed by Perzyna (1966) has been used for many elastic-viscoplastic formulations, such as Yin & Graham (1989), Hinchberger & Rowe (1998), Zhu & Yin (2000) or Kim & Leroueil (2001). All of these models consider the soil to be a non-linear and isotropic medium and thus are not applicable to over-consolidated clays. This is due to the fact that the viscoplastic strain rate is always defined as a positive value, and therefore they are not capable of modelling the behaviour on the 'dry' side of the critical state line.

More recently, following the idea of the overstress theory and incorporating the ideas enclosed in the elasto-plastic S-CLAY1S model (Karstunen *et al.* 2005), the EVP-SCLAY1S model was proposed by Karstunen & Yin (2010). This model is an elasto-viscoplastic formulation, which is capable of accounting for soil anisotropy, the destructuration of interparticle bonds and viscosity. Three elliptical surfaces are incorporated within the EVP-SCLAY1S formulation: a dynamic loading surface, a

static yield surface and an intrinsic yield surface, see Figure 2.14. The elastic behaviour in the EVP-SCLAY1S model is assumed to be similar to MCC to be isotropic and the inclination of the yield surfaces and the application of the hardening law ensures that the erasure of fabric anisotropy with viscoplastic strains is accounted for. Moreover, the expansion of the intrinsic yield surface, thus the change in the current amount of bonding, is assumed to be due to inelastic volumetric strains. As EVP-SCLAY1S is a hierarchical formulation, it can be reduced to EVP-SCLAY1 (where only creep and plastic anisotropy is considered) or to EVP-MCC (where isotropic time-dependent behaviour is the subject of study) by simply setting certain input parameters to zero.

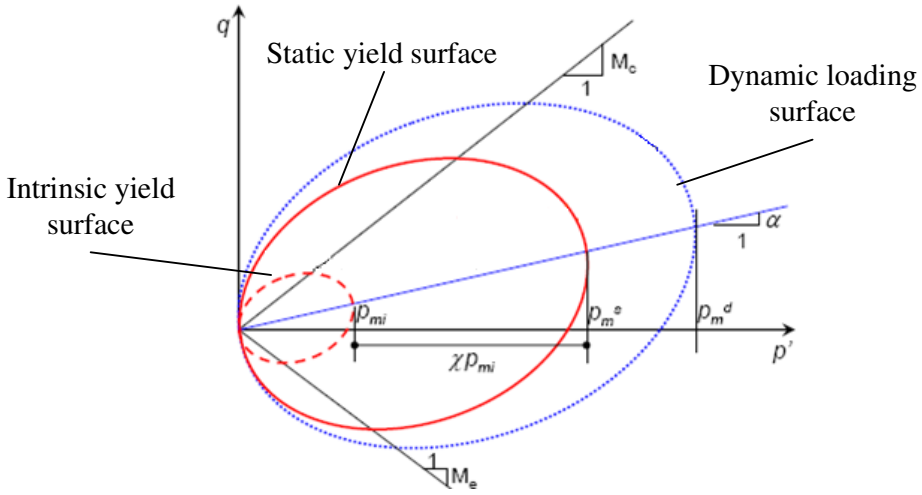

Figure 2.14: Three surfaces for EVP-SCLAY1S model in triaxial stress space.

The abilities of EVP-SCLAY1S model have been demonstrated through numerical studies of triaxial and oedometer tests on intact samples and in a simple

boundary value problem of an instrumented test embankment constructed on a Finnish soft clay. Comparison of the numerical predictions with experimental data and field measurements show that the predictions given by the EVP-SCLAY1S model are in reasonably good agreement with the measurements. However, the application of this type of model requires input values for viscous parameters, which do not have a clear physical meaning. Hence, EVP-SCLAY1S requires a calibration of the viscous input parameters by curve fitting, and as showed by Karstunen *et al.* (2010) these are not unique. This might limit the applicability of the model for use among engineering practitioners.

Another line of research used in rate-dependent modelling is the time resistance concept, initially introduced by Janbu (1969), where time resistance R is defined as the ratio of increment in time to the increment in strain. Based on evidence of fabric anisotropy and the destructuration process, Grimstad and his co-workers proposed a new constitutive model, which extends the existing S-CLAY1S model (Karstunen *et al.* 2005) using the time resistance theory, see Grimstad *et al.* (2010). The formulation enables advanced modelling of a soft soil mass by accounting for anisotropy (including cross-anisotropic elasticity), destructuration and rate effects. The volumetric strains may be positive or negative, depending on which side of the critical state line is the state of the soil. This leads to the possibility of modelling the 'dry' side of the critical state with a zero value of mean stress at non zero values of volumetric strain. The evolution of anisotropy on the reference yield surface in this model is governed by a rotational hardening rule, which is related to the viscoplastic strains, whereas the development of the viscoplastic strains is described by the time resistance concept. Moreover, the destructuration process is modelled by a

destructurational rule, similar to the idea proposed by Gens and Nova (1993). Numerical tests have also shown that this model is capable of simulating the variation of time resistance with stress level. However, at the time of writing this thesis no validation of this model against laboratory tests or boundary value problem had been performed for a natural soft clay.

2.5.2 Soft Soil Creep Model

The Soft Soil Creep model (Brinkgreve, 2002) is a formulation which is able to predict reasonably well the behaviour of an isotropic soft soil which is prone to creep at the element test level and in boundary value problems, (Vermeer *et al.*, 1998; Vermeer & Neher, 1999 and Neher *et al.,* 2001).

The Soft Soil Creep model (SSC) incorporates two yield surfaces: the current state surface (CSS) and the normal consolidation surface (NCS), presented in triaxial stress space on Figure 2.15. The yield surfaces in SSC are shifted off the apex point to the left, as shown in Figure 2.15 if the non-zero value of apparent cohesion c' is assumed.

The shape of the current state surface is defined by the parameter M^* which is similar to the Soft Soil model. Its size is determined by p'_{eq}, which represents the current stress state, as follows:

$$p'_{eq} = p' - \frac{q^2}{M^{*2}(p' - c' \cdot \cot\varphi')} \tag{2.50}$$

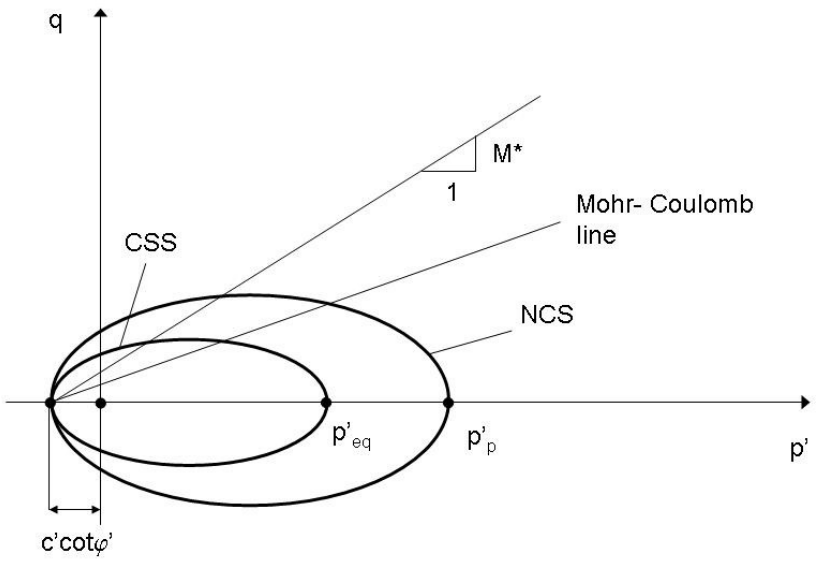

Figure 2.15: Yield surfaces of SSC model in triaxial stress space (after Brinkgreve, 2002).

The pre-consolidation pressure $p_p^{'}$ can be determined from the 24 hour compression line and it is related to the increase in the volumetric creep strain value. As a result of the hardening law, it can be expressed as below:

$$p_p^{'} = p_{p0}^{'} \exp\left(-\frac{d\varepsilon_v^c}{\lambda^* - \kappa^*} \right) \tag{2.51}$$

where: $p_{p0}^{'}$ is the initial value of the pre-consolidation pressure $p_p^{'}$.

The normal consolidation surface defines the stress state on the normal consolidation line corresponding to a given reference time. The size of the normal consolidation surface is represented by the pre-consolidation pressure $p_p^{'}$ and, unlike in the Hardening Soil and Soft Soil models, it is also a function of time. The evolution of the pre-consolidation pressure $p_p^{'}$ with time is related to the viscous

volumetric strain rate. The rate of creep is controlled via the ratio $p_{eq}^{'} / p_{p}^{'}$, which is defined as:

$$\frac{p_{eq}^{'}}{p_{p}^{'}} = \frac{1}{OCR^{*}} \tag{2.52}$$

where: OCR^{*} is the apparent over-consolidation ratio.

In the SSC model, the *NCS* expands continuously with time and with various expansion rates which are dependent on the value of OCR^{*}. In order to account for shear failure a Mohr Coulomb failure with a non associated flow rule is incorporated within the Soft Soil Creep model. Thus, similarly to SS, there is no 'dry' side in the SSC model.

The total strain increment consists of two parts: the elastic component $d\varepsilon^{e}$ and the viscous (creep) component $d\varepsilon^{c}$, which can be defined as follows:

$$d\varepsilon = d\varepsilon^{e} + d\varepsilon^{c} \tag{2.53}$$

The volumetric strain increment $d\varepsilon_{v}$ can be described in terms of stress invariants in thd p'-q plane or in triaxial stress space as below:

$$d\varepsilon_{v} = d\varepsilon_{v}^{e} + d\varepsilon_{v}^{c} \tag{2.54}$$

or

$$d\varepsilon_{v} = \frac{\kappa^{*} dp^{'}}{p^{'}} + \frac{\mu^{*}}{\tau}\left(\frac{p_{eq}^{'}}{p_{p}^{'}}\right)^{\frac{\lambda^{*}-\kappa^{*}}{\mu^{*}}} \tag{2.55}$$

where κ^{*} and λ^{*} are the modified swelling and compression indices defined from the $\varepsilon_{v} - \ln(p')$ plot (as shown in Figure 2.16), τ is the reference time, usually taken as 1 day (if the position of the normally consolidation line is defined from 24 hour oedometer tests). The first component of the volumetric strain increment describes

the elastic part of the strain increment which is directly linked to the rate of increase of the mean effective stress p', whereas the second component represents the volumetric creep strain increment.

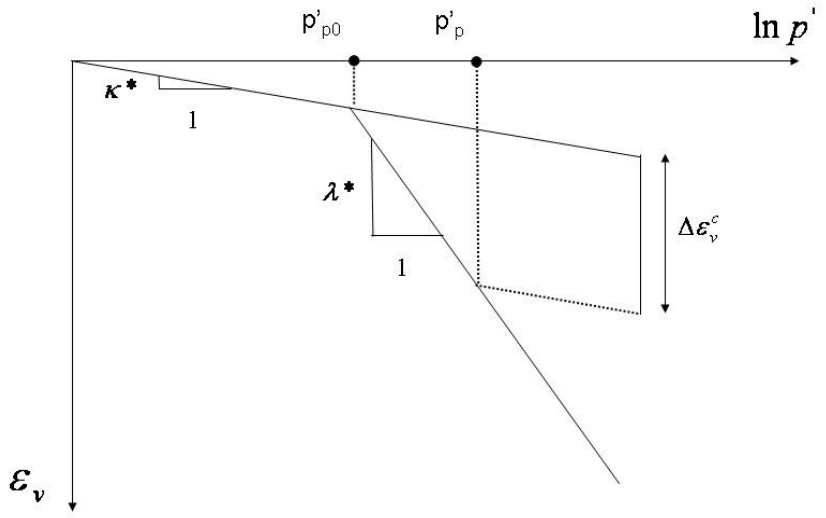

Figure 2.16: Idealised stress-strain plot: one-dimensional oedometer test.

The modified creep index μ^* can be defined from the $\varepsilon_v - \ln(t')$ plot as shown in Figure 2.17 or based on the standard creep index C_α as follows:

$$\mu^* = \frac{C_\alpha}{\ln 10(1+e)} \tag{2.56}$$

The Soft Soil Creep model requires four input parameters, λ^*, κ^*, μ^* and OCR^*, and all of these parameters can be obtained from a standard oedometer test, provided that the test has been conducted for long enough after applying each loading step. Determination of the modified compression and swelling indices, and the initial apparent over-consolidation ratio can be performed, as mentioned before,

from the $\varepsilon_v - \ln(p')$ plot and *Eq. (2.52)*. However, more emphasis should be put on the definition of the modified creep index μ^* from oedometer test results when the volumetric strain ε_v is related to the natural logarithm of time t. The modified creep index should be selected when the consolidation rate is low enough that its contribution to the settlement value is small when compared with the contribution of creep (i.e. after full consolidation).

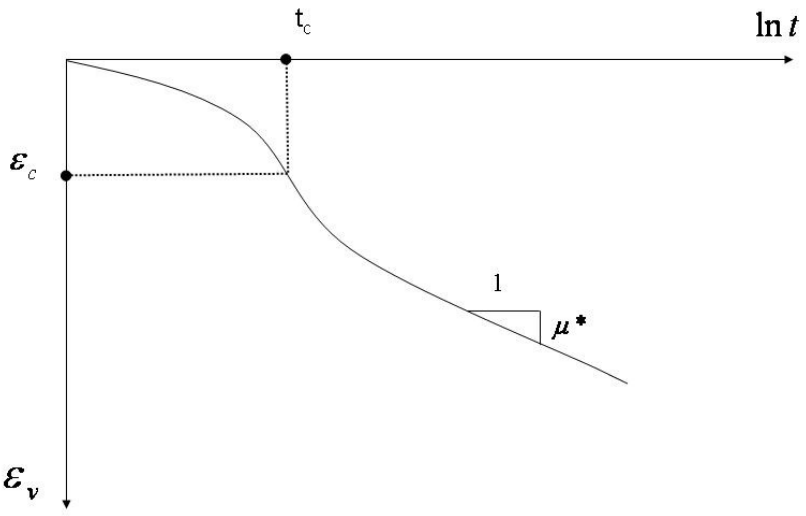

Figure 2.17: Determination of the modified compression index.

2.5.3 Anisotropic Creep Model

As most soils are anisotropic a further challenge, in addition to the viscosity of soft natural soils, is to account for initial anisotropy and the change in fabric anisotropy due to plastic straining. Leoni *et al.* (2008) incorporated these

characteristics of the stress-strain behaviour of the soft soil in one formulation called Anisotropic Creep Model (ACM).

In order to account for creep and plastic anisotropy two yield surfaces are used in this model: the normal consolidation surface (NCS) and the current stress surface (CSS), which is similar to the yield surface incorporated within the S-CLAY1 model (Wheeler *et al*., 2003). Similarly to the S-CLAY1 models, invariants can only be used when considering a cross-anisotropic sample in a triaxial stress space, with the principal axis of anisotropy coinciding with the principal stress axis. The two surfaces, presented in triaxial stress state in Figure 2.18, have the same shape and inclination α, however they are different in size.

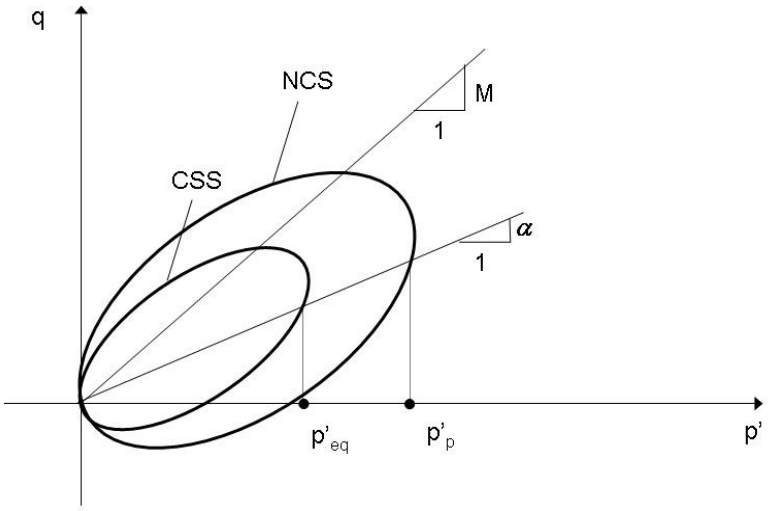

Figure 2.18: Yield surfaces of ACM in triaxial stress space (after Leoni *et al.,* 2008).

As in the SSC model, the pre-consolidation pressure $p_p^{'}$ in ACM defines the size of the normal consolidation surface and it evolves with volumetric creep strains. It can be determined as follows:

$$p_p^{'} = p_{p0}^{'} \cdot \exp\left(-\frac{\varepsilon_v^c}{\lambda^* - \kappa^*} \right) \tag{2.57}$$

where $p_{p0}^{'}$ is the initial pre-consolidation pressure, ε_v^c is the volumetric creep strains, λ^* and κ^* are the modified compression and swelling indices.

The equivalent mean stress $p_{eq}^{'}$ defines the size of the current state surface and can be determined from:

$$p_{eq}^{'} = p' + \frac{(q - \alpha p')^2}{(M^2 - \alpha^2) p'} \tag{2.58}$$

where M is the stress ratio at the critical state and q is the deviatoric stress. Within the ACM formulation an associated flow rule is assumed for the rate of the deviatoric creep strains $d\varepsilon_d^c$.

The rotational hardening law, similar to that proposed by Wheeler *et al.* (2003) for the S-CLAY1 model, controls the rotation of the NCS and CSS:

$$d\alpha = \omega \left[\left(\frac{3q}{4p^{'}} - \alpha \right) d\varepsilon_v^c + \omega_d \left(\frac{q}{3p^{'}} - \alpha \right) d\varepsilon_d^c \right] \tag{2.59}$$

where: parameters ω and ω_d are soil constants which control the rate of rotation. The parameter ω_d can be fully defined by the critical state angle of friction and therefore does not require any calibration procedure:

$$\omega_d = \frac{3\left(4M^2 - 4\eta_0^2 - 3\eta_0\right)}{8\left(\eta_0^2 - M^2 + 2\eta_0\right)} \tag{2.60}$$

where the stress ratio at critical state M, the initial stress ratio η_0 and the initial inclination α_0 are defined following the equations enclosed in the S-CLAY1 model, see *Section 2.41* and Wheeler *et al.* (2003).

Experimental data presented by Anandarajah *et al.* (1996) indicated that the initial anisotropy is erased during isotropic loading up to a pressure which is two or three times larger than the pre-consolidation pressure. Thus, the volumetric strain for erasing anisotropy can be defined as:

$$d\varepsilon_v^c = (\lambda^* - \kappa^8)\ln\frac{p_p^{'}}{p_{p0}^{'}} = (\lambda^8 - \kappa^*)\ln(2..3) \approx \lambda^* \tag{2.61}$$

Assuming a flow rule and isotropic loading with $q = 0$, the rotational hardening law can be expressed as:

$$\frac{M^2 d\alpha}{M^2\alpha - 2\alpha^2\omega_d} = -\omega d\varepsilon_v^c \tag{2.62}$$

where $d\alpha$ is the rate of inclination of the yield surface and $d\varepsilon_v^c$ is the volumetric creep strain rate. After integration of the differential equation (*Eq.(2.62)*) in the range between α_0 and $\alpha = \alpha_0 + d\alpha$ and assuming that anisotropy is practically erased when $\alpha = \alpha_0/10$, the rate of rotation of the yield surface ω can be defined as follows:

$$\omega = \frac{1}{\lambda^*}\ln\frac{10M^2 - 2\alpha_0\omega_d}{M^2 - 2\alpha_0\omega_d} \tag{2.63}$$

Hence, ω is dependent on the modified compression index λ^* and the critical state friction angle, and can also be estimated using calibration.

The volumetric creep strains are defined in the same manner as in the SSC model (*Eq. (2.55)*). The isotropic creep model can be obtained from the ACM model

by setting the inclination of the yield surfaces and the rate of the yield surface rotation to zero.

Anisotropic Creep Model has been validated in both numerical tests and boundary value problems which consider soft soil deposits. It has been shown by Leoni *et al.* (2009) that if compared with SSC the incorporation of fabric anisotropy influences significantly the predicted stress- strain behaviour. A further challenge of constitutive modelling is to incorporate creep with anisotropy and destructuration in a single model following the critical state theory. Such an attempt is presented in *Chapter 5* where the ACM model (Leoni *et al.* 2008) has been extended to take account of interparticle bonding and the destructuration process.

2.6 Comments

In this chapter a discussion on the behaviour and characteristics of soft soils has been presented, followed by a brief overview on the recent developments in constitutive modelling. Seven constitutive models, both standard and advanced, have been described; all of them are implemented into the 2D PLAXIS v. 9.02 and 3D PLAXIS Foundation finite element code as standard models (MCC, SS, HS and SSC) available or user defined models (S-CLAY1, S-CLAY1S and ACM). The formulations discussed in this chapter were divided into four groups: isotropic models (MCC, SS and HS), anisotropic models (S-CLAY1), models which account for interparticle bonding and destructuration (S-CLAY1S) and lastly, time-dependent models (SSC and ACM).

Accurate numerical modelling of real engineering problems involving natural soft clays requires adequate constitutive models that can take account of the true behaviour of a considered geo-material, such as anisotropy, destructuration and creep. If advanced constitutive models are to be widely used in engineering practice, they must be relatively simple to use and understand and the determination of input parameters should be straightforward, and preferably determined via laboratory or field testing. Very complicated formulations with parameters with no physical meaning will most probably never be widely used, and are likely to be only useful for academic research.

3

STONE COLUMNS INSTALLED IN SOFT SOIL

The installation of stone columns by applying of a heavy vibrating poker to displace the in-situ ground and to compact the imported material is widely used within most countries as a successful ground improvement technique (Watts 2000). As the amount of congested urban areas increases, so does the proportion of the structures which must be constructed on poor soft materials. Subsequently, ground improvement techniques, such as stone columns are increasingly required. For a range of different locations and ground conditions, the stone column technique has been found to be an adequate solution, varying the type of the granular material introduced into the soil in terms of the grading or the stiffness of the material.

In this chapter first an overview on the concept, applications and limitations of stone columns is briefly presented. Then, a general review of design methods is given, followed by a brief insight into the modelling of the granular columns, in particular using numerical simulations. Finally, an overall summary and some comments are given.

3.1 Overview

An acute need to develop a better understanding of the interaction between soil and ground improvement techniques, and the desire to provide satisfactory foundation performance at low costs are both major challenges for a geotechnical engineer. Aside from the economical aspect of the geotechnical design, the application of ground improvement methods should ideally in the case of soft soils, increase the shear strength and reduce the compressibility of the in-situ material. Additionally, in some cases the application of stone columns is designed to influence soil permeability and to improve homogeneity.

The stone column technique is an economical and environmentally friendly method, which treats the ground in order to withstand various loading conditions. This type of improvement method forms continuous columns from the maximum depth of penetration up to the ground surface, using a deep vibrator.

3.1.1. Concept

The concept of introducing stiff inclusions into soil has been well known for over hundreds of years. At first, wooden piles were inserted into soil to provide additional bearing capacity and to reduce the settlements. However, the application of wooden piles has been limited due to the negative effect of water on the durability of such piles and therefore with time alternative ground improvement techniques have been developed, including amongst the others the stone column concept.

The first application of limestone columns was carried out in soft estuarine deposits to support the heavy foundations of the ironworks at an artillery arsenal. The

stone columns used in that case were 0.2 m in diameter, 2 m long and they bore the load of 10 kN each. According to Moreau & Moreau. (1835) the columns improved the considered area so successfully that the expected settlements were reduced by a factor of four. After that, the use of granular material in columns was not used until the beginning of the last century.

In the 1930s stone columns (termed also as vibro stone columns) were used for the first time in a German project which involved the densification of river-borne granular soils. Afterwards the application of granular columns became a common practice in Europe. In contrast, the stone column technique arrived in the United States of America relatively late, at the beginning of the 1970s, with the first application of stone columns in 1972.

The installation of stone columns results in forming a stiff composite system consisting of the soil and a column of inserted granular material which itself is densified. The stone column installation consists of a strictly specified sequence of processes. First, the depth vibrator with a rotating eccentric mass is inserted into the soil. The nose of the vibrator is tapered to aid penetration into the ground, whilst vertical fins prevent the vibrator from rotating during the penetration (EN 14731:2005). Once the design depth is reached, the vibrator is withdrawn in lifts and the cavity is backfilled with granular material. During each lift the vibrator is then reinserted, which results in expanding the stone column diameter. This procedure is repeated until a limiting condition, measured in terms of amperage drawn by the vibrator, is achieved. The column construction is executed for additional columns at a predetermined spacing to deliver the desired treatment.

Three installation processes of stone columns may be distinguished as follows:

- dry top-feed process (termed as vibro-displacement),
- dry bottom-feed process (termed as vibro-displacement).

- wet process (termed as vibro-replacement),

All three processes use a similar type of depth vibrator, but differ from each other by the grading of the granular material and the method of introducing the material into the soil. The grading of the granular material varies from 8..50 mm for dry bottom-feed method to 25..75 mm and 40..74 mm for dry top-feed and wet method, respectively, see EN 14731:2005.

In the dry bottom-feed installation the granular medium is delivered directly to the tip of the vibrator through a permanent feed tube along its side and the vibrator remains in the ground during the column construction to maintain the stability of the cavity. In contrast, during the dry top-feed installation process the cavity formed by the vibrator remains open and the granular material is fed directly into the top of the created hole. Additionally, compressed air is used as the jetting medium to assist the vibrator during penetration to the desired depth. A very similar construction of the vibrator is used in the wet method, where the flushing water (as the jetting medium) removes soft material, stabilises the cavity and allows the specified granular material to reach the tip of the tool. Figure 3.1 shows an example of the vibrator with two tubes; one of the tubes delivers the granular material to the tip of the vibrator and the second assists in penetration into the soil and flushes the hole as necessary.

3.1.2. Applications

Stone columns are usually installed from a working platform in single or multiple rows beneath a strip footing and in groups beneath pad foundations. The treatment is performed using a grid, the arrangement of which depends on the soil conditions and the loads to be carried by the structures.

Figure 3.1: End of vibrator with two tubes (Boulanger & Duncan, n.d.).

Stone columns have been used in nearly every type of civil construction, such as residential, commercial and industrial buildings, dams, storage tanks and silos, power stations, highways, airport taxiways and runways, road and railway embankments, pipelines, bridge abutments, landslide corrections and stabilisation of cofferdams. Granular columns have also been successfully utilised in offshore engineering, as breakwater and quay walls, offshore bridge abutments, and in land reclamation projects, reaching typically up to 35 m in depth. The wide number of applications for this technique is intensified by the fact that stone columns can be used adjacent to existing buildings without causing damage from vibrations. Nevertheless, for every geotechnical application stone columns should be carefully compared with other alternative methods to consider the advantages and limitations of each treatment.

With the stone columns technique, columns of dense crushed stone are introduced into the soil in order to reduce settlement and to increase bearing capacity, allowing a reduction in the foundation size. The stone columns may also provide slope stabilisation and enable the construction of fills and shallow footings.

This type of ground improvement has proven to be successful in reducing total and differential settlements, as well as in increasing the rate of settlements. Installation of stone columns in loose sandy soils below the water table reduces the liquefaction potential and has an additional effect of draining the deposit. The installation of granular columns helps to compact loose sand and gravel layers, reinforces soils that cannot be compacted and generally facilitates drainage (particularly in very silty sands to sandy silts).

In granular soils, the effect of the vibrations is to produce a marked improvement in the relative density of the surrounding material, thus significantly improving the allowable bearing capacity and settlement characteristics. In cohesive soils, although some improvement occurs in the geotechnical properties of the clays between stone columns, most of the improvement of the formation is achieved by the combined effect of the weak soils and the stiffer columns. Indeed, in sensitive clays the installation may have a negative effect on the surrounding soil.

Ground improved by vibrations alone (vibro compaction) can be executed in soils which have a granular content greater than ≈ 90%, see Figure 3.2. In cohesive and layered soils vibrations have a minimal effect, so the penetration of the vibrator is followed by construction of the stone column. The range of soils that might be improved by vibratory techniques (including cohesive soils) has been extended to silty deposits by the installation of stone columns, see Figure 3.2.

The expected results of the application of stone columns in different types of soil are presented below in Table 3.1 (Hayward Baker, 2004). Excellent and very good results, regarding densification, can be expected in sands and silty sands, where the diversification of the size of soil particles and high friction angle result in easier densification. Considering the reinforcement effect, excellent and very good results should be expected in clays, sands, silts and mixtures of the latter two.

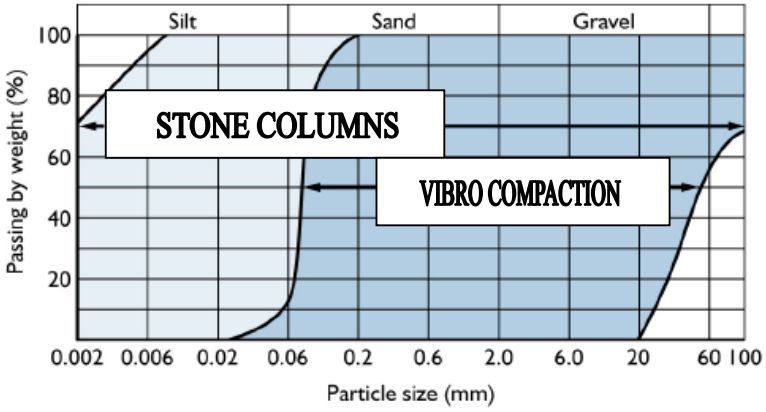

Figure 3.2: Particle size distribution illustrating the applicability of vibro compaction and stone columns (after: Hayward Baker, 2004).

Table 3.1: Stone columns- expected results of application (Hayward Baker, 2004).

Type of soil	Relative effectiveness	
	Densification	Reinforcement
Sand	Excellent	Very good
Silty sand	Very good	Very good
Non plastic silt	Good	Excellent
Clay	Marginal	Excellent
Mine spoil	Excellent, depending on gradiation	Good
Dumped fill	Good	Good
Garbage	Not applicable	Not applicable

3.1.3. Limitations

The selection of the treatment technique, as well as the method of execution, is usually based on the local ground conditions, type of loading, purpose of construction and preferences/skills of the contractor.

The wet process can be used when the soil is not contaminated and when the soil does not consist of a highly plastic clay, which could lead to a problem when handling the slurry in the process water. This method is usually chosen when the compaction of sandy and gravelly layers is required and these layers are located below the water table. Compaction is generally better accomplished with the wet rather than the dry process, as the flushing water assists in compacting the sandy soil around the column. Finally, the wet technique is used where the dry top-feed process cannot be performed because of unstable ground, such as in running sand conditions. The predominant disadvantage of the wet method is the requirement of a water supply and the final disposal of the effluent without causing pollution (EN 14731:2005). A large quantity of water is required to prevent collapse of the created cavity or contamination of the column, therefore environmental regulations may restrict drainage and the deposition of the slurry in lagoons.

The dry top feed method of installing the stone columns is suitable only where the cavity formed by the vibrator remains open during construction of the column. This technique is used in soil with a high water table and in granular soils it is only possible above the water table.

Organic soils tend to have a high moisture content, plasticity index and compressibility, hence it is difficult to reduce the settlement in these soils. Nevertheless, most organic silts and clays may be improved by introducing stone columns. If stone columns are chosen as the ground improvement method, some additional considerations should be taken into account while planning the ground investigation in order to estimate the future difficulties with construction and serviceability of the structure. Many situations can cause difficulties on site during

the installation of stone columns or after construction has been completed. Some of these issues are discussed below in separate sections.

Peat

The planned ground investigation should locate and fully evaluate extensive deposits of peat or other organic soils. The structure of peat is also an important consideration during the design of stone columns as there could be a lack of sufficient lateral support. If the discrete layer of peat is thin (less than 0.6 m) granular columns may be installed. However, for deposits with larger thicknesses or multiple thin bands of organic soil it is unlikely that peat will provide an adequate passive resistance to confine the column, see Mitchell & Jardine (2002).

To confine the stone columns in a peat layer with thickness larger than 0.6 m, a dry plug of lean-mix concrete may be constructed during the formation of the column. Another solution may be to use geogrids or geotextiles, which, if installed around the perimeter of the column, may help to encase the granular column in the peat layer.

Clay fill

It is difficult to predict the self-weight settlement of clay layers, especially if there has been little control during placement. Therefore, it is common practice that stone columns should not be used in clay fill which has been placed less than 10 years ago. In loose fills which are susceptible to collapse settlement (such as back-filled quarry pits) the installation of stone columns will be of little benefit. Collapse settlement might be caused by first-time inundation of water directly through the ground surface, underneath the ground surface or a rising groundwater table. Constructing the granular columns may facilitate the passage of water unless suitable precautious

are taken. An instant loss of lateral support at the top of the column would take place due to sudden settlement of the fill, see Mitchell & Jardine (2002).

Permeable strata

Stone columns act like vertical drains, thus for sites with relatively low natural horizontal permeability they can greatly accelerate consolidation. To make the most of this advantage with respect to the rate of primary consolidation settlement, the vertical and horizontal consolidation characteristics of the soil should be evaluated. This means that the presence and extent of thin deposits or lenses of permeable soils (such as sand, gravel or shells) should be very carefully determined. If the natural horizontal permeability is sufficiently high, the use of columns may not significantly accelerate primary consolidation.

Stability

Granular columns beneath an embankment are generally used to provide an adequate margin of safety against failure, therefore evaluation of the representative shear strength of the soil and that of the improved ground is very important. Thin soft layers of cohesive soils, in which pore water pressures may build up, can have a dominant effect on the overall stability of an embankment. For an embankment, the control of the design is generally taken to be the short-term (undrained) shear strength. For landslide problems, the occurrence and movement of water is very significant and the long-term (drained) shear strength is usually critical.

Settlement

The immediate settlement is usually complete by the end of application of load, hence generally it is of little practical significance. Primary consolidation and

secondary compression are often very important when the stone columns technique is used for embankments and abutment supports on soft soils. For organic and soft clays deposits, the secondary compression settlement can be as important as the primary consolidation. Therefore, the secondary compression requires special consideration when determining geotechnical properties. Differential settlement which may occur between approach embankments and bridges is always of important concern.

Limit of undrained strength

According to guidelines for ground improvement using stone columns, the method should be restricted to soils with a minimum undrained shear strength c_u of 15 kPa, see Forschungsgesellschaft für das Straβenwesen (1976) and NHBC (1988). However, since the guidelines for this method were developed, the use of the technique has already expanded and the equipment has improved in order to enable safe installation of columns in very soft soils. In such cases, soil improvement is often achieved by drainage rather than by reinforcement (Priebe, 2005). There are reported cases where stone columns were successfully installed in soils with an undrained shear strength as low as 5 kPa, see Raju (1997) and Raju *et al*. (2004). It should be noted that the treatment of extremely soft soils requires the utmost care and it is not sufficient to consider the undisturbed strength of cohesive soil alone.

Sensitivity

The sensitivity of the soil to disturbance, S_t, is an important design consideration and is defined as follows:

$$S_t = \frac{c_{u\ \ undisturbed}}{c_{u\ \ remoulded}} \tag{3.1}$$

where $c_{u\ \ undisturbed}$ and $c_{u\ \ remoulded}$ are the undrained cohesion of the undisturbed soil with its natural structure (bonding) intact and of the remoulded soil, e.g. soil where the natural structure has been destroyed, respectively.

Lightly over-consolidated clays are likely to be sensitive; for example widely investigated Scandinavian and Canadian quick clays have sensitivity values around 150, see Rankka *et al.* (2004). Vibrations during column installation can cause significant loss of strength in very soft soils and impact the trafficability of sites, adjacent structures and slope stability, McCabe *et al.* (2007).

Plasticity index

The installation of stone columns in soils with a high plasticity index I_p might improve such soils but it will not control swelling and shrinkage behaviour. As the volume change of the soil in terms of swelling potential is described by the plasticity index, I_p, the UK National House Building Council suggests that stone columns should not be used when $I_p > 40\%$ see NHBC (1988).

3.2. Design considerations

While considering the design and execution of stone columns, every engineer should remember that some design steps should be distinguished:

1. *Site investigation;* information regarding the type of soil, physical and geotechnical properties (such as compressibility, consistency limits, undrained shear strength, sensitivity, relative density, degree of saturation or

permeation), location/extent of peat, organic soils or biodegradable fill, comprise the basic data which are very important for design purposes.

2. *Requirements of ground improvement;* it should be established what settlement, level of safety, etc. are allowable in the project. Information on the type of foundation and the total loads are necessary to enable correct design of the stone column treatment.
3. *Predicted improvement;* calculations of the predicted improvement factor, settlement improvement factor or compressibility of the column should be performed at this stage.
4. *Stone columns scheme;* effective design requires the selection of the proper grid spacing, column diameter and type of backfill. Along with and strict consistency in the installation method, these are the elements which have a significant influence on the degree of improvement which may be achieved.
5. *Testing criteria;* As part of the design of stone columns a Production Monitoring and Quality Control procedure should be established, see Priebe (1995).

Stone columns transfer some load to the soil by shear stress along the column-soil interface and some by end bearing at the column base. One of the load transfer mechanisms (unless the granular columns are very short) is lateral bulging of the column towards the surrounding soil. At a depth more than two to three times the diameter of the stone column, the bulging of the column no longer occurs, according to Murugesan & Rajagopal (2006). The behaviour of the column under load is dictated by the passive resistance of the soil. Different trends of the bulging mechanism can be found when the stone columns are constructed beneath wide and small foundations according to Kirsch (2004). In Figure 3.3 the expected extent of the surface settlement and bulging for footings and embankments is presented. One

can see that stone columns close to the centreline (either of the footing, or of the embankment) experience lateral bulging in the lower part of the column, whereas columns near to the edge (of the footing or next to the toe of embankment) bulge closer to the top of the column.

This thesis aims to investigate the deformation patterns of floating stone columns underneath an embankment using the three-dimensional finite element method and results of the analyses are presented in *Chapter 4.*

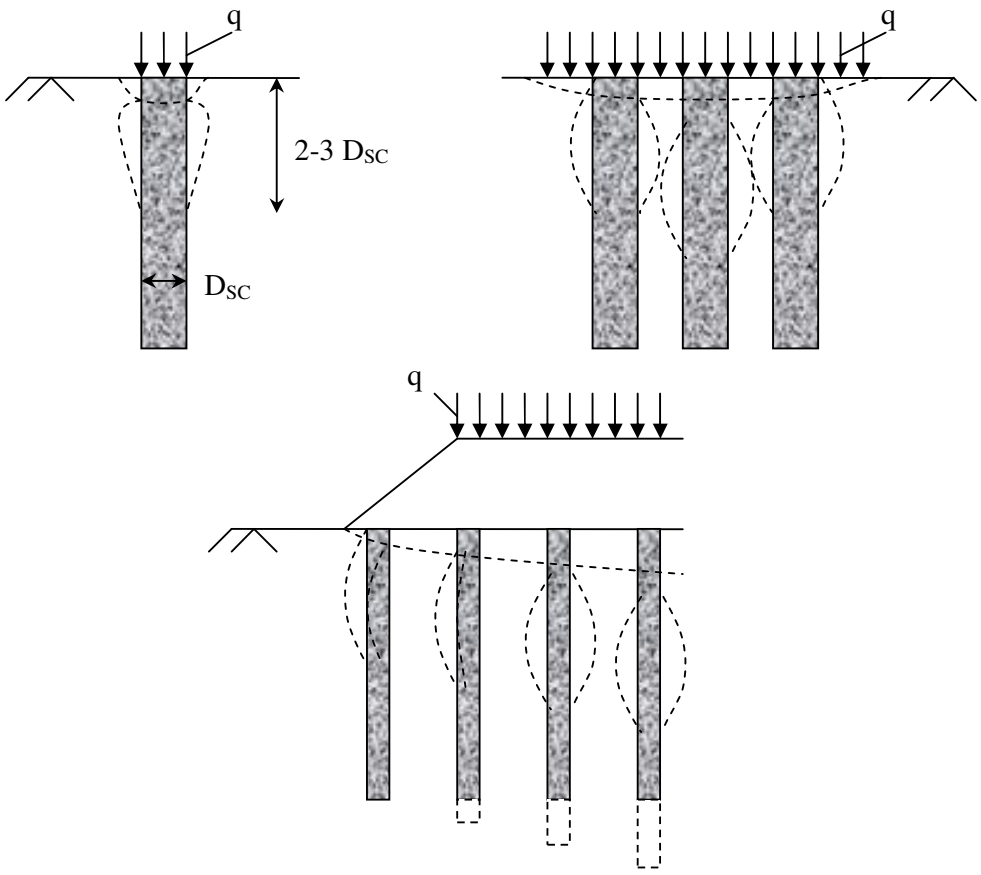

Figure 3.3: The bulging failure mechanism for stone columns under different foundation types (after: Kirsch, 2004).

3.2.1. Review of selected design approaches

The design of stone columns can be separated into bearing capacity and settlement calculations. There are several ways of designing stone columns. The most common method of design of the column for bearing capacity follows the ideas proposed by Baumann & Bauer (1974) and Hughes & Withers (1974). For settlement calculations, Priebe's approach (1995) is extensively used in Europe, with Baumann & Bauer (1974) as an alternative. However, the latter is believed to give predictions which are not as good as Priebe's method (Priebe, 1995) and has a weaker theoretical basis for clays, according to McCabe *et al.* (2007).

In the US the design method of Goughnour & Bayuk (1979) is usually used, which is an extension of the work presented by Hughes & Withers (1974) and Baumann & Bauer (1974). The incremental method (as it is sometimes called) requires consideration of the unit cell along with an incremental, iterative, elasto-plastic solution. This method is common practice in the US despite the fact that it is a much more complex approach than the Priebe method and the necessary parameters are not easy to obtain from routine site investigations.

The continuous development of constitutive modelling, in conjunction with the Finite Element (FE) method, offers new opportunities to simulate stone column foundations. The ground improvement scheme may be modelled in unison with the slab or foundation, which is one of the most important advantages of using FE methods, thus it is very useful in parametric studies and in design optimization.

Method based on Cylindrical Cavity Expansion Theory

Cylindrical Cavity Expansion Theory (CCET) is an approach which is applied in many geotechnical problems, such as interpretation of the pressuremeter test or

modelling the bulging effect, see Wroth (1984). It is based on the assumptions of a unit cell approach where the complex soil-columns systems is reproduced by an axisymmetric model with one column and the surrounding soil.

Pioneering laboratory studies on sand columns constructed in clay were presented by Hughes & Withers (1974). Their work was based on CCET and considered a cylindrical chamber in which deformations within and outside the columns were observed. By tracing the superposition of the radiographs of lead shot markers, the displacements in the column and in the surrounding soil mass were measured. One should note that Hughes & Withers (1974) considered the loading on a single column, without the loading of the surrounding soil. The load-displacement relations were determined separately for both the column and the surrounding unimproved soil to allow for superposition in order to calculate the total load-displacement behaviour of the improved soil. However, Hughes & Withers (1974) assumed equal displacement for both the column and the soil. Moreover, the principle of superposition is only valid if considered materials are assumed to be elastic.

The predicted ultimate vertical stress in the stone column can be described as follows:

$$q = \frac{1+\sin\varphi'}{1-\sin\varphi'} \quad (\sigma_{ro}^{'} + 4c_u) \tag{3.2}$$

where φ' is the friction angle of the column, $\sigma_{ro}^{'}$ is the free-field lateral effective stress and c_u is the undrained cohesion. This equation steams from studies on the field records of quick expansion pressumeter tests and it is widely used in practice to this day.

An analytical and relatively simple approach for granular columns has been proposed by Balaam & Booker (1981). The equivalent cylindrical unit (following the

Cylindrical Cavity Expansion Theory) with the stone column and the surrounding soil is approximated by assigning to them the corresponding Poisson's ratios and elastic moduli. It is assumed that the stone column and the surrounding soil will respond to the same vertical strain and that the horizontal stresses in the soil are equal to the horizontal stresses in the column. Balaam & Booker (1981) concluded that the errors arising from the assumption of the equivalent circular area for calculations are negligible.

The approach has been extended to take account of confined yielding of the frictional material of the column by Balaam & Booker (1985). The analytical solution is created separately for the clay and the stone column by developing a set of equations concerning both materials. The clay and granular material are assumed to be perfectly elasto-plastic dilatant solid satisfying the Mohr-Coulomb yield criterion with non-associated flow rule. Then, the complete solution may be found using the continuity of the lateral normal stresses and displacements at the soil-column interface. Additionally, the shear stresses at the bottom of the soil-column interface are neglected. This enables time-dependency in the settlement calculations to be taken into account and, in addition, is validated against the FE results with very good agreement according to Balaam & Booker (1985). A major drawback of the method is that it can be applied for only one soil layer improved by an end-bearing stone column. Moreover, due to assumption about rigid boundary, this solution provides additional lateral confinement, which may result in under-predictions of the anticipated settlement and bearing capacity values.

Baumann & Bauer's approach

The mathematical solution for the immediate, consolidation and total settlement estimation has been proposed by Baumann & Bauer (1974) for soils improved with

stone columns soil under the certain load conditions. The method relates the shear strength of the untreated ground to the bearing capacity of the improved soil. The estimation of both the immediate settlement and the consolidation settlement is achieved. The settlement of the column and the immediate settlement of the untreated soil are calculated based on the lateral deformation (bulging) of the stone column due to the pressure difference between the soil and the column. Following that, an assumption of the constant modulus of deformation of the stone column with regard to the depth and horizontal extent is made. Then, the ratio between the bearing stress on the column and on the untreated soil is used to obtain the immediate settlement as a function of the modulus of deformation of the untreated soil and column, and the ratio between the foundation area and the column diameter. The approach of Baumann & Bauer (1974) is still sometimes used by European engineers, but the method seems to give worse results in comparison with the real case data than the idea proposed by Priebe (1995), according to Slocombe (2001).

Priebe's method

The most common method of estimating post-treatment settlement of stone columns in Europe is the approach proposed by Priebe (1995). This method is based upon Cylindrical Cavity Expansion Theory and although it is applicable to an infinite array of columns and has some empiricism in its development, it is found to work reasonably well for most applications.

Priebe (1995 & 2005) considers a unit cell with area A with a single column and surrounding soil with cross sections A_{SC} and A_S, respectively (see Figure 3.4). Some idealisation of the column conditions is assumed. Therefore, the bulk density of the column is ignored and the granular material of the column itself is considered as

incompressible. Moreover, this method does not include the dilatancy of the granular material into consideration.

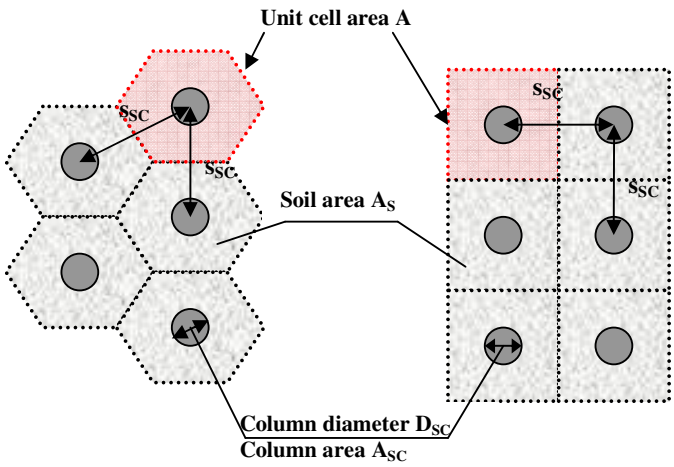

Figure 3.4: The definition of the unit cell and column area in triangular and square grid.

In the case of end-bearing stone columns, it is assumed that the column is founded on a rigid layer and that a failure in the end-bearing cannot take place. Any settlement of the load results in the bulging of the column, which remains constant over its entire length. Additionally, an assumption that the column material shears from the beginning and that the surrounding soil reacts elastically is needed. Furthermore, the soil is assumed to be displaced during installation of granular column to such an extent that the hydrostatic stresses develop and the initial resistance of soil corresponds to the liquid state. This idea has been replicated in many numerical simulations (e.g. Gäb *et al.* 2008 or Castro & Karstunen 2010) and the coefficient of earth pressure of the surrounding soil is assumed as $K_0 = 1$. This value is within the range proposed by other researches, see Elkasabgy (2005) and Elshazly *et al.* (2006), who back-calculated the coefficient of earth pressure of the

surrounding soil from several full scale load tests performed on stone columns within a few extended arrays of columns.

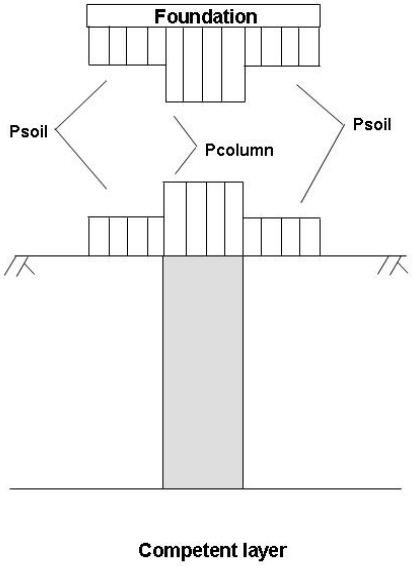

Figure 3.5: Load distribution for an end-bearing stone column.

By incorporating all of the assumptions above, Priebe (1995) derived a final improvement factor, which is assumed for settlement calculations. For estimation of the bearing capacity of the footing, a fictitious width is calculated using the actual footing width, and the angles of friction of the improved soil below the footing and of the surrounding untreated soil. In the case of ground failure, a fictitious footing will develop the same line of sliding outside of the improved area as the actual footing under actual conditions. The bearing capacity for a fictitious width of footing can be determined by the proportion of the fictitious footing width and failure width outside the footing by using the angle of friction of the untreated soil and an averaged cohesion. For more complicated soil profiles (with several soil layers) the shear values change with depth. Thus, the determination of bearing capacity is more complicated as the fictitious footing width used for calculations should be changed at

each layer. For a practical solution, the safety against ground failure and the maximum depths of the ground failure lines are proposed, see Priebe (1995).

For the case when floating stone columns are considered, the columns are not suitable to bear concentrated loads and at the boundary between the column and underlying soil balancing of stress and strain occurs. Balancing of stress and strain takes place in the upper improved layer and in the soil below the treatment, respectively. To design a floating column in soft soil, an assumption that the stress balancing takes place solely either in the upper treated zone or in the underlying zone below should be made by Priebe (2005). The treated zone can be divided into a zone with full effectiveness of the stone column and a transitional zone, as shown in Figure 3.6.a.

In the zone of full effectiveness of the column the stress distribution between the soil and column is derived from conventional calculations similar to the case of end-bearing columns, such as with proportional load on the column. At the bottom of the transitional zone, using the assumption based on dismissing the unit weight of column and soil, a certain uniform stress p exists, see Figure 3.6a. The differential load, defined for the top and bottom of the transitional zone, is transferred from the column to the soil by shear resistance. The height of the transitional zone is defined as a ratio between the differential load and the shear resistance. As it is assumed that the improvement decreases in a linear manner with depth, the settlement of the transitional zone should be calculated using a reduced average improvement factor.

In the untreated underlying zone, the load acting on the stone column is assumed to be transferred down the full thickness of the treated layer, as shown in Figure 3.6b. Therefore, the column is compressing the underlying soil with an increased load which results in a depression. The depression caused by a single

column in the underlying soil might be compared with the settlement of a circular footing and thus calculated accordingly.

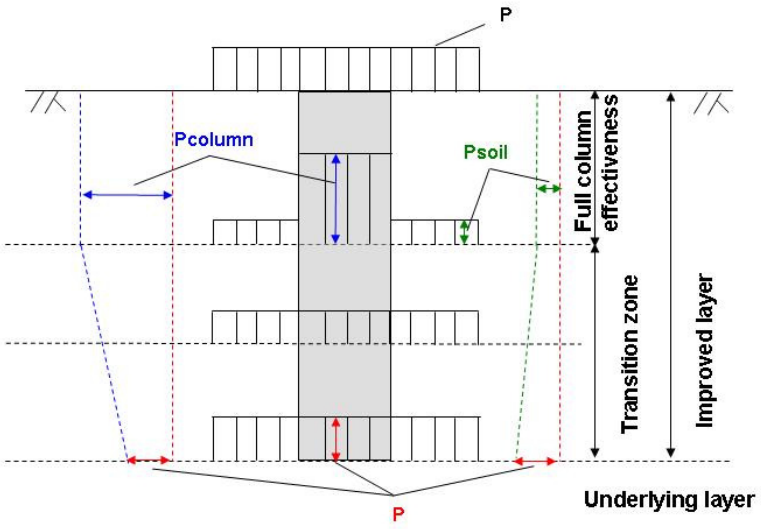

a)

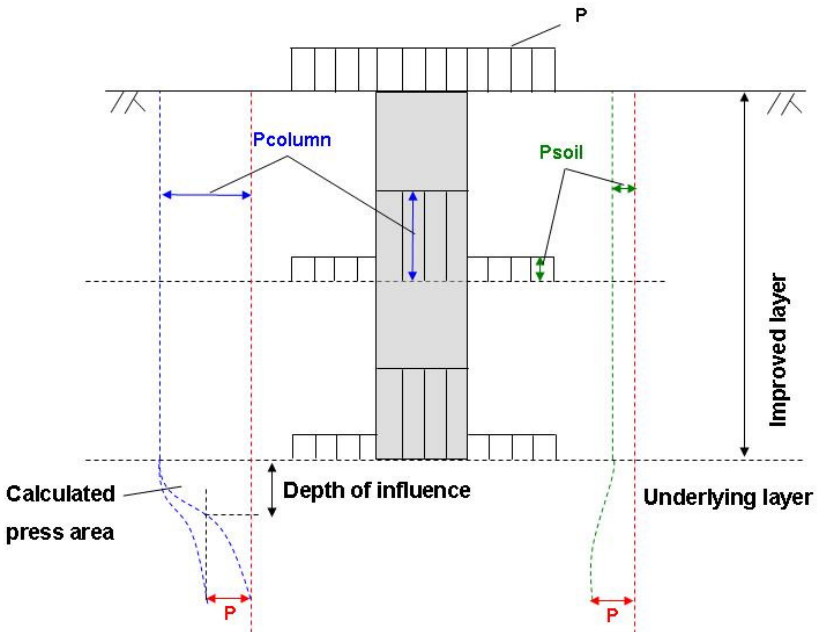

b)

Figure 3.6: Vertical stress distribution with stress equalisation for floating stone column in: a) upper treated layer and b) substratum (after: Priebe, 2005).

It is not a necessity to calculate the settlement using the difference between the column and the soil pressures, as the settlement can be determined using the total proportional load of the column and the depth of influence. The first, depends on the area ratio and the improvement factor, and the latter is defined as the depth where the pressure decreases by load distribution to the value p, see Figure 3.6b.

Approach by Etezad *et al.*

To estimate the bearing capacity of a single column and a group of columns, the method presented by Etezad *et al.* (2006) can be used. The theoretical model is based on failure mechanisms, which have been determined from a combination of Finite Element analyses and experimental data. The ultimate bearing capacity of the soil improved with stone columns consists of three components: the bearing capacity related to the unit weight of the soil, to the stone column material and to the loading applied. For each element of the ultimate bearing capacity, the chart for an equivalent angle of friction is prepared. The results presented by Etezad *et al*. (2006) for the Mohr-Coulomb constitutive model are in good agreement with the theoretical method proposed by Etezad *et al.* (2006) and give a good approximation of the expected ultimate bearing capacity range.

Method by Castro & Sagaseta

Castro & Sagaseta (2009) proposed recently an analytical solution in order to calculate the settlements after undrained loading and consolidation process, and at the final stages. This method is an extension of previous approaches and considers the radial consolidation around end-bearing stone columns under constant loading. The column is assumed to behave in an elastic-perfectly plastic manner and was described by the Mohr-Coulomb yield criterion combined with a non-associated

plastic flow with a constant dilatancy. The soil material, however, is considered as an elastic material. To account for the deformation of the column the equivalent coefficients of consolidation are used, and a few calculation steps have to be considered. First, it should be considered that the soil mass and the column behave in an elastic manner and that the consolidation process starts from the elastic solution proposed by Balaam & Booker (1981) for undrained loading. Next, it is assumed that the column deforms in a plastic manner during both undrained loading and consolidation, until the final stage is reached. It has been demonstrated by Castro & Sagaseta (2009) that this solution is in good agreement with some existing semi-empirical methods, such as Priebe (1995), and can be relatively easily utilised for the calculations of a grid of end-bearing stone columns constructed underneath an embankment. However, this solution does not account for non-linearity of constituents. Moreover, this solution does not consider any smear zones around stone columns as a result of column installation.

3.3. Previous studies on stone columns

Research on stone columns started with the granular columns themselves, first as experimental tests and nowadays increasingly with computer simulation. The numerical modelling will be discussed later in this chapter, but first a brief summary of the experimental research which has been carried out in recent years is given.

Single or singular gravity (1g) model tests are very popular amongst geotechnical engineers, however, one should not forget about some shortcomings associated with this type of test. One of the greatest drawbacks of 1g model tests is the fact that the soil mass used for such studies is always a reconstituted material, which is in contrast to the real in-situ situation. Also, as tests are performed under 1g

conditions, the stress level achieved during studies does not represent the stress level of the soil material found in-situ, where behaviour is highly non-linear and stress dependent. Hence, the frictional nature of the column and the soil is largely ignored. If used for the investigation of stone column foundations, there are also some concerns about the column installation methods when conducting singular gravity model tests. In most cases the stone columns are constructed by filling pre-bored holes with granular material which is compacted in layers. Hence, no densification of the surrounding soil mass as a result of vibrations during insertion of the poker into the ground, is considered, see e.g. Sivakumar *et al.* (2010).

Comprehensive 1g laboratory model tests on large groups of stone columns installed in kaolin were carried out at the University of Glasgow by Muir Wood *et al.* (2000). Model stone columns have been created using a replacement technique by inserting an auger into the clay (in order to form a cavity), followed by pouring sand material into the hole during removal of the lining. Muir Wood *et al.* (2000) reported that the pre-failure mechanisms and failure modes of a group consisting of a few columns is different from those of a single stone column. Muir Wood and his co-workers proved that the bearing capacity significantly increases in cases where the area replacement ratio (defined as A_{SC} / A) is greater than or equal to 25 %. Furthermore, they concluded that the area replacement ratio influences the extent of column interaction, the load sharing between the columns and the surrounding soil and the depth of the failure wedge. The majority of the failure mechanisms occurred within the region directly beneath the foundation. Figure 3.7 shows photographs of the cavities left by the sand columns, which were subsequently filled with gypsum (for imaging purposes) at the end of a footing penetration test and for the cases where L_{SC}/D_{SC} is equal to 9 and 14.5, respectively (where L_{SC} is the column length and D_{SC} is the column diameter). The red dotted line indicates the original level of the

columns base. A four-part failure mechanism scheme was proposed by Muir Wood *et al.* (2000), including the areas with no deformation, with plastic deformation and failure modes, and the region where the soil provides the lateral support to the failure wedge underneath the footing, see Figure 3.8. As a final part, the 'extension' zone mechanism is distinguished.

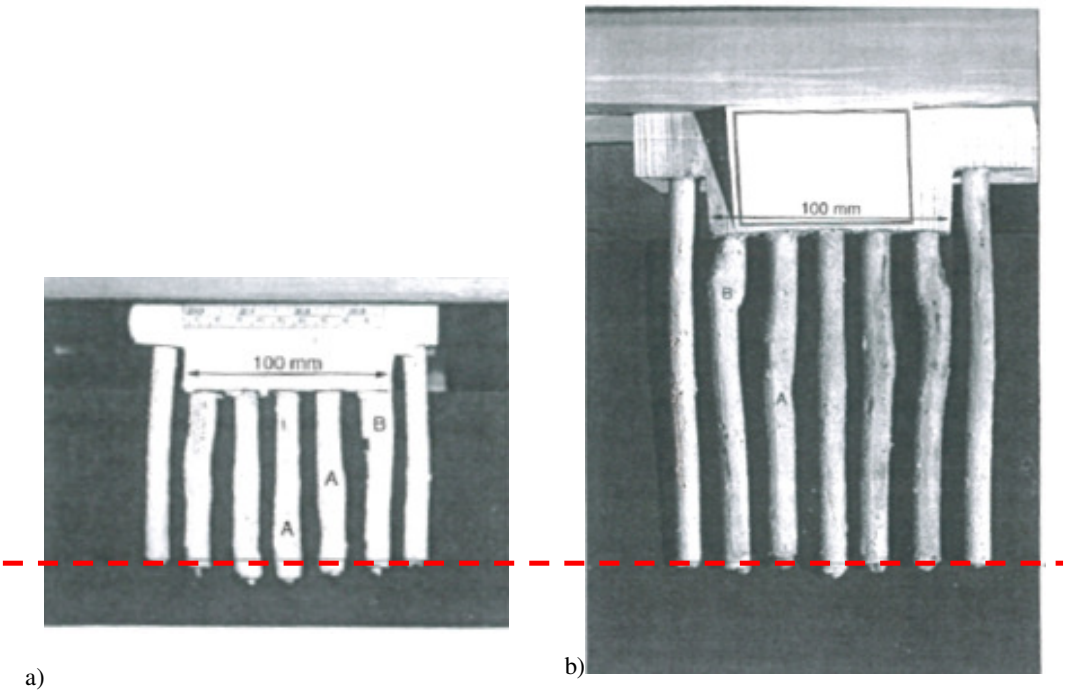

Figure 3.7: Deformed sand columns exhumed at the end of footing penetration with L_{SC}/D_{SC} equal to: a) 9 b) 14.5 (Muir Wood *et al.,* 2000).

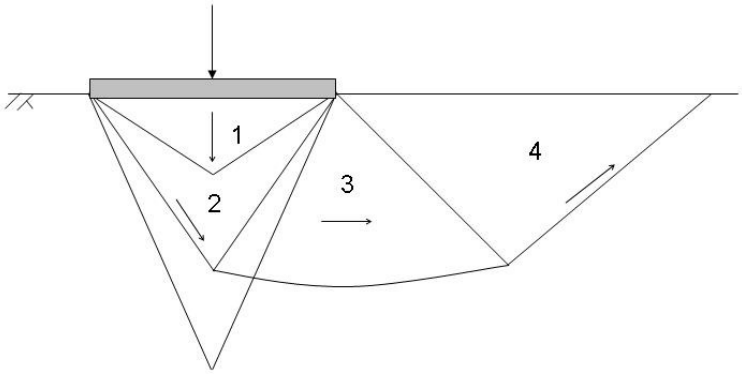

Figure 3.8: Four-zone failure mechanism for a group of stone columns (Muir Wood *et al.,* 2000).

A transparent medium with 'clay-like' properties was used in the research conducted under 1g by McKelvey *et al.* (2004). The digital photographs taken during the loading of floating columns underneath the foundation were analysed. The optimum column aspect ratio, defined as L_{SC} / D_{SC}, was found to be six times the diameter of the stone column D_{SC}. Columns longer than this value appeared not to increase the load-carrying capacity, which might suggest that the length beyond this value may be more significant in terms of reducing of settlements. Moreover, it was proven by McKelvey *et al.* (2004) that in 'short' columns (where $L_{SC} / D_{SC} = 6$) punching took place at the bottom and bulging occurs over the entire length of the columns. In the case of 'long' columns (where $L_{SC} / D_{SC} = 10$), bulging was found in the upper area only whereas the base of the stone columns remained undeformed.

During centrifuge modelling a 1/N scale model is subject to gravitational acceleration of Ng. If, during a test, the same soil material as found on site is used and the self-weight stress distribution is the same as in-situ, the experimental model experiences the same stress-strain behaviour as the in-situ model. However, a major drawback of centrifuge modelling, as in the case of 1g tests, is the fact that the soil used for modelling is reconstituted. There are also major concerns regarding scaling effects, which in most cases are unavoidable, given the model size limitations and the restrictions in tool design and manufacturing.

In the past extensive centrifuge modelling has been carried out for studies of behaviour of the soft soil deposits, the stability of embankments and consolidation process, see amongst others e.g. Davies (1981), Springman (1984) or Bolton & Sharma (1994). Many research projects have also been carried out on stone column foundations, however the column installation techniques in centrifuge modelling remain problematic as most of them do not simulate the disturbance of the

surrounding soil due to installation of the stone column. Shinsha *et al.* (1991) conducted an investigation into the influence of the stone columns on the embankment performance, filling pre-bored holes with column material. Huat & Craig (1994) and Lee *et al.* (2001) used a frozen column method in order to install in-flight columns in their studies, and Pooley *et al.* (2009) used a metal tube which was driven radially outwards, withdrawn and re-inserted incrementally to allow for column compaction. As mentioned by Pooley *et al.* (2009), the scaling effect may be significant during both column installation and the test, especially if the ratio between the material particle size and the column installation tool size is low.

The study conducted by Weber (2007) and Weber *et al.* (2010) considered physical modelling including a post-test experiment and image processing of the in-flight installation of the stone columns constructed in soft soils. Installation of the columns considered insertion, withdrawn and re-insertion of the metal tube and studies of the radial compression during column installation by the compaction of the granular material in excavated cavity were performed. Moreover, the parametric study by Weber (2007) and Weber *et al.* (2010) resulted in the identification of various zones around the installed stone column, as the smear zone analysis was conducted at a particle scale. The change in the porosity and density of the surrounding soil is determined. An influence zone with higher density and lower porosity than greenfield soil was measured up to 2..2.5 times the diameter of the column.

Over the past decades field studies have been utilised for various analyses of foundation behaviour, such as settlement performance or the bearing capacity of stone columns, see amongst others Barskldale & Bachus (1983), Greenwood (1990), Raju (1997), Van Impe (2001) or Kirsch (2004). Field trials have also been used for studies of new applications of stone columns in order to achieve sustainable

engineering solutions, such as the use of recycled railway ballast or recycled crushed concrete for column material as described by Serridge (2005). However, there are some drawbacks associated with field studies. First and foremost, field studies consider only specific configurations of stone columns. Therefore, the results are limited to only a specific type/configuration of stone columns application. Secondly, in many cases there is a lack of site investigation data available and a reliable interpretation of the field trial results is impossible. Moreover, the repetitiveness of field studies is greatly restrained by logistics and economics. One of the well known examples calling for repeated engineering investigation is a study conducted by McKenna *et al*. (1975), where a trial embankment was constructed to study the effectiveness of stone columns in reducing settlements in soft soil deposits. Little increase in the excess pore water pressure values during construction of the stone columns was recorded by piezometers and no difference between the untreated and improved zone in terms of displacement values and the settlement rate were measured by rod settlement gauges. Monitoring devices registered greater settlements in sand and silt below the columns than in the clayey alluvium layer, during construction and for some part of the serviceability period. McKenna *et al.* (1975) reported no effect on the reduction of the settlement, which caused great discussion in the geotechnical society. Various explanations for the situation occurred have been proposed: from an effect of the granular material being too coarse and the presence of slurry resulting in preventing the drainage through columns, to the comment on the transfer of the stresses down the stone columns as they performed as friction piles punched into clay, see Greenwood (1991).

The laboratory and field studies form the foundation for numerical studies and for the development of the constitutive modelling. However, the numerical studies are less time consuming and less expensive than elaborate experimental

investigations. Numerical studies allow for comprehensive studies in a relatively more economic and faster way than traditional experimental/field research.

3.3.1. Modelling of stone columns

The complexity of the modelling of the three-dimensional behaviour of a soil improved with stone columns has resulted in many approximate solutions in numerical modelling. As a consequence of those attempts four major streams can be distinguished:

a) unit cell approximation (2D axisymmetric approach),
b) 2D plane strain approach,
c) volume averaging techniques (3D problem solved using 2D finite element methods),
d) 3D finite element methods.

In the unit cell approach the soil improved with stone columns is analysed in terms of a representative unit cell with the column placed in the centre, as suggested by Hughes & Withers (1974), Balaam & Booker (1981 & 1985), Priebe (1995 & 2005). The dimensions of the representative unit cell depend on the column arrangement and spacing, see Figure 3.9. The domain of influence of the column in each arrangement has a different shape, from triangular to hexagonal and is approximated area of an equivalent circle. There is one major disadvantage of this method; it can only be used where the loads are applied in a vertical direction. Therefore, when that is not applicable other solutions should be used, such as homogenization techniques and the finite element method. More importantly, the method can only be applied to large groups of columns.

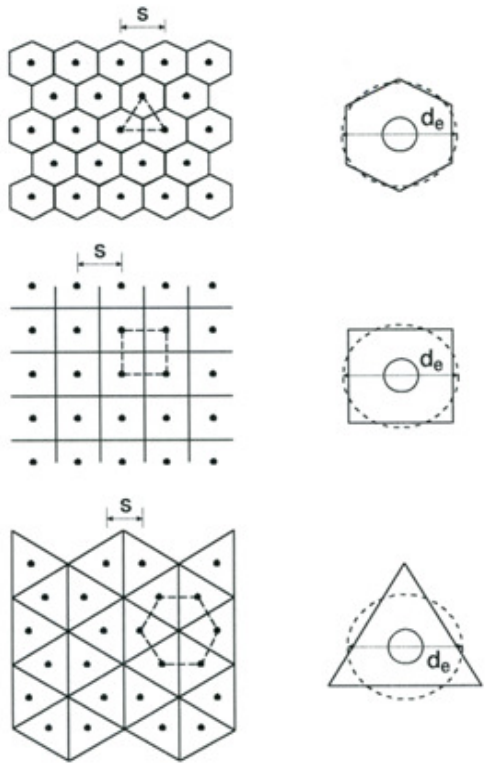

Figure 3.9: Domains of influence for particular stone column arrangements (Balaam & Booker, 1981).

In the 2D plane strain approach stone columns are represented by continuous walls with an equivalent thickness by keeping the same area ratio of the ground improvement and walls, as proposed by Van Impe & De Beer (1983) and Barksdale & Bachus (1983). In this method, a constant volume deformation is assumed. The self-weight of both the column and the soil, and the shear stresses between the column and surrounding soil are neglected. Bergado & Long (1994) proposed, in addition to the assumptions made by Van Impe & De Beer (1983) and Barksdale & Bachus (1983), that the spacing between the granular walls should be kept the same as for the stone columns, and that the wall thickness should be calculated as a proportion of the area and the spacing of the columns. Therefore, a need for

adjustments of the modelling to account for geometrical changes has been recognised. Nevertheless, as discussed by Castro & Sagaseta (2010), the equivalent column stiffness and the equivalent permeability are of significant importance when considering the correct modelling of the lateral deformations and the consolidation process. Moreover, effects of the stone column installation and smear zone should be also taken into account, as mentioned by Weber *et al.* (2009).

In the volume averaging technique the soil reinforced by the stone columns is treated as a composite material. In the simplest volume averaging approach (so-called homogenisation) the stress-strain response of the composite is defined and the behaviour of the soil-column block under the applied loading is studied. This approach was first applied under axisymmetric conditions by Mitchell & Huber (1985), where the soil treated by the stone columns was 'wished-in-place' using cylindrical rings with the same area ratio without considering any installation effects, see Figure 3.10. However, this approach does not differentiate between the stiffness of the two constituents, the column and the surrounding soil, and the highly non-linear and stress dependent behaviour of soft clays and the column is not taken into account.

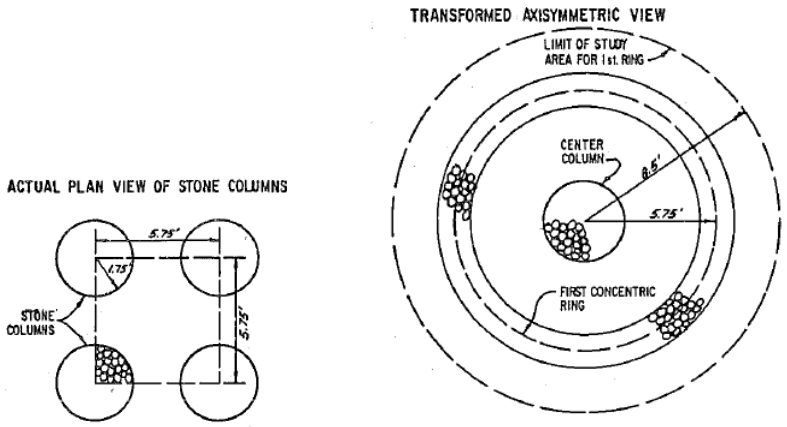

Figure 3.10: Actual and transformed view of the stone column foundation using cylindrical ring approach (Mitchell & Huber, 1985).

A more sophisticated version of volume averaging method was proposed by Schweiger (1989) and Schweiger & Pande (1988 &1989), in which an equivalent material stiffness matrix from the individual stiffness matrices of the two constituents and their respective volume fractions was developed. Later, Lee (1993) and Lee & Pande (1998) presented a method where the correction of the stress/strain difference was proposed by adding the stress/strain difference into granular material which is contrast to in-situ situation. Vogler (2008) utilised the volume averaging technique to deep-mixing method and validated his results by comparative 3D FE simulations. Although Vogler (2008) only considered cement columns, the method could also be used for stone columns. This method takes account of the non-linearity of constituents by using an elasto-plastic advanced constitutive model for both the soil and the column materials. For the case of an embankment, the results of three-dimensional FE simulations showed a good match with the proposed volume average technique in terms of settlement and stress distribution predictions. Nevertheless, in case of a footing for two or three columns per symmetric cross-section the volume averaging approach is able to predict global behaviour, but when compared with conventional 2D numerical analysis no match has been found. As a result, the volume averaging method developed by Vogler (2008) is limited to studies on the stress-strain response of a group of columns, as this approach is not suitable for the investigation of the behaviour of a single column. Moreover, proposed by Vogler (2008) method is not capable to account for installation effects and column bulging.

3.3.2. Finite element studies of stone columns

In this section some selected finite element studies of stone column foundations are briefly described. The studies presented here are reviewed by type of simulation (2D plane strain, 2D axisymmetic and 3D), rather than chronologically. A short summary of selected finite element analyses is presented in form of a table, see Table 3.2.

A comparison between numerical predictions and analytical methods has been presented by Wehr & Herle (2006) for an embankment constructed on fine-grained soil improved with floating stone columns. Plane strain analysis was performed using PLAXIS 2D software, applying elasto-perfectly plastic Mohr-Coulomb model for both soil and granular column material without any consideration of material non-linearity or stress-dependence, see Table 3.2. Continuous stone walls are used in the simulations, replacing isolated stone columns, with the restriction that the volume of the improved soil should remain unchanged. For analytical methods, authors have considered Priebe's approach (1995) to estimate the final settlements and the Balaam & Booker method (1981) to calculate time-dependent settlement. Wehr & Herle (2006) concluded that a simple analytical procedure might be more preferable to the complex numerical analysis as the analytical methods and the numerical predictions resulted in a close match both at the centreline and the crest of an embankment. That may be true for this particular case, however, the FE method gives some additional benefits, such as the prediction of horizontal displacements and distribution of an incremental shear strain in each calculation step.

Table 3.2: Summary of selected FE studies on stone columns presented in thesis.

Research			Andreou & Papadopoulos (2006)	Poorooshasb & Meyerhof (1997)	Ambily & Gandhi (2007)	Elshazly *et al.* (2008A & B)	Kirsch & Sondermann (2003)	Wehr & Herle (2006)	Gäb *et al.* (2008)	Castro & Karstunen (2010)
Aim of study	Bearing capacity		•				•			
	Settlement			•	•	•		•	•	•
	Consolidation			•				•	•	•
Type of calculation	Class A predictions									
	Benchmark		•	•	•				•	•
	Back-calculation					•	?	•	•	
Type of simulation	2D	Axisymmetry	•	•	•	•				•
		Plane strain						•		
	3D						•		•	
Type of columns	Single		•	•	•	•				•
	Group				•	•	•	•	•	
Length of columns	Floating						•	•	•	
	End-bearing		•	•	•	•				•
Column installation	Wished-in-place		•	•	•	•	•	•	•	
	Coefficient of earth pressure increased					•			•	•
	Densification								•	
	Cavity expansion									•
Type of loading	Uniform		•	•	•	•				
	Other						•	•	•	
Constitutive model used	Standard		•	•	•	•		•	•	
	Advanced						•		•	•

A comprehensive study on the behaviour of end-bearing stone columns conducted by Poorooshasb & Meyerhof (1997) is a milestone in the parametric study on the influence of factors, such as the column spacing, the soil properties or the changes in-situ stresses caused by the installation technique and compaction of the granular material. Poorooshasb & Meyerhof (1997) concluded after their 2D axisymmetric study, that the greatest influence on the performance of stone column foundations has the column spacing and the compaction of the granular material. The latter, in turn, results in changes of the stone column strength, stiffness and dilatation characteristics. Additionally, based on the assessment of the initial stresses in the surrounding soil, design charts regarding the performance ratio were produced for standard stone columns, stone columns of lower stiffness (than standard) and for floating stone columns stiffer than standard. However, in the analyses were not able to account for the shear stresses produced at the bottom of soil-column block, which was represented by simple linear Mohr-Coulomb model.

The influence of several factors, such as the applied load, the area replacement factor, the friction angle of the granular material or the effect of the undrained shear strength of the surrounding soil on predicted horizontal displacements, have been described by Andreou & Papadopoulos (2006). The conversion of an axisymmetric unit cell with end-bearing stone column was created and simple Mohr-Coulomb elastic-perfectly plastic model wass assigned to both, the granular material and the surrounding soil, not taking account of the non-linearity or undrained behaviour of the material, see Table 3.2. Only one arrangement of columns was considered in simulations, but 5 different load levels and 4 different replacement factors were investigated. The friction angles of columns varied from 38˚ to 44˚. As confirmed by other studies, the upper part of the stone column tends to experience bulging failure, see Ambily & Gandhi (2007). Moreover, in the deeper part of the soil layer and at

low applied load, column bulging is less pronounced. However, in the case of increased applied load, the column material tends to move towards the surrounding soil. Furthermore, Andreou & Papadopoulos (2006) concluded that the higher the value of the friction angle and the area replacement factor, the smaller the plastic zone becomes and the bulging is more limited. In addition, the influence of the undrained shear strength of the surrounding soil seems to be negligible as the horizontal displacements remained unchanged during the simulations as an effect of the applied linear Mohr-Coulomb model. Therefore, it should be noted that this simple elastic-perfectly plastic formulation does not account for the non-linearity of the soil, the stress dependency or the directional-dependent stiffness of the material.

Drained axisymmetric unit cell finite element analyses using 2D PLAXIS software were performed by Ambily & Gandhi (2007) to study the drained behaviour of end-bearing columns: both single and in a group of seven. For both soft clay and granular material the Mohr-Coulomb model was used, see Table 3.2. Between the column and soft soil no interface element was applied as the column deforms mainly by radial bulging and significant shear is not possible. For the group of columns, the surrounding columns were replaced with a ring following the idea by Mitchell & Huber (1985). The numerical studies presented by Ambily & Gandhi (2007) are not capable of taking into account the non-linearity and stress dependency of the soil and the column. In addition, the impact of spacing between the columns, the angle of friction of the granular material and the shear strength of the soft clay were studied and good agreement between numerical modelling and experimental results was shown. Two types of loading were used to check the influence of the loading conditions; at the beginning only the column area was loaded and then the entire area was subjected to loading. Ambily & Gandhi (2007) suggested that if the ratio S_{SC} / D_{SC} reached or exceeded the value of 3, the change in the deformation is

negligible for the predictions of the settlement. It was found that the settlement reduction ratio s_r (defined as an inverse of Priebe's improvement factor *n*) depends mostly on the centre-to-centre column spacing and the friction angle of the surrounding soil. Ambily & Gandhi (2007) concluded that the shear strength of the adjacent soil has no influence on the stiffness improvement factor, which is described as the ratio between the stiffness of treated and untreated soil.

A series of simulations of flexible foundations supported by end-bearing stone columns were conducted by Elshazly *et al.* (2008A) using 2D axisymmetric finite element analyses. According to Elshazly *et al.* (2008A) the rate of improvement decreased as the foundation size increased. In order to take account of the installation of stone columns, the post-installation soil parameters and the load-settlement records for full-scale field load tests were used to back-calculate the post-installation earth pressure coefficient and then adopted for numerical simulations, see Table 3.2. The experience of Elshazly *et al.* (2006), based on literature studies, indicates that a slight improvement may occur up to a distance of 6 m from the vibrator during the stone column installation sequence. Evidently, the extent of this improvement depends on soil properties, especially the void ratio. Soils with lower values of void ratio will experience more effective improvement than those with higher value of void ratio. The procedure proposed by Elshazly *et al.* (2008A), although effective, cannot easily be applied in practice due to limitations in availability of post-installation tests. The experience gained from one site cannot be directly transferred to another project, as installation effects depend on site specific conditions, such as ground, loading, ground improvement type and others.

The effect of column spacing on the stress response due to end-bearing stone column installation under a shallow foundation was investigated by Elshazly *et al.* (2008B), see Table 3.2. The paper presents both experimental and numerical

modelling of stress state alterations using a coupled finite element elasto-plastic model, which accounts for time-dependent soil deformations (namely the Hardening Soil model). Three different spacing patterns and columns lengths were studied. Different spacing patters were idealised using 'wished-in-place' single column surrounded by concentric rings with adequate width and granular material applied in axisymmetry conditions, similar to the idea proposed by Mitchell & Huber (1985). The effects of stone column installation were taken into account by applying the post-installation earth pressure coefficient, as defined by Elshazly *et al.* (2008A). This study can be used as a guide for engineers to estimate the optimum design for similar soil-column systems. However, again it requires derivation of post-installation material parameters to account for any changes in the soil properties caused by vibrations during installation process, and the knowledge about the settlement response; only then the post-installation horizontal to vertical stress ratio K^* can be back- calculated.

A full understanding and reproduction in numerical simulations of the installation effects for both the end-bearing and the floating stone columns is a very challenging task. So far, only the installation process of end-bearing stone columns has been simulated successfully by Castro & Karstunen (2010) by simulating cylindrical cavity expansion with 2D FE analyses in combination with the advanced constitutive model, S-CLAY1S (for model details see *Chapter 2*), see Table 3.2. However, the installation process of floating granular column seems to be more challenging to model due to the presence of competent soil layers below the column's base and its representation in the geometry model in FE software.

The results from numerical modelling compared with the experimental data on an embankment site in Kuala Lumpur regarding the stress distribution between floating stone column material and surrounding soil have been presented by Kirsch

& Sondermann (2003). A three-dimensional numerical analysis was performed using the Drucker-Prager yield criterion with a non-associated flow rule. Estimation of the ratio between the actual and the necessary shear strengths enabled the calculation of the factor of safety to be determined. The comparison of both the analytical and numerical results led Kirch & Sondermann (2003) to the conclusion that the complex load bearing system can be designed by engineers using analytical semi-empirical solutions (such as Priebe, 1995) or the numerical modelling. However, no information regarding how the stone column material was modelled (as undrained or drained material) was given by Kirsch & Sondermann (2003). Additionally, it is not clear from the paper whether the stiffness parameters used for the simulations were defined as part of desk study or of they were back-calculated from field measurements.

An attempt to simulate of stone columns performance at an Austrian field trial in Klagenfurt by means of more advanced constitutive models for both floating stone columns and soil matrix was described by Gäb *et al*. (2008), see Table 3.2. The study focused on the comparison of measured and predicted settlements and excess pore water pressures with different constitutive models simulating the soft deposits. Beneath an embankment floating stone columns were installed in soft Lacustrine clay (clayey silt) overlaid by loose to medium dense sand. The ground water table was found at depth of approximately 3 m, but the water level changes according to seasonal variation. The site was well instrumented with multilevel piezometers and extensiometers, and some CPT and dynamic probing tests were performed, see Gäb *et al.* (2007). Numerical simulations of that case study were performed using PLAXIS 3D Foundation software, considering only a representative slice of the full three-dimensional geometry. For the granular material of the stone columns the Hardening Soil models was applied and various constitutive models were used to

simulate soft deposits: the Hardening Soil model, the HS-Small model (which accounts for the effect of small strain stiffness), the isotropic Modified Cam Clay and its anisotropic extension S-CLAY1 (see *Chapter 2*). The stone columns were 'wished-in-place' and the installation effects were generally not considered. However, as the densification of the shallow layer of sand was proven by CPTU tests, for simulations the coefficient of earth pressure at rest was set to $K_0 = 1$. Installation of the stone columns results in higher stresses than in the untreated case, as the unit weight of the gravel material also acts on the soil mass. Moreover, as a result of column installation the sand layer is densely compacted, but the volume of the sand material remains unchanged. In order to account for this in FE simulations, the unit weight of the column material was assumed to be greater than in reality, see Gäb *et al.* (2007). As, in addition to this, the unit weight of the sand prior and post installation was kept constant, the stresses were calculated as a result of application of combined unit weights of the sand and the granular material. This procedure can be seen as a simplification of the installation process in sandy materials, however in clayey soils the column installation will not lead to compaction of the material to such extend. Some simplifications were undertaken for the numerical simulations, such as homogeneity of the soil layers and the geometry of the considered embankment in the longitudinal direction. Despite extensive monitoring, due to the lack of laboratory data, the stiffness parameters and the permeability of the soil were calibrated to match the deformation behaviour and the drainage conditions using the Hardening Soil model. Due to difference in the constitutive modelling approach, different values of the vertical displacement have been predicted by different constitutive models. The inspection of the vertical deformations with the vertical profile showed that the majority of the settlement was caused by the clay deposit and that the participation of the sand layer was negligible. The excess pore water

pressures were over-predicted at all depths when compared with the measured values. In general, the rate of consolidation predicted by all of the constitutive models was too fast and a closer match was not possible to achieve at that time; further calibration of the permeability values has not been carried out.

3.4. Summary and comments

Stone columns are a ground improvement method used increasingly for a wide range of foundations types. As the stone column technique results in the reinforcement and improvement of soft soil deposits, the method has gained increasing popularity worldwide.

The stone column improvement method along with its applications and limitations has been briefly described and discussed. Additionally, the important role of craftsmanship and quality control of the installation of the stone columns has been emphasised. Next, a short overview of the various design approaches for granular columns has been given, with a special emphasis put on the most common semi-empirical method. However, current design methods do not take account of the non-linearity of the soil-column systems and most of them are developed for end-bearing columns. Finally, recent studies on stone columns along with the numerical modelling of soil-column system have been presented.

Although model tests are important, singular gravity (1g) and centrifuge model tests always use a reconstituted material, which is not true representation of in-situ soil mass. The installation method rarely is analogous to that in the field. Limitations of field studies, such as consideration of specific type and configuration of stone columns and concerns associated with reliable site investigation and its

interpretation, restrain in-depth investigation of the behaviour of the column foundation constructed in soft soil deposits.

As an alternative, numerical modelling can be employed for studies of the soil-column systems. Two-dimensional plane strain approach is commonly used, however it is not true representation of the problem and reliable mapping procedures can be difficult to develop when material behaviour is non-linear. Axisymmetric modelling gives a possibility of application FE to simple studies, nevertheless it can be only used to study behaviour of a single column or large groups of columns under constant load. Most of engineering problems are however three-dimensional in nature. That calls for the numerical studies conducted in three-dimensional space. Moreover, as the true representation of the soft soil behaviour must be ensured, appropriate constitutive models shall be applied. Due to diversity of 3D FE, they can be applied to various geotechnical problems by both academics and practitioners. Nonetheless, some difficulties in numerical modelling of column installation effects remain still an engineering challenge.

Constant development in the constitutive modelling and the three-dimensional numerical codes allow for realistic and easier capturing of the complex nature of soil-column interaction. Current research aims for improved expertise in numerical modelling and simulation of soft soil deposits treated with stone columns, by using advanced constitutive formulations in 3D FE analysis. Behaviour of a stone column foundation is largely governed by the surrounding soil, its compressibility characteristics and the stress-strain-strength response. The models commonly used by civil engineering practitioners are the simple linear Mohr-Coulomb or elasto-plastic Modified Cam Clay (Roscoe & Burland, 1968) models. Nevertheless, these often result in inaccurate and over-conservative numerical predictions, as characteristics of soft soils are ignored and the complexity of the soil-column

interaction is neglected. By developing new enhanced advanced constitutive models, as presented in *Chapter 5*, the numerical predictions of the behaviour of the soft soil deposit can be improved, resulting in engineering and economically efficient geotechnical solutions.

Current stone column design procedures are based on relatively simple assumptions, such as the semi-empirical Priebe's method (1995). However, the interaction between the column and the surrounding soil is very complex and may differ from the simplifications used in existing design methods. Numerical methods are not yet fully implemented in industrial design. Nevertheless, they could be used, as discussed in the following chapters, for gaining a better understanding of the behaviour of soil improved with stone columns and for the optimisation of existing design procedures.

4

STONE COLUMNS BENEATH AN EMBANKMENT: PARAMETRIC STUDY

This chapter investigates the influence of selected characteristics of stone column foundations by conducting 3D numerical simulations of a benchmark problem. The benchmark considers an embankment constructed on Bothkennar clay, soft clay from Scotland, improved with floating stone columns using advanced constitutive soil models. The benchmark boundary value problem represents a typical application of the stone columns: reducing settlements in earth structures.

The parametric studies investigate the effect of parameters such as stiffness and angle of friction of the granular material, diameter and arrangement (length and spacing) of the stone columns, and the thickness of the soft deposit. The aim is to understand the complex behaviour of stone columns installed beneath an embankment, and to improve the analyses for design of the granular columns.

A three-dimensional representative slice of full geometry is used in numerical simulations. Undrained stone column and embankment construction is followed by a consolidation stage. Based on the results obtained, some conclusions and closing remarks on the factors influencing the behaviour of the stone column foundation and some design aspects are discussed

4.1. Numerical model

The geometry of the embankment considered is shown in Figure 4.1. Due to the symmetrical conditions only half of the model has been considered in the simulations. The embankment is assumed to be 2 m high and 10 m wide (at the crest), and the gradient of embankment slope is taken as 1:2. The underlying deposit is idealised by two layers: an over-consolidated dry crust and a slightly over-consolidated soft Bothkennar clay. The groundwater table is assumed to be located at depth of 1 m. Consolidation is assumed to occur through the top and bottom boundary of the mesh model.

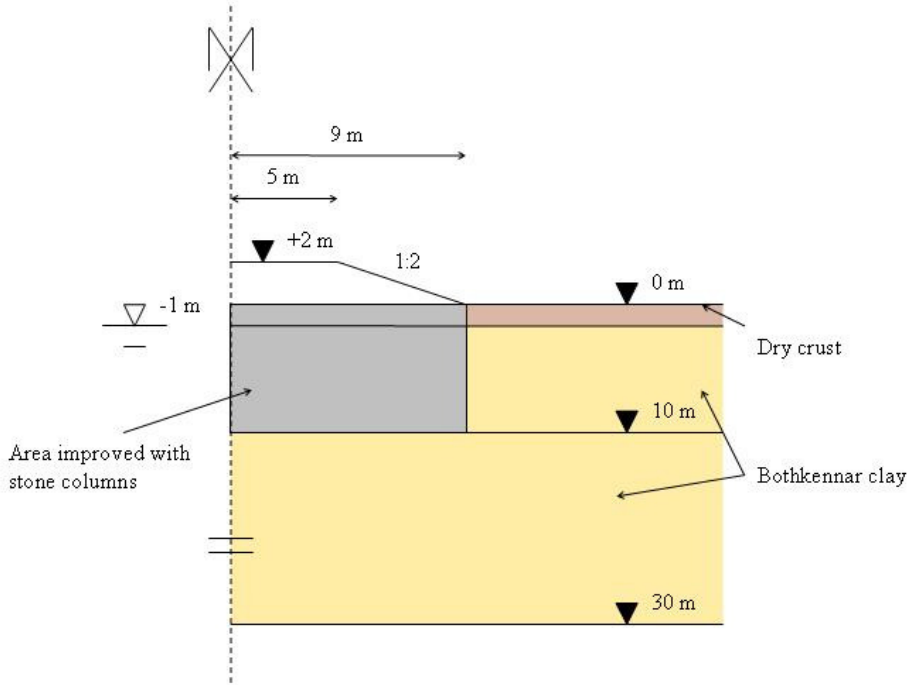

Figure 4.1: Benchmark problem: the geometry of an embankment and assumed soil profile.

For all simulations PLAXIS 3D Foundation v.2.2 finite element code has been used, taking advantage of three-dimensional modelling. A mesh with 7 200 tetrahedral elements and 80 000 degrees-of-freedom has been used in simulations, if not stated differently. Mesh sensitivity studies were carried out before conducting the parametric studies in order to reduce the influence of the mesh on the results of the simulations. First of all, a two-dimensional mesh with triangular elements was created, then the mesh was extended in the depth direction forming the three-dimensional shape. The top view of the benchmark problem along with the representative slice of full geometry is shown in Figure 4.2. Due to symmetry of the boundary value problem and the square arrangement of the stone columns constructed beneath an embankment, the full three- dimensional model can be represented by the representative slice of full geometry. The width of this slice is dependent on the spacing in which the columns have been installed and it is assumed to be equal to the columns' spacing, as shown in red solid lines in Figure 4.2a.

In order to allow for correct calculation of the initial stresses, first the Bothkennar site was considered, without any ground improvement or embankment in place. Next, the granular material was applied to selected clusters, followed by activating embankment clusters one layer at a time. Installation of the stone columns and construction of the embankment were simulated as undrained events during which the dissipation of any excess pore water pressures is not possible. Afterwards, a consolidation phase was simulated using a maximum excess pore water pressure of 1 kPa as the end criterion for calculations.

For numerical simulations the S-CLAY1S model was used to represent the layers of the dry crust and the Bothkennar clay. This model enables the anisotropy

and bonding effect present in natural soft soil to be simulated, and is described in detail in *Chapter 2*. More details with regard to the geotechnical properties of the soil at the Bothkennar site are presented in the following section.

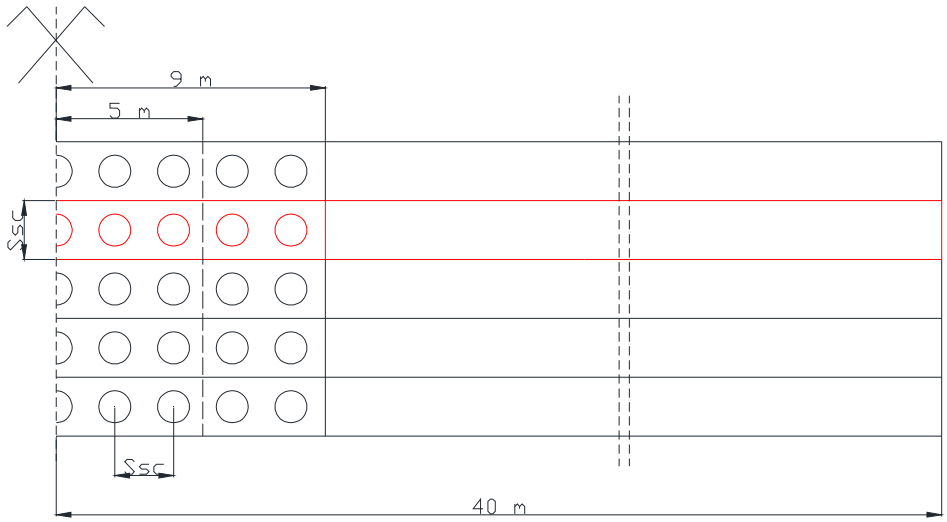

a)

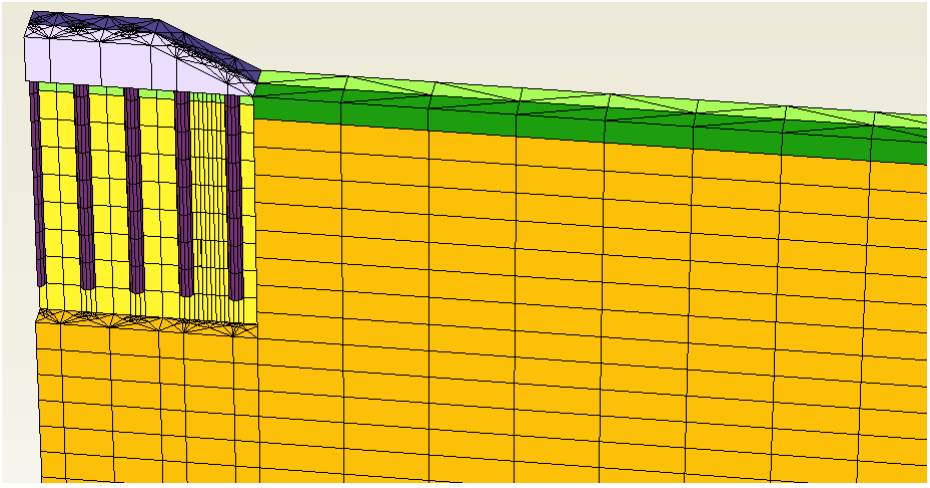

b)

Figure 4.2: Benchmark problem:
a) top view b) representative slice of full 3D geometry.

4.2. Material properties

The construction of the embankment on the soft soil deposit was simulated in two stages; two layers of 1 m embankment fill each were placed within 5 days. Krenn (2008) proved using FE modelling that the influence of the constitutive model used for the embankment fill constructed on soft soil is negligible, when the embankment is not close to failure. Hence, a simple Mohr Coulomb model was used to represent the granular fill in the benchmark problem considered. The parameters assumed are shown in Table 4.1. The cohesion of the embankment fill c' was chosen to be equal to 1 kPa for computational reasons. The embankment is assumed to be made from granular fill, and thus, it is assumed to behave in a drained manner.

Table 4.1: Embankment fill parameters.

Material	γ [kN/m^3]	E' [kN/m^2]	ν' [-]	φ' [°]	ψ' [°]	c' [kPa]
Embankment	20	30 000	0.3	38	0	1

4.2.1. Soft soil

The parameters for the soft soil used in the simulation were chosen to represent Bothkennar clay, soft clay from Scotland (UK). The Bothkennar site is situated between the cities of Edinburgh and Glasgow, on the Forth River estuary. The site was previously owned and managed by the UK Government through the Science and

Engineering Research Council (SERC) and covers an area of approximately 11 ha and 20 m depth of soft saturated natural soils, see Nash *et al.* (1992A and B).

The slightly over-consolidated Bothkenar clay, which is overlain by a dry crust, is a soft recently deposited marine sediment. It has been strongly influenced by the changes in relative sea level over the past 13 000 years. The composition of the clay is relatively consistent with depth, which is in contrast with many other soft clay sites found in the United Kingdom. Bothkennar clay has a significant organic content (determined by loss of ignition) of 3..4 %, see Leroueil *et al.* (1992). This soft soil contains approximately 30..40% clay content, 50..60% silt content and a small amount of sand, and is classified as a silty clay. The undrained shear strength is in the range of 15..55 kPa and has been determined in the laboratory using undrained triaxial tests and in-situ using vane tests, see Nash *et al.* (1992A).

Undrained and drained triaxial tests carried out on soil from depths of 5.3..6.3 m were used for the determination of the yielding characteristics, and a high degree of anisotropy of the Bothkennar clay was found, see Smith *et al.* (1992) and McGinty (2006). Moreover, the isotropic loading/unloading/reloading tests on vertically and horizontally orientated samples conducted by McGinty (2006) showed some evidence of cross-anisotropy in the elastic behaviour. Given that the plastic strains dominate in the problem considered here, the latter has been ignored.

Smith *et al.* (1992) performed oedometer tests on samples from a depth of 5..6 m to study the apparent interparticle bonding in the Bothkennar clay by comparing the behaviour of natural and reconstituted soil samples. They found that the yield stress for the natural sample was 1.5 times greater than for the reconstituted soil at

the same void ratio. Additionally, triaxial tests conducted on natural samples from 6.5..8.5 m depth showed that the breakdown of the bonding is progressive, see Clayton *et al.* (1992) and McGinty (2006). Hence, it appears to be necessary to use an advanced constitutive model that accounts for interparticle bonding and destructuration.

The considered soil profile used in the benchmark problem is shown in Figure 4.1. In the simulations the deposit is idealised in two layers: a slightly over-consolidated soft clay which is overlain by a 1m thick over-consolidated dry crust. Both layers are simulated using the S-CLAY1S model presented in *Chapter 2*. The soil constants and state variables describing the clay and dry crust are shown in Tables 4.2, 4.3 and 4.4.

Table 4.2: Standard soil constants: S-CLAY1S model.

Layer	Depth [m]	γ [kN/m^3]	k [m/s]	ν' [-]	M [-]	κ [-]	λ_i [-]
Dry crust	0-1	19.0	$1\text{x}10^{-9}$	0.2	1.51	0.02	0.15
Bothkennar clay	1-30	16.5	$2.89\text{x}10^{-9}$	0.2	1.51	0.02	0.15

Table 4.3: Advanced soil constants: S-CLAY1S model.

Layer	Depth [m]	ω_d [-]	ω [-]	ξ [-]	ξ_d [-]
Dry crust	0-1	1	30	9	0.2
Bothkennar clay	1-30	1	50	9	0.2

Table 4.4: State variables: S-CLAY1S model.

Layer	Depth [m]	e_0 [-]	K_0 [-]	POP [kN/m^2]	OCR [-]	α_0 [-]	χ_0 [-]
Dry crust	0-1	1.37	0.7	30	-	0.59	4
Bothkennar clay	1-30	2.0	0.5	-	1.5	0.59	8

Due to its consolidation history the clay can be assumed to be cross-anisotropic in terms of its elasto-plastic behaviour. Therefore the initial inclination α_0 of the yield surface of the S-CLAY1S model may be derived following the procedure outlined by Wheeler *et al*. (2003) which is recalled in *Chapter 2*.

The pre-consolidation of the dry crust was modelled using the vertical pre-overburden pressure (*POP*), listed in Table 4.4, which is defined as the difference between the maximum past value and the in-situ value of the vertical effective stress. The vertical overconsolidation ratio (*OCR*) was used for the soft clay. The in-situ coefficients of the earth pressure at rest K_0 for both the dry crust and Bothkennar clay (Table 4.4) was calculated based on the equation given by Mayne & Kulhway (1982):

$$K_0 = (1 - \sin\varphi') \cdot OCR^{\sin\varphi'} \qquad (4.1)$$

Additional advanced soil constants, ω and ω_d describing the rotation of the yield surface, were calculated following the procedure described by Wheeler *et al*. (2003) and outlined in *Chapter 2*. During the site investigation the sensitivity of the Bothkennar clay, which is used for the determination of the initial amount of structure χ_0, was found to be on average around 5 (Nash *et al.* 1992A) and that value was assumed for the numerical modelling. Moreover, to differentiate between the sensitivity of the two deposits, different values of the initial amount of structure χ_0 for both the dry crust and the Bothkennar clay were assumed. Due to insufficient data, parameters ξ and ξ_d were assumed based on the typical values for soft deposits according to the range of values outlined by Wheeler *et al.* (2003).

4.2.2. Stone columns

Floating stone columns were assumed to be installed in a square arrangement with spacing between the columns, S_{SC} equal to 2 m beneath the embankment for the first set of analyses. The diameter of the columns D_{SC} was taken as 0.6 m and the length L_{SC} was considered to be 10 m. In the FE analysis the stone columns were 'wished-in-place' during an undrained process without considering any installation effects. In fact, the installation of stone columns on structured soils reduces the amount of bonding (and sometimes also the strength) of the soil next to the columns, as well as changes the anisotropy and the coefficient of earth pressure at rest, as shown by Castro & Karstunen (2010), which is in line with the field observations presented by Guetif *et al.* (2007) and Kirsch (2006). However, the effects of installation of stone columns are not the subject of this research.

The Hardening Soil Model, described in *Chapter 2*, was used to model the granular material of the stone columns and the material parameters are presented in Table 4.5 and 4.6. The reference Young's modulus E_{50}^{ref} was assumed to be the same as the reference oedometer modulus E_{oed}^{ref}, whereas the reference unloading/reloading modulus E_{ur}^{ref} was assumed to be 3.25 times greater than the E_{50}^{ref}, see Table 4.5.

The critical state friction angle of the granular material $\varphi_{SC}^{'}$ was chosen to be 42° and the dilatancy angle ψ_{SC} was assumed to be 30° smaller than the $\varphi_{SC}^{'}$, see Table 4.6. Poisson's ratio $\nu^{'}$ and an exponent m equal to 0.3 were assumed, in line with previous simulations of stone columns, see Gäb *et al.* (2008) and Weber *et al.*

(2009). A unit weight of 19 kN/m^3 for the granular material was applied, following the experience of industry. Such a value is also justified in recent physical and numerical studies of stone columns in undrained and drained conditions underneath an embankment (Weber, 2007).

Table 4.5: Stone column stiffness parameters.

Material	γ [kN/m^3]	ν'_{ur} [-]	$E_{50}^{ref} = E_{oed}^{ref}$ [kN/m^2]	E_{ur}^{ref} [kN/m^2]
Stone column	19	0.3	80 000	260 000

Table 4.6: Additional stone column parameters.

Material	k [m/s]	c' [kN/m^3]	φ'_{SC} [^{o}]	ψ_{SC} [^{o}]	m [-]
Stone column	1.97x10^{-4}	0.1	42	12	0.3

Note: m = power for stress-level dependency of stiffness.

As the stone columns were assumed to be installed in a square grid, the representative slice of the full three-dimensional geometry for a square pattern of floating columns was determined, see Figures 4.1 and 4.2. The width of the three-dimensional slice was assumed to be equal to the column centre-to-centre spacing.

4.3. Reference analysis

As a reference model (REF) to all further simulations a three-dimensional numerical analysis was performed considering that the soft soil was improved with stone

columns up to a depth of 10 m. To simulate the behaviour of the Bothkennar clay and dry crust, the S-CLAY1S model was used. The stone column material parameters used are presented in Tables 4.5 and 4.6. The columns with diameter equal to 0.6 m were assumed to be installed in a 2 m square grid up to depth of 10 m.

The computational time required to calculate the benchmark problem considered was equal to approximately 1 day due to the great number of degrees-of-freedom in each of the simulations.

4.3.1. Vertical displacement

A plot of the surface settlement at the ground level versus the horizontal profile after construction and at the end of primary consolidation is shown in Figure 4.3. The location of the stone columns is indicated in grey.

After construction, a small amount of heave was predicted next to the embankment (0.003 m). The unrealistic extent of the heave (also at the outer boundary of the geometric model) could be eliminated (and the distribution of the heave changed) by using the small strain stiffness soil constitutive model. Due to the nature of the stone columns, the surface settlement was smaller in the granular columns than in the surrounding soil. The differential settlements at the ground surface slowly but steadily decreased as the distance from the symmetry axis increased. Moreover, at the top of the embankment differential settlements were not present as the granular fill of the embankment mitigated any differences between the settlement of the columns and the surrounding soil. Installation of the floating stone

columns resulted in a reduction of the surface settlements by a factor of 2, from 0.059 m to 0.029 m at the inner boundary of the geometry model, respectively.

At the end of consolidation, heave was no longer an issue, see Figure 4.3. The surface settlement was much smaller then at the end of the construction, resulting in approximately four times greater settlement at the end of the consolidation process at the symmetry axis. Similar to the case of surface settlements after construction, the greatest surface displacements were predicted in the soil located next to the symmetry axis of the earth structure. Installation of the floating stone columns resulted in a surface settlement reduction of 22%, from 0.148 m to 0.116 m at the inner boundary of the geometry model, see Figure 4.3.

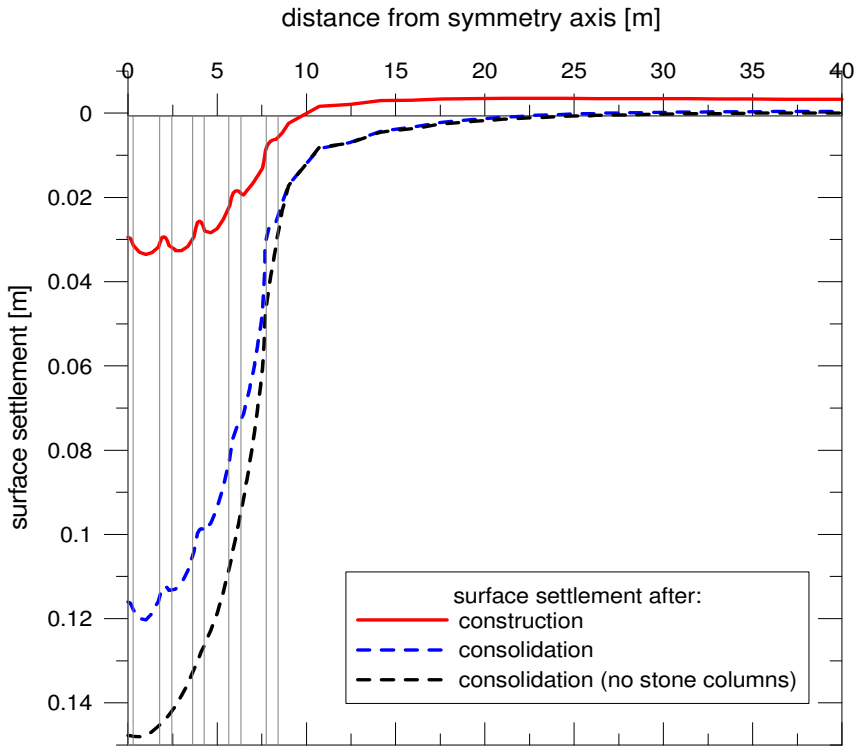

Figure 4.3: Surface settlement at the end of construction and after consolidation: reference analysis.

4.3.2. Horizontal displacement

The horizontal displacement contours at the centreline of the representative slice are presented in Figure 4.4. In Figure 4.4a the horizontal displacement contours after construction are plotted, whereas Figure 4.4b shows the contours at the end of consolidation. The location of the stone columns is indicated by the red lines. As the lateral movement of the improved soil is of greater importance beneath the embankment, the treated zone is magnified for clarity.

Looking at Figure 4.4a it is evident that after construction of the embankment, the highest values of horizontal displacements were predicted under the embankment slope, which is in agreement with previous findings, see Krenn (2008). Underneath the crest of the embankment the soil was subject to high loading, which resulted in notable vertical displacements. Due to the compressibility characteristic of the ground (governed by Poisson's ratio and also the flow rule of the constitutive model) settlements induce lateral movement in the soil block, which in some cases may result in failure. In the case of the embankment slope, no constraints are found at the other side of the loaded area and the soil displaces laterally in a greater manner. That is the case in this simulation, where under the embankment the horizontal movement of the soil-column block was found to be the highest, see Figure 4.4.

Inspection of Figure 4.4b clearly indicates that at the end of the consolidation process the horizontal displacement predictions in the improved soil zone increased by a factor equal to 1.67. The distribution of the lateral movement before and after consolidation process is different- the depth of the horizontal displacements contours reduced with time.

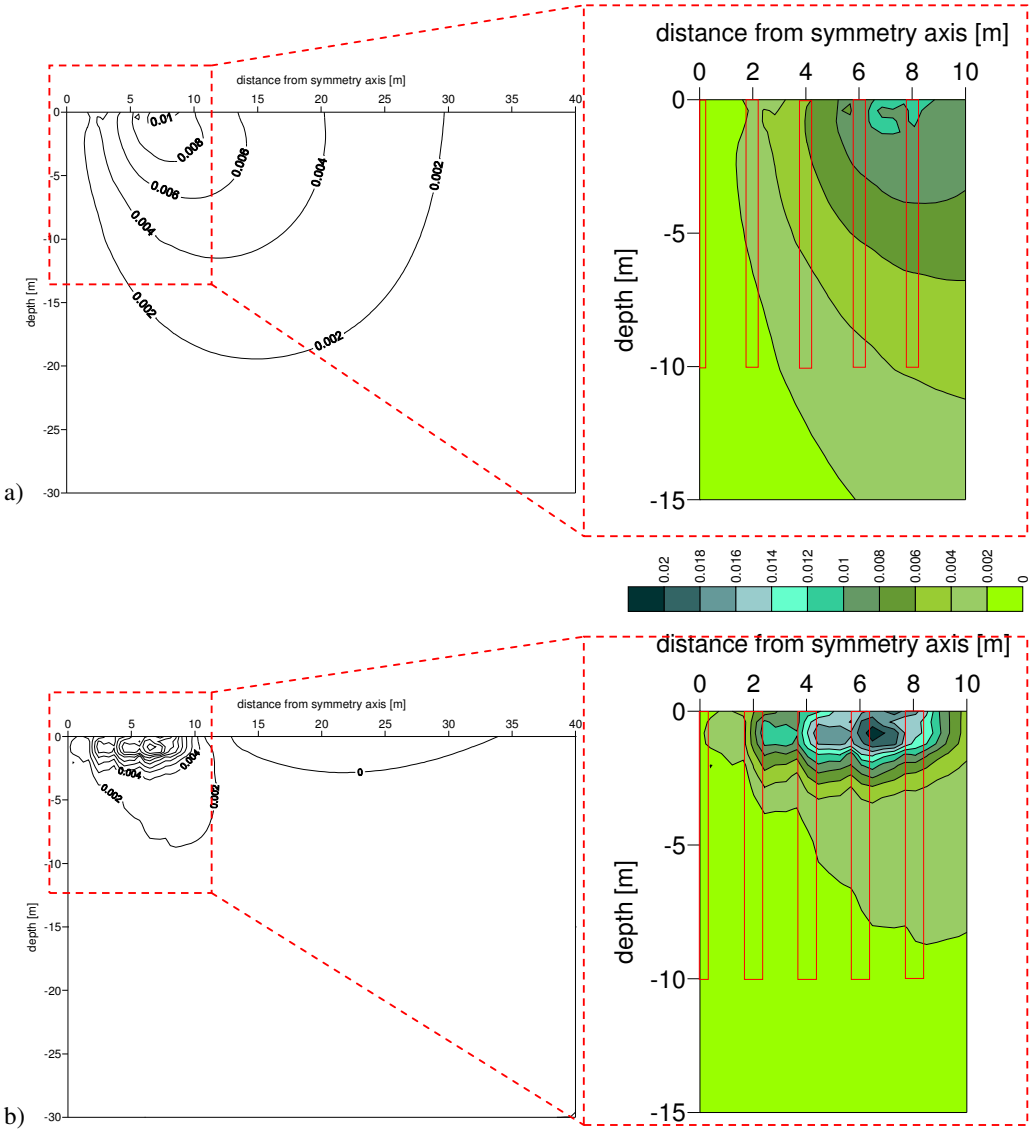

Figure 4.4: Horizontal displacement contours (in m) for reference analysis at the end of: a) construction and b) consolidation.

Horizontal displacements at the toe of the embankment (at the centre of the representative slice) at the end of the construction and consolidation processes are presented in Figure 4.5. It can be noted that after construction the relatively stiff material of the dry crust displaces laterally less than the soft Bothkennar clay. At the

end of consolidation the horizontal displacement increases from the ground surface with depth up to approximately 1.6 m and then reduces with depth. The maximum horizontal displacement occurs at a depth which is equal to 2..3 times the column diameter, which is in agreement with Murugesan & Rajagopal (2006).

4.3.3. Differential settlement

Two points were chosen for the investigation of differential vertical displacements versus depth: a point at the centreline of the granular material (named A) and a point corresponding to the surrounding soil (named B), see Figure 4.6.

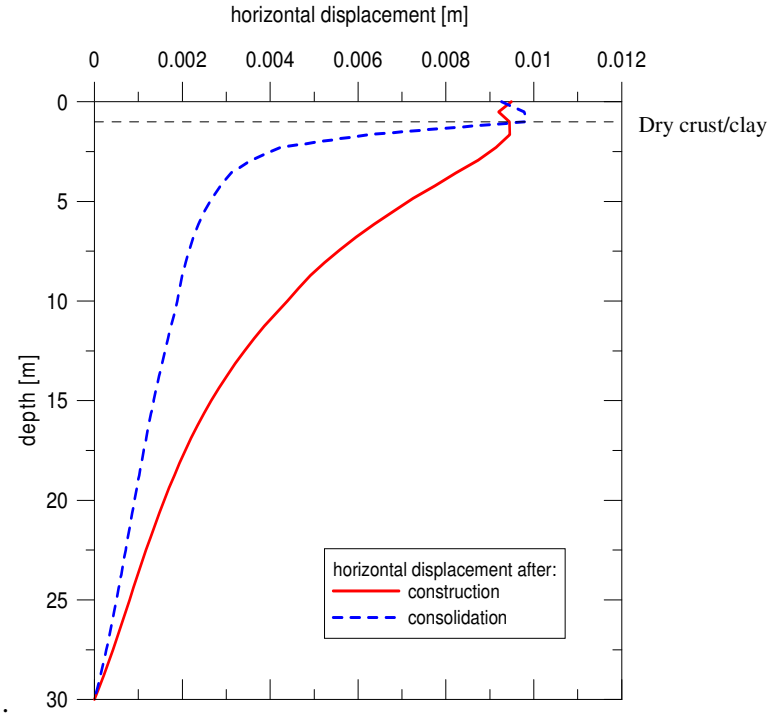

Figure 4.5: Horizontal displacement at the toe of the embankment (at the centre of the representative slice): reference analysis.

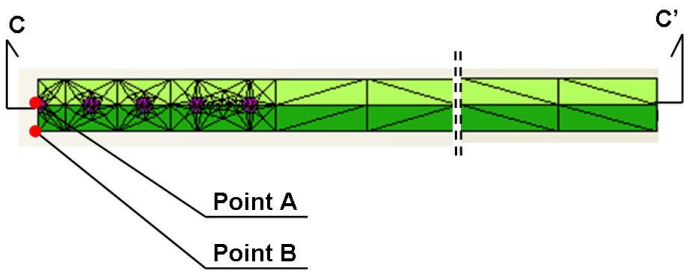

Figure 4.6: Chosen points for reference analysis: top view of geometry.

The evolution of the differential vertical displacements with depth at the centreline of the embankment (for points A and B) after the construction and consolidation is plotted in Figure 4.7.

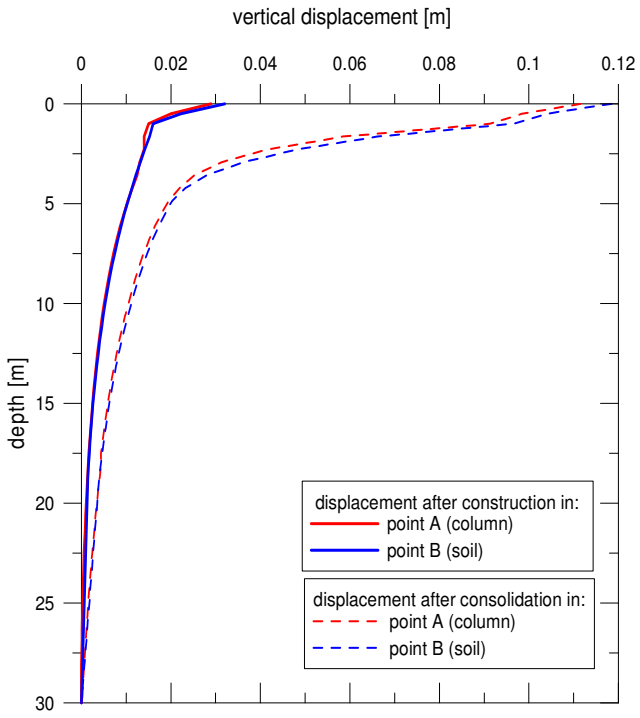

Figure 4.7: Vertical displacement vs. depth for reference analysis at the end of construction and consolidation: for points A and B.

It can be observed that after construction predictions are different for points A and B only at shallow depths of the soil mass, with a value of the differential vertical displacements equal approximately to 0.027 m. Differential vertical displacement reduces with depth and diminishes completely at a depth of $Y / D_{SC} = 5$ (=3 m), where Y is the depth and D_{SC} is the column diameter. A similar situation was observed after consolidation, although the value of the differential settlements was smaller and negligible.

4.3.4. Vertical effective stresses

Vertical stress contours along cross-section *C-C'* (see Figure 4.6) after construction and consolidation are plotted in Figure 4.8. The overall response looks reasonably similar despite the different stages of analysis. The difference between the predictions of vertical effective stresses for the soil and the columns is small although higher stresses are found throughout the column material than in the soil. As in the benchmark problem floating stone columns are considered, i.e. the columns do not penetrate any competent stiff layer of soil. Therefore they do not transfer the load into a rigid stratum but into the surrounding soil as part of a load transfer process. This process can be seen in Figure 4.8: in upper part of plot granular material transfers more load than the surrounding soil. At the base of the columns the load is transferred from the columns to the soil underneath. In between this base level and the ground surface at a depth of approximately 9 m the 'neutral point' can be

found. This point indicates that the amount of load held by the column and surrounding soil is of the same value.

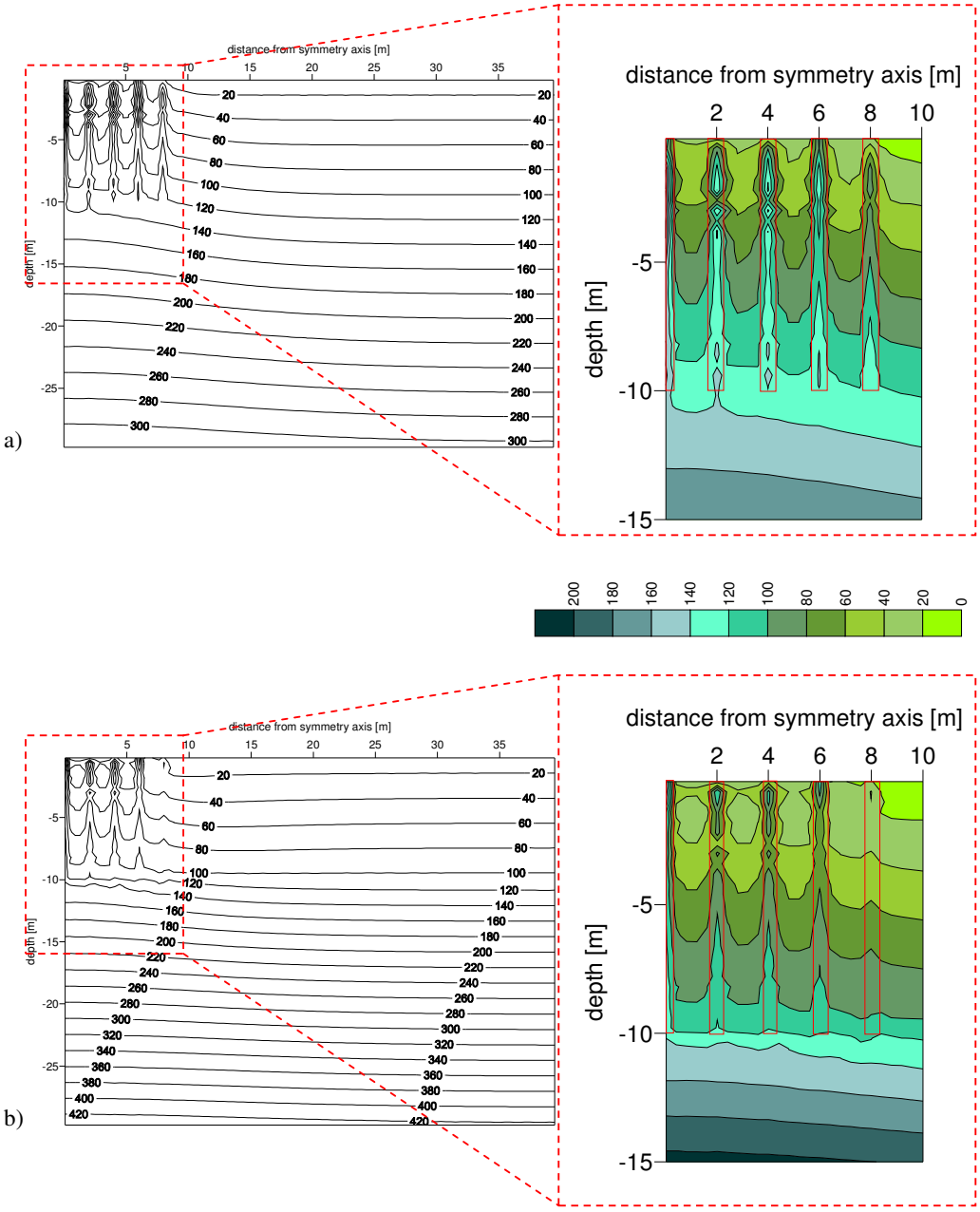

Figure 4.8: Vertical effective stress contours (in kPa) for reference analysis at the end of: a) construction and b) consolidation.

4.3.5. Stress paths

Figure 4.9 shows the selected stress paths in the granular material if the column (point A) and in the surrounding soil (point B) at three different locations below the centreline of the embankment. Plots are presented in terms of t' and s', where $t' = \frac{\sigma_1' - \sigma_3'}{2}$ and $s' = \frac{\sigma_1' + \sigma_3'}{2}$. The figures represent the stress conditions at the ground surface (Figure 4.9a), at the top of the clay layer (Figure 4.9b) and at the base of the stone column (Figure 4.9c). The loading applied at the ground surface (as embankment fill) has been transferred along the stone column length into the deeper layers. The change in depth profile from dry crust to the Bothkennar clay layer induces a higher level of stress due to the greater stiffness of the upper layer compared to the soft soil below. At the column base the stress paths for points A and B are almost identical. The surrounding soil experiences, obviously, less stresses as the stiff granular material of the stone column takes most of the applied loading during the construction of the embankment.

4.3.6. Excess pore water pressures

Stone columns speed up the dissipation of excess pore water pressures, therefore an inspection of the excess pore water pressures at chosen depths should be performed. Figure 4.10 shows a schematic sketch of the various points in the soft deposit chosen for the inspection of the excess pore water pressure.

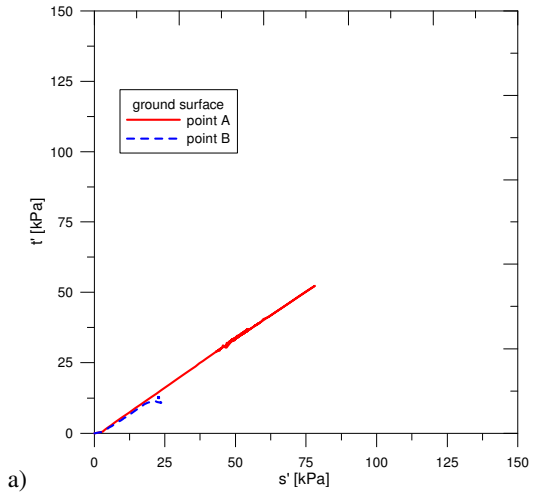

a)

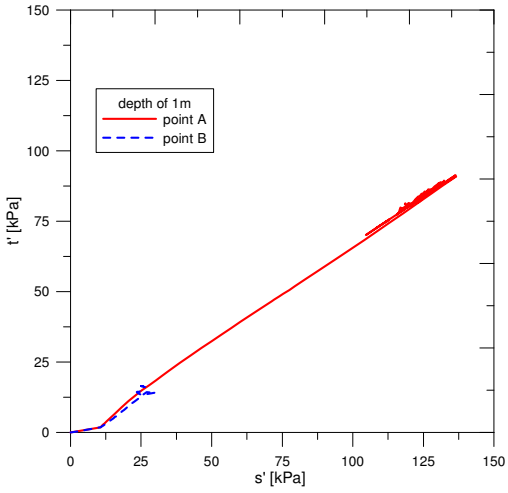

b)

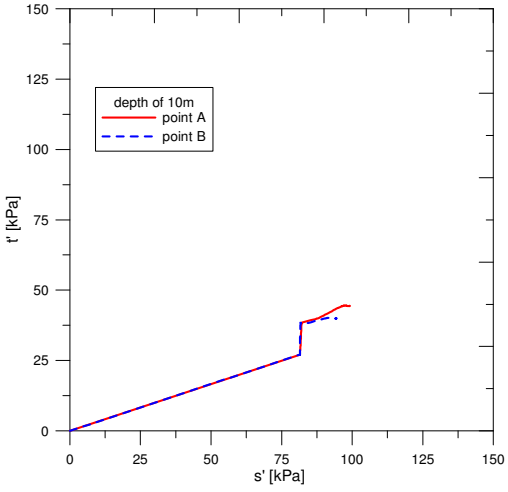

c)

Figure 4.9: Stress paths for reference analysis for points A and B at:
a) ground surface, b) depth of 1 m and c) depth of 10 m.

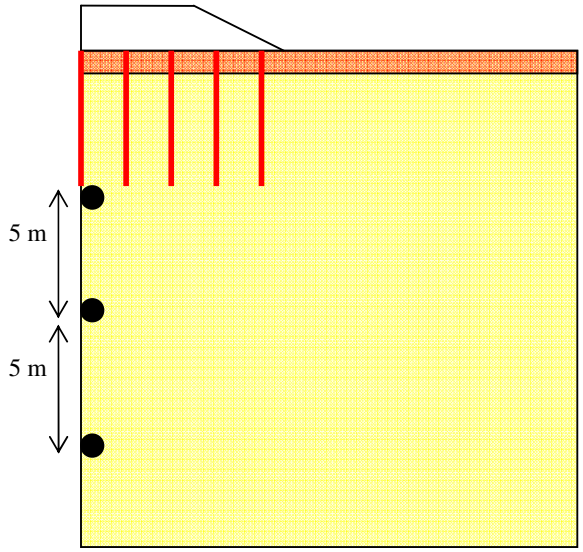

Figure 4.10: Sketch of the benchmark geometry with chosen points for the excess pore water pressure predictions: reference analysis.

The evolution of the excess pore water pressures with time is plotted in Figure 4.11. The plot has been prepared for the stone column base and 5 m and 10 m below the column base. The geotechnical sign convention for pore water pressure has been applied, where negative values refer to suction (when pore air pressure is atmospheric).

The excess pore water pressures build up and then dissipate as the consolidation process evolves, see Figure 4.11. This phenomenon is due to the Mandel-Cryer effect (Mandel, 1950 and Cryer, 1963) during coupled consolidation. Decay of the excess pore water pressure is particularly rapid at the column base, where the interface between the granular material with good hydraulic conductivity properties and the surrounding soil (of poorer permeability characteristics) is located.

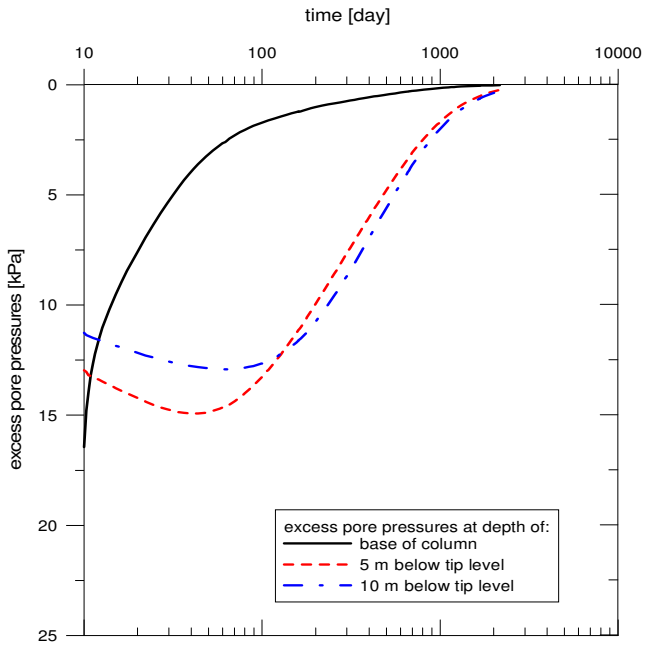

Figure 4.11: Excess pore water pressure evolution with time: reference analysis.

The excess pore water pressures contours after construction and after approximately 6 months and 3 years during the consolidation process are plotted in Figure 4.12. Again, the geotechnical sign convention has been applied for those plots and for clarity the improved zone has been magnified in an additional plot (with the location of the stone columns indicated by the red solid lines).

After construction, the predicted excess pore water pressure distribution shows greater values in the granular material, of approximately 35..48 kPa, than in the soil mass, of approximately 30 kPa. The pore pressure concentration in the improved zone will be gradually erased by dissipation of the excess pore water pressures during the consolidation process.

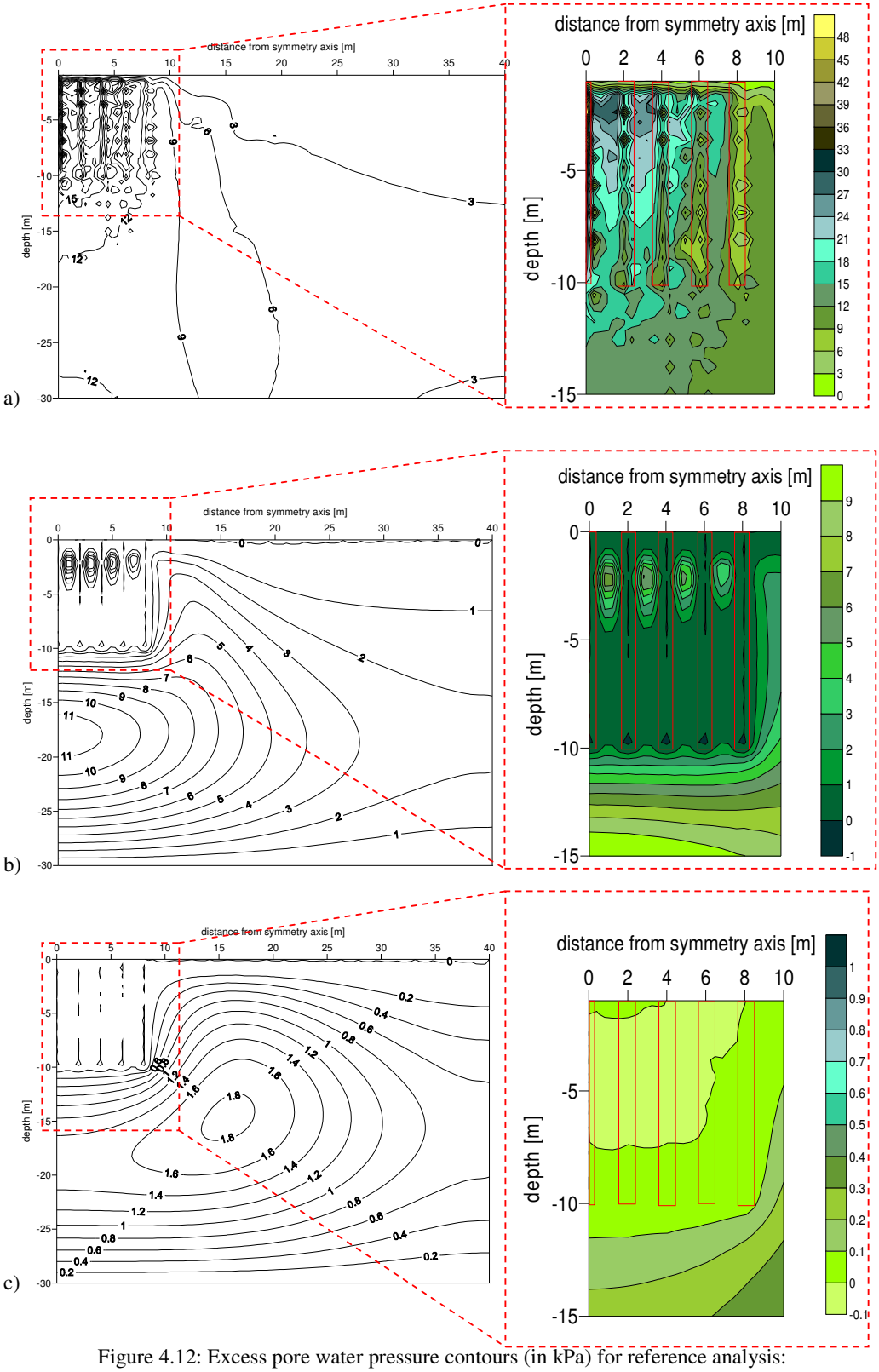

Figure 4.12: Excess pore water pressure contours (in kPa) for reference analysis:
a) after construction, b) 6 months into consolidation and c) 3 years into consolidation.

Local concentration of the excess pore water pressures in the stone column material is due to local numerical inaccuracies during undrained construction. This process can be seen during inspection of the predicted excess pore water pressures after approximately 6 months of consolidation, see Figure 4.12b. In the soft unimproved soil mass a concentration of the excess pore water pressure at a depth of 15..20 m is observed with a maximum value of 11 kPa. In the treated zone the value of predicted pore pressures in the column material is approximately 1 kPa and in the surrounding soil is approximately 6..7 kPa. The excess pore water pressure contours after approximately 3 years of consolidation are plotted in Figure 4.12c.

4.3.7. Mobilised shear strength

Figure 4.13 shows the contours of the mobilised shear strength τ_{mob} , determined as $q/2$ (where q is the deviatoric stress) at the end of the consolidation process. On the left hand side the overall response is presented, whereas on the right hand side the scaled picture of the improved zone is plotted. The contours of the stone columns are indicated by the red solid lines. At a distance of approximately 15 m from the symmetry line of the embankment (or Z/B = 1.67, where Z is the distance from symmetry axis and B is the width of the embankment) the distribution of the mobilised shear strength is similar to the expected response for an embankment constructed on unimproved soil. Closer inspection of the treated zone concludes that the mobilised shear strength is predicted to be higher for the column material than for surrounding soft soil. For columns 1..4 in the centreline of the

embankment, the mobilised shear strength is predicted to be a value of 55 kPa up to a depth of approximately 5 m and then remains at 45 kPa in the lower part of the columns. The column which is located nearest to the embankment toe has a shear strength of 45 kPa up to a depth of 5 m. Below that depth, the mobilised shear strength decreased to a value of 35 kPa.

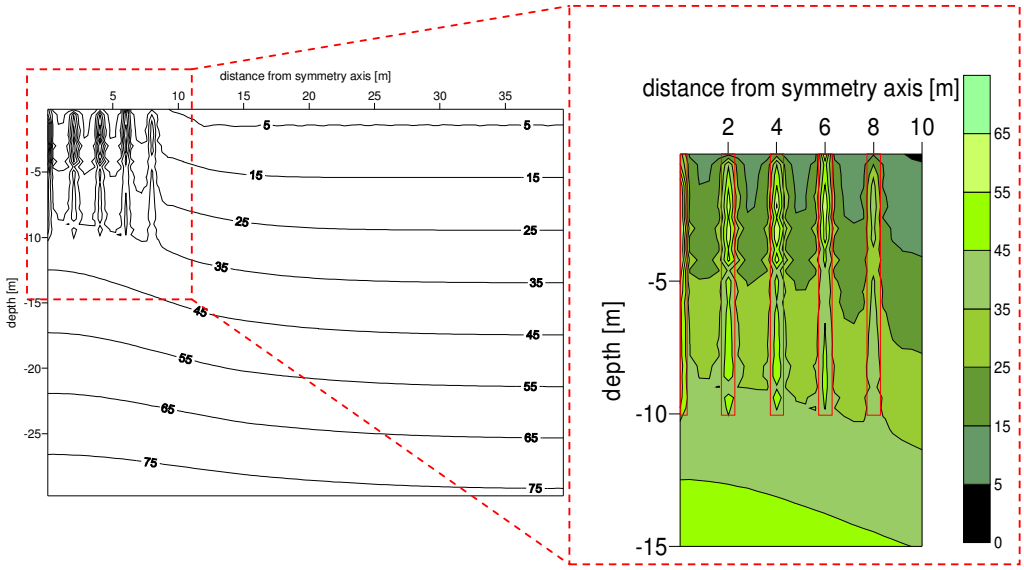

Figure 4.13: Mobilised shear strength contours (in kPa) at the end of consolidation: reference analysis.

4.4. Influence of mechanical properties of the stone columns

For the construction of the stone columns a gravelly material is usually used, which meets the specified requirements regulated by the various standards or guidelines (national or worldwide), see BS EN 14731:2005, Forschungsgesellschaft für das

Straβenwesen (1979) or NHBC (1988). As the column is formed using different types of gravel, the mechanical properties of the stone column will vary depending on the mechanical properties of the material used. Therefore, numerical simulations were performed, in order to asses the influence of the compaction and stiffness of the stone column material on the settlement predictions.

Values of the mechanical characteristics assumed in the numerical analysis are compared to the typical values for the stone column material widely used in industry. The same three-dimensional mesh as in the case of the reference analysis was used. The geometry of the embankment benchmark and the soil profile were not altered.

4.4.1. Strength of granular material

The friction angle plays a crucial role in the calculations of the bearing capacity of a soil improved with stone columns and the dilatation, expressed as the volume increase of the granular material, has a significant effect on the settlement reduction. As the columns are usually designed to yield, the friction and dilatancy angles of the granular material will influence the overall behaviour of the system. Thus, a parametric study to investigate the impact of those two factors on the numerical predictions was carried out, considering separately the influence of strength and column stiffness.

The effect of column strength (expressed as the angle of friction) is investigated in this section by varying only the angles of friction φ'_{SC} and dilatancy ψ'_{SC}. The most compacted stone column material chosen for the numerical simulations had an

angle of friction φ'_{SC} of 50˚ and resulted in a relatively high angle of dilatation (ψ'_{SC} = 20˚), see Table 4.7. The stiffness of the granular material was kept constant (see Table 4.5) and is considered separately in *Section 4.4.2*.

Table 4.7: Variation of angle of friction and dilatancy angle due to column compaction.

Set of parameters	φ'_{SC} [˚]	ψ'_{SC} [˚]
M1	40	10
REF	42	12
M2	44	14
M3	50	20

In large scale shear box tests in dense samples of granular material very high friction angles (above 50˚) have been measured at low normal stresses, see Herle *et al.* (2007). Herle *et al.* (2007) reported that the in-situ value of the friction angle of the stone column material is much closer to the value of 50˚ than previously thought. Therefore assuming an angle of friction below 40˚ cannot be justified, and the range of the friction and dilatancy angles in some recent studies is rather theoretical, e.g. see Poorooshasb & Meyerhof (1997) or Borges *et al*. (2009).

The importance of the column strength is evident looking at the plot of the settlement reduction ratio s_r in relation to the angles of friction and dilatancy of the stone column material, see Figure 4.14. The settlement reduction ratio s_r is determined as the ratio between the settlement with stone columns and settlement in the case of no ground improvement. One can observe a greater reduction of settlement in columns which allow a higher concentration of the stresses.

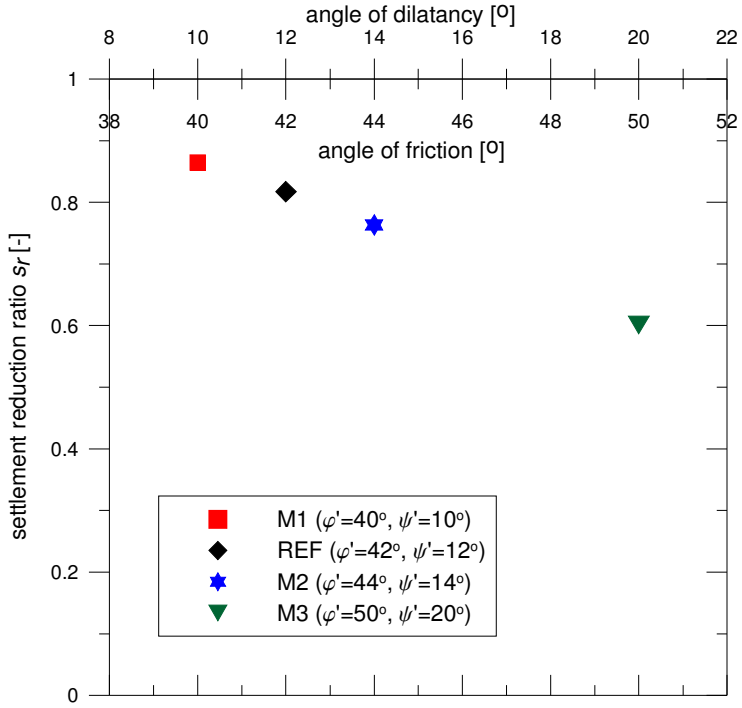

Figure 4.14: Relation between the densification of the stone column and the settlement reduction ratio.

Plots of the surface settlements after construction and at the end of primary consolidation are shown in Figure 4.15. After construction some surface heave is predicted (0.003 m), the magnitude is the same regardless of the friction angle of the granular material. The actual magnitude of the settlement is rather similar for all four cases, however the differences are more pronounced close to the centreline of the embankment. The reduction of the surface settlement of 25% just after construction is noticeable for the stone column material with a higher friction angle. Due to the nature of the stone columns, the surface settlements are smaller in the granular columns than in the surrounding soil.

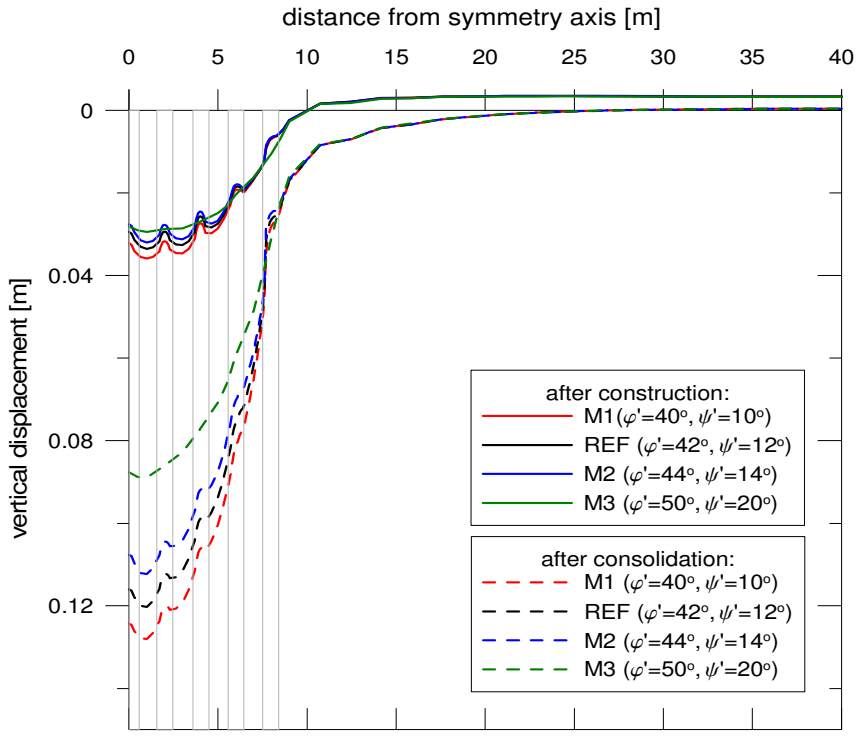

Figure 4.15: Surface settlement for different compaction levels of the granular material after construction and consolidation process.

The differential settlement (between the column and the surrounding soil at the centreline of the embankment) after the construction varies from 0.004 m to 0.001 m for simulations M1 and M3, respectively, and is hence insignificant. At the end of consolidation the same magnitude of differential settlements is predicted for simulations M1 and M3, respectively. Therefore it may be concluded that the angle of friction of the granular material has some influence on the differential settlements, and that angles of friction and dilatancy have greater impact when their values are around 50° and 20°, respectively. Moreover, at the end of consolidation the heave is no longer an issue. Again, the greatest displacements are predicted in the soft soil

next to the symmetry axis. An increase in the friction and dilatancy angles resulted in a reduction in the surface settlements at the end of consolidation of approximately 32% from 0.124 m to 0.084 m for M1 and M3, see Figure 4.15. The surface settlement plots converge at a distance of approximately 9 m from the symmetry axis and no difference can be seen outside the embankment footprint.

Looking at the settlement- time curve at the centreline of the embankment, one can see that an increase in the friction angle of the granular column leads to a noticeable reduction in the settlement, Figure 4.16. The influence of the friction angle of the gravelly material is pronounced during consolidation process.

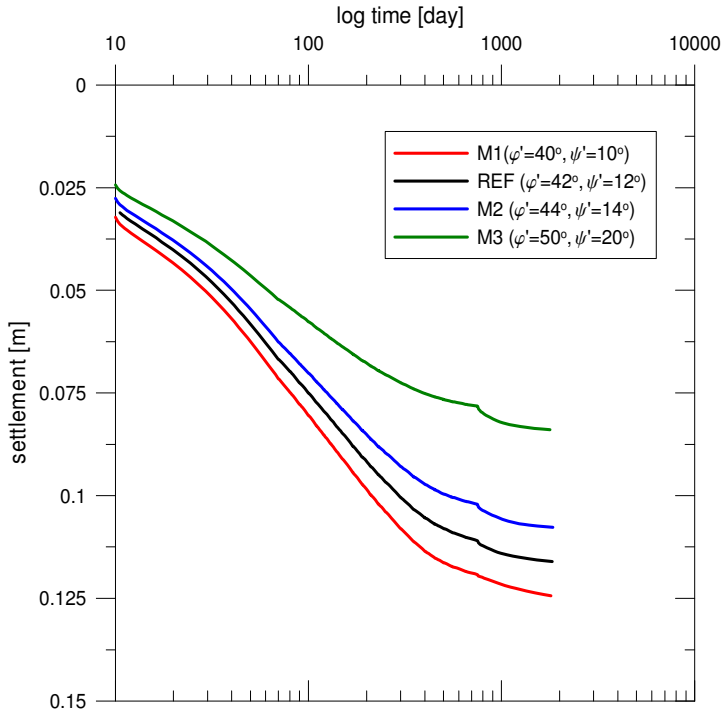

Figure 4.16: Settlement- time curve at the centreline of an embankment for different angles of friction of granular material.

4.4.2. Stiffness of granular material

In addition to the friction/dilatancy angle, compaction also influences the stiffness of the granular material. The stiffness of the granular material used for stone column construction varies depending on the origin of the material, the stiffness of the surrounding soil and the installation method. Talking about the influence of the column stiffness on the behaviour of the complex soil-column system one usually considers the modular ratio $E_{oed,SC} / E_{oed,soil}$, which is defined as the ratio between the one- dimensional deformation modulus of the column and the soil. Given both materials (soil and column) are non-linear, this ratio is never constant with depth, and will vary as soon as one of the stiffness or geometry parameters changes. It is usually expected that well compacted gravelly material will improve the settlement and bearing capacity of the treated soil, however the optimum modular ratio $E_{oed,SC} / E_{oed,soil}$ for the soil-column system may limit the reinforcing effect of the stone columns.

The impact of the stiffness of the granular material has been explored using three sets of parameters for the stone columns, see Table 4.8. The unit weight, Poisson's ratio, angle of friction and dilatancy have been assumed to be the same as stated in Tables 4.5 and 4.6.

Table 4.8: Variation of the column stiffness.

Set of parameters	$E_{50}^{ref} = E_{oed}^{ref}$ [kN/m^2]	E_{ur}^{ref} [kN/m^2]
REF	80 000	260 000
M4	100 000	325 000
M5	120 000	390 000

It would be worth investigating the impact of the predicted modular ratio $E_{oed,SC} / E_{oed,soil}$ on the obtained results. However, the column and soil are non-linear materials and are allowed to deform radially thus, the predicted modular ratio cannot be considered as oedometric. Moreover, their stiffness changes with depth. Therefore, the equivalent stiffness modulus in the vertical direction $E_{eq,v}$ was determined using the relationship between the incremental vertical effective stress to the incremental vertical strain at specific depth:

$$E_{eq,v} = \frac{\Delta\sigma'_y}{\Delta\varepsilon_y} \tag{4.2}$$

The evolution of the equivalent vertical modular ratio $E_{eq,v,SC} / E_{eq,v,soil}$ with depth is presented in Figure 4.17. The plot is limited to the treatment depth only. Increasing the column stiffness has no apparent influence on the evolution of the equivalent vertical modular ratio for simulations M4 and M5, see Figure 4.17. One can see that in the over- consolidated dry crust layer the increase in the stiffness of the granular material is less pronounced than in the soft clay strata and that the value of the equivalent stiffness modulus in the vertical direction $E_{eq,v}$ decreases with depth. It is expected that the magnitude of $E_{eq,v}$ will change also with time (e.g. after construction and consolidation, different values of $E_{eq,v}$ will be determined due to changes in the vertical effective stress and strains).

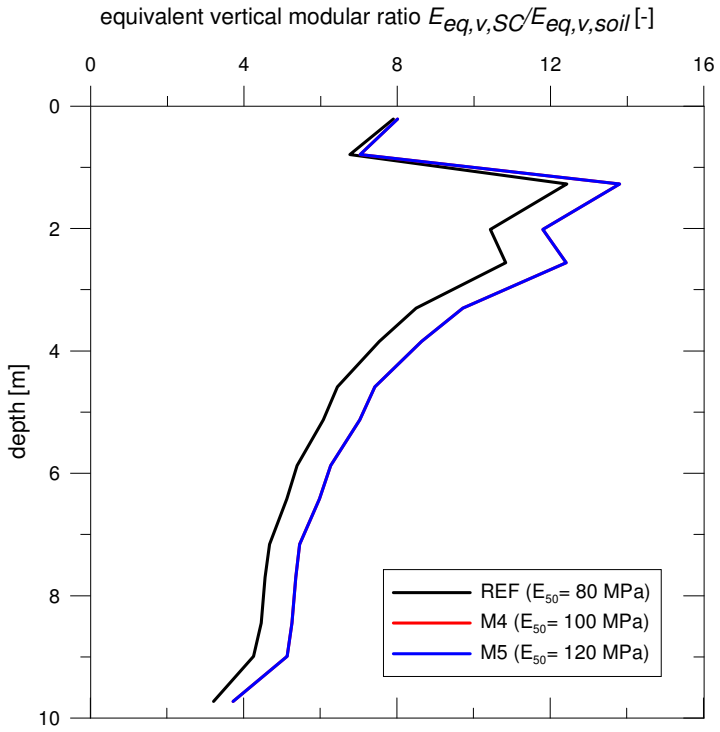

Figure 4.17: Evolution of the equivalent vertical modular ratio with depth.

As shown in Figure 4.18, the settlement reduction ratio s_r decreases with the increase of the equivalent vertical modular ratio $E_{eq,v,SC} / E_{eq,v,soil}$. The effect of the $E_{eq,v,SC} / E_{eq,v,soil}$ ratio is however almost negligible, so in terms of design the friction and dilatancy angles of the columns and the properties of the surrounding soil are more influential than the stiffness of the granular material. Moreover, the value of the equivalent vertical modular ratio $E_{eq,v,SC} / E_{eq,v,soil}$ will be limited by the compression modulus of the hosting soil and the mechanical properties of commercially available granular materials.

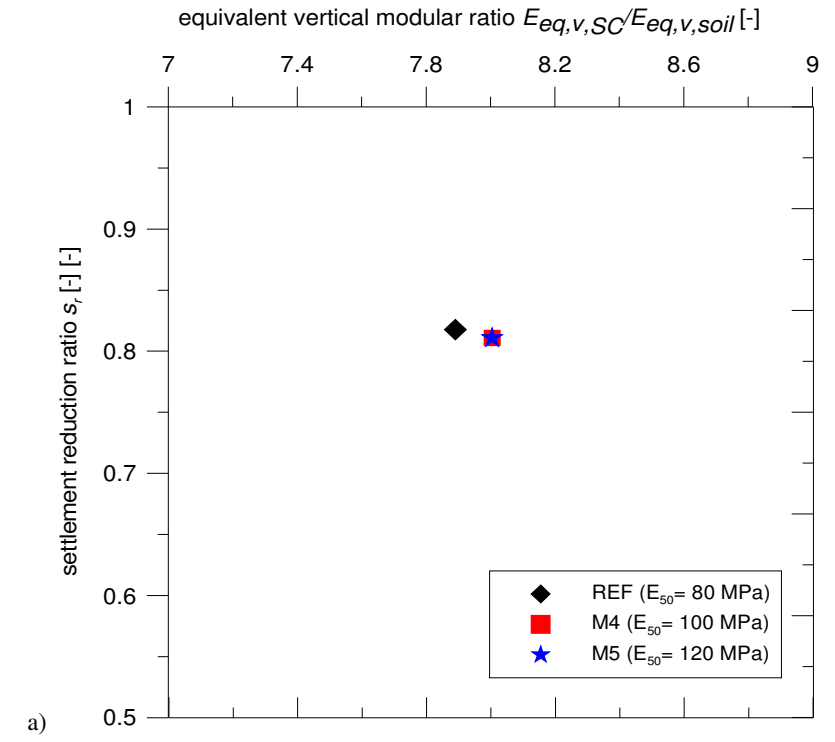

a)

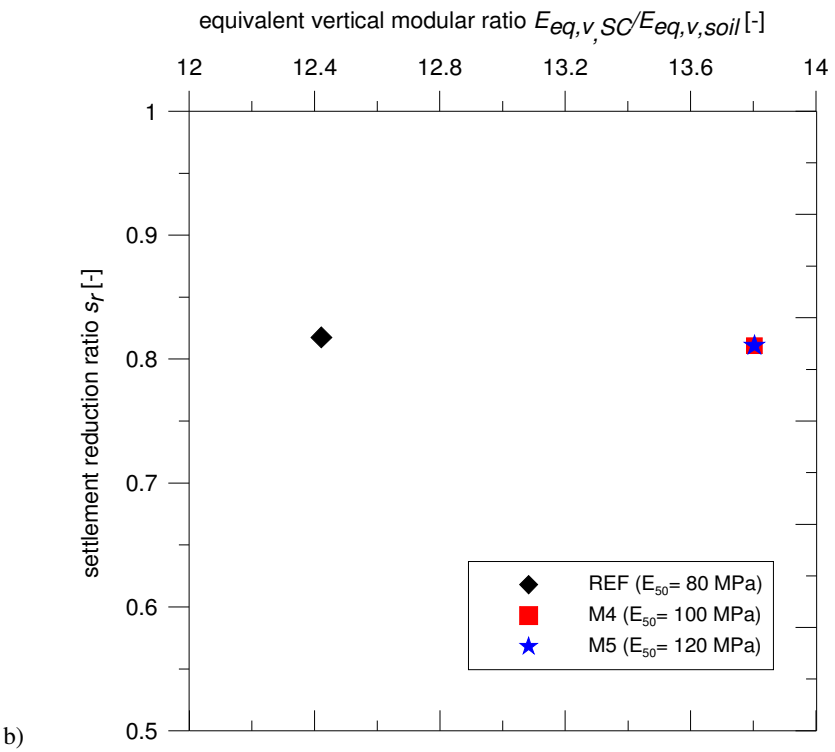

b)

Figure 4.18: Influence of the equivalent vertical modular ratio on the settlement reduction ratio at the top of layer: a) dry crust and b) Bothkennar clay.

4.4.3. Conclusions on the mechanical properties impact

The influence of mechanical aspects on the behaviour of stone column foundations has been investigated using three-dimensional FE analyses.

The angle of friction of the granular material was found to influence greatly the settlement reduction during the current parametric studies. Increasing the oedometric stiffness modulus of the stone column material had a minor influence on the predicted settlement response within the considered range of values. Some reduction in the predicted settlement values was shown to occur by increasing the equivalent vertical modular ratio. However, it can be concluded that the angle of friction of the granular material is a dominant mechanical aspect influencing the behaviour of the stone column foundations.

4.5. Influence of physical properties of the stone columns

In the next section of the parametric study, the influence of the column diameter D_{SC} is investigated, followed by the centre-to-centre spacing S_{SC} and the length of the granular column L_{SC}.

The geometry of the embankment benchmark and the soil profile are the same as presented in Figure 4.1 and 4.2. The mesh used for the numerical simulations considering column diameter and spacing is different than for that used for the

reference analysis in order to take account of changes in the physical properties of the column foundations.

4.5.1. Diameter of stone columns

The column diameter seems to be one of the easiest parameters to alter in the geotechnical design to satisfy the project requirements. As the most common stone column diameter used in the industry in Europe is 0.6 m, a parametric study considering the values close to that range was performed. The geometry of the area improved with stone columns was changed in the numerical simulations, taking into account the column diameter. The properties of the granular material, the spacing and the length of the stone columns were all kept constant when varying the diameter of the granular column, see Table 4.9.

Table 4.9: Variation of the column diameter.

Set of parameters	D_{SC} [m]	A_r [-]	Vr [-]	S_{SC} / D_{SC} [-]	L_{SC} / D_{SC} [-]
REF	0.6	0.07	0.02	3.33	16.67
P1	0.7	0.10	0.03	2.86	14.29
P2	0.8	0.13	0.04	2.50	12.50

The numerical predictions in relation to the settlement reduction ratio s_r and the area replacement ratio A_r are presented in Figure 4.19. The area replacement ratio A_r is the proportion of the area of the stone columns to the total area of the improved soil. In the case where the area ratio A_r is equal to zero, (i.e. no columns), the settlement ratio s_r is equal to one. According to analytical solutions, the

reduction in the settlement value by 50 % or more (when $s_r \leq 0.5$) can be obtained by installing the stone columns with an area ratio A_r equal to 0.2, see Figure 4.19. That might suggest in theory that the stiffer the soil-column area is, the greater the improvement in the performance for the same area ratio when compared to the untreated soil. Nevertheless, this has not been confirmed in many case histories which conclude differently.

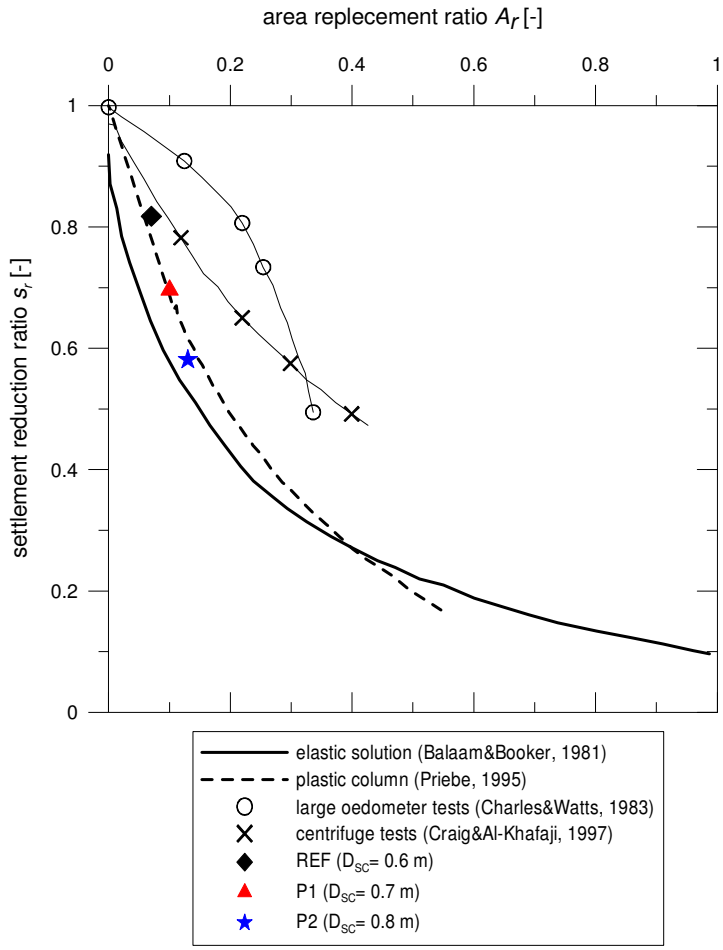

Figure 4.19: Stiffening effect of column diameter: parametric study and chosen solutions.

Additionally, the theoretical solutions and the laboratory data for stone columns described by various authors are compared with the numerical simulations. Four types of solution are presented within Figure 4.19; the elastic approach presented by Balaam & Booker (1981) along with the plastic solution by Priebe (1995) and two laboratory tests: the large oedometer test conducted by Charles & Watts (1983) and the centrifuge test on a tank foundation on sand columns in clay performed by Craig & Al-Khafaji (1997). Charles & Watts (1983) considered 5 configurations of the stone column in their study, varying the area replacement ratio from 0.002 to 0.330, whereas Craig & Al-Khafaji (1997) investigated 4 configurations of columns in the centrifuge model tests of a tank foundation, varying the area replacement ratio from 0.1 to 0.4. One can see that the numerical predictions are in a reasonably good agreement with previous experience. Indeed, larger differences would have been expected, given the analytical solutions by Balaam & Booker (1981) and Priebe (1995) are for end-bearing stone columns, which demonstrate how conservative the elastic solution given by Balaam & Booker (1981) is. The settlement reduction ratio s_r reduces as the column diameter increases.

The plot of the impact of the S_{SC} / D_{SC} on the settlement reduction ratio s_r is presented in Figure 4.20 based on the results of the parametric study. Additionally, the results for the experimental tests conducted on a group of 7 end-bearing stone columns constructed in soft clay in a cylindrical tank are plotted, see Ambily & Gandhi (2007). Ambily & Gandhi (2007) considered a triangular grid of columns and a sand layer was placed at the top of the clay to simulate a working platform. Furthermore, the numerical results for predictions obtained by Ambily & Gandhi (2007) using an axisymmetric approach with the Mohr-Coulomb's criterion for clay

and granular material are included. For the experimental and numerical study Ambily & Gandhi (2007) used the angle of friction for the stone column material values of 43˚ and 40˚, respectively, whereas for the current study a friction angle of 42˚ has been used.

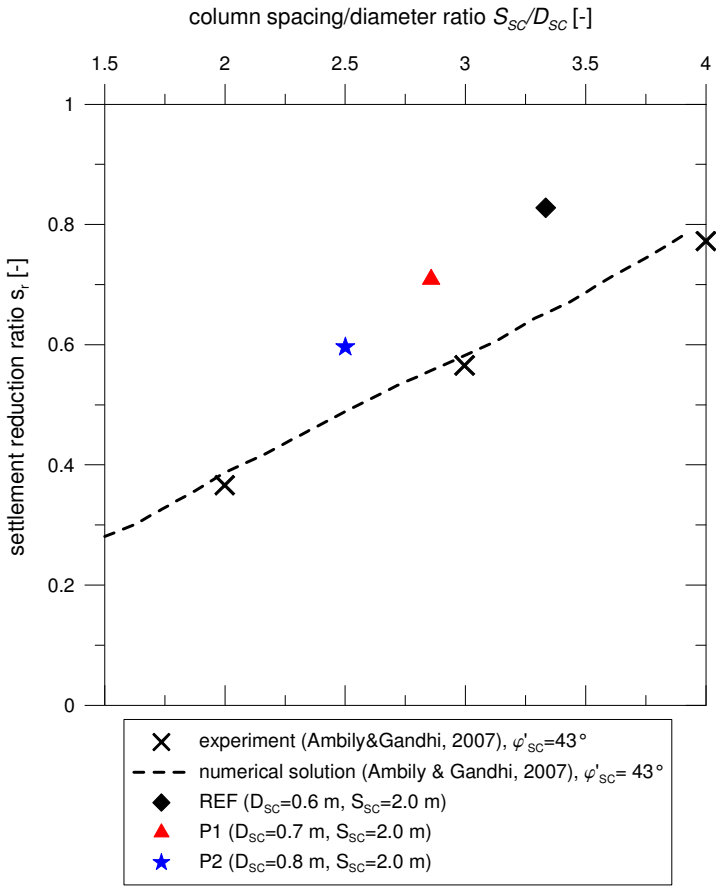

Figure 4.20: Effect of S_{SC} / D_{SC} on settlement reduction ratio.

It can be observed that the ratio S_{SC} / D_{SC} has a significant influence on the obtained settlement reduction ratio s_r. The stiffness effect reduces as the S_{SC} / D_{SC} ratio increases, see Figure 4.20. In contrast to the numerical studies carried out by Ambily

& Gandhi (2007), the numerical simulations presented in this parametric study considered the non-linearity of the material. Predictions by Ambily & Gandhi (2007) appear to be quite conservative when compared with the current study, however they considered end-bearing stone columns, whereas in this thesis the behaviour of floating columns is investigated.

4.5.2. Stone column spacing

Most research on the behaviour of stone columns has indentified the centre-to-centre spacing of the granular columns as having a significant impact. Therefore, numerical simulations were performed for this parametric study for three different column centre-to-centre spacings, see Table 4.10. The column diameter was kept constant at 0.6 m. The chosen range of column spacing was that which is typically used in the industry. Again, the width of the representative slice of the full three-dimensional geometry varied for each calculation, taking into account the arrangement of the stone columns.

Table 4.10: Variation of the column spacing.

Set of parameters	S_{SC} [m]	A_r [-]	Vr [-]	S_{SC} / D_{SC} [-]	L_{SC} / S_{SC} [-]
P3	1.7	0.08	0.03	2.83	5.88
REF	2.0	0.07	0.02	3.33	5.00
P4	2.3	0.06	0.02	3.83	4.35

The evolution of the surface settlement for three chosen points (the centreline, crest and toe of the embankment) with the centre-to-centre spacing is shown in

Figure 4.21. Inspection of the plot results in the conclusion that the column spacing is of greater importance at the centreline of the embankment, and with increasing distance from the axis symmetry its significance reduces, most likely due to the flexibility of the system, as the toe is not affected at all. As expected, smaller stone column spacing resulted in the reduction of the surface settlement.

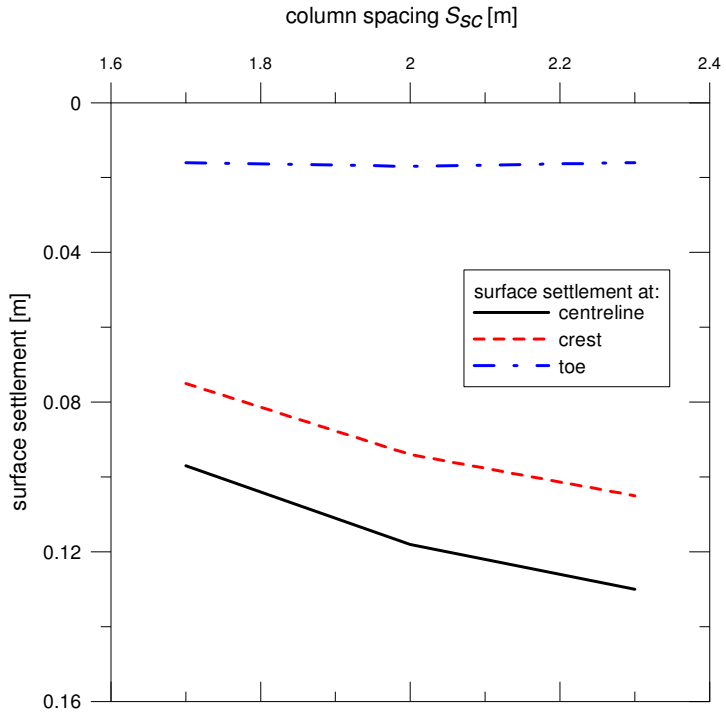

Figure 4.21: Evolution of the surface settlement with column spacing.

The evolution of the settlement reduction ratio s_r with column spacing S_{SC} is shown in Figure 4.22. One can see that as the S_{SC} increases the s_r value reduces: given the column spacing changes from 1.7 m to 2.3 m, the settlement reduction ratio decreases by approximately 23 %, see Figure 4.22.

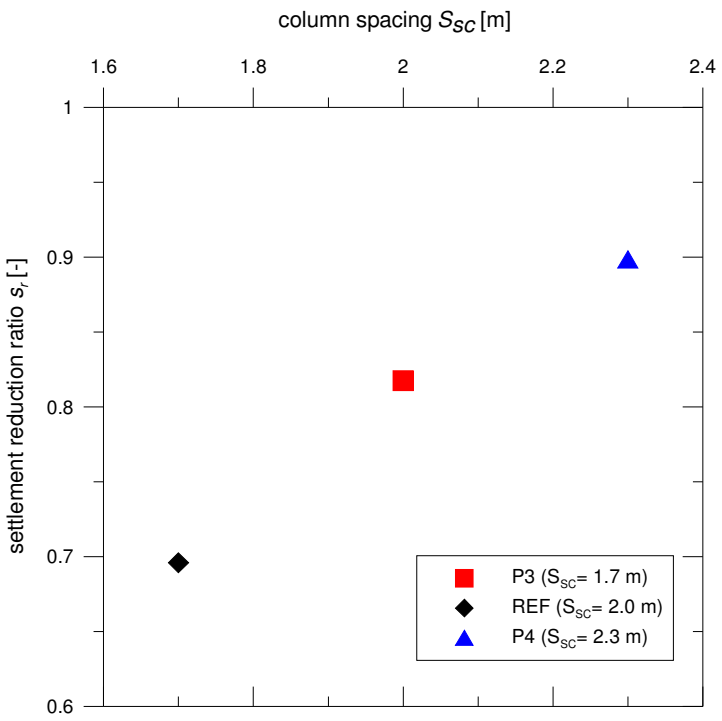

Figure 4.22: Evolution of the settlement reduction ratio with column spacing.

4.5.3. Length of stone columns

Column length is one of the key design parameters for stone column foundations and would be expected to influence the stress-strain behaviour of the column-soil system. To asses that impact, a parametric study of a simple benchmark problem was performed in which the column length was varied, see Table 4.11. Lengths of the stone columns of 5 m, 10 m and 15 m were considered. The three-dimensional mesh was created in advance, enabling the column material to reach the desired level. This excluded the possibility of the mesh-dependency influencing the results obtained.

Table 4.11: Variation of the column length.

Set of parameters	L_{SC} [m]	A_r [-]	Vr [-]	L_{SC} / S_{SC} [-]	L_{SC} / D_{SC} [-]
P5	5.0	0.07	0.01	2.50	8.33
REF	10.0	0.07	0.02	5.00	16.67
P6	15.0	0.07	0.04	7.50	25.00

Again, the properties of the soft soil, stone column and embankment fill materials were assumed according to Tables 4.1..4.6. The stone columns had a diameter of 0.6 m and a centre-to-centre spacing was 2.0 m.

A schematic sketch of the various points in the soft deposit chosen for the inspection of the excess pore water pressure is plotted in Figure 4.23.

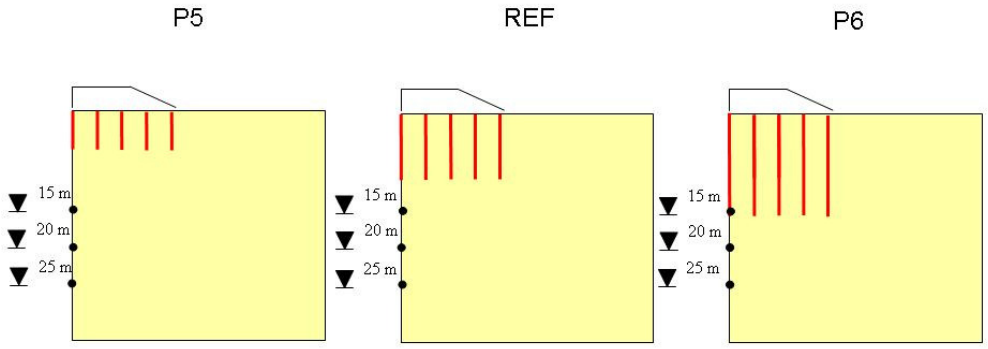

Figure 4.23: Geometry sketch with chosen points for study of the excess pore water pressure evolution: influence of column length.

The predicted evolution of the excess pore water pressures over time is shown in Figure 4.24. The plots have been prepared for depths of 15 m, 20 m and 25 m from the ground surface. The geotechnical sign convention has been applied, where negative values refer to suction. As observed in Figure 4.24, the process of building

up and subsequent dissipation of the excess pore water pressures during consolidation is associated with the Mandel-Cryer effect (Mandel, 1950 and Cryer, 1963), which is commonly present during coupled consolidation.

The plot of the excess pore water pressures at a depth of 15 m is presented in Figure 4.24a. The stone columns of length of 15 m (P6) reduce the consolidation time by factors of 10 and 19 when compared to simulations with a column length equal to 10 m (REF) and 5 m (P5), respectively. In the case of simulation P6, the stone column base is situated at a depth of 15 m.

Figure 4.24b presents the excess pore water pressures evolution with the consolidation time at a depth of 20 m from the ground surface. The differences between the numerical predictions for the three different column lengths are less pronounced. Longer columns (REF and P6) reduce the time needed for the excess pore water pressure dissipation more efficiently than the 5 m long columns (by a factor of approximately 1.6 and 3.3, respectively). However, the steepness of the excess pore water pressure dissipation curve for simulations REF and P6 (especially in the final part) is similar.

The plot of the excess pore water pressures with time at a depth of 25 m is shown in Figure 4.24c. At this depth the influence of the length of the granular columns is less pronounced than at shallower depths. Inspection after approximately 500 days into the consolidation process revealed that for the simulation with 5 m long columns (P5) the values of the excess pore water pressures were almost 2 times greater than for the calculation where 15 m long columns were considered (P6).

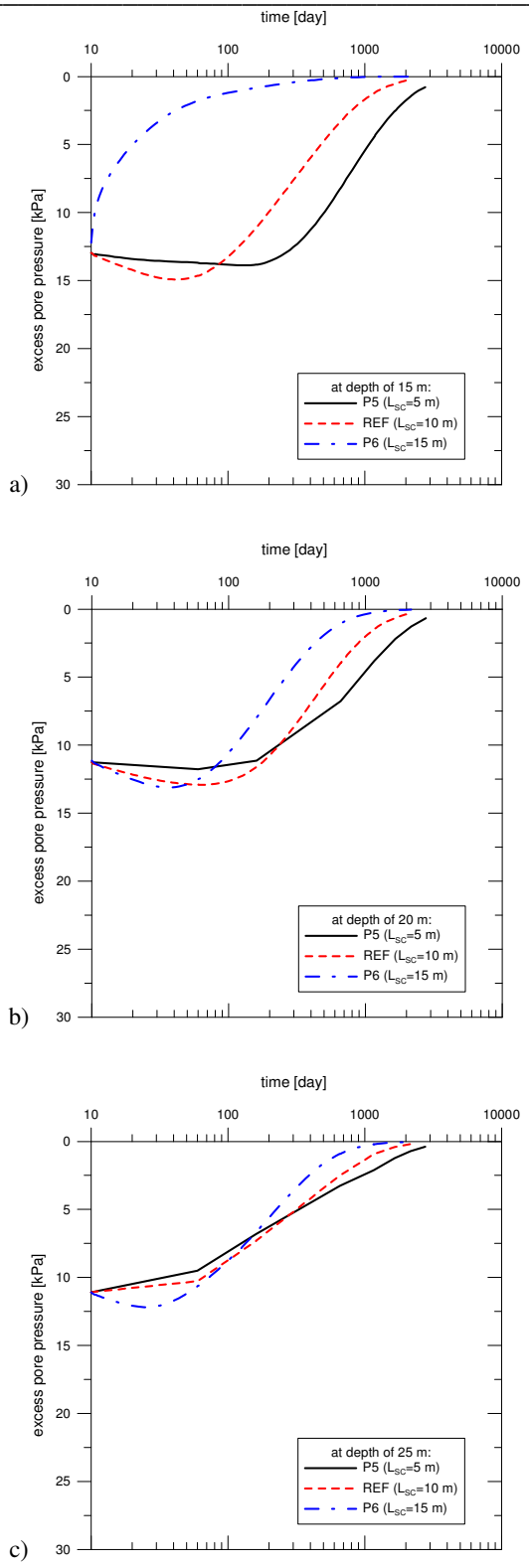

Figure 4.24: Excess pore water pressure vs. time at depths of a) 15 m, b) 20 m and c) 25 m.

The excess pore water pressure contours after construction and after approximately 3 years of consolidation are plotted in Figures 4.25 and 4.26. As expected, after construction the distribution of the excess pore water pressures at a distance of 10 m from the embankment symmetry axis are not influenced by the stone columns length, whereas the pattern underneath the embankment seems to be affected, see Figure 4.25. The general distribution of the excess pore water pressures is found to be similar. The predicted excess pore water pressure at the base of the stone column at the centreline of the embankment is double in the case of the 5 m long columns than for cases of the 10 m and 15 m long columns. However, the base of the column close to the toe of the embankment experienced almost an identical amount of excess pore water pressure build up during construction (approximately 12 kPa). Some local concentration of the excess pore water pressures in the stone column material can be seen in Figure 4.25 which is due to local numerical inaccuracies during undrained construction.

The excess pore water pressure contours after approximately 3 years of consolidation are plotted in Figure 4.26. Different excess pore water pressure distributions were predicted for the various column lengths. Inspection of the untreated soil zone revealed a still notable concentration of excess pore water pressures in the case of the short (5 m long) stone columns, compared to the other cases. For simulations with 5 m long columns (P5), at the bases zero excess pore water pressures were predicted, however excess pore water pressures in-between the columns were not fully dissipated and the area beneath the treated soil experienced a greater amount of excess pore water pressures than in the case of the granular column with a length of 10 m or 15 m.

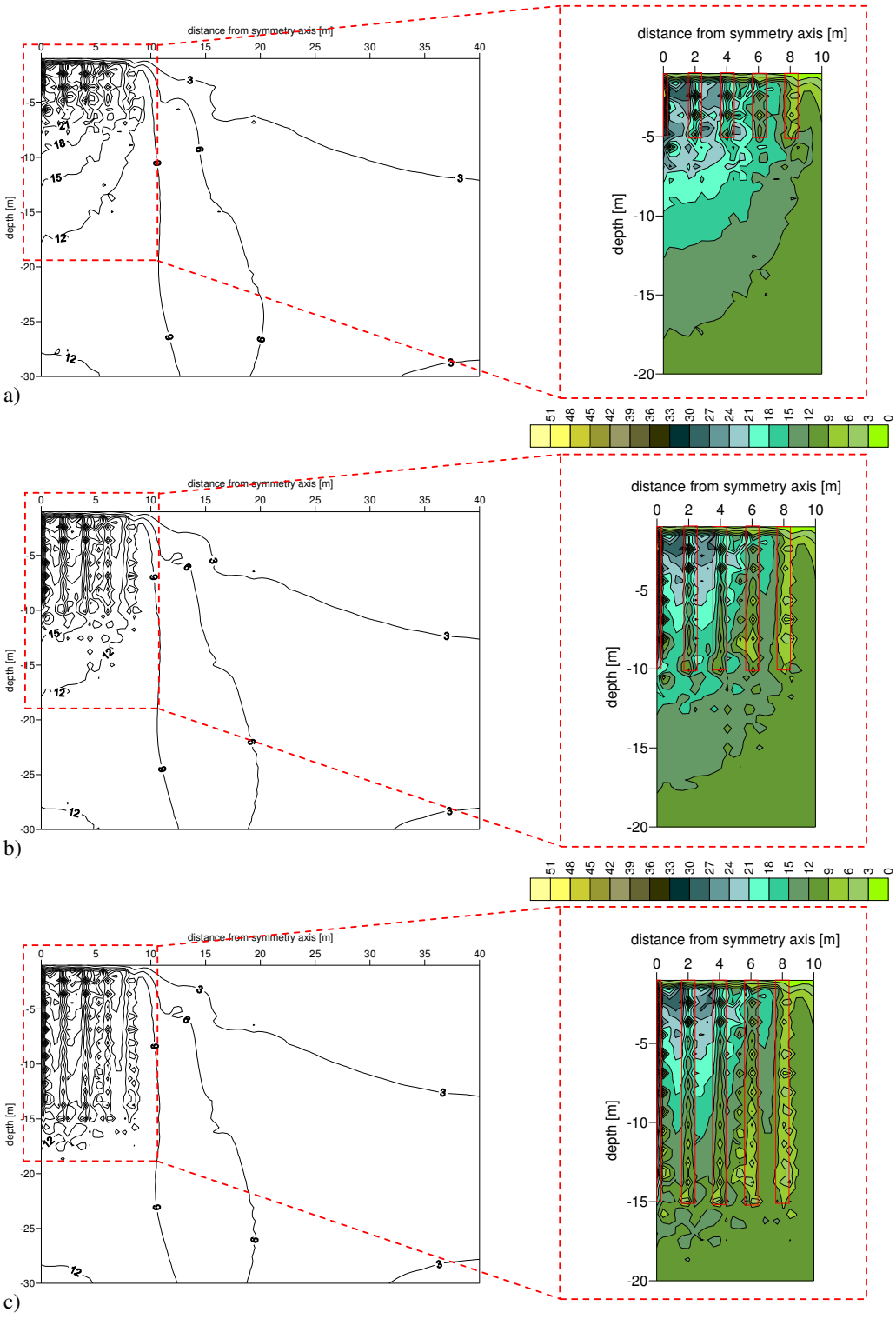

Figure 4.25: Excess pore water pressures contours (in kPa) after construction for:

a) P5 (L_{SC} = 5 m) b) REF (L_{SC} = 10 m) and c) P6 (L_{SC} = 15 m).

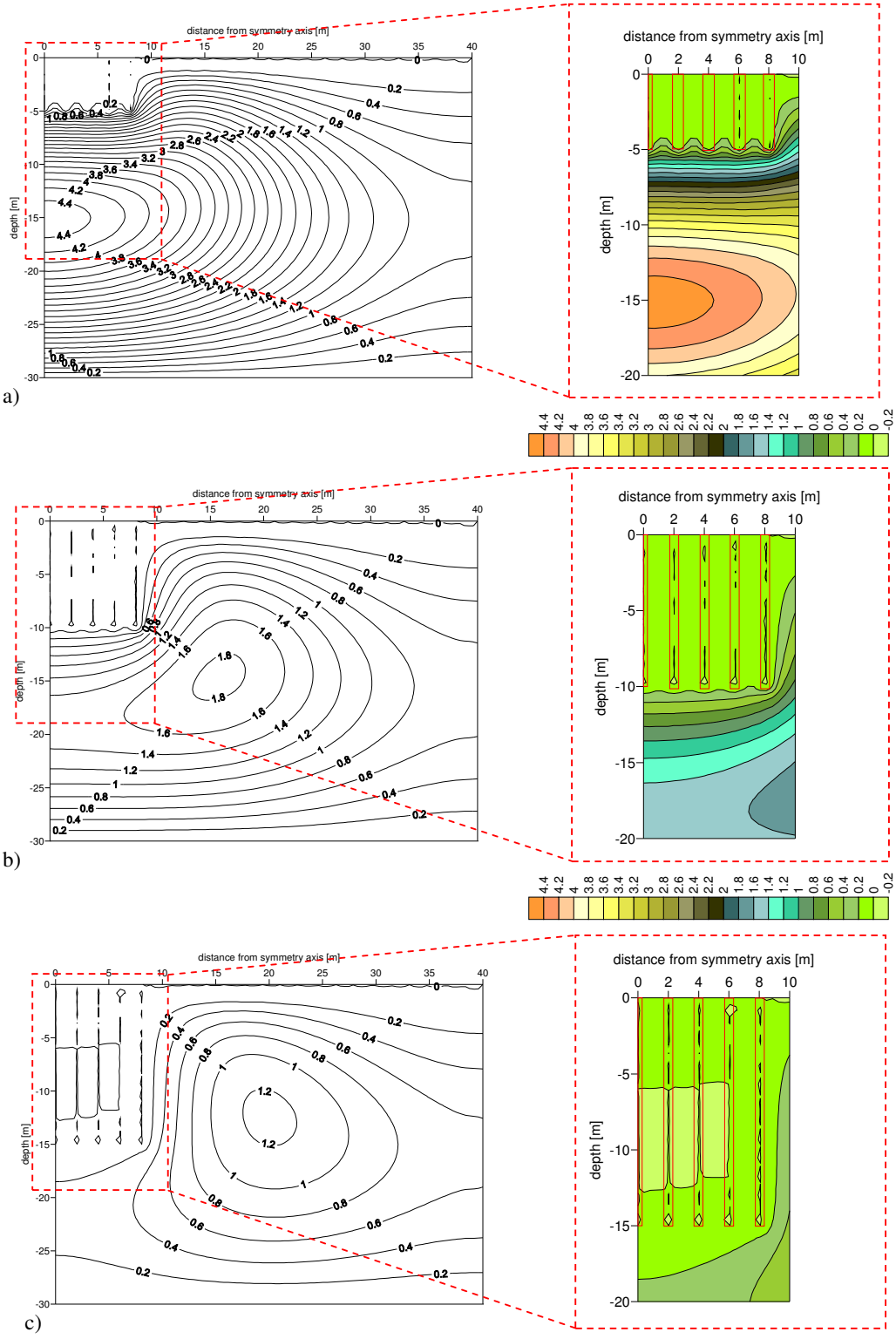

Figure 4.26: Excess pore water pressures contours (in kPa) after 3 years into the consolidation for:

a) P5 (L_{SC} = 5 m) b) REF (L_{SC} = 10 m) and c) P6 (L_{SC} = 15 m).

The predicted magnitude of the excess pore water pressures for simulations REF (L_{SC} = 10 m) and P6 (L_{SC} = 15 m) was similar. It seems that the efficiency of the column foundation in terms of the dissipation of the excess pore water pressures can be ensured by installing the stone columns with the L_{SC} / D_{SC} and L_{SC} / S_{SC} equal to 17 and 5, respectively. Above these values, the granular columns have a less pronounced effect on the numerical predictions.

The evolution of the settlement reduction ratio s_r with the volume replacement ratio V_r is presented in Figure 4.27. The volume replacement ratio is the ratio between the volume taken by the stone columns and the total soil volume.

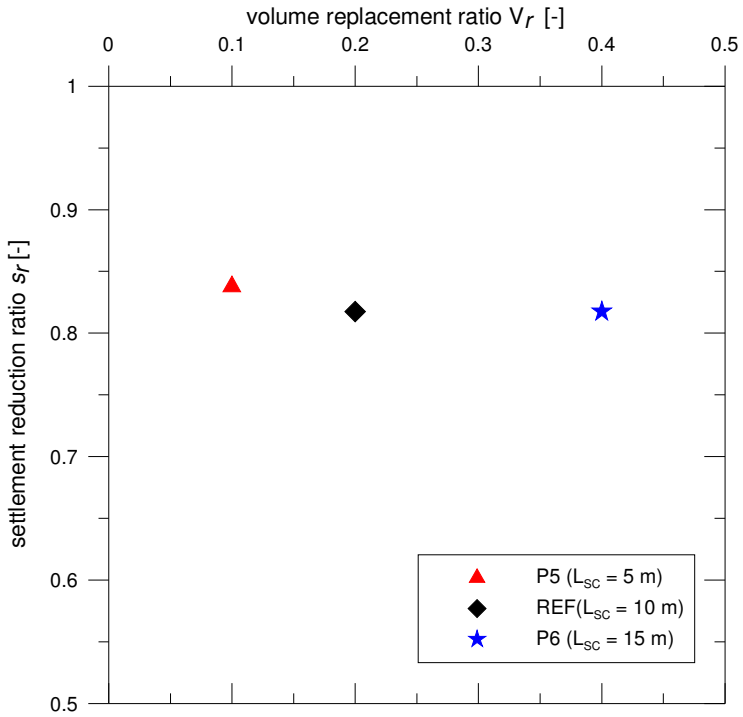

Figure 4.27: Evolution of the settlement improvement ratio with the volume replacement ratio: column length.

It is obvious that the column length is one of the determining factors for the settlement predictions of the stone column foundation. However, although an increase in the settlement reduction ratio was predicted, when the length was beyond 10 m no notable improvement was predicted. This suggests that the improvement occurs when the ratios L_{SC} / D_{SC} and L_{SC} / S_{SC} are less or equal to approximately 17 and 5, respectively.

Figures 4.28..4.30 show the predicted column deformation after construction and at the end of consolidation for the three different column lengths. All the deformation plots have been scaled up by 25 times to enhance the mechanisms. One can see that the predicted deformation at the end of construction occurs in the upper part of the stone column, regardless of the column length, whereas the bases of the columns remained undeformed. The deformation occurs in the upper part of the stone column at a depth of 2.8 to 3.7 times the column diameter. For short stone columns, where the ratio L_{SC} / D_{SC} is equal to 8.33 the deformation occurred at a depth of 2.8 to 3.2 times the diameter of the stone column, whereas for 15 m long columns (with ratio $L_{SC} / D_{SC} = 25$) the bulging occurred at a depth of 3.4 to 3.7 times the column diameter. This confirms previous studies which have suggested that the bulging mechanism occurs at a depth equal to 2 to 3 times the column diameter.

McKelvey *et al.* (2004) indicated that the critical column length is $L_{SC} / D_{SC} = 6$ and concluded that above that value the deformation in the floating stone column beneath a footing occurs in the upper region of the column. The base of the granular column remains undeformed, which suggests little or no load transfer in that area. As the

presented parametric studies consider columns with the ratio $L_{SC} / D_{SC} > 6$, the deformation would be expected in the upper column zone only.

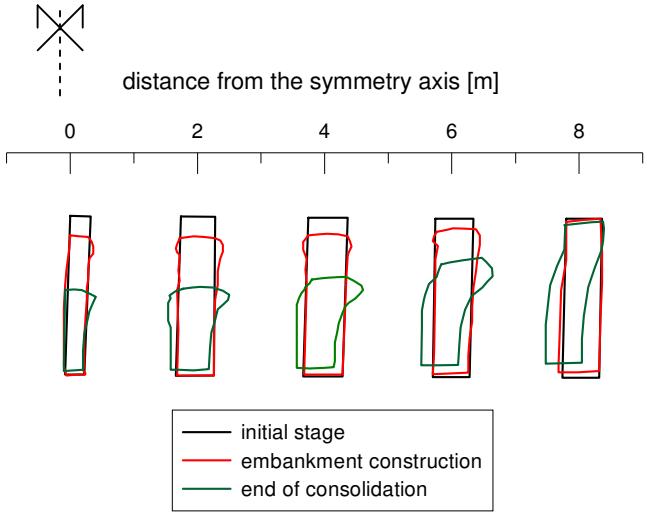

Figure 4.28: Deformation pattern for simulation P5 (L_{SC} = 5 m); scaling factor 25.

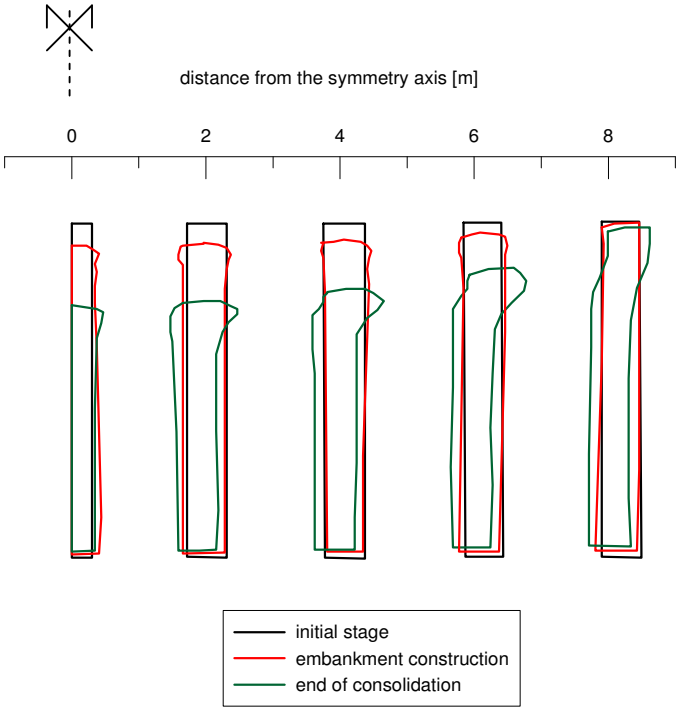

Figure 4.29: Deformation pattern for simulation REF (L_{SC} = 10 m); scaling factor 25.

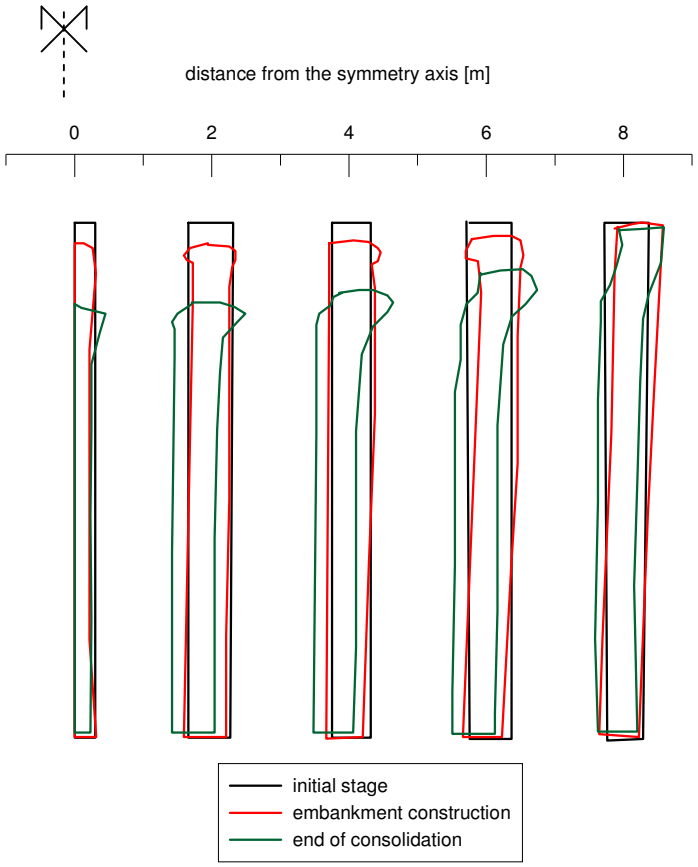

Figure 4.30: Deformation pattern for simulation P6 (L_{SC} = 15 m); scaling factor 25.

The bulging predicted by the FE simulations matches largely the mechanisms described by Kirsch (2004). However, the mechanism predicted by the numerical simulations of the outer stone column is somehow more pronounced than that presented by Kirsch (2004). The centre column experiences a much smaller deformation than the columns located close to the embankment toe which can be explained by the restraint provided by neighbouring columns.

For the stone column at the symmetry axis of the embankment a more uniform deformation is observed, whereas the mechanism of bending and bulging is noticed for the edge columns. The stone columns close to the toe of an embankment have undergone a non-restrained deformation in the direction towards the untreated zone and experienced non-uniform loading from the fill material weight.

In order to investigate the influence of the embankment height (i.e. the magnitude of the loading applied onto the improved area of the soft soil layer) on the optimum column length, additional simulations were performed. Evolution of the surface settlements with the column length L_{SC} is presented in Figure 4.31. One can see, as expected, that with an increase in the embankment height, the corresponding surface settlement increases. The rate at which the predicted surface settlements vary dependent on the column length is influenced by the embankment height; the change in settlements is more pronounced in the case of the higher embankment than in the case of a lower one.

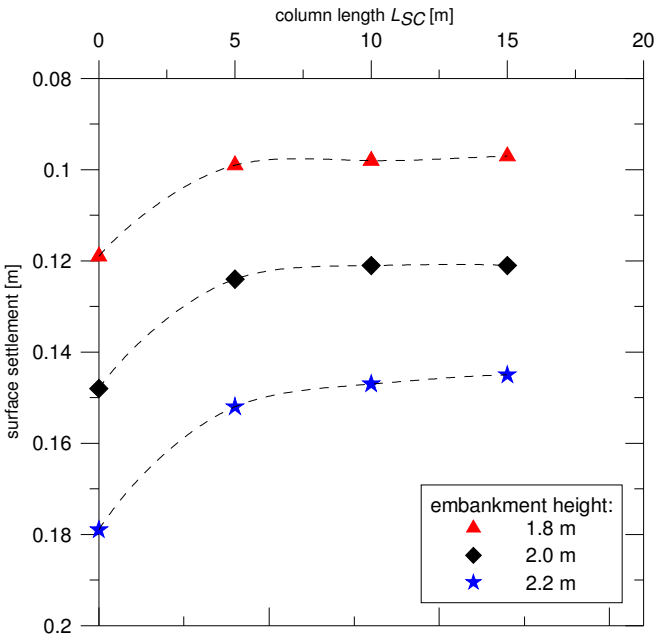

Figure 4.31: Evolution of the surface settlement with the column length: influence of embankment height.

Prediction of the settlement reduction ratio s_r as a function of the column length/spacing ratio L_{SC} / S_{SC} and the column/diameter ratio L_{SC} / D_{SC} for calculations in which the embankment heights (loading regime) have been varied are presented in Figures 4.32a and b, respectively. Research suggests that there is a certain L_{SC} / S_{SC} ratio and L_{SC} / D_{SC} ratio beyond which improvement is less pronounced. The current study indicates that the optimum ratio is about 5 and 17 for the L_{SC} / S_{SC} and the L_{SC} / D_{SC} ratios, respectively.

4.5.4. Conclusions on the effect of the physical properties

The assessment of the physical properties of the stone columns has been conducted, by varying the column diameter, spacing and the length. The studies considered both the short and long term behaviour of the stone column foundation on a soft soil deposit.

As expected, the settlement reduction ratio s_r reduced as the column diameter increased. Additionally, increasing the column diameter reduced the horizontal displacement contours at depth. When the soil is the subject of non uniform loading (as in the case of an embankment slope) it displaces laterally in a greater manner.

The columns spacing/diameter ratio S_{SC} / D_{SC} had a significant influence on the settlement reduction ratio s_r.

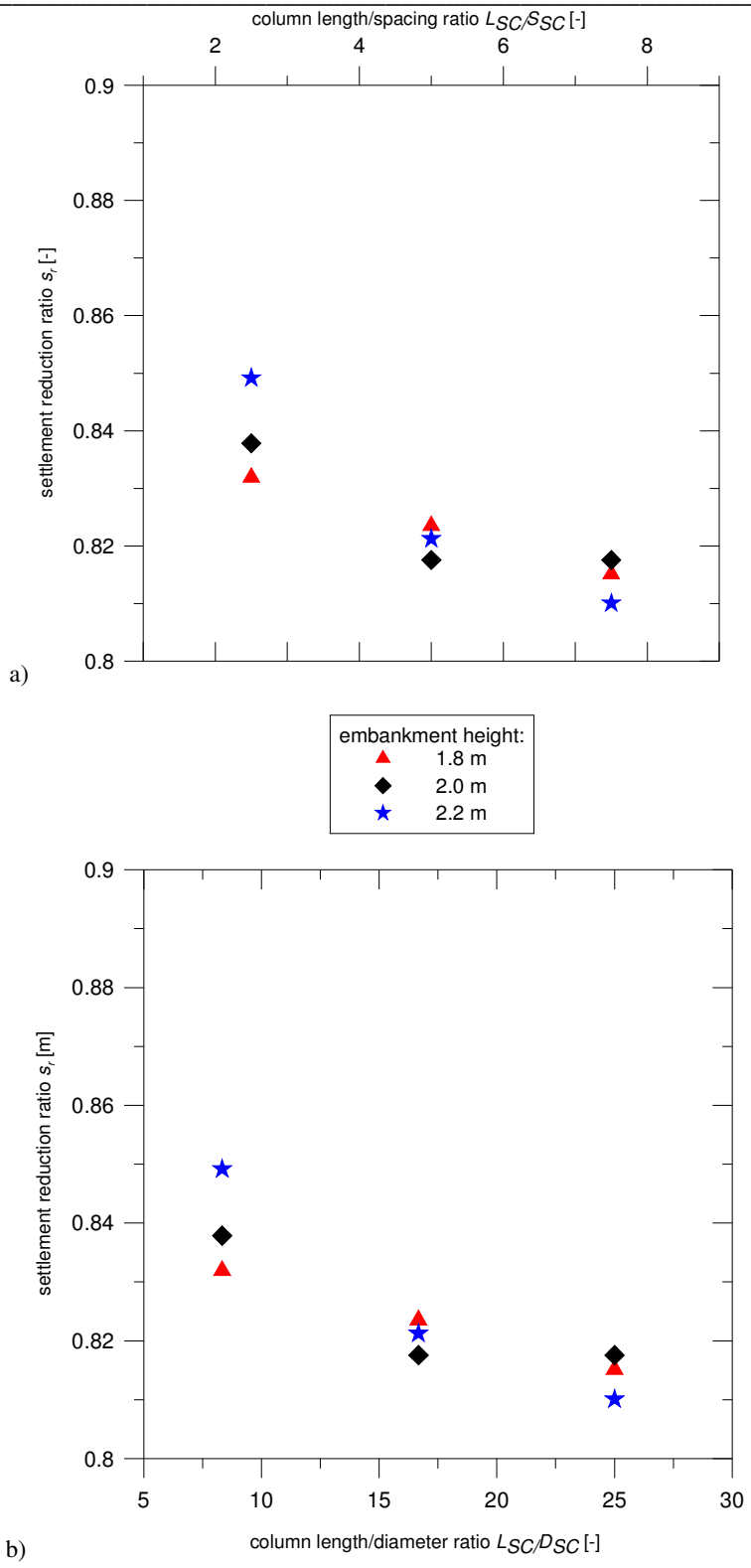

Figure 4.32: Influence of the embankment height on the: a) L_{SC} / S_{SC} and b) L_{SC} / D_{SC} .

To illustrate that, results for the whole set of parametric studies dealing with the geometry of the stone columns are summarised in Figure 4.33 by plotting the impact of the S_{SC} / D_{SC} on the s_r.

Following the findings from this research, a relationship between the settlement reduction ratio s_r and the column/spacing ratio S_{SC} / D_{SC} was established using two different approaches. First, a logarithmic relationship going through all the data points was determined, this is drawn in Figure 4.33 as a bold black line. This relationship is defined as:

$$s_r = 0.74 \times \ln(S_{SC} / D_{SC}) - 0.08 \tag{4.3}$$

Then, an alternative simple bi-linear relationship for the considered benchmark problem was also defined, and is plotted in Figure 4.33 as dotted red lines, for case $S_{SC} / D_{SC} \langle 2.8$ and $S_{SC} / D_{SC} \geq 2.8$, respectively. This relationship can be described as follows:

$$s_r = \begin{cases} 0.33 \times S_{SC} / D_{SC} - 0.25 & if \quad S_{SC} / D_{SC} \langle 2.8 \\ 0.21 \times S_{SC} / D_{SC} + 0.11 & if \quad S_{SC} / D_{SC} \geq 2.8 \end{cases} \tag{4.4}$$

In order to check the validity of *Eq.(4.3)* and *(4.4),* some hand calculations and a few additional numerical simulations were performed: with the S_{SC} / D_{SC} equal to 2 and 4, respectively. Predictions in the form of the settlement reduction ratios related to the column spacing/diameter ratio are presented in Figure 4.34.

Application of the FE leads to a corresponding value of the settlement reduction ratio for the case where $S_{SC} / D_{SC} = 2$ and $S_{SC} / D_{SC} = 4$ of 0.40 and 0.92 respectively, see Figure 4.34.

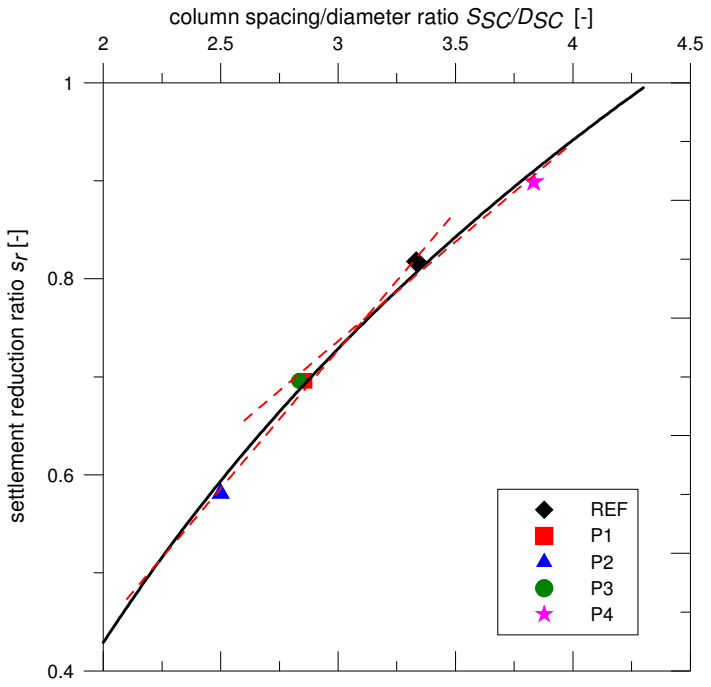

Figure 4.33: Evolution of the S_{SC} / D_{SC} ratio with the settlement reduction ratio.

Using *Eq. (4.3)* one can calculate an expected settlement reduction ratio s_r as:

$$s_r = \begin{cases} 0.74 \times \ln(2) - 0.08 = 0.43 & if \quad S_{SC} / D_{SC} = 2 \\ 0.74 \times \ln(4) - 0.08 = 0.95 & if \quad S_{SC} / D_{SC} = 4 \end{cases} \tag{4.5}$$

However, using *Eq.(4.4)* one can calculate an expected settlement reduction ratio s_r as:

$$s_r = \begin{cases} 0.33 \times 2 - 0.25 = 0.41 & if \quad S_{SC} / D_{SC} = 2 \\ 0.21 \times 4 + 0.11 = 0.94 & if \quad S_{SC} / D_{SC} = 4 \end{cases} \tag{4.6}$$

Although, the differences between calculations with *Eq. (4.3)* and *Eq. (4.4)* are small, it seems that the bi-linear relationship describes the predicted settlement reduction

ratio for the certain S_{SC} / D_{SC} values considered in the boundary value problem better, see Figure 4.34. Additionally, field data corresponding to floating stone columns installed in a square grid as a support for embankments as presented by Raju *et al.* (2004) and Raju (1997) are presented in Figure 4.34.

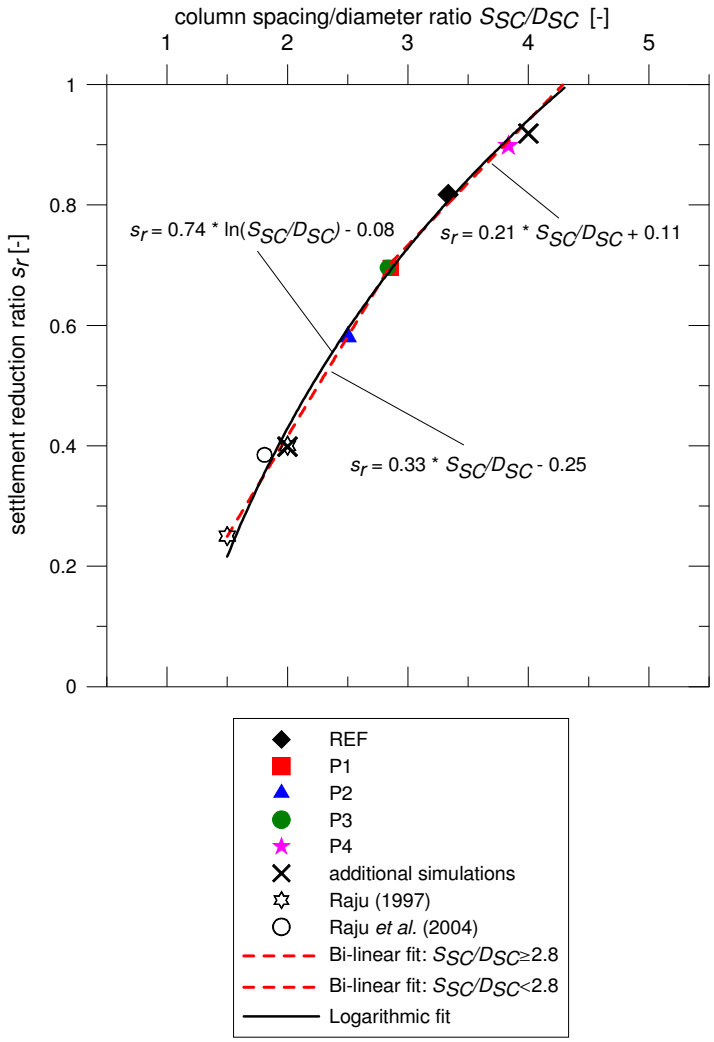

Figure 4.34: Validation of the linear and logarithmic relationships between the s_r and the S_{SC} / D_{SC} ratio.

In each case the stone columns were constructed in soft Malaysian silt and clay. The lack of field data, where the S_{SC} / D_{SC} ratio is equal to or more than 2.8, means that only preliminary conclusions can be drawn, however the bi-linear relationship shows good agreement with the reported field data. Current numerical simulations suggest that there is a certain S_{SC} / D_{SC} ratio beyond which improvement in terms of settlement is marginal. The current study indicates that the optimum ratio, beyond which the rate of increase of the benefits reduces, is about 2.7..2.8. Proposed relationships can be used as guidance on the expected settlement reduction ratio when z specific S_{SC} / D_{SC} ratio is assumed. Future research should be conducted in order to study the sensitivity of the over-consolidation ratio on the S_{SC} / D_{SC} ratio and to determine the existence and possible form of similar relationships for different geotechnical problems where stone columns are used as a foundation in various engineering structures.

Column spacing has a great influence on the settlement predictions, especially at the centreline of the embankment. This importance reduces with distance from the symmetry axis.

The column length is of great significance for the consolidation process: longer columns enabled faster and more efficient dissipation of excess pore water pressures. However, when the L_{SC} / D_{SC} and the L_{SC} / S_{SC} ratios were more than 17 and 5, respectively, the influence on the predicted speed of the consolidation process was found to be marginal. Deformations in the upper part of the columns were found regardless of the column length. The stone columns under the embankment and the embankment slope are to experience little deformation as the neighbouring columns

provide restraint. The columns close to the toe of the embankment experience non-restrained deformations in the direction towards the unimproved soil.

The optimum L_{SC} / D_{SC} and L_{SC} / S_{SC} ratio value was found to be less or equal to 17 and 5, respectively. The numerical results suggest that the magnitude of load (embankment height) has little influence on the optimum L_{SC} / D_{SC} and L_{SC} / S_{SC} ratios in the case considered. As expected, it was found that the rate at which the surface settlements occur for the different column lengths varies with the embankment height and that the change in settlement value is more pronounced in the case of a higher rather than a lower embankment.

4.6. Influence of thickness of the soft deposit

As stone columns in practice are installed either as floating or end-bearing columns, numerical simulations considering granular columns constructed on a rigid layer were also performed. Additionally, an analysis varying the soft deposit thickness from 10 to 30 m was conducted.

Similar to the other FE analysis of the reference analysis, the soft deposit was simulated using the S-CLAY1S model and the bedrock, on which the stone columns were founded, was modelled using the simple Mohr-Coulomb model. The soil profile of all cases is presented in Figure 4.35 and the summary of the different simulations is collated in Table 4.12.

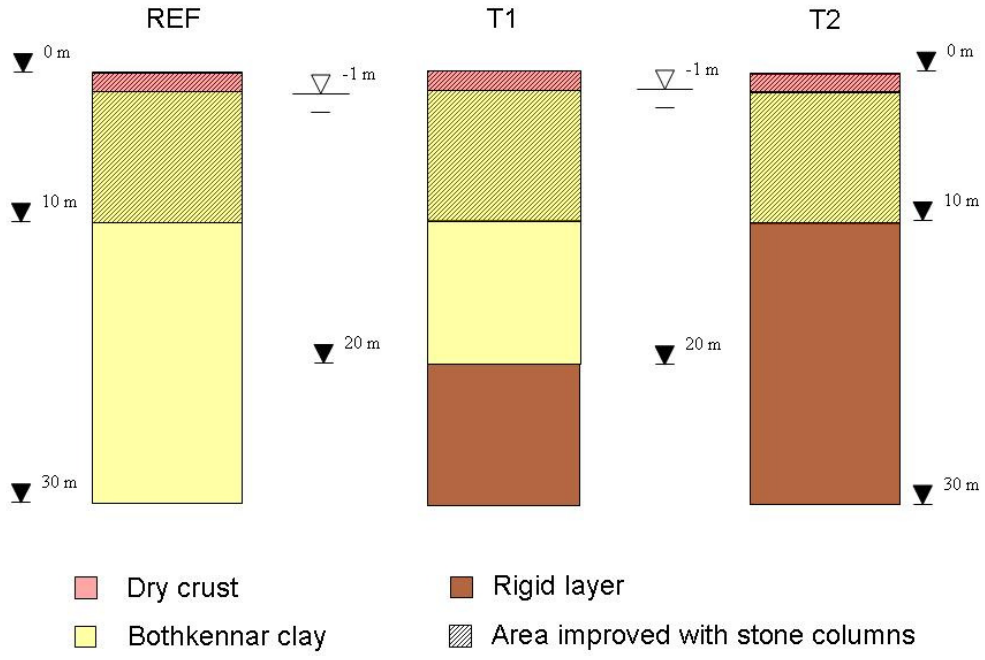

Figure 4.35: Soil profile used in simulations investigating the influence of the soft deposit.

Table 4.12: Variation of the soft deposit thickness.

Set of parameters	Thickness of soft layer d_{ss} [m]	Type of columns	A_r [-]	V_r [-]
REF	30.0	Floating	0.07	0.02
T1	20.0	Floating	0.07	0.04
T2	10.0	End-bearing	0.07	0.07

Figure 4.36 shows the stiffening effect of the soft deposit thickness along with selected field data results for end-bearing granular columns. The predictions for the numerical simulations considering floating stone columns and columns founded on the rigid strata are also presented.

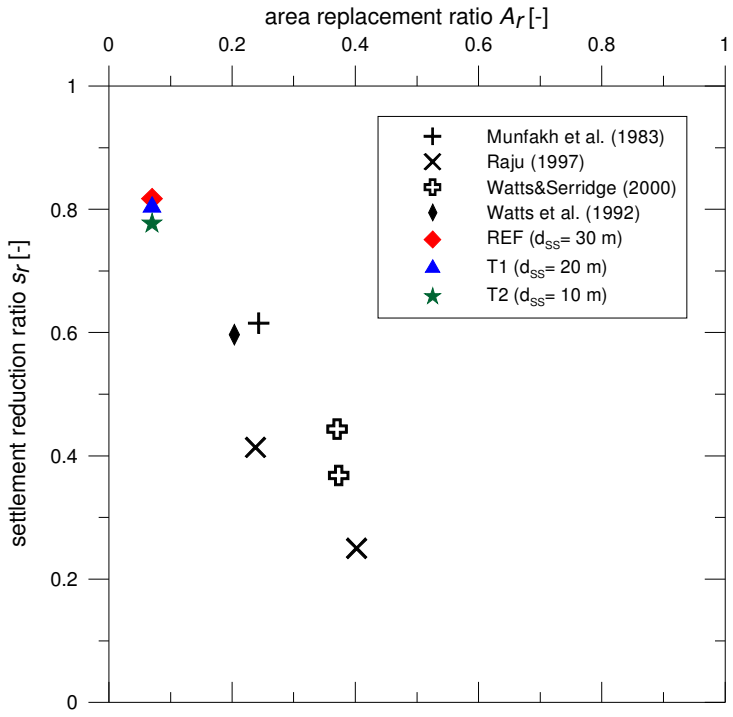

Figure 4.36: Stiffening effect of thickness of soft deposit: parametric study and selected field data.

It can be observed that end-bearing stone columns founded on a rigid layer gave a lower settlement reduction ratio s_r than both cases of floating columns (constructed in 20 m and 30 m thick soft layer, simulation REF and T1, respectively), which means that a greater amount of improvement was noticed for those granular columns. The field data presented on the plot considers the end-bearing stone column for different column diameters and lengths along with different column applications. An exceptional high settlement reduction ratio s_r for floating stone columns installed in a 30 m thick soft deposit (simulation REF) was due to the lack of the stiffening effect of a deeper bedrock layer.

Figure 4.37 shows the influence of the soft deposit thickness on the settlement reduction ratio s_r. One can notice that an increase in the soft soil thickness resulted in an increase in the s_r value, however from a practical point of view the differences are marginal. In the case of the 10 m thick soft layer (T2), the stone columns were founded on the rigid stratum which gives additional support to the columns.

The impact of the thickness of the soft deposit on the numerical predictions in terms of consolidation time is presented in Figure 4.38. For this plot the results for end-bearing and floating stone columns have been collated. One should remember that the numerical simulation considering the soft deposit thickness equal to 10 m was conducted for end-bearing granular columns (T2), whereas the results for the floating stone columns reflected the thickness of the soft stratum of 30 m (REF). Again, it can be observed that the time needed to finish the consolidation process is shorter in the case of the soft deposit with a smaller thickness (approximately by a factor of three). The effect of the thickness of the soft deposit on consolidation time is an important factor, far more important than the total settlement. Consequently, although floating stone columns can be very effective in overall settlement reduction, in the case of a thick soft stratum, column lengths may need to be extended in order to reduce the consolidation time.

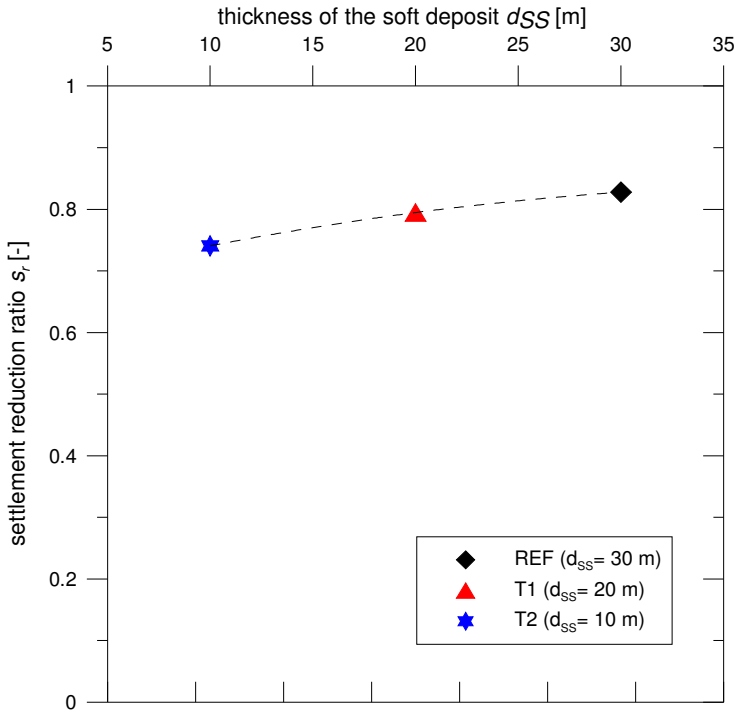

Figure 4.37: Impact of the soft deposit thickness on the surface settlement.

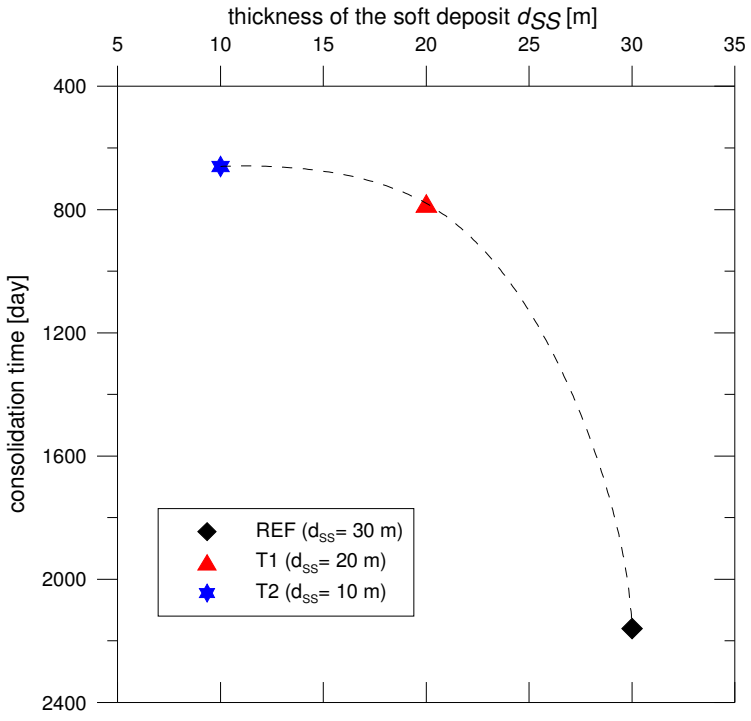

Figure 4.38: Impact of the soft deposit thickness on the consolidation time.

4.6.1. Conclusions on the influence of thickness of soft deposit

The impact of the soft deposit thickness on the stress-strain behaviour of soft clay improved with the floating and end-bearing stone columns was investigated in the above section. Thickness of the soft soil deposit is a significant factor for the predicted consolidation time and is of lower importance for the settlement reduction ratio s_r. As floating stone columns can effectively reduce the settlement response, longer floating columns speed up the process of excess pore water pressure dissipation. Therefore, in the case of thick soft soil layer, optimisation of the column length is necessary, in order to achieve a desired rate of consolidation.

4.7. Economical aspects of chosen stone column-soil systems

The economical cost of column construction has been calculated thanks to the courtesy of several leading geotechnical contractors in the United Kingdom who agreed to give an estimated average cost of the dry feed stone column, determined as approximately £54 per cubic meter of the column, (Bell, 2009 and Wlaź,2009). However, one should remember that the cost of applying stone columns into the soil is a combination of several factors, such as:

- Local gravel price,

- Method of treatment,
- Soil type,
- Depth of construction,
- Productivity,
- Other (including the commercial aspects).

In the calculations below none of these factors have been taken into consideration.

Nevertheless, the numerical studies conducted allowed for determination of the most and the less effective application of the stone columns in the soft clay of Bothkennar. For the best system one can take the application where both the greatest settlement reduction ratio value was obtained and the amount of granular material required to form the stone columns is minimal. The information required for the determination of the first part of the above definition is presented in terms of the settlement reduction ratio s_r in Figure 4.39 and tabulated in Table 4.13. For determination of the most and the less effective column foundation only simulations where the influence of the physical properties of the stone columns were investigated are used.

Table 4.13: Summary of presented numerical simulations: parametric study.

Simulation	Parameter						Settlement reduction ratio s_r [-]
	φ_{SC} [°]	$E^{ref}_{oed,SC}$ [kN/m^2]	D_{SC} [m]	S_{SC} [m]	L_{SC} [m]	d_{SS} [m]	
REF	42	80 000	0.6	2.0	10.0	30.0	0.818
P1	42	80 000	0.7	2.0	10.0	30.0	0.696
P2	42	80 000	0.8	2.0	10.0	30.0	0.581
P3	42	80 000	0.6	1.7	10.0	30.0	0.696
P4	42	80 000	0.6	2.3	10.0	30.0	0.899
P5	42	80 000	0.6	2.0	5.0	30.0	0.838
P6	42	80 000	0.6	2.0	15.0	30.0	0.818

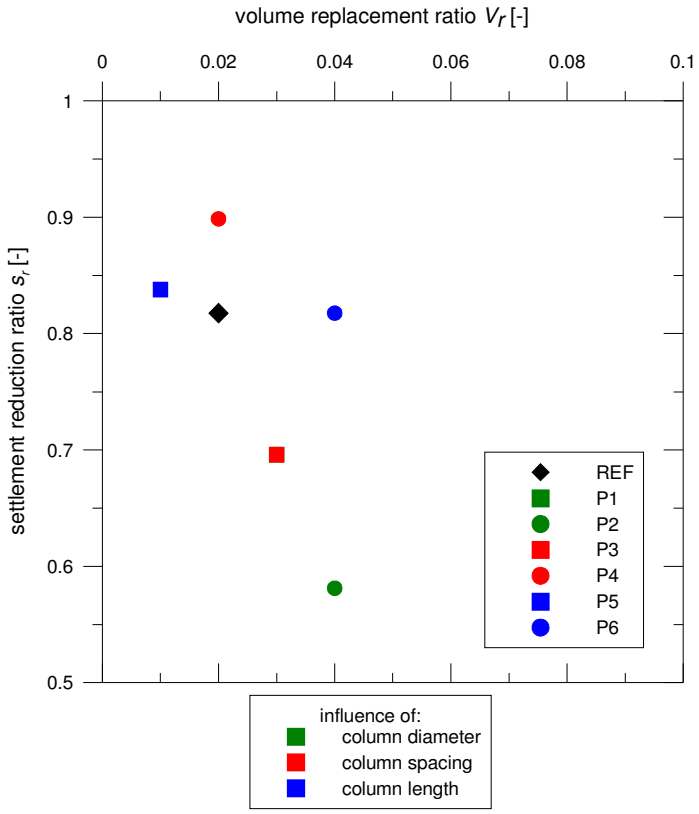

Figure 4.39: Settlement reduction ratio vs. volume replacement ratio: economical aspects of the construction.

One can see that the P2 stone column foundation gave the lowest settlement reduction ratio, which means that the improvement in the settlement response was the greatest. Moreover, the numerical predictions concluded that the P4 column foundation had the highest settlement reduction ratio resulting in the smallest improvement of the settlement response when compared with the unimproved soft soil beneath the embankment. From all of the analysed simulations the most effective system in terms of settlement reduction appears to be P2, which considers stone column with a diameter of 0.8 m installed up to a depth of 10 m and a c/c spacing of

2.0 m. The columns have an oedometric stiffness equal to 100 000 kN/m^2, and the friction and dilatancy angles for the granular material are 42˚ and 12˚, respectively.

Inspection of Figure 4.39 indicates that the less effective solution is application P4, where 0.6 m diameter columns were constructed at 2.3 m spacing up to a depth of 10 m. Again the columns used for this system have an oedometer stiffness equal to 100 000 kN/m^2, and the friction and dilatancy angles for the granular material are 42˚ and 12˚, respectively. One should note that the volume replacement ratio V_r, and subsequently the area replacement ratio A_r are of different values for simulations P2 and P4.

To take account of the economical aspects of application of the granular material, the costs associated with all the improvement systems considered in this chapter are presented in Figure 4.40 and are listed in Table 4.14. The cost of the particular systems was determined as the price for 1m^3 of the improved soil beneath an embankment, and one should note that it does not take account of the array of factors listed above, such as local gravel price, productivity or mobilisation/de-mobilisation of contractor. As the cost of application is calculated based on the volume of granular material required for the execution of the improvement technique, the systems in which the influence of the mechanical properties of stone column material and the thickness of soft soil are not taken into account in this study. The price of the most efficient system in terms of settlement reduction (P2) is almost twice as high as the less efficient system, however the required performance should be the determining factor in the design process, not the cost of the execution.

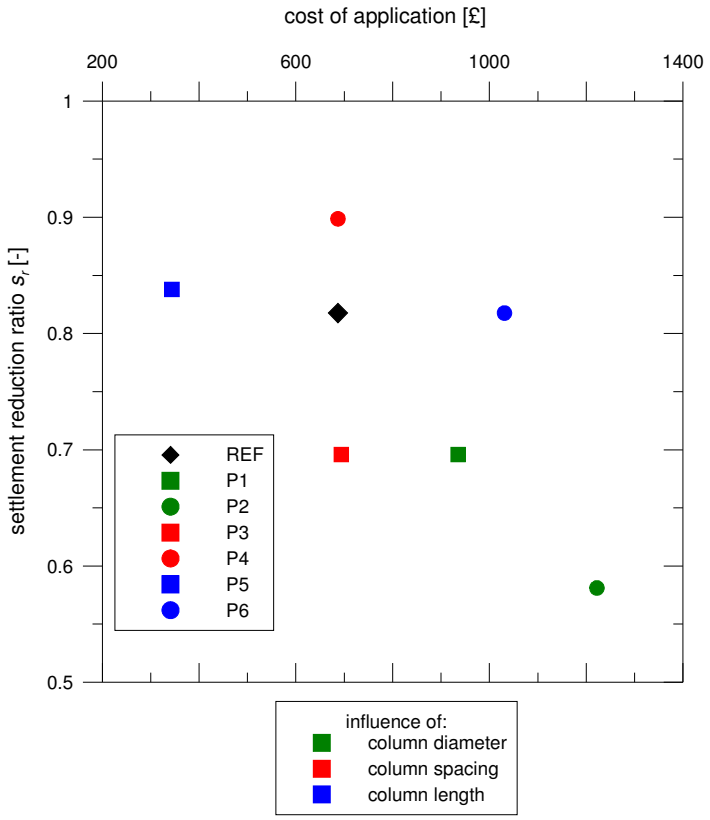

Figure 4.40: Cost of all considered systems: parametric study.

Table 4.14: Economical aspect of all considered stone column-soil systems: parametric study.

System	Cost per 1m^3 of column [£]	Cost per application [£]
REF	54	687
P1	54	935
P2	54	1222
P3	54	694
P4	54	687
P5	54	344
P6	54	1031

In Table 4.15 the most and the least effective (in terms of settlement reduction) systems are listed along with the estimated cost per application and the predicted settlement reduction ratio s_r. The simulation indicated as P2 results in a 35% reduction of the settlement in comparison with P4, see Table 4.15.

Table 4.15: Economical aspect of the most and the least efficient stone column-soil system.

System	Predicted surface settlement [m]	Predicted settlement reduction ratio s_r [-]	Cost per application [£]
P2	0.086	0.581	1222
P4	0.133	0.899	687

4.8. Summary and Conclusions

In this chapter the influence of several factors on the behaviour of the stone column foundation has been assessed. The benchmark study considered stone columns that were installed underneath an embankment in a soft soil stratum, represented by the Bothkennar clay. Simulations were performed using advanced constitutive S-CLAY1S model to take account of anisotropy and destructuration of the soft soil deposit, implemented in the three-dimensional commercial finite element code PLAXIS.

The evaluation of different aspects has been divided into three parts. The impact of the mechanical and physical properties of the stone column was investigated by varying factors such as the strength (expressed as angle of friction) and the stiffness of the granular material, and the diameter, spacing and length of the

stone columns. Afterwards, the effect of the thickness of the soft deposit was studied, considering both floating and end-bearing stone columns. Finally, the economical cost of the most and the least effective stone column-soil system determined during the numerical calculations has been briefly evaluated. It should be general practice that meeting the engineering requirements and not the cost of the execution of the ground improvement is the most important criterion during the design process.

In order to emphasise the influence of the considered aspects on the numerical predictions, results for all the simulations conducted are presented as settlement-time plots in Figure 4.41. The greatest influence on the numerical stress-strain predictions was found for the column strength (expressed as angle of friction), column diameter and spacing. The length of the stone columns was found to be a secondary design parameter. The actual stiffness of the column material and the thickness of the soft soil deposit were found to have little influence on the numerical settlement predictions of considered column foundations.

The column spacing/diameter S_{SC} / D_{SC} ratio is one of the key design parameters suggested by the parametric studies presented herein. Numerical simulations and field data collected from the literature suggest typically a value of S_{SC} / D_{SC} ratio of about 2.7..2.8, as with higher ratios the differences in settlement reduction ratio s_r are rather marginal.

Additionally, a simple bi-linear relationship between the S_{SC} / D_{SC} ratio and the settlement reduction ratio s_r was presented in *Eq. (4.4)*:

$$s_r = \begin{cases} 0.33 \times S_{SC} / D_{SC} - 0.25 & if \quad S_{SC} / D_{SC} \langle 2.8 \\ 0.21 \times S_{SC} / D_{SC} + 0.11 & if \quad S_{SC} / D_{SC} \geq 2.8 \end{cases}$$

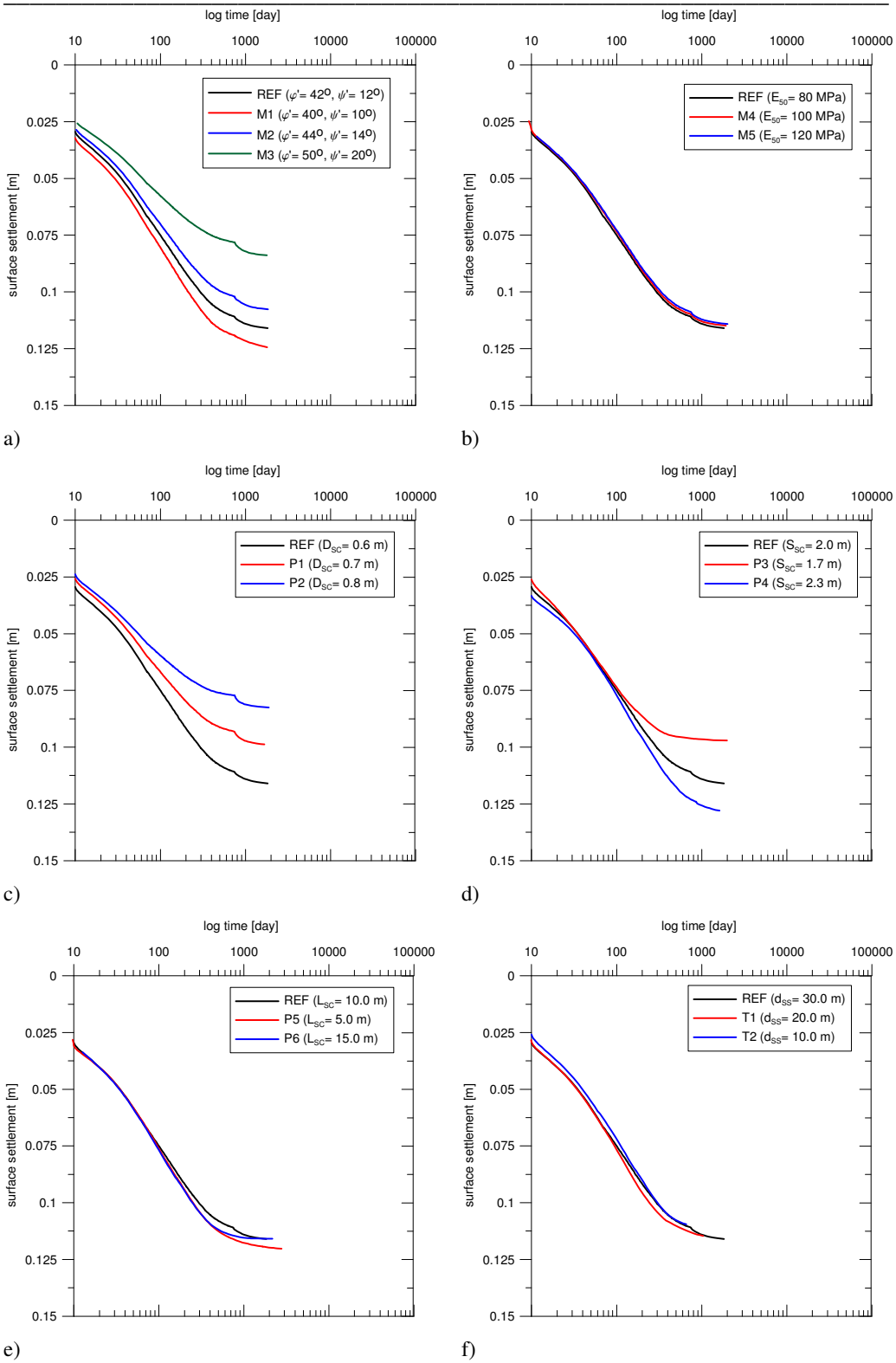

Figure 4.41: Time- settlement curve for parametric study- influence of: a) column strength, b) column stiffness, c) column diameter, d) column spacing, e) column length and f) soft soil thickness.

Future research should be conducted in order to determine the existence and possible form of similar simple relationships for different geotechnical problems where the stone column technique is used in engineering practice.

Numerical simulations indicated also that the optimum column length can be defined as $L_{SC} / D_{SC} \leq 17$ and $L_{SC} / S_{SC} \leq 5$. Moreover, the current research indicates that different loading regimes (expressed as the embankment height) within the studied range of values had little influence on the optimum L_{SC} / D_{SC} and L_{SC} / S_{SC} ratios.

In terms of settlement reduction, floating columns appear to work as well as end bearing columns. Indeed, the results are very similar to those predicted by simple design methods for end bearing columns. This demonstrates how conservative the simple design methods are. However, as the thickness of the deposit increases, so does the time required for consolidation. Therefore, in deep deposits the length of the stone columns needs to be optimised in order to achieve a desired rate of consolidation.

In all the simulations conducted, the columns were 'wished-in-place'. The installation of stone columns changes the structure of the soil and also causes an increase in excess pore water pressures. Provided these excess pore water pressures are allowed to dissipate before construction, the installation effects are likely to be very beneficial.

5

DEVELOPMENT AND VALIDATION OF THE ACM-S MODEL

This chapter introduces the ACM-S model, a formulation developed based on the Anisotropic Creep Model (Leoni *et al.* 2008), which has been enhanced to account for interparticle bonding and destructuration. A brief description of the proposed model is given, followed by a validation of the model at the element test level (oedometer, long-term oedometer and undrained triaxial creep tests). This is then complemented by the analysis of a simple 2D benchmark problem to demonstrate that the ACM-S model can be applied at boundary value level. The comparison between the predictions by ACM-S and experimental results from laboratory tests shows that a model which considers destructuration can significantly increase the quality of the predictions of the ACM (Leoni *et al.* 2008), thus extending the applicability of the model to time-dependent behaviour of structured soft clays. The work presented in this chapter was carried out under the supervision of Dr Martino Leoni from Wechselwirkung- Numerische Geotechnik, Office Italiano (formerly of

the University of Stuttgart, Germany).

5.1 Constitutive model ACM-S

The proposed time-dependent model for soft soils, named ACM-S, is based on the Anisotropic Creep Model (ACM) by Leoni *et al*. (2008). Leoni *et al.* (2008) demonstrated that this viscous model, which accounts for the evolution of large strain anisotropy, predicts the viscous strains in both compression and extension stress paths for normally consolidated (NC) and lightly over-consolidated natural soft soils.

The ACM model incorporates rotated ellipsoidal surfaces adopted from Wheeler *et al.* (2003) as the normal consolidation surface (NCS) and the current stress surface (CSS), as shown on Figure 5.1 for the simplified case of triaxial stress space considering a cross-anisotropic sample. In general stress space these ellipses are defined in terms of a mixed formulation, that includes a deviatoric fabric tensor to describe the arrangement of the fabric, see Wheeler *et al.* (2003) for details and Leoni *et al.* (2008) for the general formulation of ACM. The ACM-S model incorporates in addition to the rotational hardening law a destructuration law, which describes the evolution of the particle bonding.

Following the classical elasto-plastic theory, the total strains are composed from elastic and irrecoverable components:

$$\dot{\varepsilon}_{ij} = \dot{\varepsilon}^{e}_{ij} + \dot{\varepsilon}^{c}_{ij} \tag{5.1}$$

where $\dot{\varepsilon}_{ij}$ is the total strain rate tensor and the superscripts *e* and *c* refer to the elastic and creep components, respectively.

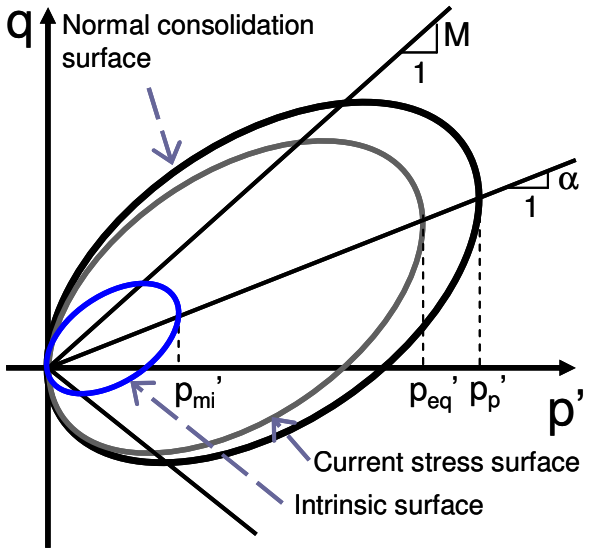

Figure 5.1: Yield surfaces of the ACM-S model in triaxial stress space.

The current stress point defines the so-called Current Stress Surface (CSS). In triaxial stress space the size of the CSS is defined as:

$$p_{eq}^{'} = p' + \frac{(q - \alpha \cdot p')^2}{(M^2 - \alpha^2) \cdot p'} \tag{5.2}$$

where the scalar parameter α describes the orientation of the NCS in triaxial stress space.

The normal consolidation surface (NCS) is defined by $p_{eq}^{'} = p_p^{'}$, where $p_p^{'}$ is the pre-consolidation pressure. The pre-consolidation pressure $p_p^{'}$ evolves the volumetric creep strain ε_v^c according to the hardening law:

$$p_p^{'} = p'_{p0} \cdot \exp\left(-\frac{\varepsilon_l^c}{\lambda_i^* - \kappa^*}\right) \tag{5.3}$$

where λ_i^* and κ^* are the intrinsic modified compression index and modified swelling index, respectively defined as $\lambda_i^* = \lambda_i /(1+e_0)$ and $\kappa^* = \kappa/(1+e_0)$, where λ_i and κ are the slopes of the intrinsic compression and swelling line in the $e - \ln p'$ plane and e_0 is the initial void ratio.

The distance between the CSS and NCS is treated as a generalised over-consolidation ratio $OCR^* = p_p' / p_{eq}'$. Creep volumetric strains are defined as:

$$\dot{\varepsilon}_v^c = \frac{\mu_i^*}{\tau}\left(\frac{1}{OCR^*}\right)^{\beta} \tag{5.4}$$

where μ_i^* is the intrinsic modified creep index , β is the creep exponent and τ is the reference time. The creep exponent is defined as:

$$\beta = \frac{\lambda_i^* - \kappa^*}{\mu_i^*} \tag{5.5}$$

and μ_i^* can be linked to the coefficient of secondary compression, C_α by:

$$\mu_i^* = \frac{C_\alpha}{\ln 10(1+e_0)} \tag{5.6}$$

The admissible stress states are bounded by the Argyris failure criterion (AR) (Argyris *et al.,* 1974), which is analogous to the Matsuoka-Nakai failure envelope (Matsuoka & Nakai, 1982), but has a simpler mathematical form than the Matsuoka-Nakai model. This failure criterion is presented in both triaxial stress space and the octahedral plane in Figure 5.2. One can see that the AR criterion coincides with Mohr-Coulomb (MC) at all apexes corresponding to triaxial extension and compression, Figure 5.2.

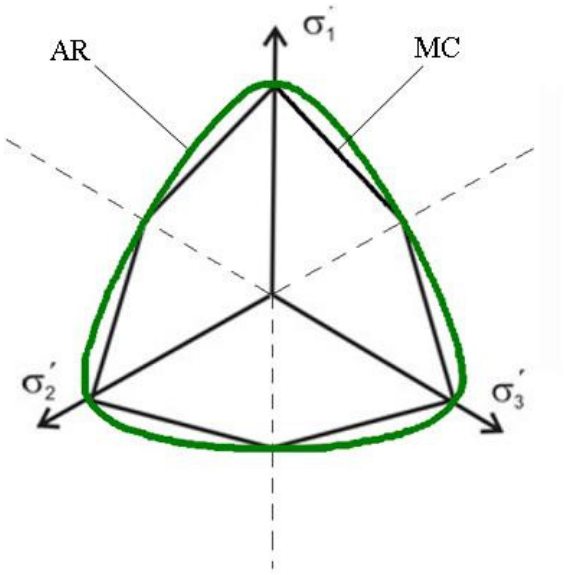

Figure 5.2: The Argyris failure criterion in octahedral plane.

5.1.1 Anisotropy

The ACM-S model incorporates the same rotational hardening law describing the rotation of the constitutive surfaces as used in the ACM model. The rotational hardening law in ACM was described in *Chapter 2* and will be not repeated here.

5.1.2 Destructuration

ACM-S incorporates a destructuration law, which relates the reduction of bonding to volumetric and deviatoric creep strains. The scalar state variable χ_0 describes the

amount of particle bonding and with the degradation of the bonds the value of χ_0 ultimately reduces to zero, following the ideas by Karstunen *et al.* (2005):

$$d\chi_0 = -\xi \cdot \chi_0 \cdot (\left|d\varepsilon_v^c\right| + \xi_d \cdot d\varepsilon_d^c) \tag{5.7}$$

where χ_0 is the initial amount of bonding and the parameters ξ and ξ_d control the absolute and relative rate of destructuration of bonds. Further detail on the calibration of the destructuration parameters is given in the following section.

5.1.3 Soil constants and state variables of the ACM-S model

The proposed model incorporates two additional soil parameters, ξ and, ξ_d and one additional state variable χ; the initial value for χ and the soil parameters ξ and ξ_d can be estimated based on standard laboratory tests. Advice regarding how to evaluate each of them is given in Tables 5.1 and 5.2. The parameters used for the ACM-S model can be divided into four groups. The first group refers to standard constants and state variables, whereas the second group of parameters are related to time-dependency (Table 5.1). The third group relates to anisotropy (Table 5.2) and the fourth group are parameters related to interparticle bonding and destructuration (Table 5.2).

Table 5.1: Soil constants, initial state parameters and time-dependency constants for ACM-S.

Group	Parameter	Notation	Estimated from
Soil constants and initial state parameters	c'	Apparent effective cohesion	Undrained consolidated triaxial test or drained consolidated triaxial test
	φ'	Angle of friction at critical state	Undrained consolidated triaxial test, drained consolidated triaxial test
	ψ	Angle of dilatancy	Assumed to be equal to zero for soft normally consolidated or slightly over-consolidated clays
	POP/OCR	Pre- overburden pressure/ Over- consolidation ratio	Oedometer test as: $POP = \sigma'_{p0} - \sigma'_{v0}$ $\quad OCR = \sigma'_{p0} / \sigma'_{v0}$
Time-dependency constants	μ_i^*	Modified intrinsic creep index	$\mu_i^* = \frac{C_{\alpha,i}}{\ln 10(1+e)}$, where $C_{\alpha,i}$ is estimated from the consolidation curve obtained from an oedometer test with constant load at high stress level
	τ	Reference time	Duration of the test, equal to 1 if the test lasts for 1 day

Table 5.2: Initial state parameters and constants for anisotropy and destructuration for ACM-S.

Group	Parameter	Notation	Estimated from
Anisotropy constants	α_0	Initial anisotropy	Critical state stress ratio as: $\alpha_0 = \eta_{K0} - \frac{M^2 - \eta_{K0}^2}{3}$, where $\eta_{K0} = \frac{3M}{6-M}$
	ω	Absolute rate of yield surface rotation	$\omega = \frac{1}{\lambda^*} \ln \frac{10M^2 - 2\alpha_0\omega_d}{M^2 - 2\alpha_0\omega_d}$
	ω_d	Relative rate of yield surface rotation	$\omega_d = \frac{3(4M^2 - 4\eta_{K0}^2 - 3\eta_{K0})}{8(\eta_{K0}^2 + 2\eta_{K0} - M^2)}$
	λ_i^*	Modified intrinsic compression index	$\lambda_i^* = \lambda_i/(1+e)$, where λ_i is determined from the one-dimensional oedometer test on a reconstituted sample or on a natural soil at very high stress levels
	κ^*	Modified swelling index	$\kappa^* = \kappa/(1+e)$, where κ is determined from the one- dimensional oedometer test on a natural soil
Destructuration initial state parameters and constants	χ_0	Initial bonding parameter	Sensitivity of the soil S_t using $\chi_0 = S_t - 1$
	ξ	Absolute effectiveness of destructuration	Typically 8 .. 12, can be determined from triaxial test at very low value of stress ratio
	ξ_d	Relative effectiveness of destructuration	Typically 0.1 .. 0.3, can be determined from triaxial test at very high value of stress ratio

In-house data on soft clays from Finland and that published on Scottish Bothkennar clay by McGinty (2006) indicate that the relationship between the intrinsic modified compression index λ_i^* and modified swelling index κ^* can be expressed as $\lambda_i^* / \kappa^* = 4..8$, but that this ratio is likely to be highly dependent on clay mineralogy.

Many researchers investigated the relationship between the intrinsic modified creep index μ_i^* and the intrinsic modified compression index λ_i^*, see among others Mesri & Godlewski (1977), Kabbaj *et al.* (1988), Kim & Leroueil (2001). The lower and upper bound of μ_i^* / λ_i^* ratio can be found in the literature, as that presented by Mesri *et al.* (1995) and recalled in Table 5.3.

In light of the above considerations, the large amount of model parameters is compensated by their simple determination. In very preliminary calculations, the calibration of the model parameters can be carried out by means of well-established correlations (i.e. presented by Mesri *et al.,* 1995), thus not requiring major effort. However, in all the cases where laboratory tests need to be performed, only routine tests are required. For all of these reasons, there is the potential for the practical application of ACM-S in the day-to-day engineering of soft soils.

Table 5.3. Viscous parameters for geotechnical materials (adopted from Mesri *et al*., 1995).

Material	μ_i^* / λ_i^* [-]
Granular soils, including rockfill	0.02±0.01
Shale and mudstone	0.03±0.01
Inorganic clays and silts	0.04±0.01
Organic clays and silts	0.05±0.01
Peat and muskeg	0.06±0.01

5.2 Numerical validation of ACM-S

A constant strain-rate oedometer test, a long-term oedometer and undrained triaxial creep test were numerically simulated to demonstrate the capability of the proposed model to qualitatively describe the behaviour of soft natural soils. Additionally, a benchmark embankment was simulated to check the performance of the ACM-S model in a simple geotechnical boundary value problem.

The soil constants and state variables of the natural clays considered, namely Batiscan clay (Canada), Berthierville clay (Canada), Vanttila clay (Finland) and Bothkennar clay (Scotland) are shown in Table 5.4 and 5.5. For comparison, all simulations were additionally performed with the ACM model, which ignores the effect of bonding and destructuration. The apparent pre-consolidation of the soil has been represented by the pre-overburden pressure POP, defined as the difference between the apparent pre-consolidation stress (based on 24 hour oedometer tests) and the in-situ vertical effective stress.

5.2.1 Constant strain rate oedometer test

The constant strain-rate oedometer tests on Batiscan clay were conducted by Leroueil *et al.* (1985) on samples that were 19 mm height and 50.8 mm in diameter. Drainage was only allowed at the top of the specimens and the strain rate varied from $1.43 \cdot 10^{-5}$ s^{-1} to $1.07 \cdot 10^{-7}$ s^{-1}. The vertical effective stress in the field σ_v' at a depth of 7.3 m, corresponding to the depth from which the samples were taken, was estimated to be equal to 65 kPa, and this was taken as the initial stress for the simulations.

Values of the apparent effective cohesion, angle of friction at critical state and dilatancy angle were assumed after Rocchi *et al.* (2003). The slopes of the compression and swelling lines in $e - \ln p'$ plane and the void ratio were determined from oedometers tests on natural samples from a depth of 7.3 m using the laboratory test results from Leroueil *et al.* (1985): λ and λ_i were calculated from plots at strain levels of 3..9% and 20..25%, respectively. Based on results from oedometer tests, the void ratio and the initial amount of bonding were found to be 1.92 and 2, respectively. Using results from oedometer tests, the intrinsic modified compression index λ_i^* and the modified compression index used in the ACM model was determined as 0.1404 and 0.5616, respectively. A value of the modified swelling ratio κ^* was calculated as 0.0127 and this value was applied for simulations carried out with both the ACM-S and ACM models.

Different values of the modified creep index had to be input for the case of the structured material (simulations with ACM-S) and for the case without any structure and bonding effects (modelled with ACM). If results of an oedometer test on a natural sample with a high stress level applied are not available, one can use the lower and upper bound μ_i^* / λ_i^* range established by Mesri *et al. (*1995). In the case of simulations of constant strain rate oedometer tests on Batiscan clay, the ratio μ_i^* / λ_i^* of 0.05 was defined.

The value of the relative effectiveness of destructuration ξ_d and the absolute effectiveness of destructuration ξ was taken from typical values for soft clays, see Table 5.2.

The input parameters for ACM-S and ACM models are summarised in Tables 5.4 and 5.5. As during one-dimensional consolidation no further rotation of the yield

surface is expected, the numerical simulations should highlight only the effect of destructuration on the predictions.

Table 5.4: Soil constants, initial state parameters and time-dependency constants for constant strain rate oedometer test on Batiscan clay.

Soil	Model	ν' [-]	c' [kPa]	φ' [°]	POP [kPa]	μ_i^*/μ^* [-]	τ [day]
Batiscan	ACM-S	0.3	0	25	35	0.007	1
	ACM					0.020	

Table 5.5: Anisotropy soil constants and destructuration initial state parameters and constants for constant strain rate oedometer test on Batiscan clay.

Soil	Model	λ_i^*/λ^* [-]	κ^* [-]	ω [-]	ω_d [-]	χ [-]	ξ [-]	ξ_d [-]
Batiscan	ACM-S	0.1404	0.0127	10	0.5	2	10	0.3
	ACM	0.5616				-	-	-

The agreement achieved between the experimental and numerical results using both the ACM-S and ACM models is shown in Figure 5.4. Both models are able to represent the strain-rate effect on the pre-consolidation pressure. The ACM-S model is able to predict the curvature in the oedometer tests very well, whereas the ACM model over-predicts the final part of the curve. These results show that taking account of destructuration enables accurate predictions of the stress-strain behaviour over the whole stress range.

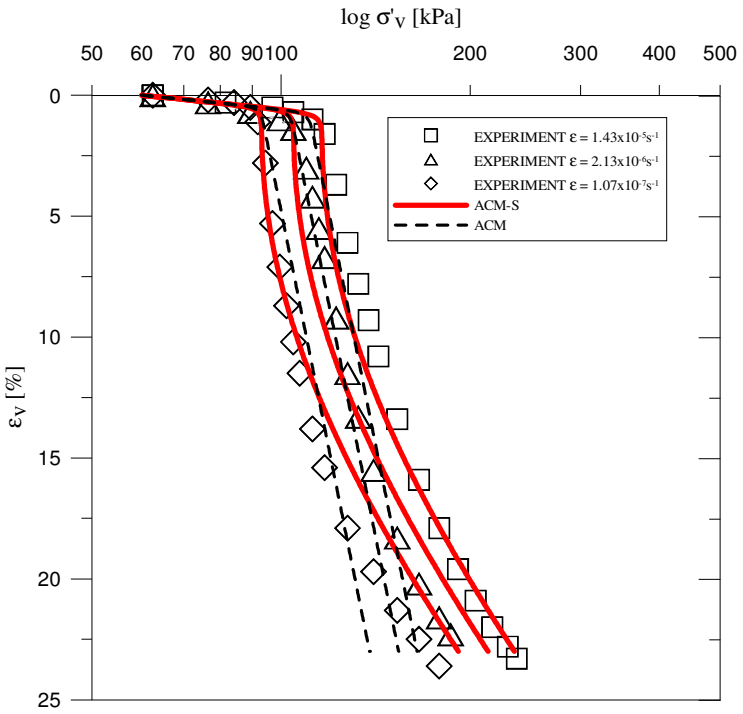

Figure 5.4: Oedometer test on Batiscan clay: experimental data versus numerical simulations using the ACM-S and ACM models.

5.2.2 Long- term oedometer test

Long-term oedometer tests were performed on Berthierville clay by Kabbaj (1985) and Kabbaj *et al.* (1988). On samples with a height of 20 mm and a diameter of 75 mm, a vertical stress was applied varying from 39 to 135 kPa. As previously mentioned, in oedometer tests the influence of anisotropy is insignificant and therefore only the effect of destructuration can be investigated with the model predictions. As the values of the destructuration parameters were assumed (ξ, ξ_d and χ_0), the simulations of the long-term oedometer test on Berthierville clay can give qualitative predictions only.

For numerical simulations the slopes of the swelling and the intrinsic compression lines were determined independently using long-term oedometer tests performed by Kabbaj *et al.* (1988) on Berthierville sample from a depth of 3.4 m. The relationship between the secondary compression index C_α and the compression index C_c and, subsequently between the modified intrinsic compression index μ_i^* and the intrinsic value of the modified compression index λ_i^*, was assumed to be equal to 0.04, as indicated by Mesri & Castro (1987) and Leroueil & Marques (1996). Due to a lack of laboratory test results, to calibrate the destructuration parameters (ξ, ξ_d and χ_0) a typical range of values were assumed, see Tables 5.6 and 5.7.

Table 5.6: Soil constants, initial state parameters and time-dependency constants for long-term oedometer test on Berthierville clay.

Soil	Model	ν' [-]	c' [kPa]	φ' [°]	POP [kPa]	μ_i^*/μ^* [-]	τ [day]
Bertherville	ACM-S	0.2	0	23	48	0.0050	1
	ACM					0.0104	

Table 5.7: Anisotropy soil constants and destructuration initial state parameters and constants for long-term oedometer test on Berthierville clay.

Soil	Model	λ_i^*/λ^* [-]	κ^* [-]	ω [-]	ω_d [-]	χ [-]	ξ [-]	ξ_d [-]
Bertherville	ACM-S	0.13	0.011	10.3	0.4	0.5	11	0.3
	ACM	0.26				-	-	-

Figure 5.5 presents the volumetric strain versus time for six applied stress levels. A good agreement between the experimental and numerical results was

achieved. For all applied stress levels the ACM-S model overestimates the settlements having predicted reasonably well the trend of the settlement for higher stress levels. The ACM model significantly overestimates the evolution of the settlements in time, which proves that destructuration heavily affects the behaviour of the soft soil.

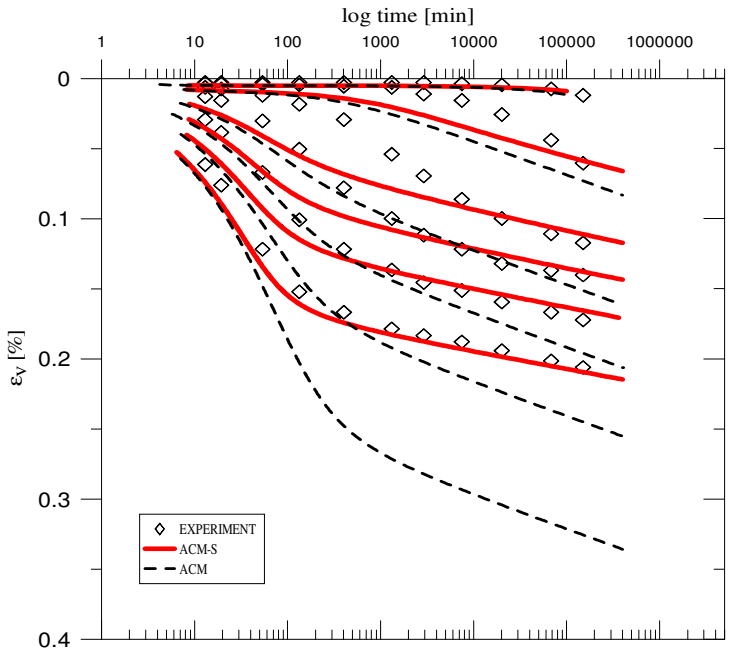

Figure 5.5: Long-term oedometer test on Berthierville clay:
experimental data versus numerical simulations using the ACM-S and ACM models.

5.2.3 Undrained triaxial creep test

Undrained triaxial creep tests were conducted on samples from a depth of 3 to 3.5 m on Vantilla clay, soft clay from Finland, by Yin *et al.* (in press). The height of the specimens was 100 mm and the diameter 50 mm. The tests were carried out under three different deviator stress levels after applying an identical consolidation stage ($\sigma_1^{'} = 26.9\,\text{kPa},\ \sigma_3^{'} = 16.5\ \text{kPa}$) which lasted for two weeks, see Table 5.8.

Table 5.8: Undrained triaxial creep tests on Vantilla clay: numerical validation of ACM-S.

Test	Depth [m]	γ [kN/m3]	e_0 [-]	Applied stress [kPa]	
				σ'_1	σ'_3
CAUCR1	3.16..3.27	13.61	3.308	31.0	16.5
CAUCR2	3.31..3.42	13.77	3.145	31.5	14.2
CAUCR3	3.05..3.15	13.54	3.308	36.5	16.5

For FE analyses, the results from standard consolidated undrained triaxial and oedometer tests on natural and reconstituted samples were used to determine the values for the soil parameters, see Koskinen & Karstunen (2004) and Karstunen & Koskinen (2008). Based on these, the intrinsic modified compression index and the modified swelling index were calculated. Then, the relationship between the intrinsic modified creep index μ_i^* and the intrinsic modified compression index λ_i^* was assumed to be $\mu_i^* / \lambda_i^* = 0.04$, in accordance with the value proposed by Mesri *et al.* (1995). An initial amount of bonding was chosen to represent the lower bound sensitivity range, based on the results from fall cone tests on intact and reconstituted samples and from oedometer tests presented by Yin & Karstunen (in press). Parameters ξ and ξ_d were assumed based on typical values for Finnish soft clay identified by Zentar *et al.* (2002). The values of the model parameters used for the numerical simulations are presented in Tables 5.9 and 5.10. The numerical creep tests were performed using the ACM-S and ACM models for three different stress levels, see Table 5.8.

Table 5.9: Soil constants, initial state parameters and time-dependency constants for undrained triaxial creep tests on Vantilla clay.

Soil	Model	ν' [-]	c' [kPa]	φ' [°]	POP [kPa]	μ_i^*/μ^* [-]	τ [day]
Vanttila	ACM-S	0.2	0	33.5	11.9	0.003	1
	ACM					0.006	

Table 5.10: Anisotropy soil constants and destructuration initial state parameters and constants for undrained triaxial creep tests on Vantilla clay.

Soil	Model	λ_i^*/λ^* [-]	κ^* [-]	ω [-]	ω_d [-]	χ [-]	ξ [-]	ξ_d [-]
Vanttila	ACM-S	0.075	0.015	19.9	0.9	50	11	0.2
	ACM	0.150				-	-	-

The plot of the axial strain versus time for three applied stress levels (Figure 5.6a) demonstrates that the ACM-S model reproduces the experimental results reasonably well, particularly for the high deviatoric stress level. ACM, in contrast, under-predicts the results for two of the three stress levels. The evolution of the change in pore pressures with time is presented in Figure 5.6b. For the intermediate deviatoric stress level (CAUCR2) the predictions given by both the ACM-S and ACM are good, whereas for the lowest and highest deviatoric stress level (CAUCR1 and CAUCR3, respectively) only ACM-S gave reasonable good predictions of the pore pressures.

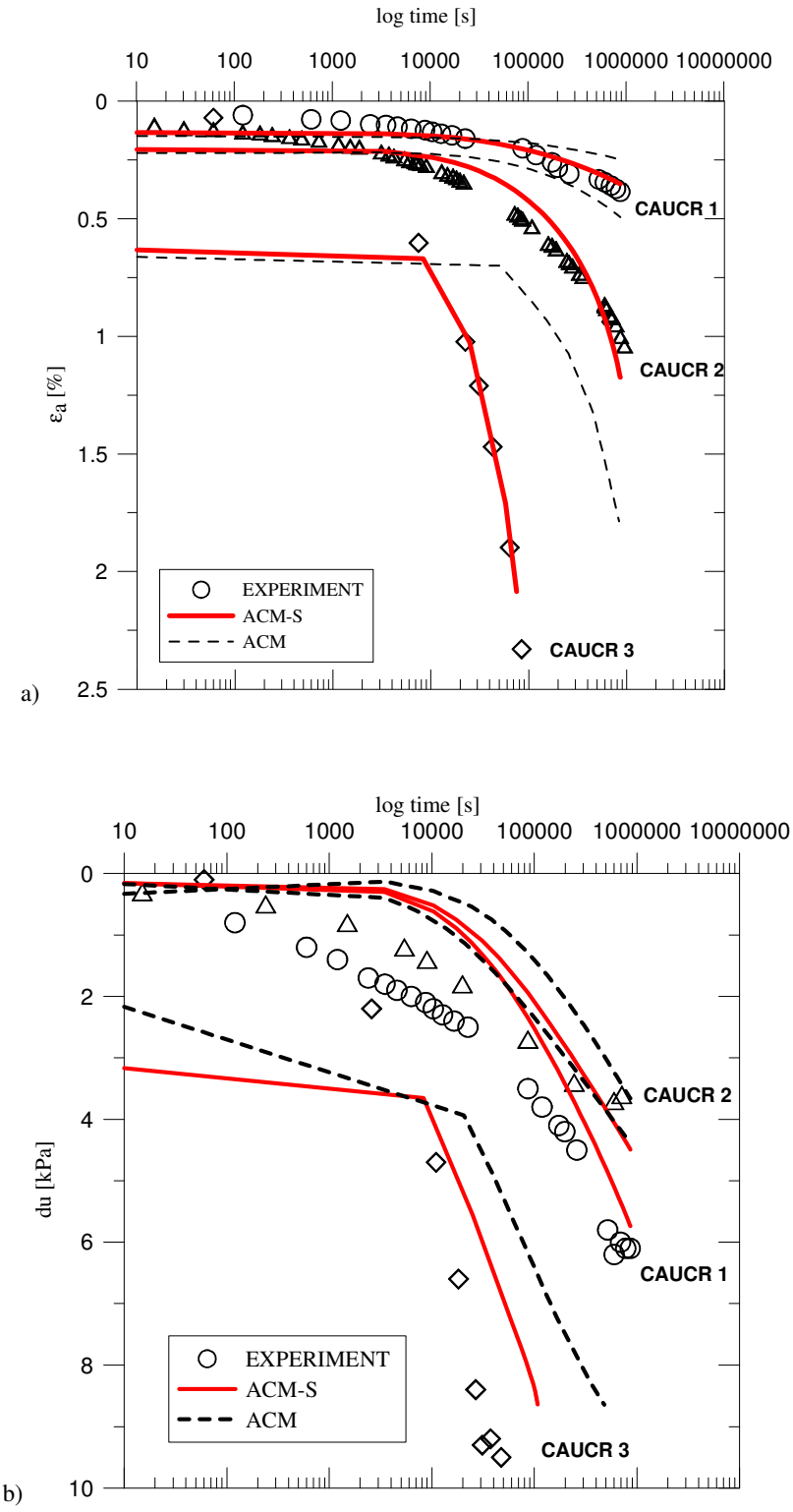

Figure 5.6: Triaxial creep test on Vanttila clay, experimental data versus numerical simulations using the ACM-S and ACM models:
a) axial strain versus time and b) excess pore water pressure versus time.

The test conducted at the three deviatoric stress levels includes examples of the primary, secondary and tertiary (rupture) creep. Figure 5.7 presents the predicted axial strain rate versus time. Figure 5.7a shows mainly primary and secondary creep during test CAUCR1, and Figure 5.7b presents both primary and secondary creep during tests CAUCR2. The ACM-S model predicts the primary and secondary creep notably better than ACM. All three components of creep during test CAUCR3 can be seen in Figure 5.7c, where the soil sample failed due to an exponential increase in the strain rate with strains at a constant deviatoric stress (creep rupture). Although ACM-S predicted the tertiary creep better than ACM, the predictions using the ACM-S model are still not fully satisfactory.

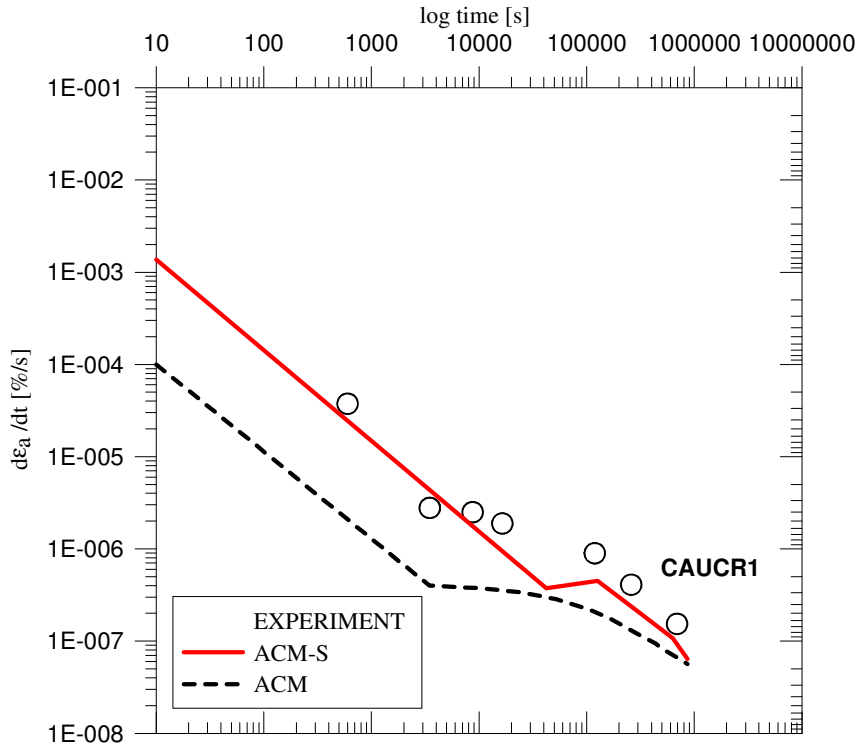

a)

b)

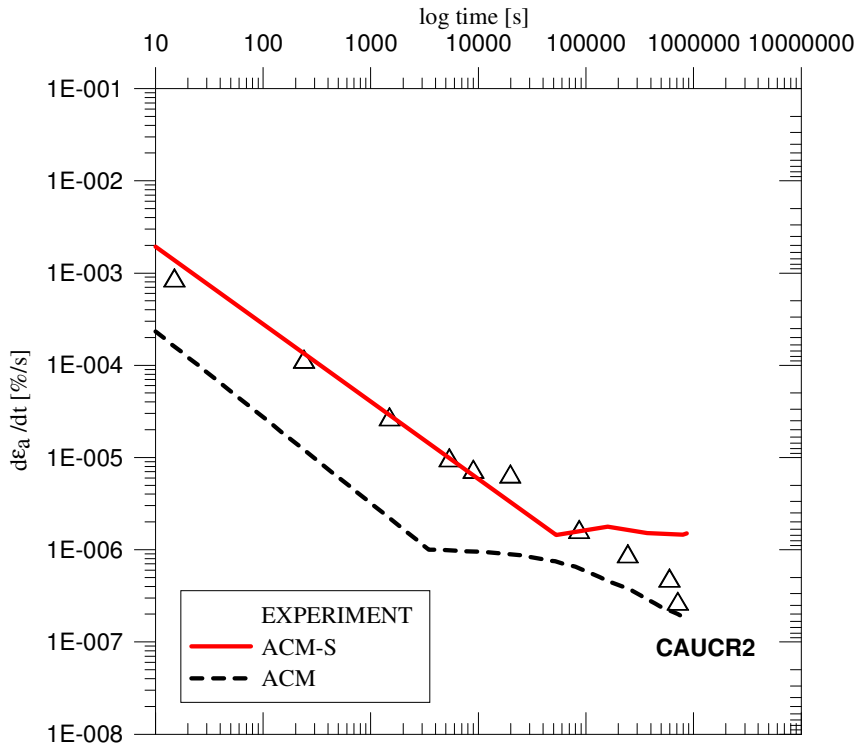

c)

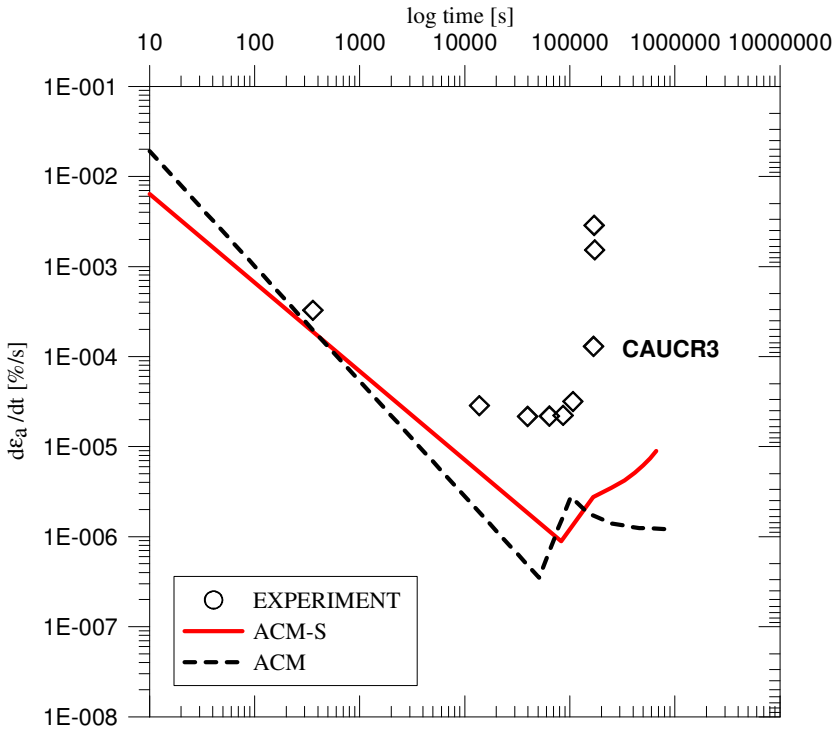

Figure 5.7: Triaxial creep test on Vanttila clay, axial strain rate versus time:.
a) CAUCR1 b) CAUCR2 and c) CAUCR3.

5.2.4 2D boundary value problem

The numerical analysis of an idealised embankment constructed on Scottish Bothkennar clay was performed to investigate the differences in the numerical predictions of the vertical and horizontal displacement of a real geotechnical problem, between the anisotropic creep model, capable of taking account of the destructuration of interparticle bonds (ACM-S) and the original model (ACM), which accounts only for anisotropy and the viscosity of the soft soil. The soft recently deposited marine sediment of Bothkennar is a cross-anisotropic and structured material which is high susceptibility for creep, and which has been studied extensively in field and laboratory tests, see Géotechnique (1992).

The homogeneous subsoil was assumed to consist of three distinct layers with varying pre- overburden pressure POP (where $POP = \sigma_p^{'} - \sigma_v^{'}$). The unit weight was assumed to be equal to 16 kN/m^3. As the deformation of the embankment is not relevant for the purposes of the present study, the embankment fill was modelled by using the elastic perfectly plastic Mohr-Coulomb model with a unit weight of 20 kN/m^3, Young's modulus E'= 40 000 kPa, Poisson's ratio ν'= 0.3, and effective friction angle φ'= 38°. Cohesion and the dilatancy angle were set to zero. The groundwater table was assumed to be located 2 m below the ground surface.

Bothkennar clay was simulated using the ACM-S and ACM models and the soil was assumed to be in a slightly over-consolidated state, with values for the lateral earth pressure at rest in agreement with Mayne and Kulhawy's formula (Mayne & Kulhawy, 1982), which reads as follows: $K_0 = K_0^{NC} \cdot OCR^{\sin\varphi'} = (1 - \sin\varphi') \cdot OCR^{\sin\varphi'}$. As the over-consolidation of the soil is defined with POP, the relevant depth of the deposit shall be considered in

calculations of OCR and, thus, of K_0. Most settlements are expected to be in the shallow soil deposits, therefore for estimation of the OCR a depth of 4 m, not half of the soft deposit, was chosen. Hence the OCR can be calculated as:

$$OCR = \frac{\sigma_p^{'}}{\sigma_v^{'}} = \frac{\gamma' d + POP}{\gamma' d} \tag{5.8}$$

Following that, the K_0 value was determined to be equal to 0.5. The model geometry of the benchmark embankment is shown in Figure 5.8. The numerical analysis was performed using small deformations assumption. The construction of the embankment was simulated in five phases. The first construction phase, in which the first layer of the embankment was built (10 days), was followed by a consolidation stage of 30 days. Secondly, the completion of the construction up to a height of 2 meters (10 days) and a final consolidation phase of 100 years were simulated.

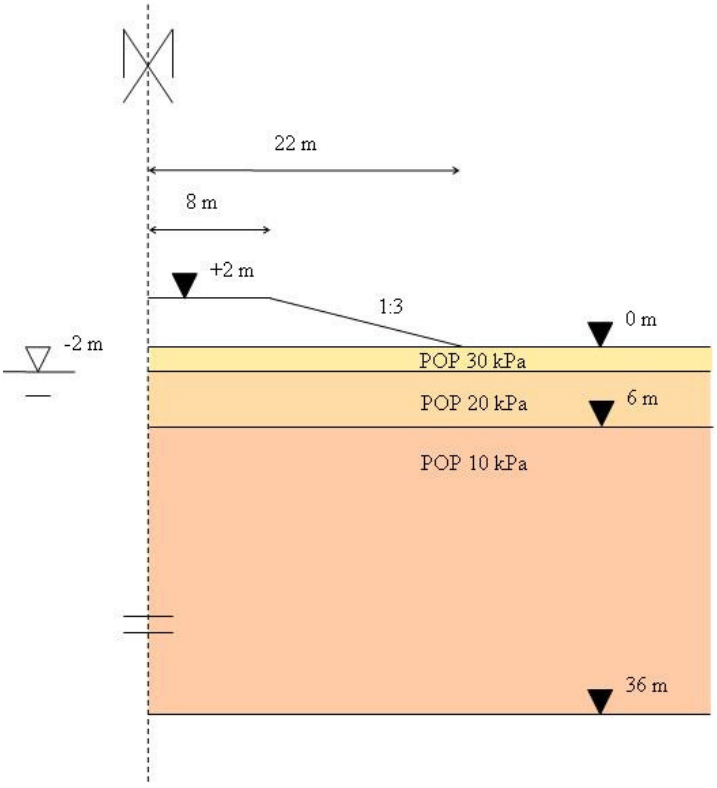

Figure 5.8: Geometry of the embankment constructed on Bothkennar clay and soil profile: numerical simulations with the ACM-S and ACM models.

According to Nash *et al.* (1992A), Nash *et al.* (1992B) and Smith *et al.* (1992) the slope of the compression line for the natural and reconstituted samples of Bothkennar clay was found to be 0.30 and 0.15, respectively. Additionally, the slope of the swelling line κ of the Bothkennar clay was determined as equal to 0.02. Those values were determined by laboratory testing, where the initial void ratio e_0 was found to be equal to 2.0.

Applying the simple relationship between the slope of the compression lines and the modified compression index, one can estimate the intrinsic modified compression index λ_i^* = 0.05 and the modified compression index λ^*=0.1. The modified swelling index κ^* was calculated as κ^* = 0.0067. The creep parameters for the reconstituted and natural soil were determined using the findings by Nash *et al.* (1992B) during the incremental loading oedometers tests that the ratio C_α / C_c is equal to 0.03..0.05, where C_α is the secondary compression index and C_c is the compression index of the natural soft soil sample.

Over the years many studies have been conducted in order to study the relationship between the secondary compression index and the compression index, see Mesri & Godlewski (1977), Mesri & Castro (1987), Mesri (2001) or Mesri & Vardhanabhuti (2005). These authors concluded that for natural soils C_α / C_c is found to be between 0.02 and 0.1. The ratio of $\mu_i^* / \lambda_i^* = 0.04$ applied for the numerical study is well within this range of values and corresponds to the values reported by Nash *et al*. (1992B). The parameters accounting for interparticle bonding effects and destructuration were assumed as suggested by Kamrat-Pietraszewska *et al.* (2008) resulting in ξ, ξ_d and χ_0 equal to 9, 0.2 and 8, respectively. All material parameters are given in Tables 5.11 and 5.12.

Table 5.11: Soil constants, initial state parameters and time-dependency constants for 2D boundary value problem on Bothkennar clay.

Soil	Model	ν' [-]	c' [kPa]	φ' [°]	POP [kPa]	μ_i^*/μ^* [-]	τ [day]
Bothkennar	ACM-S	0.2	0	37.5	10/20/30	0.002	1
	ACM					0.004	

Table 5.12: Anisotropy soil constants and destructuration initial state parameters and constants for 2D boundary value problem on Bothkennar clay.

Soil	Model	λ_i^*/λ^* [-]	κ^* [-]	ω [-]	ω_d [-]	χ [-]	ξ [-]	ξ_d [-]
Bothkennar	ACM-S	0.05	0.0067	30	1	8	9	0.2
	ACM	0.1				-	-	-

Inspection of the evolution of the surface settlement with time for points at the embankment centreline, crest and toe (Figure 5.9) suggest that the ACM-S model predicts somewhat smaller settlement values than ACM, given it predicts an non-constant apparent λ^* value.

Surface settlement after construction and after 100 years into consolidation is presented in Figure 5.10. The importance of the modelling of the soft soil complexity can be seen particularly for the material subjected to loading (under the embankment); there the difference in the numerical predictions given by the ACM-S and ACM models is the greatest. However, outside the embankment footprint (in the unloaded area) both ACM-S and ACM predict unrealistic vertical displacements. Simulations carried out with the elasto-plastic S-CLAY1S model (Koskinen *et al.* 2002, Karstunen *et al.* 2005) predicted the surface settlements of approximately 0.27

m after 100 years into the consolidation process at the centreline of the embankment, which is more than 4 times smaller than the deformation predicted by the ACM-S model in the current simulation.

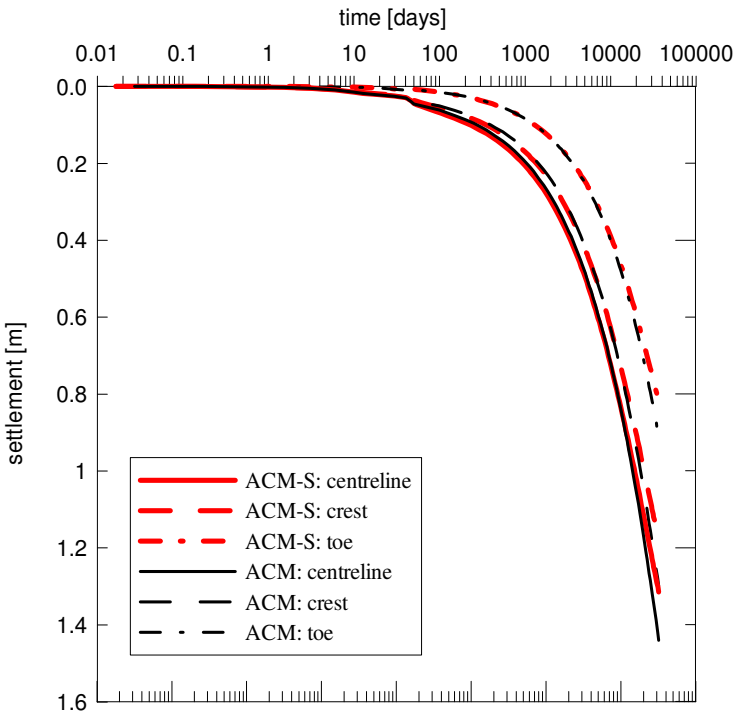

Figure 5.9: Settlement evolution with time for points at the ground surface below centreline, crest and toe of Bothkennar embankment: numerical simulations using the ACM-S and ACM models.

As mentioned before, in the case of experimental data, one can use the relationship between the secondary compression and the compression indices as an indication regarding the magnitude of the creep of the studied deposit. However, the compression parameters must be carefully selected, as the application of unrealistic input values may lead to incorrect numerical predictions of the stress-strain behaviour of the deposit.

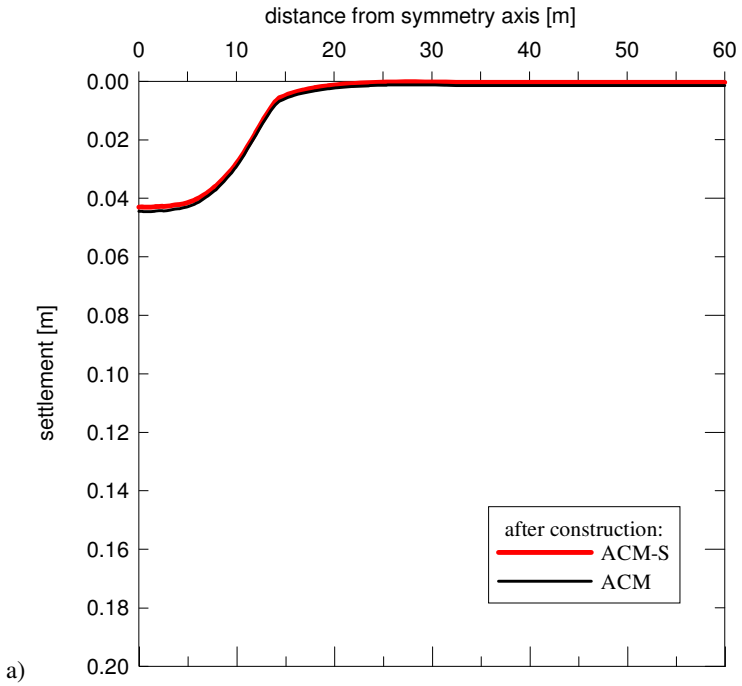

a)

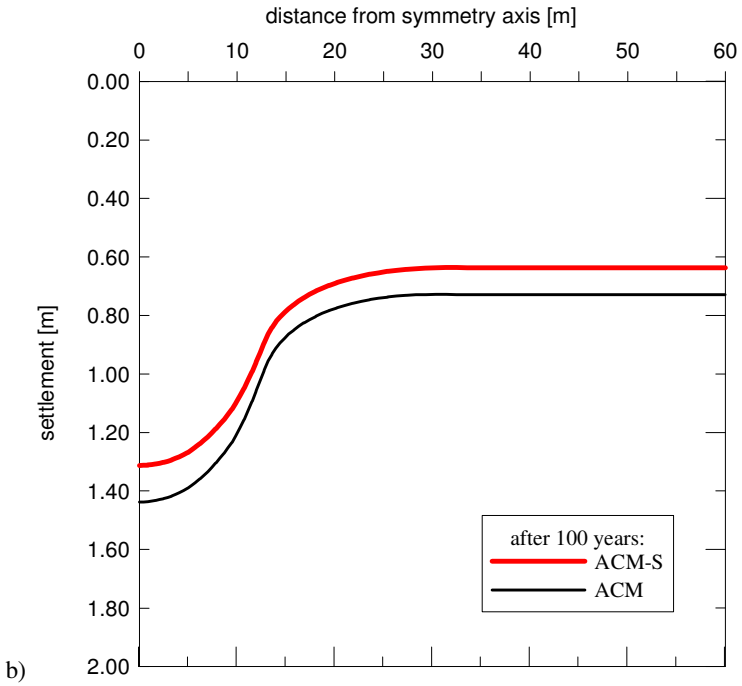

b)

Figure 5.10: Surface settlement with the horizontal profile for numerical simulations with ACM-S and ACM after: a) construction and b) 100 years.

To illustrate how the compression indices influence the settlement calculations, the μ_i^* / λ_i^* ratio applied for the soft layers in benchmark problem considered here for both the ACM-S and ACM models was assumed to be half and twice the value suggested by Mesri *et al.*, 1995. The ratio between the secondary compression and the compression indices was assumed to be equal to 0.02 and 0.08, respectively. For the sake of completeness, Figure 5.11 also includes the settlement predictions after 100 years into the consolidation process reproduced from Figure 5.10b. It is evident that the settlement changes dramatically with a change of the μ_i^* / λ_i^* ratio, see Figure 5.11.

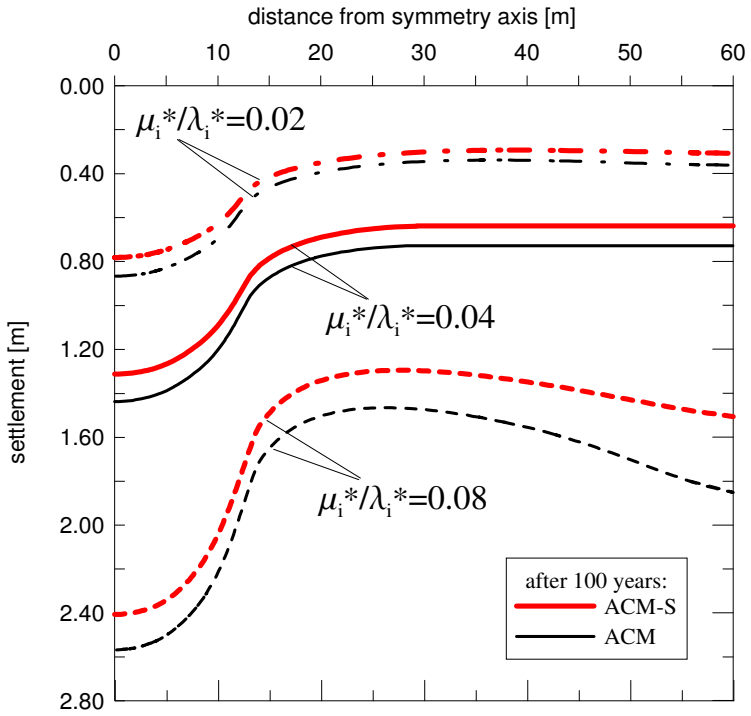

Figure 5.11: Influence of λ^* / μ^* on the surface settlement predictions, Bothkennar clay: numerical simulations using the ACM-S and ACM models.

By setting μ_i^* / λ_i^* ratio to a low value of 0.02, one reduces the viscosity of the soft soil, leading to a decrease in the settlement. However, increasing μ_i^* / λ_i^* ratio to

0.08, results in an increase of the surface settlements up to an unrealistic value of approximately 2.5 m for a 2 m high embankment. In the unloaded area for $\mu_i^* / \lambda_i^* = 0.08$ the differences between the predictions given by ACM-S and ACM are much more pronounced, see Figure 5.11. Moreover, at the outer boundary the models predict unrealistic settlement values which are higher than those located close to the embankment. The ratio between the secondary compression and the compression indices is a fundamental soil property, and its influence is evident and therefore this relationship should be carefully determined.

Horizontal movements versus depth at the toe and the crest of the embankment after 100 years into consolidation are shown in Figure 5.12. A negative value of the horizontal displacement indicates movement towards the symmetry axis of the embankment, whereas positive indicates movement towards the outer boundary of the geometry model. The effect of destructuration reduces, however only slightly, the predicted horizontal movements compared to the predictions given by the ACM model, this is also supported by Krenn (2008). Inspection of Figure 5.12 shows that the maximum horizontal movement of the subsoil occurs at a depth of approximately 6 m, which coincides with both the discontinuity in the POP value and the embankment width. Predictions of horizontal displacements presented by Karstunen *et al.* (2010) using the S-CLAY1S and the EVP-SCLAY1S models for a similar 2D benchmark problem on Bothkennar clay are significantly smaller than those calculated using both the ACM-S and ACM models. In fact, the ratio between the maximum values of the vertical surface displacement and the lateral movement $\delta_{y,\max} / \delta_{x,\max}$ for both S-CLAY1S and EVP-SCLAY1S as determined by Karstunen *et al.* (2010) was approximately equal to 9, whereas the simulations using ACM-S and ACM predicted that this ratio was equal to 14.

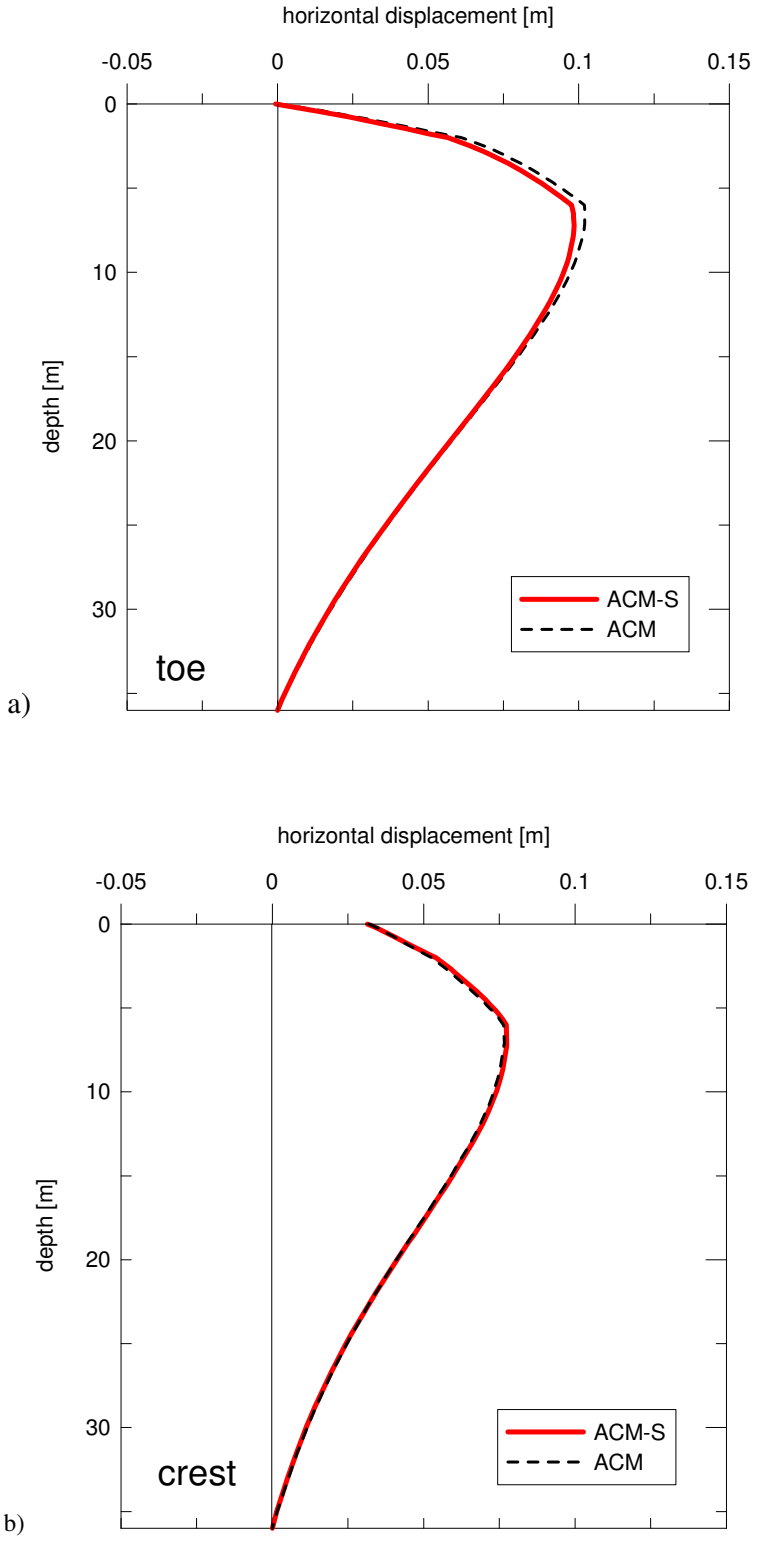

Figure 5.12 Evolution of horizontal displacement with depth after 100 years of consolidation for numerical simulations using ACM-S and ACM at the Bothkennar embankment: a) crest and b) toe.

The excess pore water pressures contours after construction and after 50 years of consolidation are plotted in Figures 5.13 and 5.14. The soil mechanics sign convention for pressure has been applied, where negative values refer suction. It can be noted that accounting for destructuration reduces the excess pore water pressure development during embankment construction, see Figure 5.13. Moreover, the extent of the excess pore water pressure bulb is wider in the case of the ACM model than was predicted using the ACM-S model. The excess pore water pressure contours after 50 years into the consolidation process are plotted in Figure 5.14. The increase in the value of the excess pore water pressures is attributed to the combined effect of creep and the Mandel-Cryer effect (Mandel, 1950 and Cryer, 1963) during coupled consolidation. That may suggest that the degree of consolidation, commonly referred to by engineering practitioners should be calculated based on settlements, rather than on the value of the excess pore water pressure.

5.3 Summary and conclusions

A new time-dependent model ACM-S, which accounts for viscosity, anisotropy and degradation of interparticle bonds, was used to simulate the behaviour of soft natural soils. The numerical validation considered constant strain-rate oedometer tests on Batiscan clay at different strain rate levels, long-term oedometer tests on Berthierville clay at different stress levels and undrained creep triaxial tests on Vantilla clay under different stress levels. Further, a benchmark embankment on Bothkennar clay was analysed using the ACM-S model. The comparison between the numerical predictions and experimental results was used to demonstrate the

capabilities of the ACM-S model in capturing soft soil features, such as viscosity, anisotropy and destructuration at the single element level.

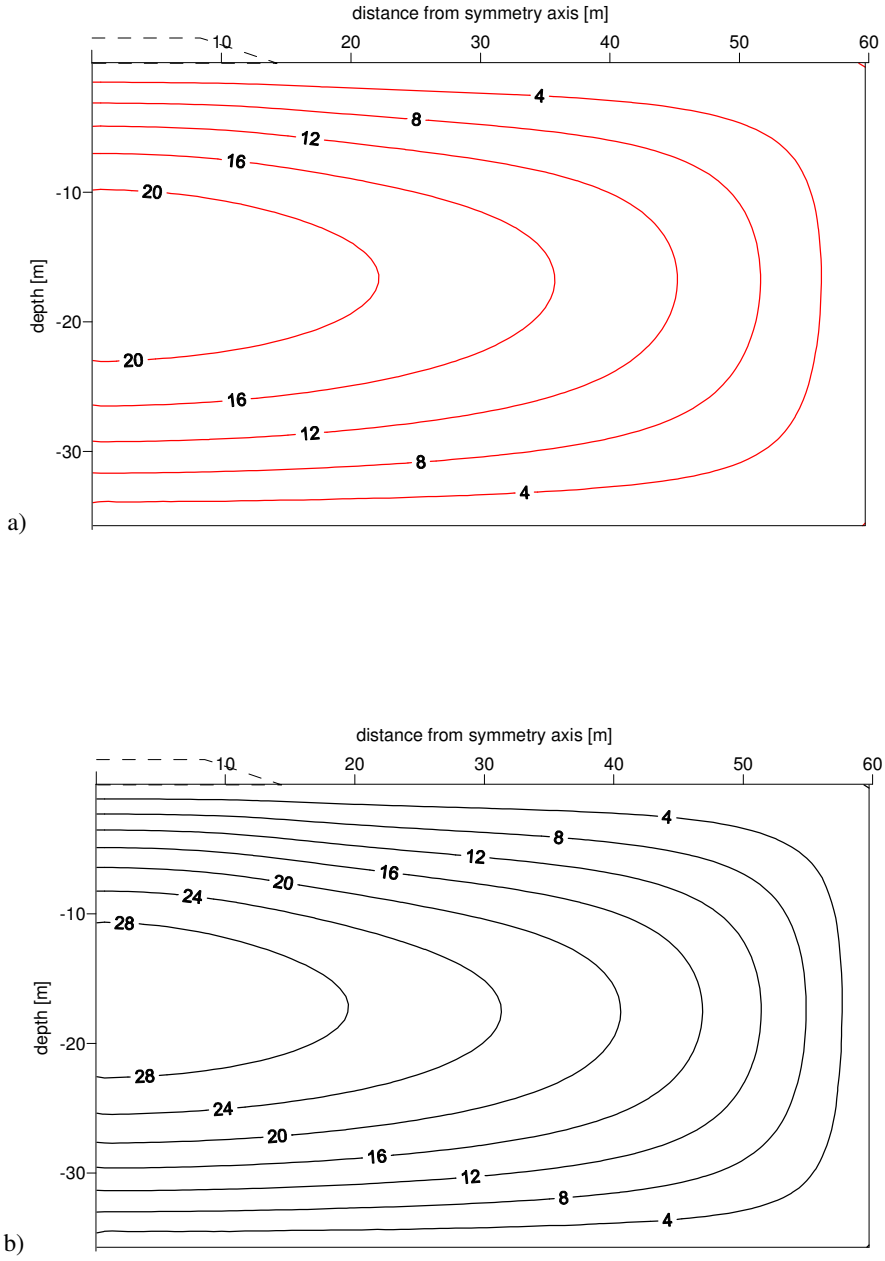

Figure 5.13: Numerical predictions of excess pore water pressures contours (in kPa) after construction for Bothkennar clay using: a) ACM-S and b) ACM.

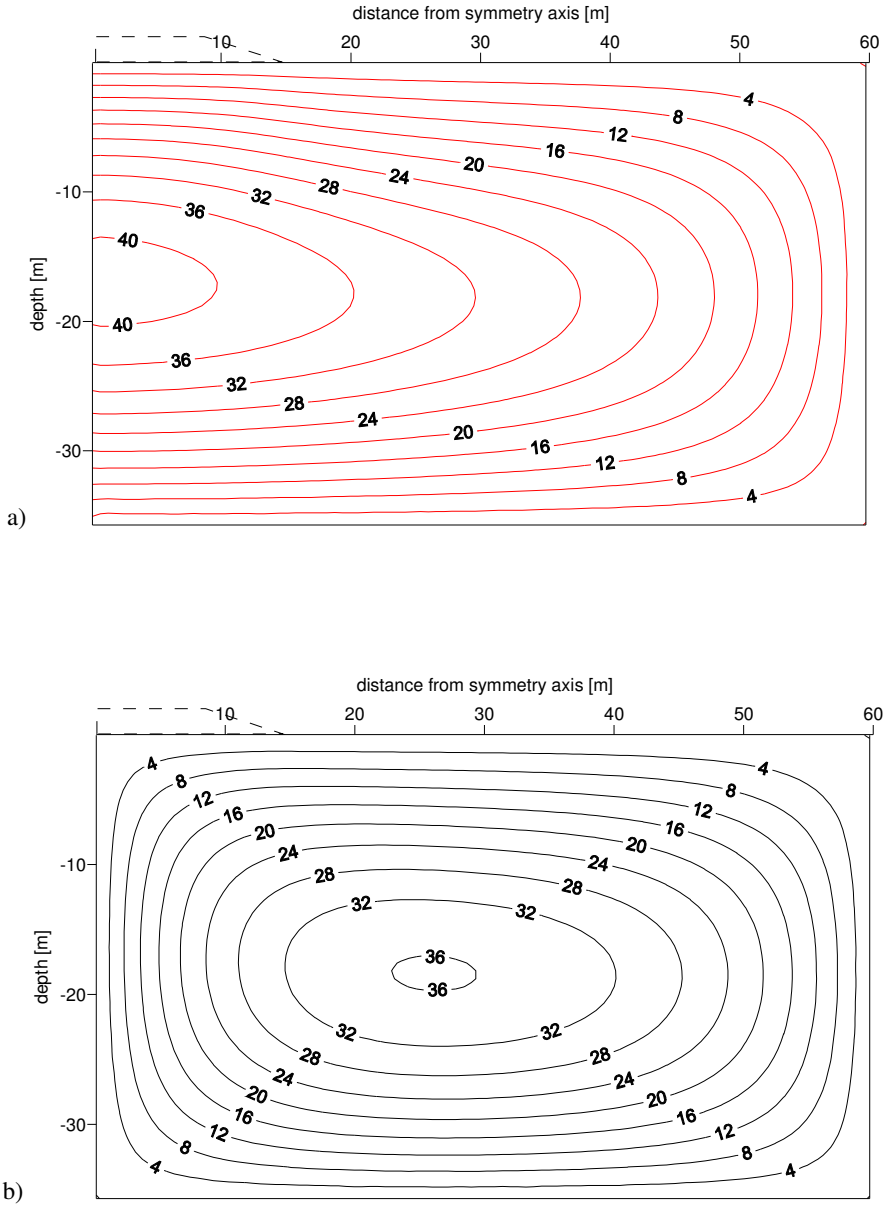

Figure 5.15: Numerical predictions of excess pore water pressures contours (in kPa) after 50 years of consolidation for Bothkennar clay using: a) ACM-S and b) ACM.

The proposed formulation is based on existing constitutive models for structured soft soils which are prone to creep (ACM and S-CLAY1S) and it has been implemented as a user-defined model into the commercial finite element code PLAXIS. The number of input soil parameters used for ACM-S has been kept to a minimum and all of them can be determined via laboratory testing of structured soft soil to ensure clarity with regard to the determination of the soil parameters. As the proposed model has a hierarchical form, some of the soft soil features, such anisotropy or interparticle bonding, can be simply switched off. The application of a coupled consolidation analysis in the finite element code PLAXIS in conjunction with the ACM-S model illustrated that boundary value problems in terms of both undrained and drained analysis can be carried out, which ensures the potentially wide applicability of the proposed model as an engineering tool.

The proposed ACM-S model predicts well the soil behaviour during constant strain rate oedometer tests, predicting both the curvature and the rate-dependence of the pre-consolidation pressure, and it also simulates reasonably well the trend of the settlement for high stress levels applied during the numerical reproduction of long-term oedometer tests. Inspecting the numerical predictions for undrained triaxial creep tests, the ACM-S model appears to reproduce the experimental results reasonably well, particularly for the higher axial stress level. Given the reasonably good agreement between the numerical simulations and the experimental results, the ACM-S model can be considered capable of capturing the essential features of soft soil behaviour, including the creep rupture phenomena. It has been shown that the model can be easily applied for both simulations of laboratory tests and boundary value problems. However, at the boundary value level the results predicted by the ACM-S model are far from satisfactory. The main limitations of the ACM-S model are (i) the over-prediction of both the vertical and horizontal displacements and (ii)

the unrealistic creep deformations predicted outside the embankment footprint (outside loaded area). The simulations using the ACM-S and ACM models indicate that the subsoil under its own self-weight (in the presence of in-situ stresses only) can result in significant creep settlements. A possible explanation for this phenomenon may lay in the formulation of ACM-S (and ACM) itself, as it is assumed that the normal consolidation surface (NCS) is the contour of the constant volumetric creep strain rate. That however, may lead to large volumetric creep strain increments between the K_0-line and the critical state line (CSL). Furthermore this may result in greater than expected horizontal movements, and following that greater vertical displacements. Therefore, this issue requires further investigation. Additionally, in the ACM-S model the concept that the μ_i^* / λ_i^* ratio is constant for a given soil is applied. This is not true for the EVP-SCLAY1S model (Karstunen & Yin, 2010).

6

INFLUENCE OF CONSTITUTIVE MODEL ON NUMERICAL RESULTS: 3D STUDY

In this chapter numerical simulations with different constitutive models have been performed to asses the impact of the constitutive models on the predicted response of an embankment constructed on soft soil improved with floating stone columns. For calculations six constitutive models were used to simulate the behaviour of the soft soil deposit:

- Modified Cam Clay (Roscoe & Burland, 1968),
- S-CLAY1 (Wheeler *et al.,* 2003),
- S-CLAY1S (Koskinen *et al,* 2002, Karstunen *et al.,* 2005),
- Soft Soil Creep Model (Brinkgreve, 2002),
- Anisotropic Creep Model (Leoni *et al*., 2008),
- Anisotropic Creep Model with destructuration ACM-S.

The constitutive models used for this study were described in *Chapters 2* and *5.* The Modified Cam Clay (MCC) and the Soft Soil Creep model (SSC) are isotropic formulations, whereas the S-CLAY1 and the ACM models account for fabric anisotropy.

The S-CLAY1S and the ACM-S models, introduced in *Chapter 5*, in addition to fabric anisotropy, also take into account the effect of interparticle bonding and the destructuration process. The MCC, S-CLAY1 and S-CLAY1S models are elasto-plastic formulations, whereas the SCC, ACM and ACM-S are viscous constitutive models. The soft deposit was assumed to have the properties of the Bothkennar clay from Scotland. The aim of this chapter is to understand and demonstrate the difference between the alternative modelling approaches, and to study the influence of anisotropy, destructuration and time-dependency, and their combinations, on the stress-strain response of a soft deposit improved with stone columns. Moreover, the impact of the over-consolidation of the soil mass (expressed as pre-consolidation stress) on the numerical predictions of the initial stresses, construction stage and subsequent consolidation process is also discussed.

6.1 Benchmark problem and numerical model

The three-dimensional boundary value problem considers a soft soil improved by floating stone columns and it represents a typical application for stone columns: reducing the settlement of earth structures. The benchmark chosen for this chapter considers an embankment constructed on Bothkennar clay, soft clay from Scotland.

Similar to *Chapter 4*, the stone columns were used in order to reduce the total and differential settlements and the consolidation time. The effect of the different constitutive models on the stress-strain behaviour of the soil matrix during embankment construction and during the subsequent consolidation process was investigated. The effects of various constitutive models on soft clay response has been the subject of many studies, see Wiltafsky *et al.* (2003), Karstunen *et al.* (2006) or Krenn (2008). However none of these studies considered time-dependency and secondary compression effects. Moreover, the majority of previous studies have investigated unimproved soft deposits, whereas especially in soft soils, ground improvement techniques, such as stone columns, are required. This chapter is an attempt to investigate that engineering problem in detail and the aspects influencing the behaviour of the soft soil are studied. The dimensions, geometry and simulation assumptions are the same as those used in the reference simulation in the benchmark study described in *Chapter 4*.

To represent the layers of dry crust and the Bothkennar clay during simulations, six different constitutive models were chosen: MCC (Roscoe & Burland, 1968), S-CLAY1 (Wheeler *et al.*, 2003), S-CLAY1S (Koskinen *et al.*, 2002 and Karstunen *et al.*, 2005), SSC (Brinkgreve, 2002), ACM (Leoni *et al.*, 2008) and as presented in *Chapter 5*, ACM-S. Table 6.1 summarises the capabilities of the constitutive models, specifying the specific soft soil characteristics which are considered in each model. The first three models (MCC, S-CLAY1 and S-CLAY1S) are incapable of taking account of the viscous behaviour of the soil, whereas the SSC, ACM and ACM-S models are viscous models. MCC and SSC are isotropic formulations. The aim of this numerical study is to apply two constitutive models widely accepted by the

engineering community and implemented in FE commercial code (MCC and SSC) and their more sophisticated and advanced extensions (S-CLAY1, S-CLAY1S, ACM and ACM-S) into a three-dimensional boundary value problem involving floating stone columns underneath an embankment.

Table 6.1: Capabilities of chosen constitutive models and soil characteristics.

Soil characteristic	Constitutive model					
	MCC	S-CLAY1	S-CLAY1S	SSC (PLAXIS)	ACM	ACM-S
Anisotropy		•	•		•	•
Interparticle bonding and destructuration			•			•
Viscosity				•	•	•

For all simulations, PLAXIS 3D Foundation v.2.2 finite element code has been used, taking advantage of the three-dimensional modelling. A representative slice of the full geometry was used in the numerical simulations. A mesh with 7 200 tetrahedral elements and approximately 80 000 degrees-of-freedom was used in the simulations. As for *Chapter 4*, mesh sensitivity studies were carried out before performing the parametric study in order to reduce the influence of the mesh on the results of the simulations. The computational time required to calculate the considered benchmark problem was equal to approximately 1 to 2 days due to the large number of degrees-of-freedom in each of the simulations and the complexity of the advanced constitutive models used. One should note that SSC is implemented

into PLAXIS 3D Foundation v.2.2 as a standard constitutive model, whereas all the other formulations were applied in FE software as user-defined soil models.

6.2 Material properties

To represent soft soil during this study, as in *Chapter 4*, the Bothkennar clay (Scotland) was selected. In the simulations the deposit was idealised by two layers: a slightly over-consolidated soft clay overlain by a 1m thick over-consolidated dry crust. This soft clay is a cross-anisotropic and structured material with a high susceptibility for creep indicated by extensive field and laboratory tests, see Géotechnique (1992). In the following section the properties for the soft soil (Bothkennar clay) and for the dry crust for each of the constitutive models used are presented.

The state parameters and soil constants used as the input parameters for all six constitutive models are presented below. First, the parameters describing the S-CLAY1S 'family' are given, as this model is a hierarchical extension of the isotropic MCC and anisotropic S-CLAY1 models. Then, the soil parameters used for the creep models (SSC, ACM and ACM-S) are presented.

6.2.1 S-CLAY1S- type models

A detailed description of the S-CLAY1S 'family' of models (MCC, S-CLAY1 and S-CLAY1S) was presented in *Chapter 2*. The state parameters and soil constants describing the clay and dry crust are shown in Tables 6.2..6.4. As emphasised in *Chapter 2*, S-CLAY1S is a hierarchical extension of the MCC model. It is possible to switch on or off certain features, such as the rotation of the yield surface or the initial amount of bonding. By setting ξ, ξ_d and χ_0 to zero values and using intrinsic rather than the apparent value of the slope of the normal compression line S-CLAY1S reduces to the anisotropic S-CLAY1 model and by setting parameters ω and α_0 to zero it further reduces to the isotropic MCC model.

6.2.2 Creep models

The state parameters and soil constants describing the soil deposit with SSC, ACM and ACM-S are shown in Tables 6.5..6.8. The ACM-S model, which accounts for anisotropy, interparticle bonding and time-dependency of soft soil, is a hierarchical formulation, similar to S-CLAY1S, which allows for switching on or off certain soil mass features. It can be reduced to the ACM model by setting the initial amount of bonding to zero.

Table 6.2: Standard soil constants: MCC, S-CLAY1 and S-CLAY1S.

Layer	Depth [m]	γ [kN/m^3]	k [m/s]	ν' [-]	M [-]	κ [-]	λ / λ_i [-]
Dry crust	0-1	19.0	$1x10^{-9}$	0.2	1.51	0.02	0.3/0.15
Bothkennar clay	1-30	16.5	$2.89x10^{-9}$	0.2	1.51	0.02	0.3/0.15

Table 6.3: Advanced soil constants: MCC, S-CLAY1 and S-CLAY1S.

Layer	Depth [m]	ω_d [-]	ω [-]	ξ [-]	ξ_d [-]
Dry crust	0-1	1	30	9	0.2
Bothkennar clay	1-30	1	50	9	0.2

Table 6.4: State variables: MCC, S-CLAY1 and S-CLAY1S.

Layer	Depth [m]	e_0 [-]	K_0 [-]	POP [kN/m^2]	OCR [-]	α_0 [-]	χ_0 [-]
Dry crust	0-1	1.37	0.7	30	-	0.59	4
Bothkennar clay	1-30	2.0	0.5	-	1.5	0.59	8

Table 6.5: Soil constants: SSC, ACM and ACM-S.

Layer	Depth [m]	γ [kN/m^3]	k [m/s]	ν' [-]	φ' [-]
Dry crust	0-1	19.0	$1x10^{-9}$	0.2	37
Bothkennar clay	1-30	16.5	$2.89x10^{-9}$	0.2	37

Table 6.6: Additional soil constants: SSC, ACM and ACM-S.

Layer	Depth [m]	POP [kN/m^2]	OCR [-]	K_0 [-]
Dry crust	0-1	30	-	0.7
Bothkennar clay	1-30	-	1.5	0.5

Table 6.7: Time-dependency and anisotropy constants: SSC, ACM and ACM-S.

Layer	μ^* / μ_i^* [-]	τ [day]	λ^* / λ_i^* [-]	κ^* [-]	ω [-]	ω_d [-]
Dry crust	0.0021/0.0011	1	0.1266/0.0633	0.0084	30	1
Bothkennar clay	0.004/0.002	1	0.1/0.05	0.0067	50	1

Table 6.8: Destructuration constants: SSC, ACM and ACM-S.

Layer	χ_0 [-]	ξ_d [-]	ξ [-]
Dry crust	4	0.2	9
Bothkennar clay	8	0.2	9

Over the years many studies have been conducted in order to investigate the relationship between the secondary compression and the compression indexes C_α / C_c, which for natural soils is found to be between 0.02 and 0.1, see Mesri & Godlewski (1977), Mesri & Castro (1987), Mesri (2001) or Mesri & Vardhanabhuti (2005). The creep parameters for reconstituted and natural soil are determined using findings by Nash *et al.* (1992) during the incremental loading oedometers tests on Bothkennar clay that the ratio C_α / C_c is equal to 0.03..0.05. Applied for the numerical study ratio of $\mu_i^* / \lambda_i^* = 0.04$ for Bothkennar clay is well within this range of values, and the intrinsic modified creep index was assumed to be equal to 0.002.

6.3 Numerical results

The construction sequence has been assumed to be the same as in *Chapter 4*: first the installation of stone columns and the construction of the embankment took place under undrained conditions and was then followed by consolidation. The end of consolidation is defined as occurring when the value of the excess pore water pressures is equal to or less than 1 kPa. As the installation effects are not the subject of this research, they have not been taken into account. The stone columns underneath the embankment were simply 'wished-in-place' by switching the appropriate clusters with dry crust and the clay properties to a granular material.

As the impact of the over-consolidation of the soft deposit on numerical predictions is a subject of some parts of this study, the value of the pre-consolidation stress has been changed for some of simulations. However, unless stated otherwise, the soft clay is assumed as slightly over-consolidated material with OCR value equal to 1.5 and the dry crust layer is considered as over-consolidated and described with POP value of 30 kPa.

6.3.1 Vertical displacement

The predicted surface settlements for the different constitutive models are presented in Figure 6.1, where both the settlement after construction (solid lines) and after consolidation (dashed lines) are shown for the S-CLAY1S and ACM-S group of models. As expected, all of the models predicted lower values of settlements in the

granular material than in the soil mass due to the greater bearing capacity of the columns than the surrounding soil. After construction the S-CLAY1S type models predict the same small surface heave (~3 mm) outside the embankment, which is not predicted by the creep models, and the predicted values are almost the same for all the elasto-plastic models. The maximum vertical displacement after construction was approximately 0.032 m and was predicted by SSC, whereas the smallest movement was predicted by the S-CLAY1S type of models, at approximately 0.025 m, see Figure 6.1.

At the end of consolidation under the embankment the isotropic MCC model predicted a stiffer response than S-CLAY1 or S-CLAY1S, proving that considering soft soils as isotropic media results in an underestimation of the settlements (see Figure 6.1a). The maximum vertical displacement predicted by all six constitutive models was at the centreline of the embankment and the zero surface settlement point was located about 10 m from the symmetry axis for all models (which corresponds to the width of the embankment base). In reality, due to the installation of the stone columns the interparticle bonds will be damaged further and a greater vertical (and subsequently horizontal) movement may be anticipated.

It has been previously proven by Karstunen *et al.* (2006) that the incorporation of plastic anisotropy increases the predicted settlements for an unimproved soft soil. In the current research ground improvement has been considered. The anisotropic S-CLAY1 model predicts the highest values of settlements compared with the other elasto-plastic models. Results from the simulation with the S-CLAY1S model are in between the other two remaining analyses (MCC and S-CLAY1). The opposite behaviour is observed for SSC, ACM and ACM-S, where the isotropic SSC model

predicts notably higher vertical displacements. As the creep models generate creep strains in both the normally- and over-consolidated range, the predicted settlements are greater than those estimated by S-CLAY1S type of formulations. The SSC model implemented in the PLAXIS finite element code predicts very different and unrealistic magnitudes of the surface settlements when compared to the other viscous and all of the elasto-plastic models. Moreover, Figure 6.1b shows that time-dependent constitutive models predict substantial (and unrealistic) vertical displacements in the area not subjected to any loading, so these deformations are simply trigged by the self-weight of the soil mass. Due to an increase of the creep strains with time in the ACM-S type of formulations, the settlement of the soil deposit and the creep process starts immediately without imposing any loading.

This issue was further analysed by conducting additional numerical simulations with ACM-S. Before the construction of the stone columns and embankment began, a stage with in-situ stresses only, where the soft soil deposit was allowed to consolidate for an excessive period of time (t = 10 000 years) under its own self-weight was simulated. Next, the vertical and horizontal displacements were set to zero and the stone columns and embankment were constructed (as undrained actions), followed by the consolidation process. Figure 6.2 presents the settlement predictions after construction and consolidation for this simulation (in red) along with the comparative results shown in Figure 6.1 (in black). The procedure carried out, of resetting the displacements to zero after allowing for reconsolidation of the soft soil deposit, has little influence on the settlement predictions after construction.

a)

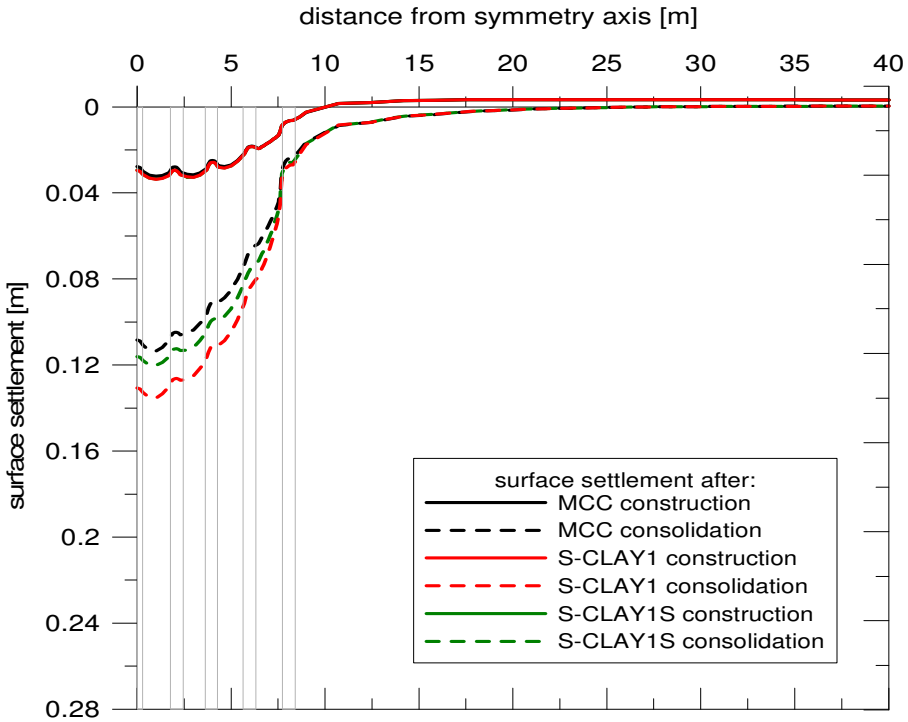

b)

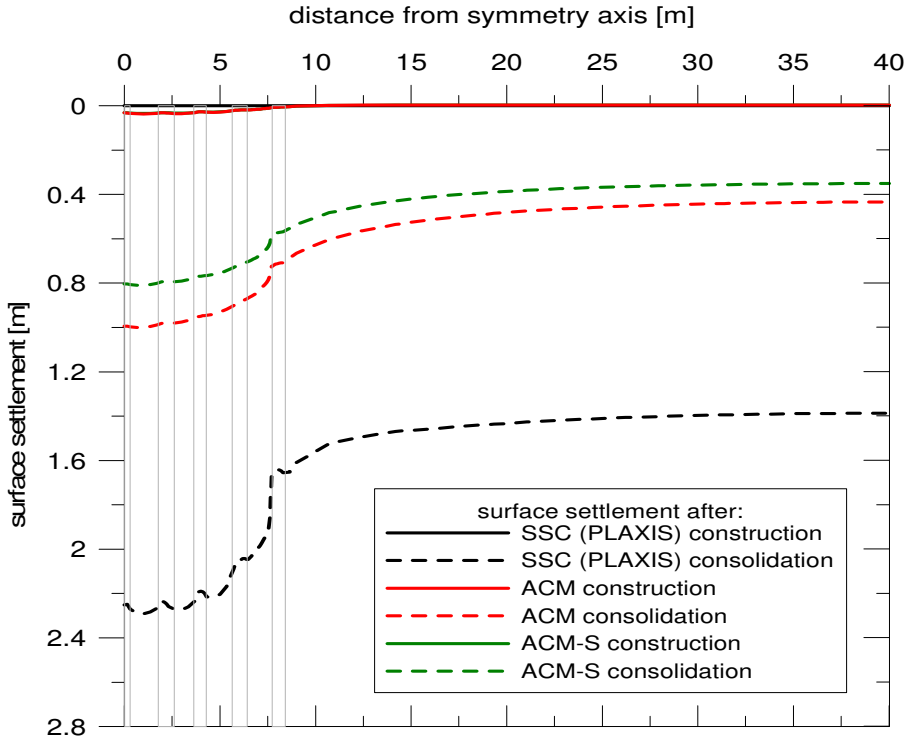

Figure 6.1: Predicted surface settlements for 3D study after construction and consolidation: a) S-CLAY1S 'family' and b) creep models.

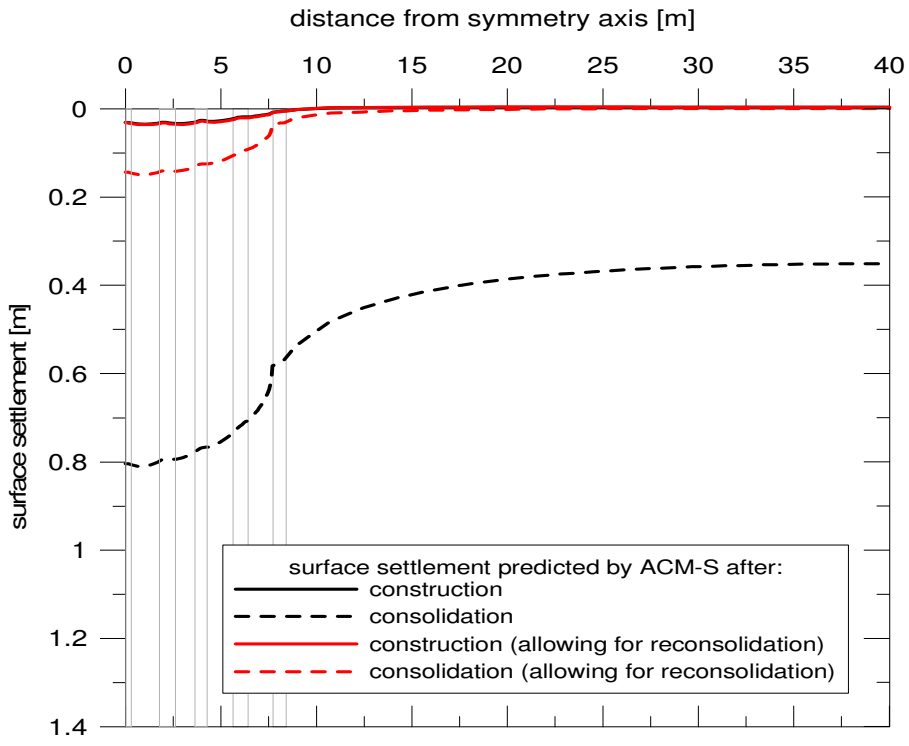

Figure 6.2: Influence of the modelling approach on predicted surface settlements for 3D study after construction and consolidation: ACM-S.

However, its major influence on the numerical predictions is obvious when looking at the surface settlements after consolidation. Allowing for reconsolidation of the soft Bothkennar deposit, results in a reduction in the vertical displacement value approximately by a factor of 6. Moreover, as the soft soil has been already reconsolidated before the stone columns and the embankments are constructed, no self-weight settlements during unloading were predicted, see Figure 6.2. In fact, allowing for reconsolidation of the soft clay resulted in predicted surface settlements after construction and consolidation of the same magnitude that were predicted by

the elasto-plastic S-CLAY1S group of models. Inspection of the contours of the bonding parameter and the over-consolidation ratio in the soft soil deposit at the initial stage of simulation for the standard modelling approach and for the modelling approach allowing for reconsolidation led to conclusion that although the reconsolidation approach can be used for the issue of the unrealistic self-weight surface settlements predicted when using the time-dependent constitutive models, it is not realistic (and thus, effective) to apply it for numerical simulations of geotechnical problems.

Following the findings in *Chapter 5*, studies of the influence of the ratio between the secondary compression index C_α and the compression index C_c on the surface settlements using ACM-S were conducted. For this part, the C_α / C_c ratio (or ratio μ_i^* / λ_i^*) was chosen to be 0.08, which is two times higher than that found by Nash *et al.* (1992B) during the incremental loading oedometers tests on Bothkennar clay and the limits found by Mesri *et al.* (1995) for natural soils. Figure 6.3 presents the settlement predictions after construction and consolidation for this simulation (in red) along with the comparative results shown in Figure 6.1 (where the C_α / C_c ratio was assumed to be equal to 0.04). It can be observed that the surface settlement changes dramatically with a change in the C_α / C_c ratio, see Figure 6.3. By setting the C_α / C_c ratio to a higher value, the viscosity of the soft soil increases, leading to an increase in the vertical displacement value. This increase is ultimately uniform, which results in a greater surface settlement at the outer boundary of the geometry model. The influence of this ratio on numerical predictions of stress-strain behaviour is evident and this relationship should be carefully determined.

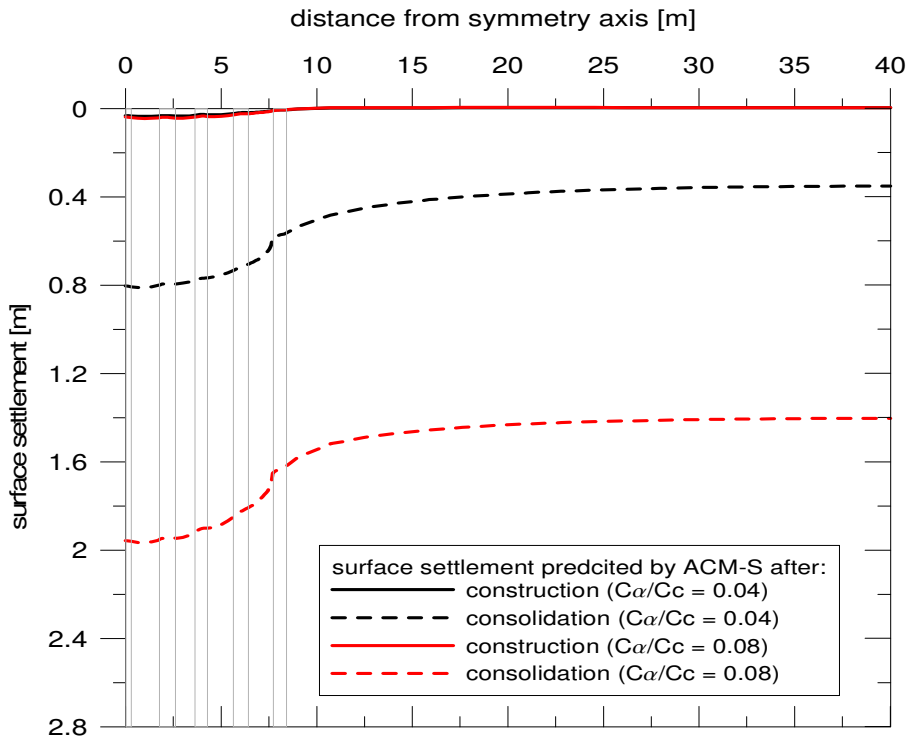

Figure 6.3: Influence of the C_α / C_c ratio on predicted surface settlements for 3D study after construction and consolidation: ACM-S.

In order to asses the settlement reduction ratio s_r (which describes the reduction of the settlements due to the ground improvement), simulations in which the improvement of the soft soil is not considered were also performed. For the case modelled using isotropic MCC the settlement reduction ratio was equal to 0.553, whereas for S-CLAY1 and S-CLAY1S it was equal to 0.829 and 0.818, respectively. Accounting for anisotropy in the simulations with the elasto-plastic models increased the settlement reduction ratio s_r from 0.553, predicted by MCC, to 0.829 estimated by S-CLAY1 (which resulted in an increase in the vertical displacement value by almost 50 %). The influence of the combination of the anisotropy and interparticle

bonding effect resulted in a slight increase of the settlement improvement ratio for the numerical analysis when compared with the predictions made by the S-CLAY1 model. For the case modelled with isotropic SSC model the settlement reduction ratio was equal to 0.424, whereas for ACM and ACM-S it was equal to 0.984 and 0.988, respectively. Accounting for anisotropy in the simulations carried out with the time-dependent models, increased the settlement reduction ratio s_r from 0.424, predicted by SSC, to 0.988 estimated by ACM-S, which resulted in a reduction of the vertical displacement by approximately 133 %. The influence of the combination of the anisotropy and bonding effect resulted in a slight increase of the settlement improvement ratio for the numerical analysis.

The evolution of the settlement with depth at the centreline of the embankment was also investigated. Point A (at the centreline of the granular material) was chosen for the investigation of vertical displacements versus depth, see Figure 6.4. Figure 6.5 presents the predicted differential vertical displacements versus depth at the centreline of the embankment for point A for all of the constitutive models used.

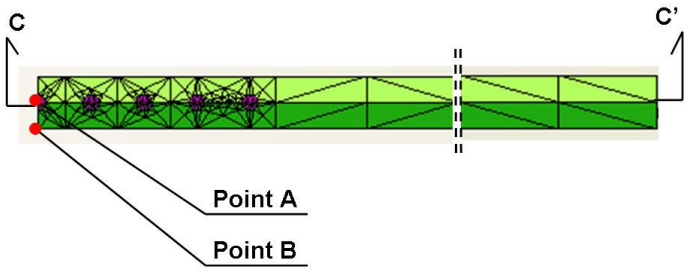

Figure 6.4: The chosen points for settlement analysis for 3D study: top view of geometry.

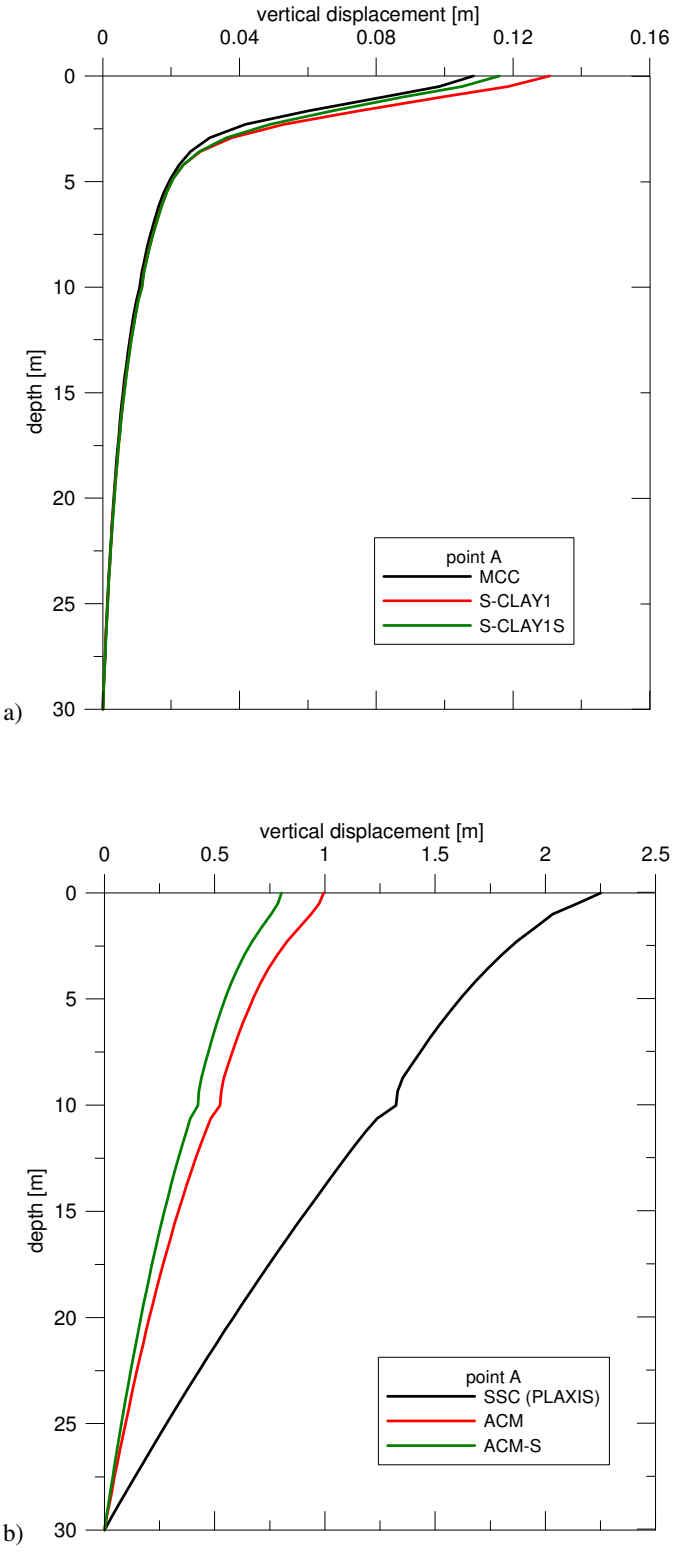

Figure 6.5: Predicted vertical displacements versus depth at the centreline of the embankment for 3D study for: a) S-CLAY1S 'family' and b) creep models.

It can be observed that both types of constitutive models predict different magnitudes of the movement and the general tendency of curvature. The time-dependent formulations estimated much greater vertical displacements at every point in the vertical profile than the elasto-plastic models (at most points by a factor of 10), see Figure 6.5. In the elasto-plastic models, the discrepancy between the predictions made by the models was observed solely at shallow depths, approximately from the ground level up to 5 m depth. This is due to the shape and inclination of the yield surfaces incorporated in the chosen constitutive models. Anisotropy influences the predictions of the vertical displacement forming the lower bound for the predictions. The vertical displacements decrease with depth, reaching 1 mm at a depth of approximately 25 m. Discrepancy between the predictions using the viscous models was much more pronounced than for the elasto-plastic models. The isotropic SSC model predicted unrealistically large movements, of different magnitude than the other models, at the ground surface of approximately 2.251 m. ACM and ACM-S predicted notably smaller values of the surface vertical displacements of 0.994 m and 0.804 m, respectively. Additionally, the predictions given by the creep models do not predict as sharp a reduction in the settlements with depth as the elasto-plastic models, and the reduction in the vertical displacement value with depth takes place at a much smaller rate, reaching only 1 mm at the bottom of the geometry model (depth of 30 m), see Figure 6.5b. Taking into account anisotropy, which was simulated with ACM, caused a reduction in the vertical settlements along the vertical profile. The vertical movement was further reduced by incorporating destructuration in the time-dependent constitutive models.

6.3.2 Horizontal displacement

The predicted lateral movements underneath the embankment toe after construction and consolidation are shown in Figures 6.6 and 6.7.

Figure 6.6 presents the predicted horizontal displacements underneath the embankment toe versus depth after construction. After construction of the stone columns and the embankment, all of the models but one (SSC) predicted similar values of the horizontal displacements at the embankment toe, of approximately 0.010 m. The isotropic SSC model predicted significantly larger horizontal displacements, of approximately 0.070 m, due to yielding at most of the stress points underneath the embankment, as found during inspection of the plastic points. Moreover, SSC predicted, in contrast to other models, that the horizontal displacement after construction was the greatest at the ground surface in the stiff dry crust layer and then gradually decreased with depth.

Figure 6.7 presents the horizontal displacements after consolidation at the embankment toe. The largest horizontal displacements at the toe of embankment were again predicted by SSC, where approximately 0.130 m of lateral movement was predicted at the ground surface. All of the constitutive models except SSC predicted horizontal deformations of different (smaller) magnitudes. Again, and as expected, the elasto-plastic models predicted the lowest value of horizontal displacements, see Figure 6.7. The maximum horizontal movements were predicted by all but one (SSC) of the models at a depth of 1 m, coinciding with the discontinuity of K_0 and the over-consolidation pressure. That mechanism is particularly apparent for the ACM

and ACM-S models, see Figure 6.7b. Negative values of the horizontal displacements were predicted by the time-dependent ACM and ACM-S models as a result of high settlements pulling the embankment toe towards the centreline of the geometry model. Accounting for anisotropy in the elasto-plastic models led to a marginal reduction of the predicted lateral movements, and taking into account both anisotropy and destructuration further reduced the value of the horizontal displacements. For the time-dependent models, considering soil anisotropy also reduced the predicted lateral movements. Again, it can be observed that the horizontal displacements predicted by the SSC model were much higher than those predicted by the other formulations; this is most probably the result of assumed creep part of the model or a possible error in the numerical implementation of the SSC model enclosed in the PLAXIS code. This should be investigated in the future by further numerical simulations using the isotropic version of the ACM model (with $\alpha = 0$ and $\omega = 0$).

6.3.3 Stress paths and stress contours

For the studies on the influence of the constitutive models on the numerical predictions of selected stress paths the point corresponding to the surrounding soil (point B) was investigated, see Figure 6.4.

Figures 6.8 and 6.9 present the selected stress paths at point B at two different depths below the centreline of the embankment: at the top of the clay layer (depth of 1 m) and at the base level of the stone column (depth of 10 m). Plots are presented in terms of t' and s', where $t' = (\sigma_1' - \sigma_3')/2$ and $s' = (\sigma_1' + \sigma_3')/2$.

a)

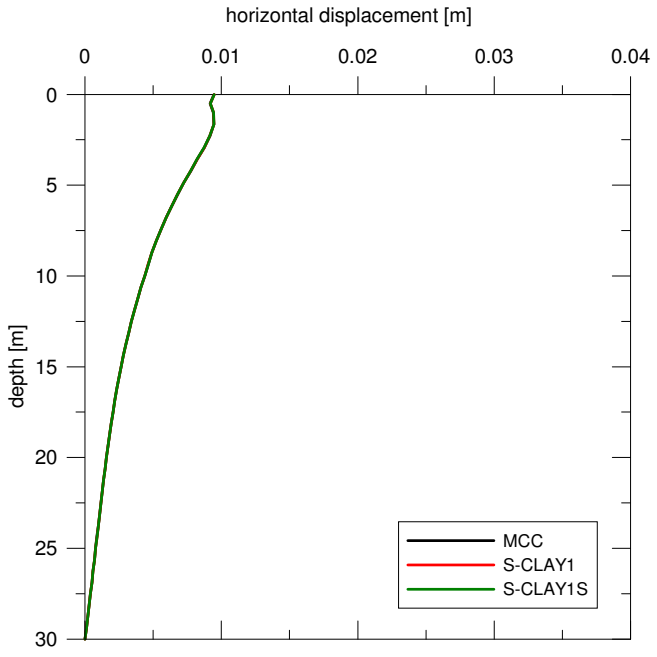

b)

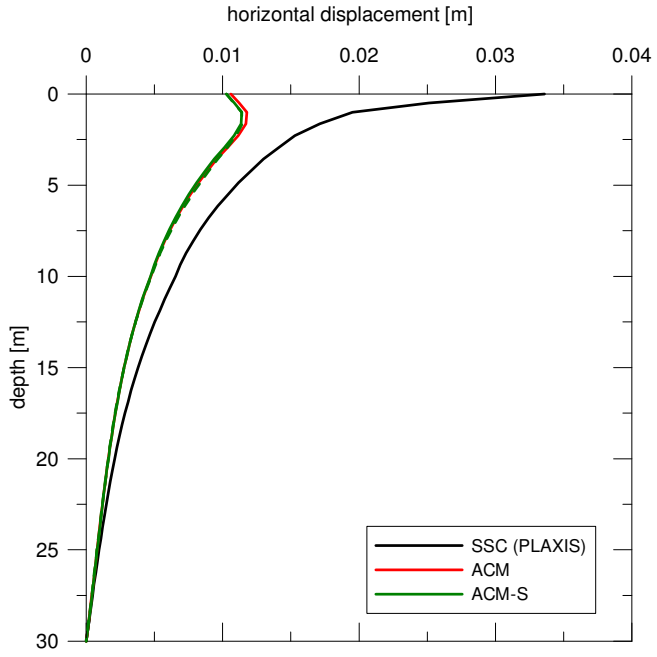

Figure 6.6: Predicted horizontal displacement versus vertical profile at the embankment toe after construction for 3D study for: a) S-CLAY1S 'family' and b) creep models.

a)

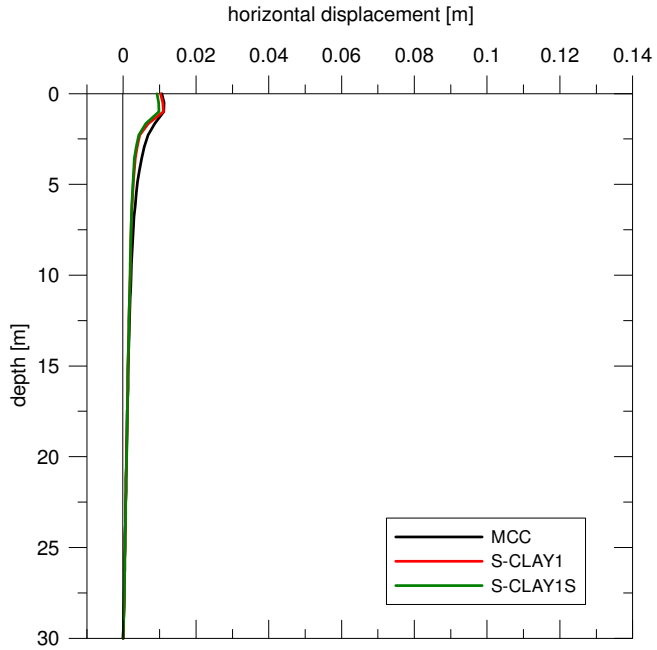

b)

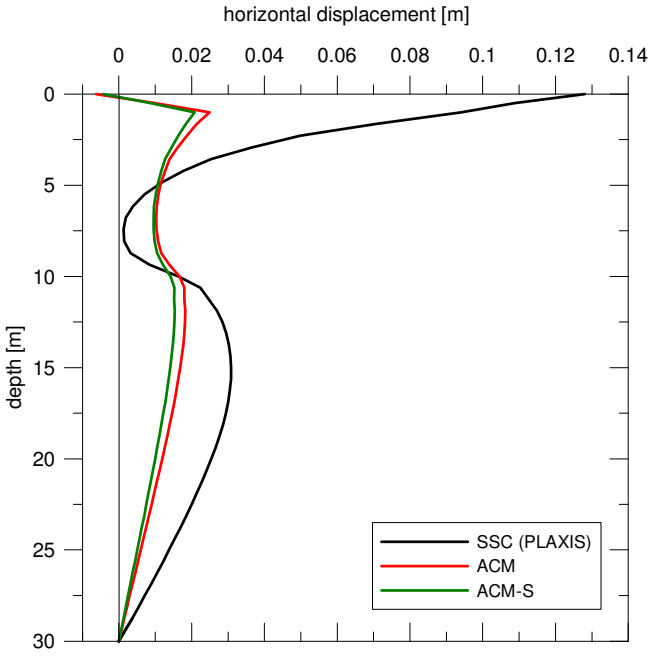

Figure 6.7: Predicted horizontal displacement versus vertical profile at the embankment toe after consolidation for 3D study for: a) S-CLAY1S 'family' and b) creep models.

For detailed inspection of the stress paths at a depth of 1 m, the predictions given by all the constitutive models at point B are presented in Figure 6.8. The steepness of the stress paths is similar except for the isotropic MCC and SSC models. As the K_0-stress ratio of 0.70 was calculated for the 1D-consolidation of the dry crust layer, the elasto-plastic S-CLAY1S and S-CLAY1S models and the time-dependent ACM and ACM-S models predicted a somewhat more realistic stress path, with a gradient of 0.60, than the other formulations, see Figure 6.8. In contrast, the isotropic MCC and SSC models predicted gradients of the stress ratio of about 0.41 and 0.24, respectively. The greatest influence on the numerical predictions was taking into account soil anisotropy, whereas the combination of both anisotropy and destructuration had little effect on the stress predictions.

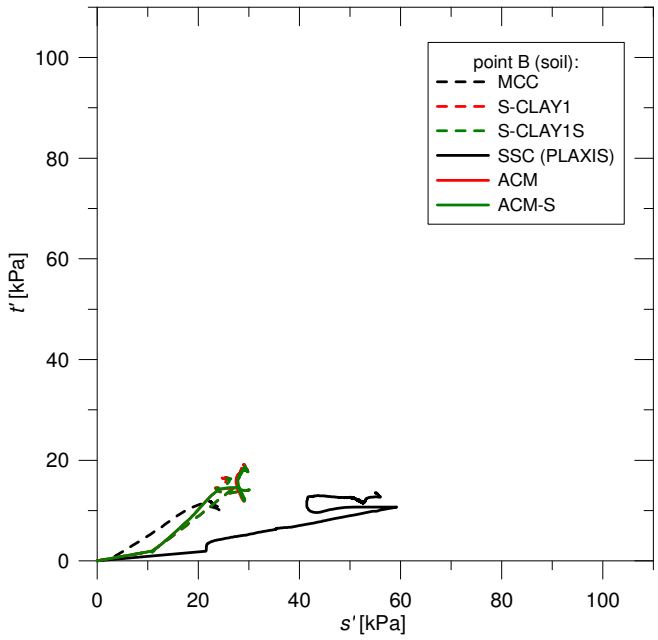

Figure 6.8: Triaxial stress paths under the centreline of the embankment at a depth of 1 m for point B for S-CLAY1S 'family' and creep models.

For detailed inspection of the predicted stress paths in the soft soil deposit Figure 6.9 is presented. Only the isotropic MCC model predicted a much smaller magnitude of stress at point B, whereas the other elasto-plastic formulations, ACM and ACM-S predicted almost identical stress paths in the soft soil deposit at a depth of 10 m. It is evident that the influence of anisotropy and destructuration is small, but that the impact of accounting for soil anisotropy solely is much more pronounced.

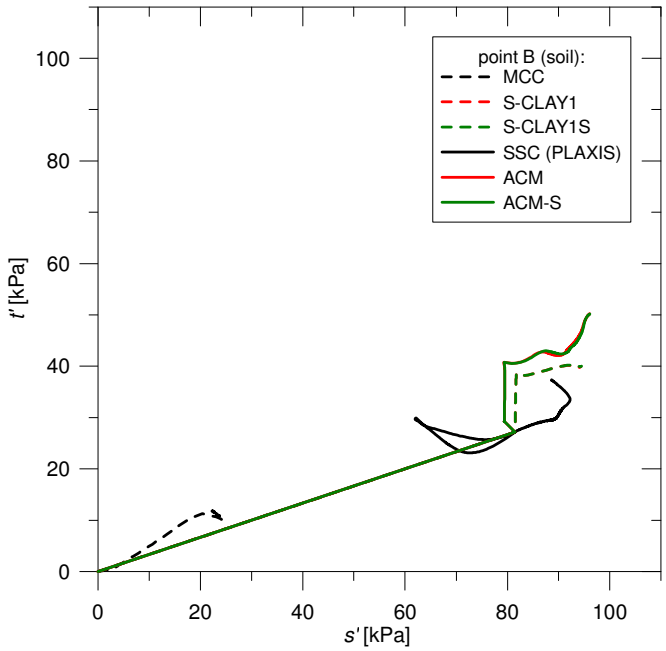

Figure 6.9: Triaxial stress paths under the centreline of the embankment at a depth of 10 m for point B for S-CLAY1S 'family' and creep models.

The predicted vertical effective stress contours along a horizontal profile at the centre of the stone columns after consolidation are presented in Figures 6.10 and 6.11. All but one of the constitutive models (SSC) predicted similar overall contours of the vertical effective stresses.

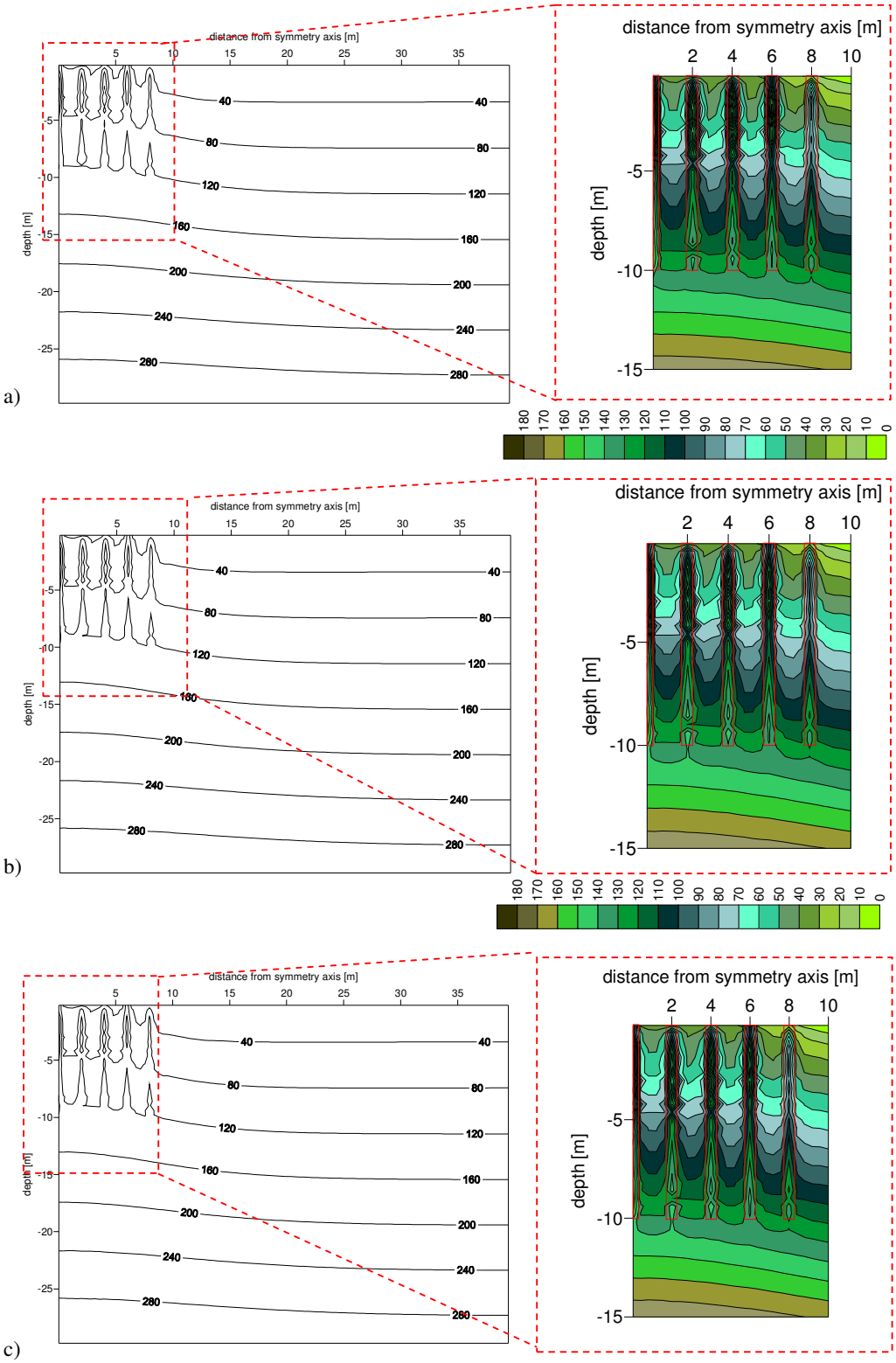

Figure 6.10: Vertical effective stress (in kPa) contours after consolidation for:

a) MCC b) S-CLAY1 and c) S-CLAY1S.

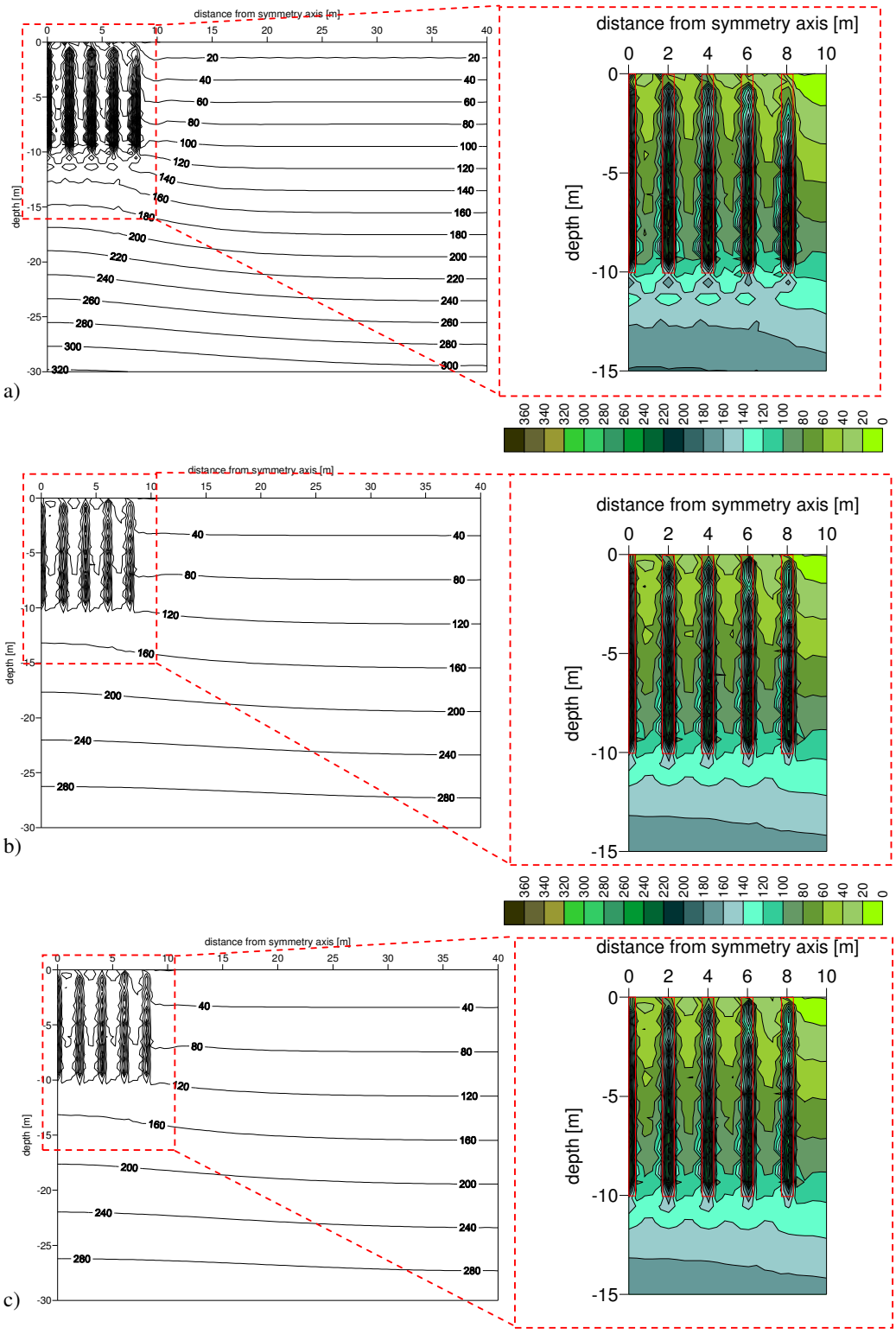

Figure 6.11: Vertical effective stress (in kPa) contours after consolidation for:
a) SSC (PLAXIS) b) ACM and c) ACM-S.

Detailed inspection of the stone column improved area confirmed that the surrounding soil in the treated zone experienced much greater vertical effective stresses when predicted by the time-dependent models rather than by the elasto-plastic formulations. Moreover, the granular columns experienced a higher amount of stress (170..180 kPa and 350..360 kPa with the elasto-plastic and time-dependent models, respectively) than the surrounding soil, especially in the shallow deposit of dry crust. Higher values of vertical effective stresses in the creep models rather than in the elasto-plastic models was due to negative skin friction.

The predicted horizontal effective stress contours along a horizontal profile in at the centre of the stone columns after consolidation are presented in Figures 6.12 and 6.13. The elasto-plastic constitutive models predicted overall higher levels of the horizontal effective stresses after consolidation than the creep models. In fact, the lowest overall maximum horizontal effective stresses were predicted by the isotropic SSC model. Moreover, in the case of the creep models some concentration of the horizontal effective stresses was predicted in the lower part of the columns, above 80 kPa in some locations and 60 kPa for SSC and ACM/ACM-S, respectively. The elasto-plastic models predicted some horizontal effective stress concentration of about 40 kPa in the upper part of the columns.

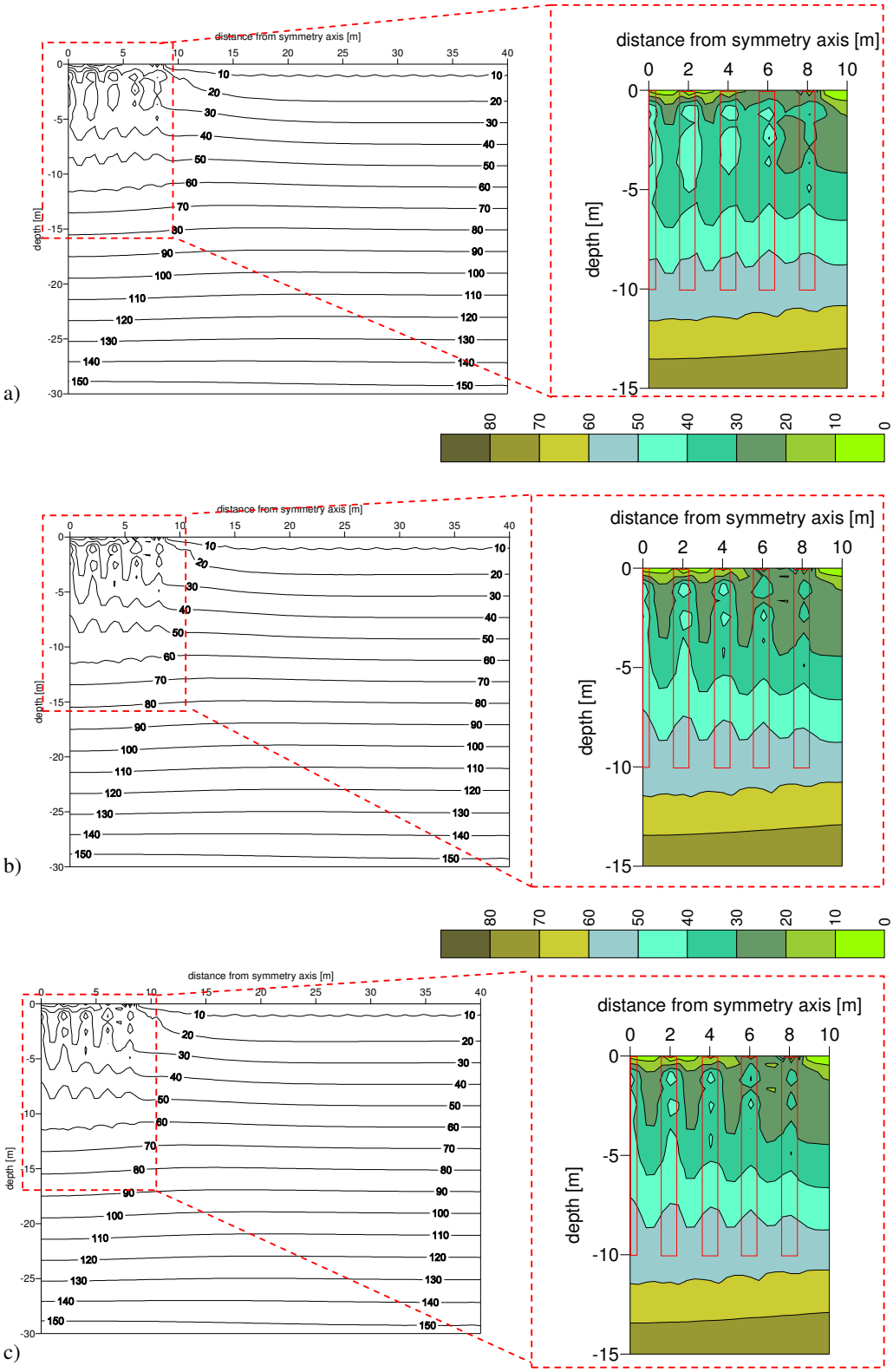

Figure 6.12: Horizontal effective stress (in kPa) contours after consolidation for:
a) MCC b) S-CLAY1 and c) S-CLAY1S.

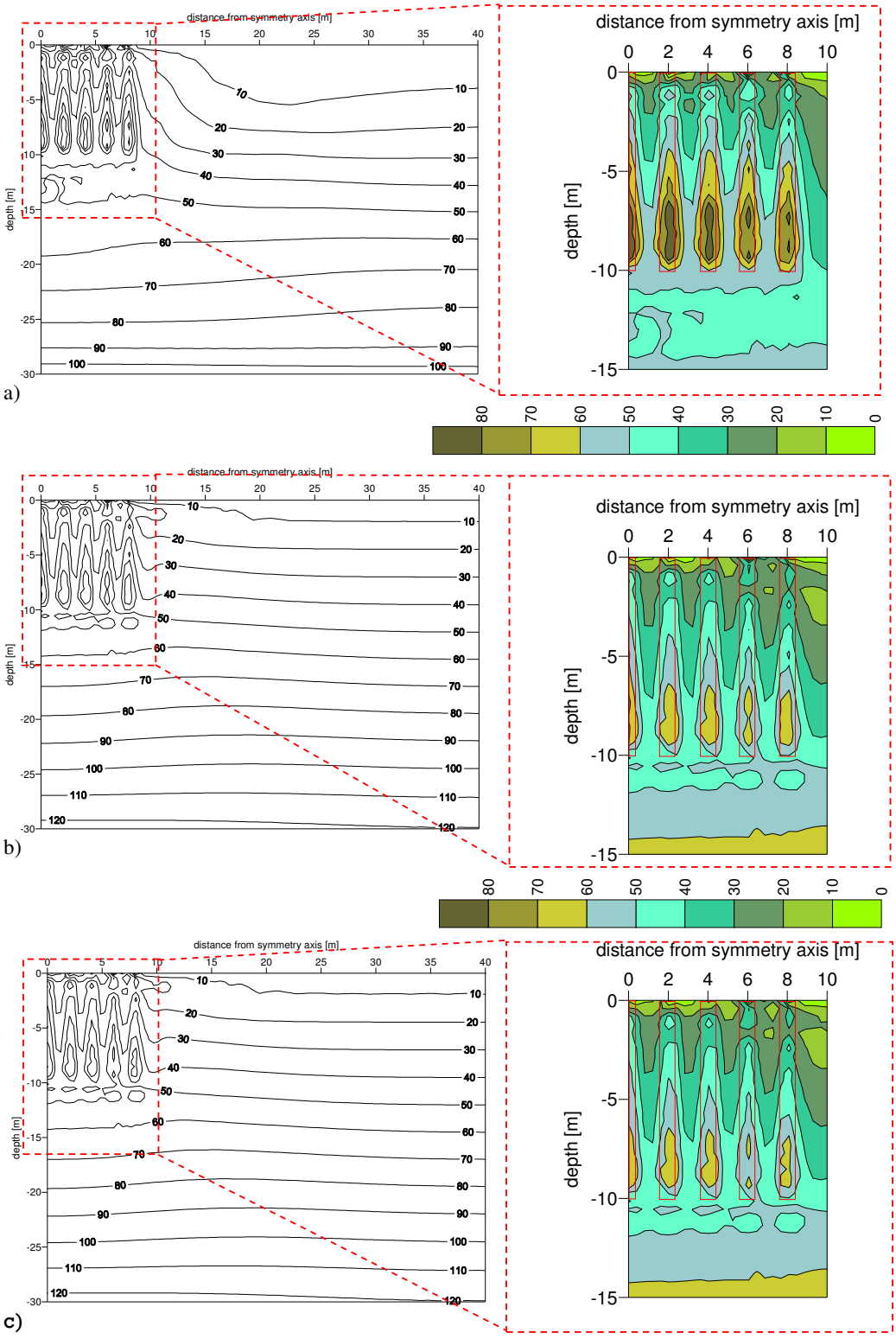

Figure 6.13: Horizontal effective stress (in kPa) contours after consolidation for:
a) SSC (PLAXIS) b) ACM and c) ACM-S.

6.3.4 Excess pore water pressures

The stone columns speed up the dissipation of the excess pore water pressure, therefore an inspection of the excess pore water pressures at selected depths is of interest, see Figure 6.14. The evolution of excess pore water pressures with time in the soil mass surrounding the stone columns at a depth of 10 m (base level of the floating stone columns) and 15 m below the ground surface for all six constitutive models is presented in Figures 6.15 and 6.16.

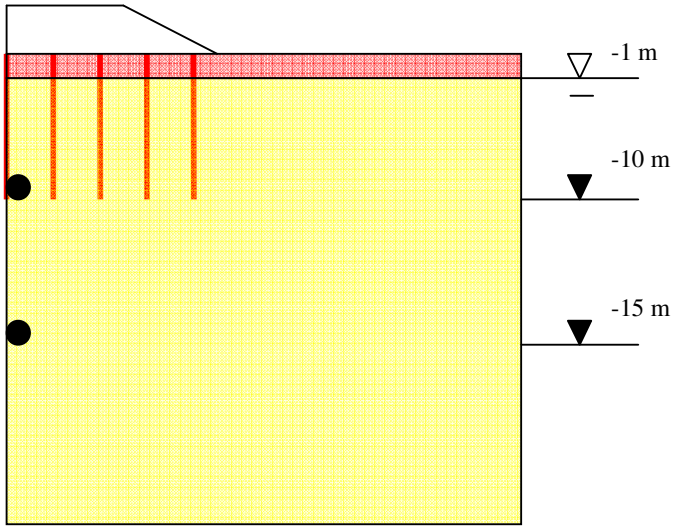

Figure 6.14: Sketch of the benchmark geometry with selected points for the excess pore water pressures predictions: 3D study.

Evolution of the excess pore water pressures at the level of the stone column bases (depth of 10 m) with time is shown in Figure 6.15. It is clear that all but one of the constitutive models (namely SSC) predicted very similar evolution of the excess pore water pressures with time.

a)

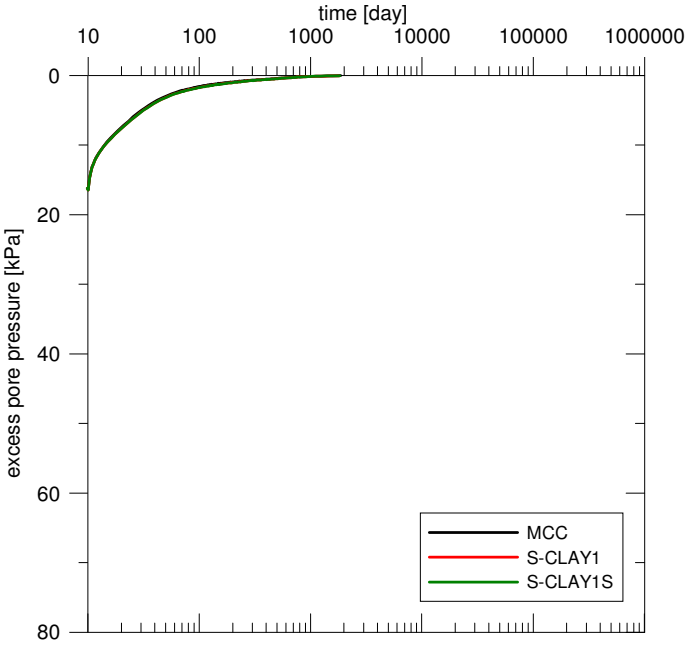

b)

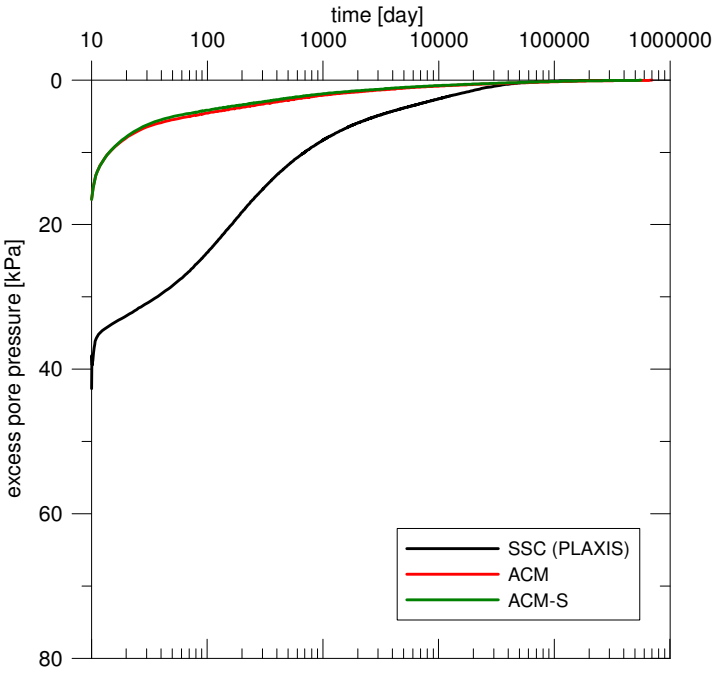

Figure 6.15: Evolution of the excess pore water pressures with time at a depth of 10 m for 3D study for: a) S-CLAY1S 'family' and b) creep models.

a)

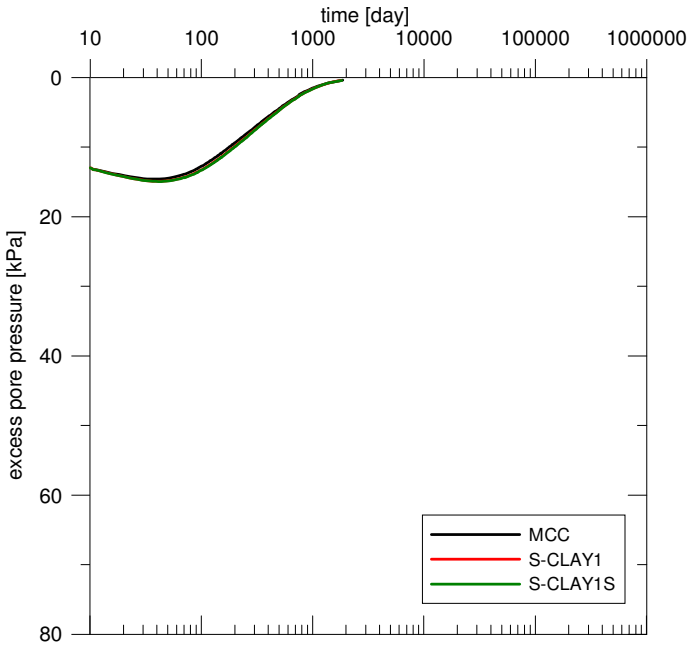

b)

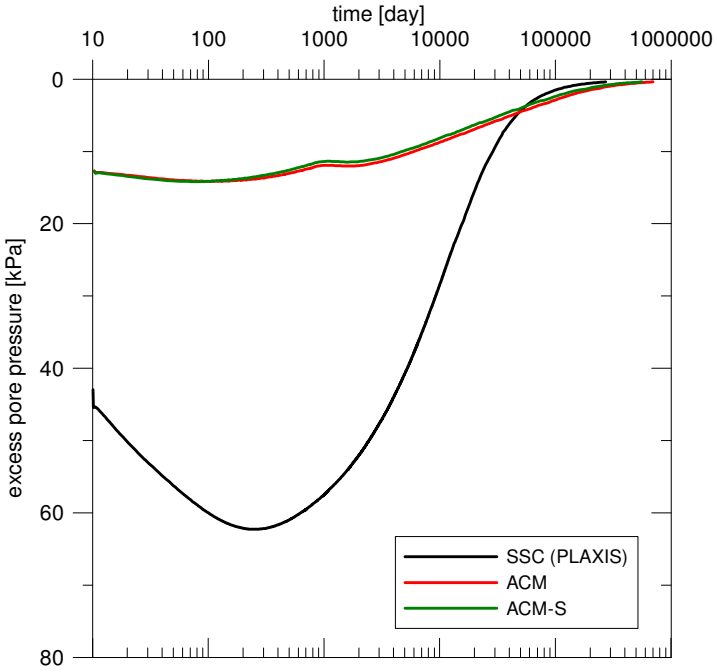

Figure 6.16: Evolution of the excess pore water pressures with time at a depth of 15 m for 3D study for: a) S-CLAY1S 'family' and b) creep models.

In fact, the isotropic SSC model predicted more than twice the excess pore water pressure at the beginning of the consolidation process compared to the other models and, in addition to this, the rate of dissipation was much higher than in the case of MCC, S-CLAY1, S-CLAY1S, ACM or ACM-S, see Figure 6.15. The influence of both anisotropy and destructuration on the numerical predictions at the stone columns base level was marginal.

Figure 6.16 presents the evolution of the excess pore water pressures at a depth of 15 m with time, corresponding to a depth of 5 m below the stone column bases. The excess pore water pressures build up and then dissipate as the consolidation process evolves, see Figure 6.16. In the case of the elasto-plastic models this phenomenon is due to the Mandel-Cryer effect (Mandel, 1950 and Cryer, 1963) during coupled consolidation. In addition to that, in the case of the creep models the increase in the value of the excess pore water pressures is also attributed to creep. The elasto-plastic models predicted similar amounts of the excess pore water pressures as a result of construction as the ACM and ACM-S models, see Figure 6.16. However, the elasto-plastic models predicted a faster process of dissipation than the viscous models. Again, the greatest excess pore water pressure value was predicted by the isotropic SSC model.

Figure 6.17 presents the excess pore water pressure contours for S-CLAY1S and ACM-S with respect to the horizontal profile 1 year from the start of consolidation. The time-dependent model predicted a maximum excess pore water pressure almost twice as high as the elasto-plastic S-CLAY1S model; accounting for the viscous behaviour of the soft soil deposit which leads to a slower water dissipation.

The excess pore water pressure contours with respect to the horizontal profile 2 years into the consolidation process for S-CLAY1S and ACM-S are presented in Figure 6.18. The scale in Figure 6.18b is different from that in Figure 6.18a. Again, the time-dependent ACM-S model predicted a slower dissipation of the excess pore water pressures and accounting for the viscous behaviour of the soft soil deposit triggered some delay in the excess pore water pressure dissipation.

6.3.5 Effect of over-consolidation on the behaviour of the soft soil deposit

In this section the effect of the over-consolidation of the soil mass on the numerical predictions is studied in detail and some conclusions on that issue are formulated.

The apparent over-consolidation of a soil can be reported using the over-consolidation ratio OCR, which is defined as the ratio between the maximum experienced effective stress (apparent pre-consolidation stress) $\sigma_p^{'}$ to the current overburden stress $\sigma_v^{'}$. A soil mass which is currently subjected to the highest stress level that it has ever experienced is normally consolidated and has an OCR equal to one.

This section aims to investigate the effects of variations in the apparent over-consolidation of the soft soil, (in terms of the pre-consolidation pressure), on the numerical results using the two advanced constitutive models: S-CLAY1S and ACM-S. Both of the models account for plastic anisotropy as well as destructuration

and the bonding process and, in addition, the ACM-S model also takes into account the viscosity of the soil.

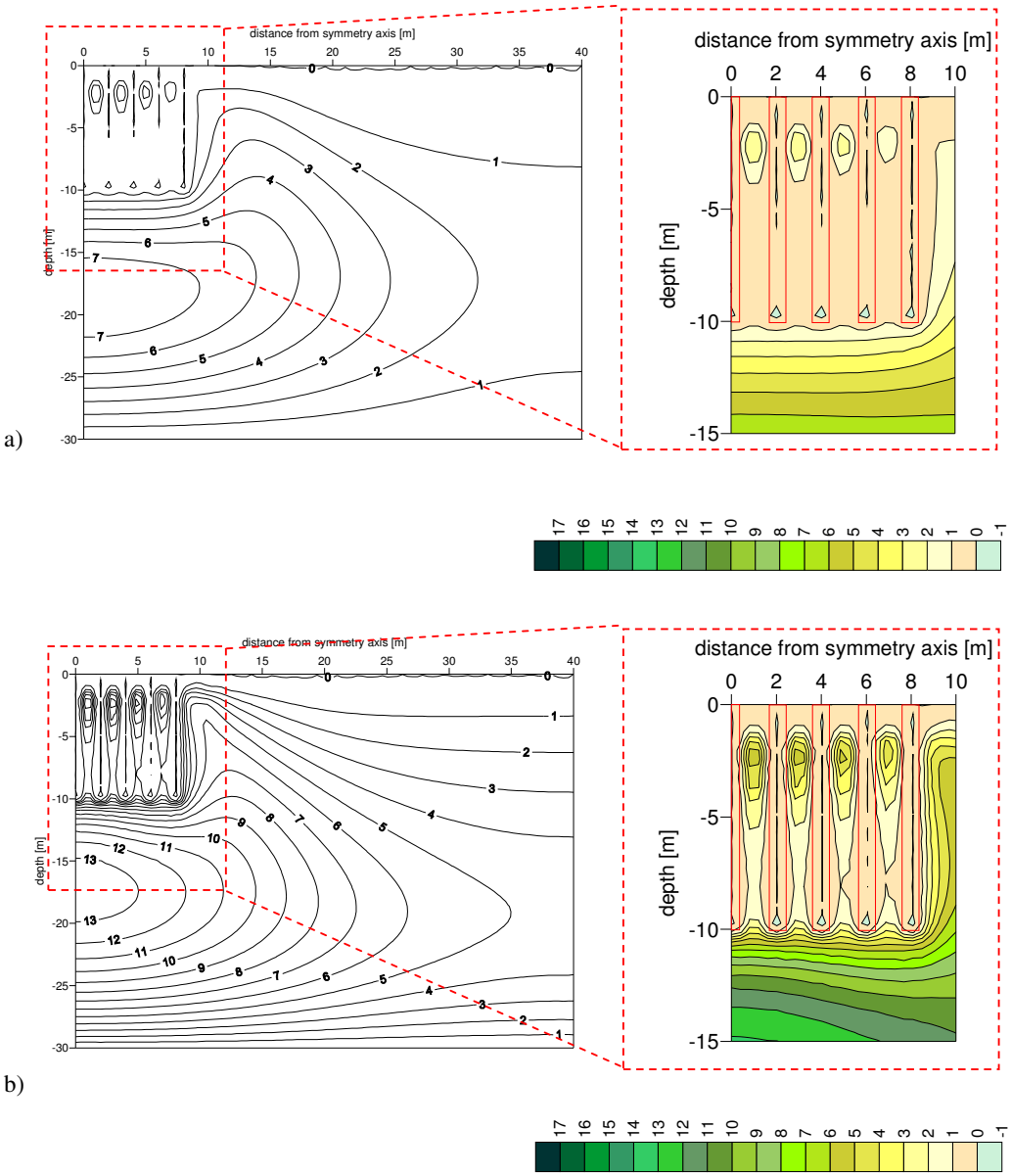

Figure 6.17: Excess pore water pressure (in kPa) contours after 1 year into consolidation for: a) S-CLAY1S and b) ACM-S.

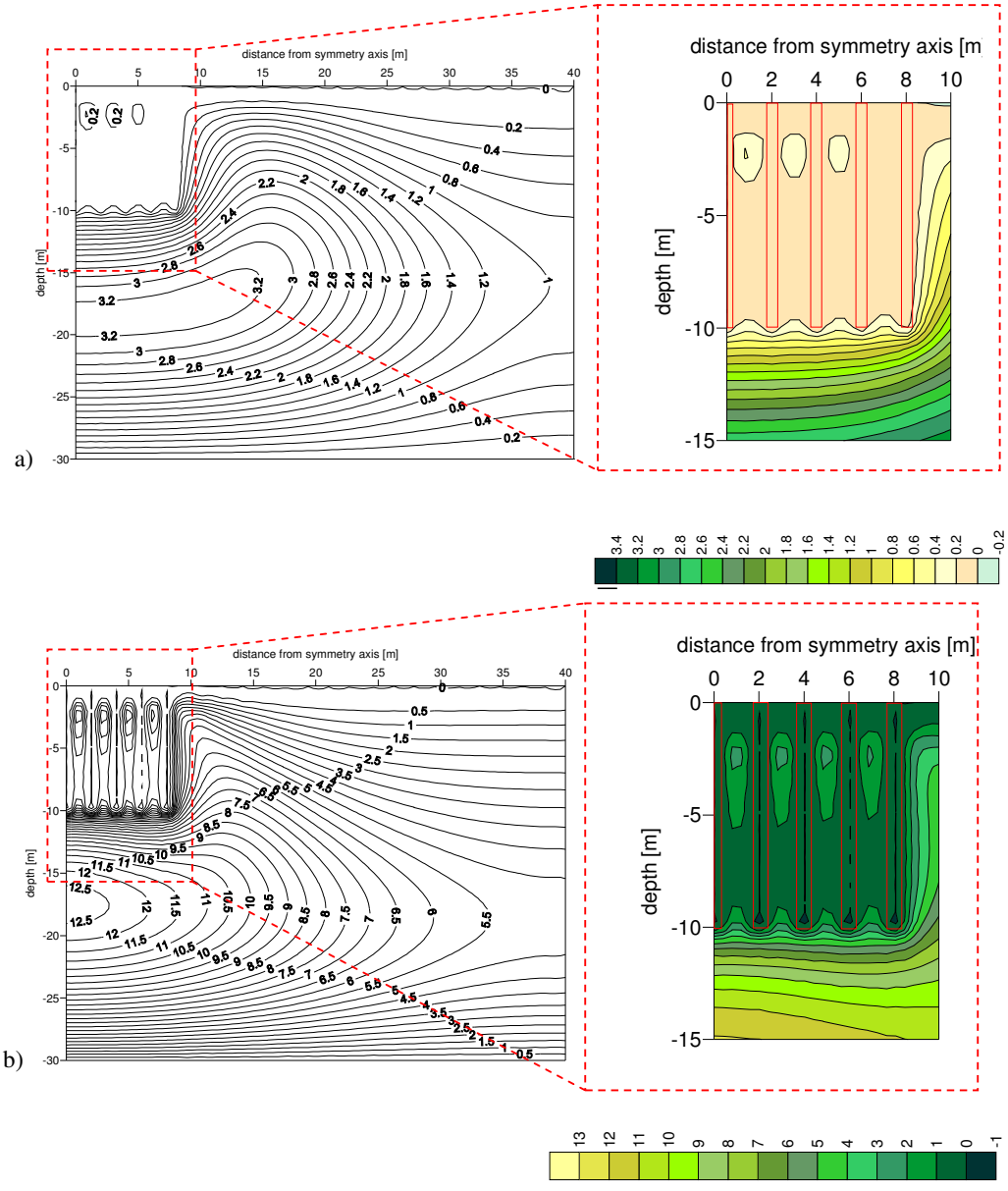

Figure 6.18: Excess pore water pressures (in kPa) contours after 2 years into consolidation for: a) S-CLAY1S and b) ACM-S.

To investigate the effect of the pre-consolidation stress, the over-consolidation ratio OCR was varied for the soft Bothkennar clay material. In previous sections of this *Chapter* an over-consolidation ratio value of 1.5 was assumed. In this section the OCR value was changed to 1.3 and 1.7, respectively.

The influence of the over-consolidation ratio (and the pre-consolidation stress) on the surface settlements after construction and consolidation is illustrated in Figure 6.19. As expected, the influence of the over-consolidation on the numerical predictions of the vertical displacement after the consolidation process was much more pronounced than in the case of construction of the embankment. Similar to the results from *Section 6.3.1,* the ACM-S model in this study predicted unrealistic settlements outside the loaded area, see Figure 6.19b. In fact, by increasing the over-consolidation ratio by approximately 30 % (from 1.3 to 1.7), the settlement was reduced by approximately two and six times for S-CLAY1S and ACM-S respectively. This demonstrates that the viscous models are super-sensitive to any changes in the apparent over-consolidation ratio. Increases in the creep strains over time in ACM-S is dependent on the ratio of the effective stress and the pre-consolidation stress, thus also on the over-consolidation ratio OCR value. Both the settlement and creep process of the soil deposit starts immediately without any load applied. It has been reported by Brinkgreve (2001) that setting the OCR value to 1 may lead in time-dependent constitutive models to excessive settlement velocities during the calculation of the initial stresses in the FE software, see Brinkgreve (2001). Structured soils, with rather high values of the over-consolidation ratio therefore results in excessive and unrealistic deformations.

a)

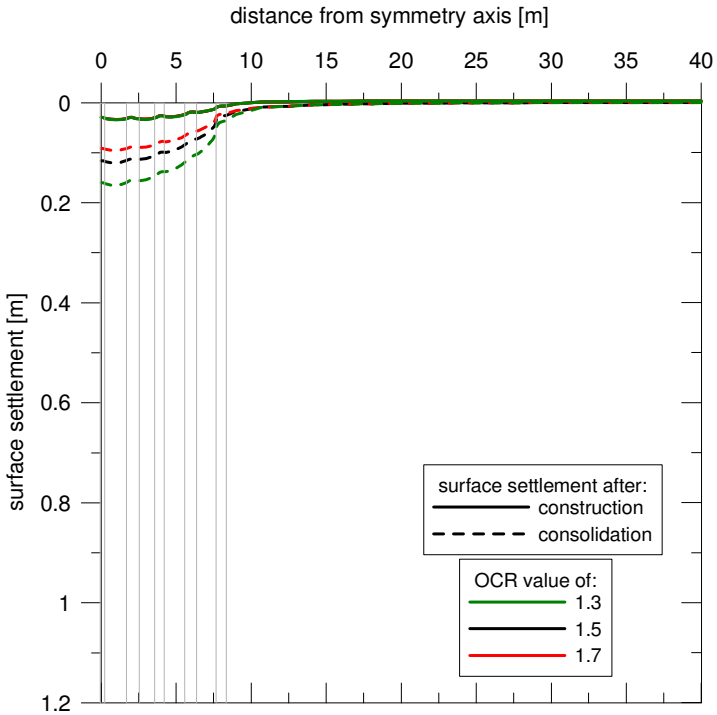

b)

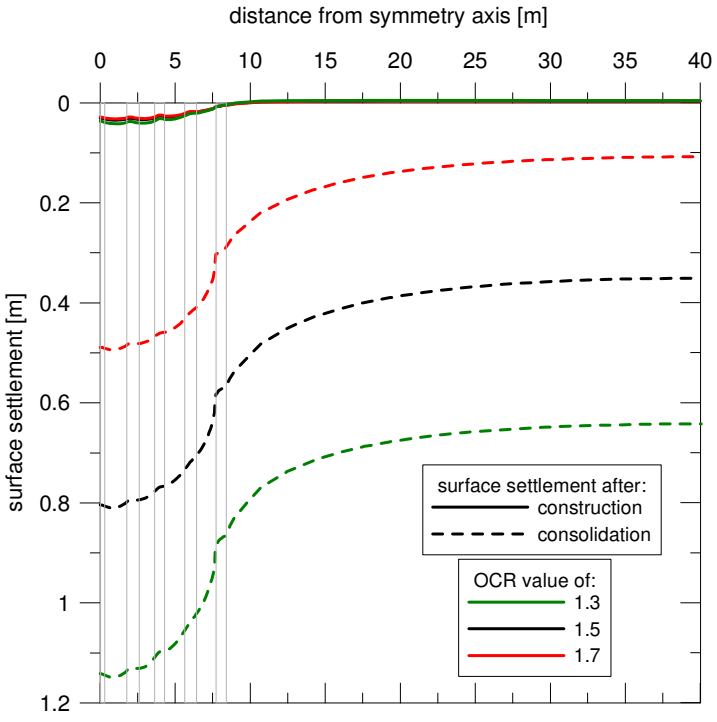

Figure 6.19: Evolution of the surface settlement with OCR value for 3D study for: a) S-CLAY1S and b) ACM-S.

Additionally, the simulations were repeated without consideration of the floating stone columns in the soft soil mass in order to determine the settlement reduction ratio s_r. Results are presented in the form of a figure, where the evolution of the settlement reduction ratio with the over-consolidation ratio is shown, see Figure 5.20. It appears that an increase in the over-consolidation of the soft clay leads to a decrease of the settlement reduction ratio s_r, with the exception of the S-CLAY1S model when using an *OCR* value of 1.5. It is recommended that this problem is investigated in the future in greater detail.

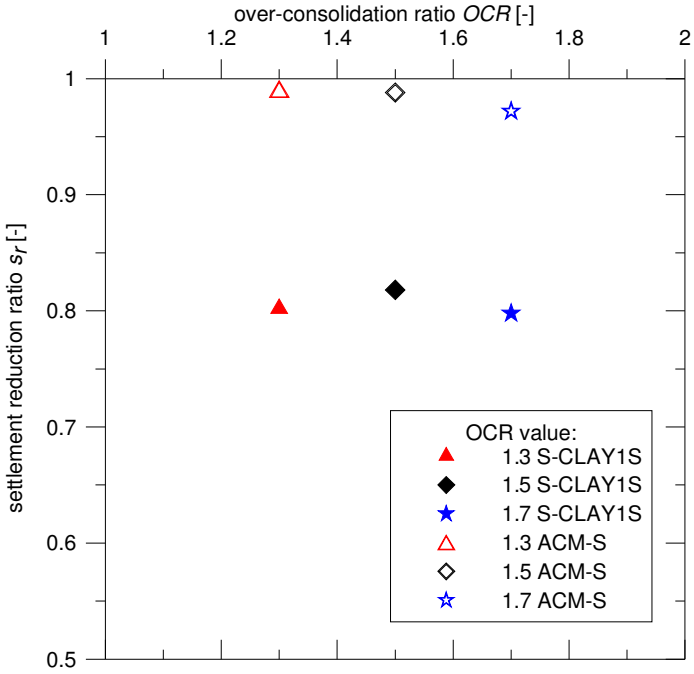

Figure 6.20: Evolution of the settlement reduction ratio with OCR value for 3D study.

The effect of the over-consolidation ratio on the evolution of the excess pore water pressures with respect to time at two different depths (10 m and 15 m) for both

advanced constitutive models is presented in Figures 6.21 and 6.22. The results correspond to point B in the soft soil, see Figure 6.4.

Figure 6.21 presents the excess pore water pressure evolution with time at the level of the stone columns bases. Inspection of the excess pore water pressures plots reveals that the influence of the over-consolidation ratio value in the elasto-plastic model is negligible, see Figure 6.21a. However, for the time-dependent formulation the OCR value is of greater importance than for the elasto-plastic model. A reduction in the over-consolidation ratio leads to an increase in the excess pore water pressures at the start of consolidation process, as well as to a higher rate of the excess pressure dissipation, Figure 6.21b.

Figure 6.22 presents the predicted excess pore water pressure evolution with time at a depth of 15 m (5 m below the stone column base level) for OCR from 1.3 to 1.7. Figure 6.22a shows the numerical predictions for the elasto-plastic S-CLAY1S model, whereas Figure 6.22b corresponds to the time-dependent ACM-S formulation. In the case of S-CLAY1S, the influence of the over-consolidation ratio has some effect in the initial stages of the consolidation process, see Figure 6.22a. The increase in the OCR of the soft soil mass leads to first an increase of the excess pore water pressure value (most probably as a result of the Mandel-Cryer effect) and a higher rate of the pore pressure dissipation. The viscous ACM-S model predicted a different pattern of the excess pore water pressure evolution: a reduction of the OCR value significantly increased the predicted value of the excess pore water pressure, see Figure 6.22b. This behaviour of the greatest excess pore water pressure of those considered is somewhat unexpected and, thus, it should be the subject of further detailed investigation.

a)

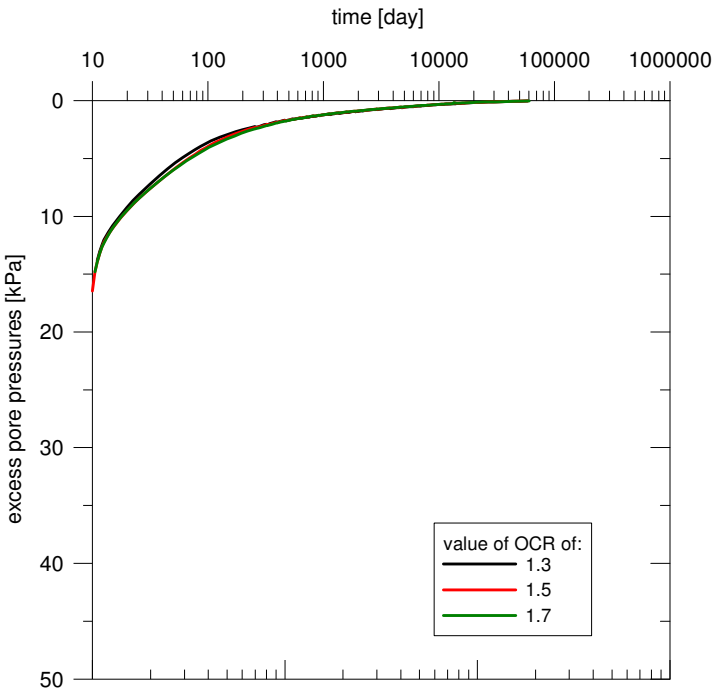

b)

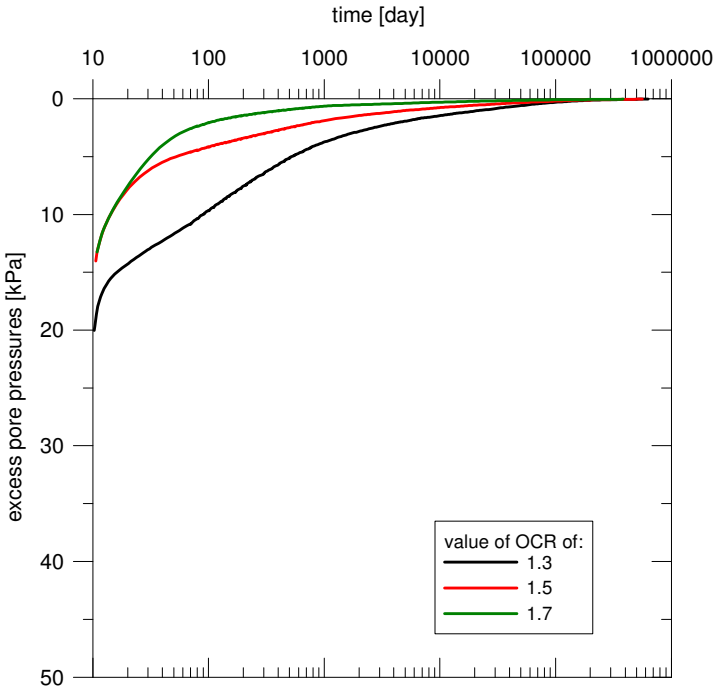

Figure 6.21: Evolution of the excess pore water pressures with time and OCR value for 3D study at depth of 10 m for: a) S-CLAY1S and b) ACM-S.

a)

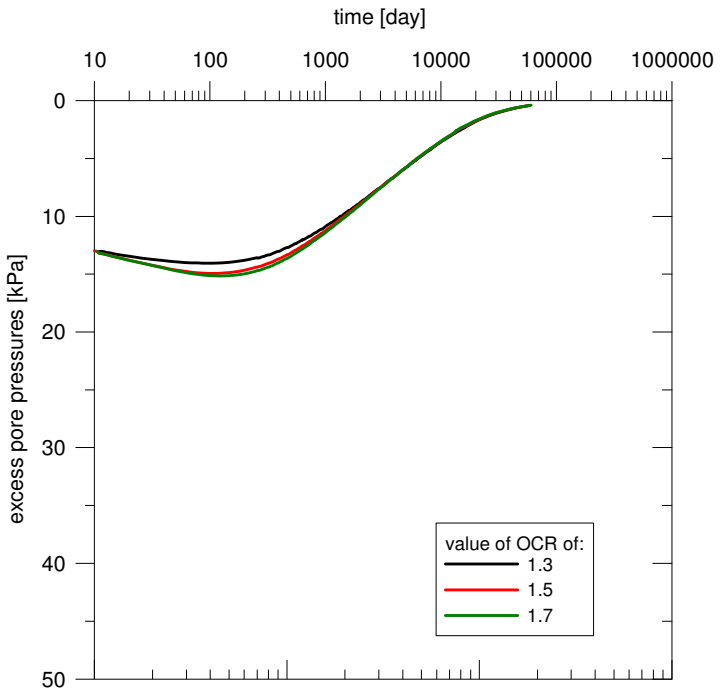

b)

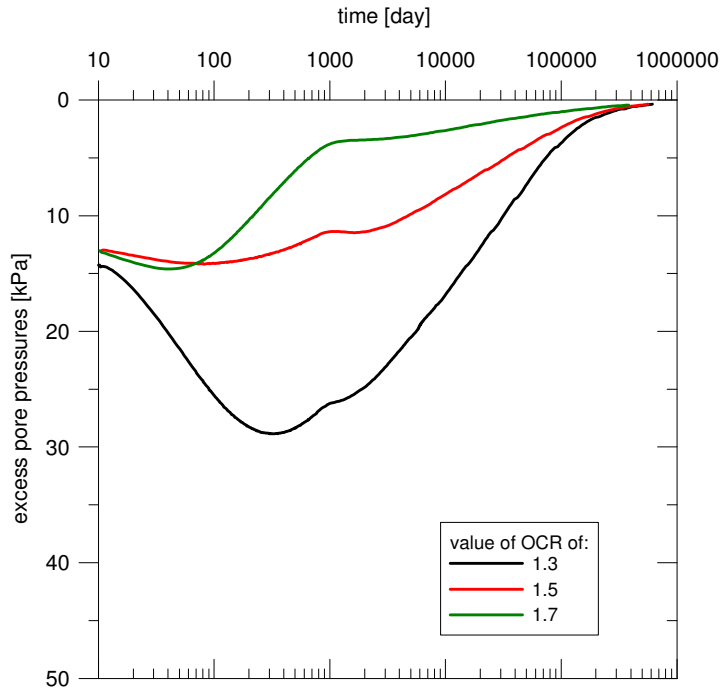

Figure 6.22: Evolution of the excess pore water pressures with time and OCR value for 3D study at depth of 15 m for: a) S-CLAY1S and b) ACM-S.

6.4 Summary and Conclusions

In this chapter the influence of the constitutive models used to represent the mechanical behaviour of a soft soil improved with floating stone columns has been assessed. Furthermore, the sensitivity of the predictions to changes in the pre-consolidation of the soft strata has been studied. The stone columns were installed below an embankment on a soft soil, represented by Bothkennar clay. Simulations were performed using both standard and advanced constitutive models (accounting for anisotropy, destructuration and viscous effects) implemented in a three-dimensional commercial finite element code. For the FE analyses four advanced constitutive models were selected to represent the soft deposit, namely the S-CLAY1, S-CLAY1S, ACM and ACM-S models. In order to assess the influence of plastic anisotropy, the well-known isotropic MCC and SSC models were applied in some of the simulations for comparison. All of the constitutive models used in the benchmark problem assumed identical initial in-situ stress states and vertical pre-consolidation stresses.

The numerical results showed that in the case of the elasto-plastic models, accounting for anisotropy and destructuration increased the settlements and reduced the lateral movement. In contrast, in the time-dependent formulations taking into account anisotropy and destructuration resulted in a reduction of the vertical and horizontal displacements. The isotropic SSC model predicted different (and unrealistic) magnitudes of both vertical and lateral movements, most probably partially due to the creep part of the model and the numerical implementation in the

finite element code, which differs from the ACM and ACM-S models used in this study.

The predictions given by the creep models overall appear to be unrealistic, because significant settlements were predicted most notably in the unloaded area beside the embankment. In order to alleviate this problem, a procedure with a consolidation phase where only in-situ stresses were present for a long period of time, after which the displacements were reset to zero before construction of the stone columns and the embankments, was studied. The application of this procedure excluded the problem of excessive self-weight settlements in the unloaded area when considering the time-dependent constitutive models. However, the application of this procedure resulted in the use of an incorrect over-consolidation state and amount of bonding in the soft soil deposit for subsequent simulation and, thus, may lead to unrealistic numerical predictions.

Studies on the impact of the pre-consolidation stress (by terms of the value of the over-consolidation ratio OCR) demonstrated that an increase in the OCR resulted in the reduction of the predicted surface settlements. This phenomenon was especially pronounced in the case of the time-dependent constitutive ACM-S model where the predicted settlement curves were super-sensitive to the value of the over-consolidation ratio. The influence of the pre-consolidation stress on the numerical predictions of the excess pore water pressures was correspondingly significantly more pronounced in the case of ACM-S than the elasto-plastic S-CLAY1S model. Additionally, this influence was observed to be greater in the deeper soil deposits than at shallow depths, where the dissipation of the excess pore water pressures was faster due to presence of the stone columns. Increasing the pre-

consolidation stress resulted in a reduction of the excess pore water pressures, for predictions using ACM-S, and a small increase in the excess pore water pressure predictions in the case of S-CLAY1S predictions.

The influence of the C_α / C_c ratio of the soft soil deposit on the predictions of the surface settlement by the creep models was investigated, suggesting that the impact of C_α / C_c ratio is important, therefore this relationship should be carefully determined. However, the settlement predictions were more dramatically dependent on the value of the over-consolidation ratio than on the C_α / C_c ratio.

7

CASE STUDY: STONE COLUMNS BENEATH A FOOTING

This chapter investigates the use of stone column foundations beneath a footing on a soft soil deposit. In order to fulfil the requirements of a typical project, special attention has been placed on the performance of the stone columns after the first three years of service. Due to the complex soil profile and heterogeneity of the ground conditions, both standard and advanced constitutive models have been used to represent the soil and stone column material. The case study considers a footing (raft foundation) constructed on lightly over-consolidated soft clay on a site in Western Scotland close to the coastline. The design of floating stone columns was proposed by the author due to their ability to reduce the total and differential settlements, and the time required for the consolidation process. Their applicability in this case is studied using detailed three-dimensional finite element analyses. Full three- dimensional geometry is used in the numerical simulations taking advantage of

PLAXIS 3D Foundation software. Total and differential settlements are first investigated. Afterwards, the stress distribution and stress paths are studied, followed by the analysis of the distribution of the excess pore water pressures and consolidation time.

7.1 Case study

The case study considers a soft soil improved by floating stone columns. The granular columns are proposed as a support of a footing (raft foundation) in order to reduce the total and differential settlements of the construction, as well as to reduce the consolidation time required for full dissipation of the excess pore water pressures. This case study demonstrates a typical application of stone columns for settlement reduction in geotechnical engineering. To represent ground conditions for this case study, a soil profile found on the site of Bishopton, Scotland, is used. Due to the former location of an explosive-manufacturing Royal Ordnance Factory at Bishopton (ROF Bishopton) and due to decontamination and remediation issues, the site was for many years omitted in the council's plans for residential and business development. In 2008 new planning consent was granted, permitting a redevelopment scheme and construction of a motorway junction (motorways A8/M8), (BBC, 2008).

7.2 Site description and soil profile

The area of Bishopton is situated approximately 15 km north-west of Glasgow on the estuary of the River Clyde, see Figure 7.1. It is a large brownfield site where a former explosive-manufacturing factory was located. The planned redevelopment on one of Europe's largest brownfield sites proposes construction of approximately 2 000 homes, a community woodland park and facilities, as well as a business park.

Figure 7.1: Raft footing case study: site location.

A notable amount of ground investigation has been carried out in this area, including cone penetration tests (CPT), standard penetration tests, standard drilling

using cable percussion method, piezometric measurements, particle size distribution analysis and laboratory triaxial compression and oedometer tests. Site investigation data has been made available courtesy of Keller Foundation (UK).

A review of the site data indicated that the soil profile consists of a layer of dry crust, which overlays a 6.7 m thick silty clay layer and a 7 m thick stratum of soft clay. Below the clay layer a sandstone stratum is found, which forms a natural boundary for the geometry considered in the case study. The groundwater table is located at a depth of 1.3 m. The soil profile assumed in the case study is shown in Figure 7.2.

For this case study, installation of floating stone columns was proposed in order to reduce the total and differential settlements of the planned raft footing. The construction scheme consists of a raft footing used as a support for residential buildings; the geometry of the foundation is presented in Figure 7.3. The results of laboratory and in-situ tests enabled the geotechnical properties of the soil deposit, to be determined; these are presented in *Section 7.5.*

7.3 Proposed design

For settlement reduction of the raft footing, floating stone columns were proposed for the project. Stone columns of length 5.5 m (from the footing level) and diameter 0.6 m were selected.

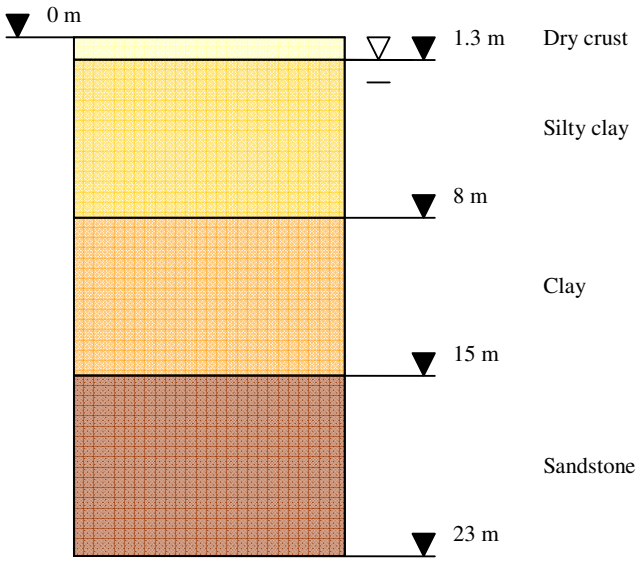

Figure 7.2: Raft footing case study: assumed soil profile.

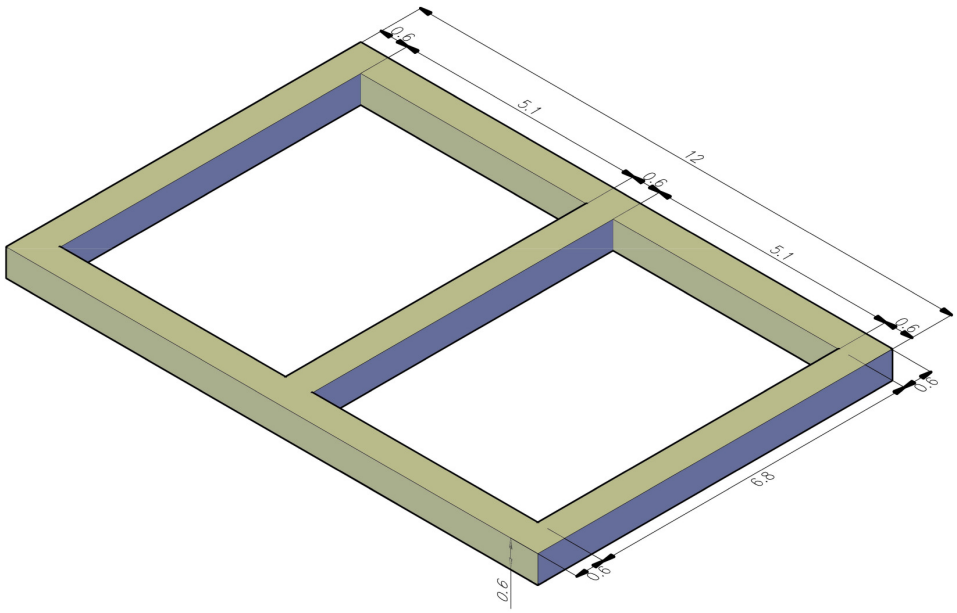

Figure 7.3: Raft footing case study: 3D view of foundation geometry.

Based on the latest standards and guidelines, such as BS (EN 14731:2005) and NHBC (1988), stone columns were proposed to be constructed in the footprint of the raft foundation. As pointed out in BRE (2000), the safe load capacity of a group of stone columns depends on the soil conditions, the column diameter, spacing and length, and the shear strength of the compacted granular material. For low-rise buildings, the minimum layout of stone columns is one column at all external corners, returns and junctions of the raft foundation in order to mitigate differential settlements. Usually, a column spacing of 2 m or less is used for raft foundations in order to support a linear load for settlement reduction.

Keeping that in mind and given the geometry of the footing, spacing of the columns in the X and Z directions is different resulting in 1.425 m and 1.480 m in both directions. The outline of the stone column design is presented in Figure 7.4.

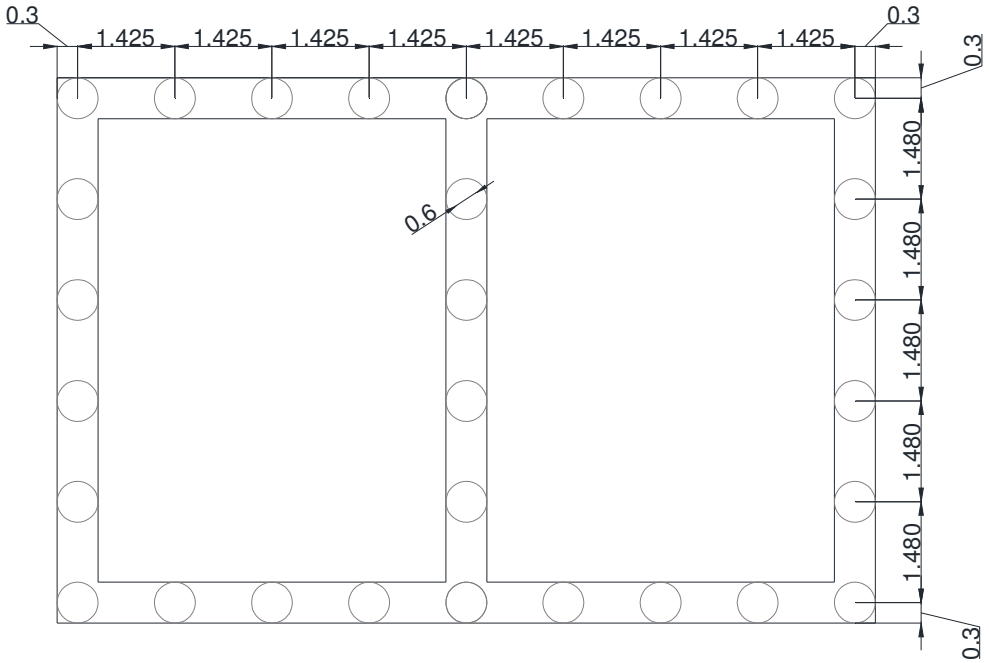

Figure 7.4: Raft footing case study: stone column design.

7.4 Numerical model

For all simulations the PLAXIS 3D Foundation v.2.2 finite element code was used, taking advantage of three-dimensional modelling. A mesh with 8 800 tetrahedral elements and approximately 960 000 degrees-of-freedom was used in the simulations, see Figure 7.5. At first, a two-dimensional mesh with triangular elements was created. Next, the mesh was extended in the depth direction forming a three-dimensional shape. Mesh sensitivity studies were carried out before performing the case study in order to reduce the influence of the mesh on the results of the simulations. The computational time required to calculate the case study considered was equal to approximately one day due to the great number of degrees-of-freedom in each of the simulations.

Only the bottom and top boundaries of the model were open for consolidation and water can freely flow out of these boundaries. The installation of the stone columns, construction of the footing and loading were simulated as undrained events during which the dissipation of any excess pore water pressures is not possible. During construction of the footing the soil material in between the raft slabs was removed in order to realistically mimic the working sequence on site. Following that, in subsequent phases the granular fill placed in between footing slabs was simulated by applying a distributed load on the foundation level of 11.4 kPa (assuming a 0.6 m high layer of fill with a unit weight of 19 kN/m^3). Construction of the foundation was followed by the application of a distributed load on top of the raft footing of 83.33 kN/m^2, which corresponds to a line load of 50 kN/m. Afterwards, a consolidation

phase was simulated until a maximum excess pore water pressure of 1 kPa was reached. In order to exclude any influences of the outer boundary, the geometry model was extended in both horizontal planes (X and Z) by approximately 2B laterally from the symmetry axis of the footing and 2B below the footing, where B is the footing width in the X direction. The depth of the geometry model extends up to 23 m, taking into account also the sandstone layer, see Figure 7.5 and Figure 7.2.

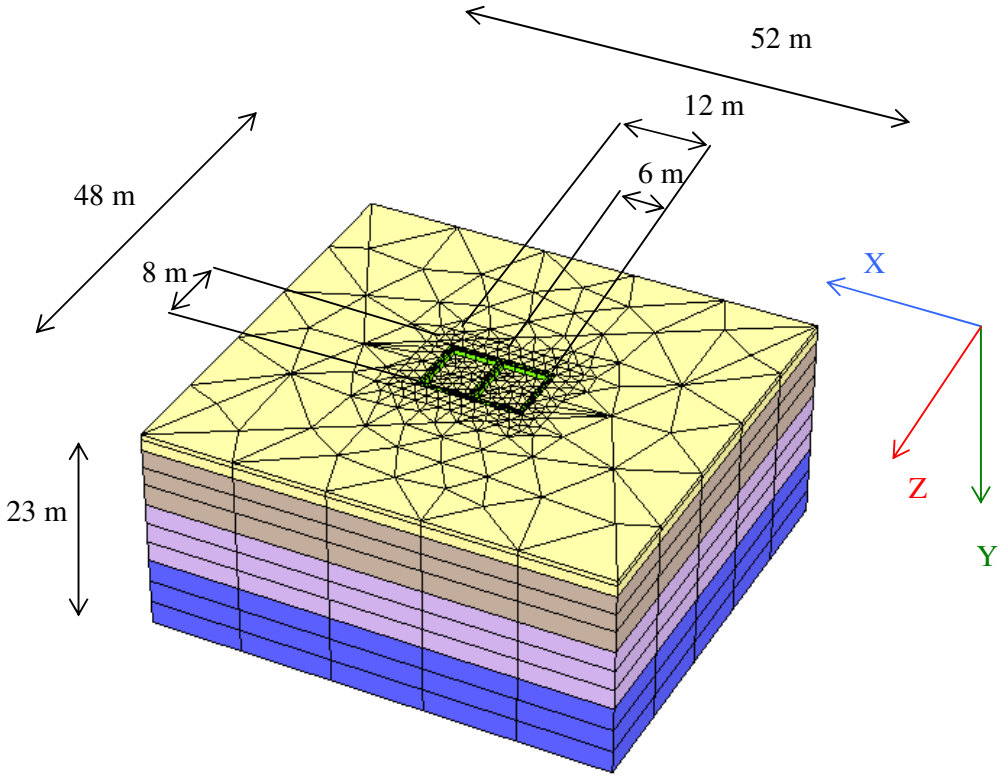

Figure 7.5: Raft footing case study: problem mesh and geometry.

More details with regard to the geotechnical properties of the soil at the Bishopton site are presented in the section below. The top view of the case study

along with the cross-sections A-A' and B-B' are shown in Figure 7.6. Additionally, five points chosen for further studies are indicated on the figure; red and blue dots indicate points chosen for evaluation of the settlement response and for evaluation of the excess pore water pressure, respectively.

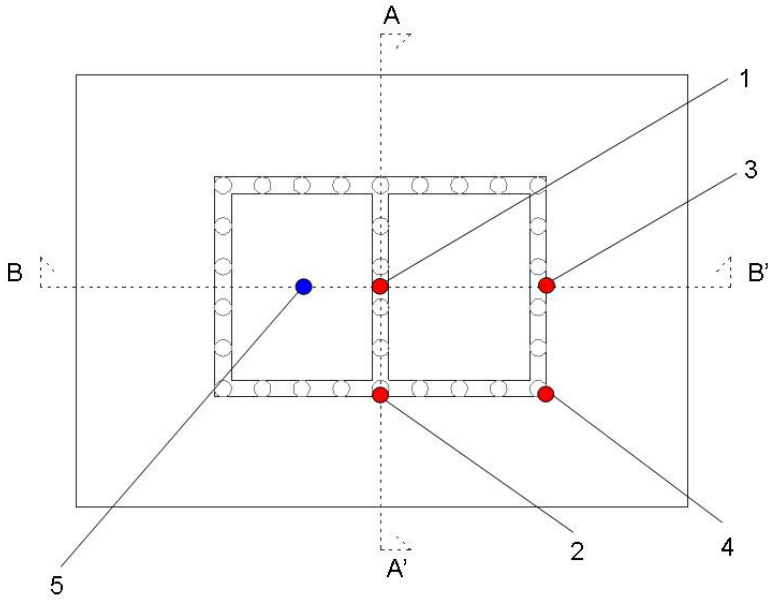

Figure 7.6: Raft footing case study: top view.

7.5 Material properties

In order to simulate the complexity of the problem three different constitutive models were used in the finite element analyses. Each soil layer was analysed and the appropriate constitutive model, in order to realistically represent the mechanical behaviour of the constituent, was applied. Both standard and advanced constitutive

models were used, taking advantage of the user-defined formulation of the S-CLAY1 model in the commercial code PLAXIS 3D Foundation.

7.5.1 Soil deposit

For the case study, the soil profile illustrated in Figure 7.2 was considered. The slightly over-consolidated silty clay and clay layers, which are overlain by a dry crust, represent soft recently deposited marine sediments. Below the clay layer a sandstone stratum forms a natural boundary for the soft deposit on Bishopton site. Due to the nature of the dry crust and the sandstone, these layers were simulated using the Hardening Soil (HS) model, which was briefly described in *Chapter 2*. In order to represent the layers of silty clay and clay, the S-CLAY1 model was applied, which takes into account plastic anisotropy of the considered soil material, and was presented in detail in *Section 2.4.1*.

Soft soil: silty clay and clay

The soft soil found at a depth of 1.3 to 8 m at the Bishopton site has approximately 20..30% clay content, 50..60% silt content and a small amount of sand, and can be classified as a silty clay. The soil stratum lying below the silty clay has approximately 30..40% clay content, 50..60% silt content and a small amount of sand, and can be classified as a slightly sandy clay. An undrained shear strength in the range of 10..55 kPa has been found for both the silty clay and clay material in the laboratory with undrained triaxial tests and with cone penetration tests in situ.

Due to close similarities between the soft soil found at Bishopton and the Bothkennar sites, the silty clay and clay of Bishopton is assumed to be, as in the case of the Bothkennar clay, highly anisotropic. One dimensional compression tests on samples from depths of 2.1..9.5 m enabled investigation of the loading-unloading response of the soil and the yield stresses. In the laboratory tests the soft soil layers exhibited extremely low compressibility, indicating high disturbance of the soil samples. As a result of the desk study, the soft soil at the Bishopton site is expected to be over-consolidated with compressibility parameters similar to the soft clay from Bothkennar, although the Bishopton clay layers would be expected to be less homogeneous and structured than the Bothkennar clay due to the differences in the sedimentation environment. In fact, the disturbance of the soil samples is so high that the intrinsic value of the slope λ_i of the compression curve in the $e - \ln p'$ determined from the one-dimensional oedometer test on a natural soil from the Bishopton site is lower by approximately 20..35 % than the λ_i values for fully reconstituted Bothkennar clay samples. Following that, some concerns about reliable estimation of in-situ compressibility and over-consolidation cannot be excluded. Therefore, for these preliminary numerical simulations, the soft soil at Bishopton was chosen to be modelled as a normally consolidated and fully reconstituted material. As Figure 7.7 suggests, for small stress increments $d\sigma'$ this leads to over-prediction of the stress-strain behaviour, and can be considered as a very conservative approach.

It is recognised that the assumption about the normally consolidated and fully reconstituted state of the soft soil at Bishopton site has some further implication for numerical predictions, such as the determination of the in-situ coefficients of the earth pressure at rest K_0 . However, as the current research is aimed only at

providing preliminary numerical predictions, the in-situ coefficient of the earth pressure at rest was based on the equation given by Jaky (1948) and calculated to be equal to 0.5. It is essential for further research to ensure that sample disturbance is minimised and that good quality samples are obtained and used for laboratory testing.

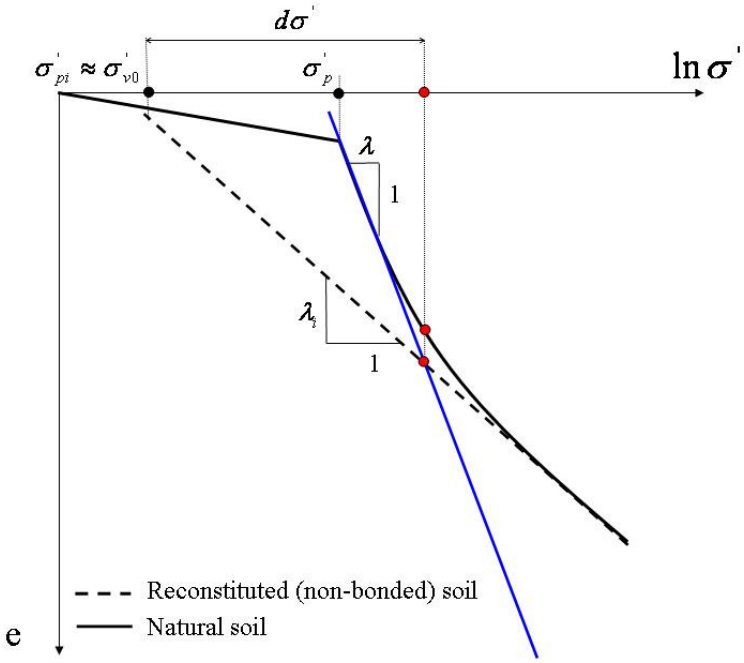

Figure 7.7: Raft footing case study: compressibility parameter for natural and reconstituted soil.

Due to its consolidation history the soft soil deposit was assumed be cross-anisotropic in terms of elasto-plastic behaviour, which led to determination of the initial inclination α_0 of the yield surface of the S-CLAY1 model following the procedure outlined in *Chapter 2*. The values for the additional advanced soil

constants, ω and ω_d describing the rotation of the yield surface, were calculated following the procedure described in *Section 2.4.1*.

The soil constants and state variables describing the silty clay and clay layers are shown in Tables 7.1, 7.2 and 7.3.

Table 7.1: Standard soil constants: S-CLAY1.

Layer	Depth [m]	γ [kN/m^3]	k [m/s]	ν [-]	M [-]	κ [-]	λ_i [-]
Silty clay	1.3-8.0	18.0	$2.2\text{x}10^{-10}$	0.2	1.2	0.015	0.133
Clay	8.0-15.0	18.0	$2.5\text{x}10^{-10}$	0.2	1.2	0.015	0.125

Table 7.2: Advanced soil constants: S-CLAY1.

Layer	Depth [m]	ω [-]	ω_d [-]
Silty clay	1.3-8.0	0.76	90
Clay	8.0-15.0	0.76	110

Table 7.3: State variables: S-CLAY1.

Layer	Depth [m]	e_0 [-]	K_0 [-]	OCR [-]	α_0 [-]
Silty clay	1.3-8.0	0.790	0.5	1.0	0.46
Clay	8.0-15.0	0.844	0.5	1.0	0.46

Other soil deposits: dry crust and sandstone

The dry crust and sandstone, due to their nature and mechanical behaviour were modelled using the Hardening Soil (HS) model described in *Section 2.3.3*. The material parameters for the dry crust and sandstone strata are listed in Table 7.4 and

7.5. It is assumed that water can freely flow through the dry crust and sandstone layers as both materials are considered to be fully drained.

Table 7.4: Dry crust and sandstone stiffness parameters.

Material	γ [kN/m^3]	$\nu_{ur}^{'}$ [-]	$E_{50}^{ref} = E_{oed}^{ref}$ [kN/m^2]	E_{ur}^{ref} [kN/m^2]
Dry crust	19.0	0.2	1 720	5 160
Sandstone	22.0	0.2	100 000	200 000

Table 7.5: Dry crust and sandstone additional parameters.

Material	k [m/s]	c' [kN/m^3]	$\varphi^{'}$ [^{o}]	ψ [^{o}]	m [-]	K_0 [-]	OCR [-]
Dry crust	3.35x10^{-9}	0.1	27	12	0.55	0.700	1.0
Sandstone	2.31x10^{-8}	200	27	12	0.3	0.530	1.0

Note: m = power for stress-level dependency of stiffness.

7.5.2 Stone columns

Floating stone columns were installed below the footing with a spacing between the columns S_{SC} equal to 1.425 m and 1.480 in the X and Z directions, as shown in Figure 7.4. The diameter of the columns D_{SC} and the length L_{SC} was assumed to be equal to 0.6m and 5.5 m, respectively. In the FE analysis the stone columns were 'wished-in-place' in an undrained process without considering any installation effects. As already mentioned in previous chapters, installation of the stone columns is expected to change a number of state variables, such as anisotropy and the coefficient of earth pressure at rest, see i.e. *Chapter 4*. However, the effects of

installation of the stone columns are not the subject of this research and therefore were not taken into consideration.

The Hardening Soil Model, described in *Chapter 2*, was used to model the granular material of the stone columns and the material parameters used for the purpose of this case study were assumed to be the same as those used for the parametric study presented in *Chapter 4*. The stone column material parameters are listed in Table 7.6 and 7.7 for the sake of completeness.

Similar to the simulations in *Chapter 4*, the critical state friction angle of the granular material φ'_{SC} was chosen to be 42 ° and the dilatancy angle ψ_{SC} was assumed to be 12°. The Poisson's ratio ν' and an exponent m equal to 0.3 were assumed. A unit weight of 19 kN/m^3 was assumed for the granular material, following the experience of the engineering industry.

Table 7.6: Stone column stiffness parameters.

Material	γ [kN/m^3]	ν'_{ur} [-]	$E_{50}^{ref} = E_{oed}^{ref}$ [kN/m^2]	E_{ur}^{ref} [kN/m^2]
Stone column	19	0.3	80 000	260 000

Table 7.7: Stone column additional parameters.

Material	k [m/s]	c' [kN/m^3]	φ'_{SC} [^{o}]	ψ_{SC} [^{o}]	m [-]	K_0 [-]
Stone column	1.97x10^{-4}	0.1	42	12	0.3	0.331

Note: m = power for stress-level dependency of stiffness.

7.5.3 Footing

A raft foundation of width and height both equal to 0.6 m was considered in this case study, see Figure 7.3. The raft footing was assumed to be built from the foundation level (a depth of 0.6 m), resulting in the top of the construction level being located at the ground surface. The footing was modelled as a linear elastic material with a Young's modulus of E' equal to 2 x 10^7 kN/m^2 and a Poisson's ratio of 0.15. The footing was loaded with distributed load of 71.4 kN/m^2 after construction and the loading was maintained constant.

7.6 Numerical simulations

Numerical simulations for the raft footing were conducted assuming the following sequence of site works:

1) construction:
    a) undrained installation of stone columns,
    b) undrained construction of footing and application of distributed load between the slabs of the foundation (simulating granular fill),
    c) undrained application of loading on top of raft footing,
2) consolidation:
    a) first period of service- consolidation phase lasting 3 years,

b) consolidation until full dissipation- excess pore water pressures are equal to or less than a 1 kPa.

Additionally, to calculate the settlement reduction ratio a numerical simulation of the case study with no ground improvement was carried out.

7.6.1 Total settlement

The plot of vertical displacements with respect to the time required for full dissipation of the excess pore water pressures is shown in Figure 7.7 for representative points in between the slabs of the footing at four different locations. The floating stone columns reduced the total settlements by approximately 75 %. In fact, the settlement reduction ratio s_r varies during construction and consolidation, resulting in the lowest value after construction and reaching a value of 0.670 after dissipation of the excess pore water pressures. Settlement reduction ratios for each phase of loading, serviceability period and full consolidation are listed in Table 7.8.

Table 7.8: Raft footing case study: evolution of the settlement reduction ratio with time.

Phase	Settlement reduction ratio s_r [-]
Construction (undrained)	0.292
Consolidation (3 years)	0.607
Full consolidation	0.670

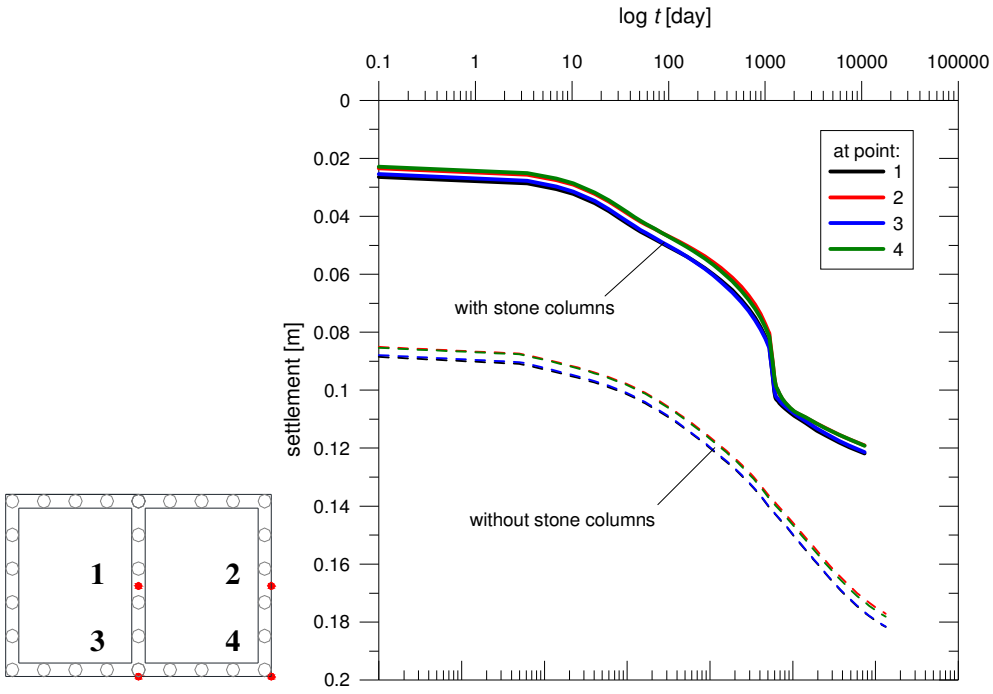

Figure 7.7: Evolution of settlement with time: raft footing case study.

Additionally, one can see that the time required for full dissipation of the excess pore water pressures is reduced by 40 % when floating stone columns are installed. Commonly used in engineering practice the degree of consolidation (expressed as $U_p = 1 - \frac{u_t}{u_0}$, where u_0 and u_t are the initial excess pore water pressures and the excess pore water pressures at time t) is determined as equal to 0.93 and 0.78 after 3 years of consolidation for the case with stone columns and the case when no ground improvement is in place, respectively.

7.6.2 Differential settlement

The plots of the settlement versus horizontal profile for the cross-sections A-A' and B-B' at the foundation level after construction are shown in Figures 7.8 and 7.9. Additionally, the results in the case of no ground improvement in place are presented. In grey and red the outlines of the foundation and stone columns in both the cross-sections are shown.

Looking at Figure 7.8 where the contours of the vertical displacement at the foundation level after construction are plotted, one can see that in the cross-section A-A', where a row of six columns support the raft foundation, the soil mass block displaces equally with distance from the model boundary in the Z axis direction and that the highest displacement is found at the footing footprint. A similar pattern is observed for the case where no ground improvement is used, as the footing induces a uniform distribution of the settlement but of higher magnitude than in the case with stone columns. The differential settlement of the raft foundation in the cross-section A-A' after construction is found to be negligible, of 1/4000, and well within acceptable limits for British housing, which is equal to 1/500, NHBC (2010).

Inspection of Figure 7.8b for the cross-section B-B' shows how well floating stone columns can carry the applied load and reduce the vertical displacements, leading to a reduction of the settlements in between the footing slabs by a factor of 11. The differential settlement of the raft foundation along the cross-section B-B' was found to be negligible (1/2000) and well in acceptable differential settlements for housing, see NHBC (2010).

Figure 7.9 presents the settlements at the foundation level for both cross-sections, A-A' and B-B', after consolidation. Again, numerical results for the case without stone columns are shown, and the outlines of footing and columns are indicated in grey and red, respectively. One can see that the settlement is much higher than after application of the loading, resulting in a value of approximately four times greater than predicted at the end of the construction phase. The greatest vertical displacements were predicted in the symmetry line of the footing. As in the case after construction, the differential settlement of the raft foundation along the cross-section A-A' was found to be negligible (1/4000) and well within the acceptable differential settlements for housing which is equal to 1/500, see NHBC (2010). It is evident that installation of the stone columns resulted in a reduction of the settlements between the footing slabs by a factor of 24 along cross-section B-B', see Figure 7.9b. Again, the differential settlement of the raft foundation along cross-section B-B' was found to be negligible (1/1500) and well within the acceptable differential settlements for housing, see NHBC (2010).

a)

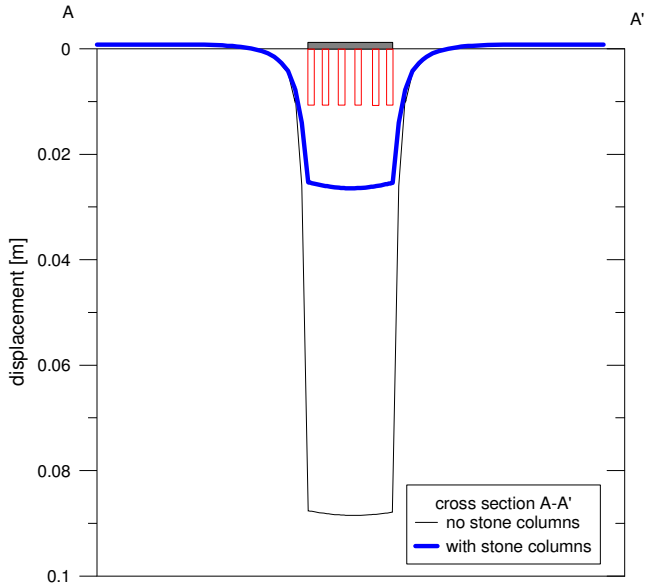

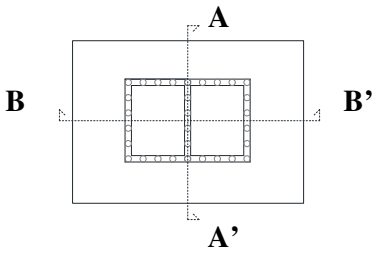

b)

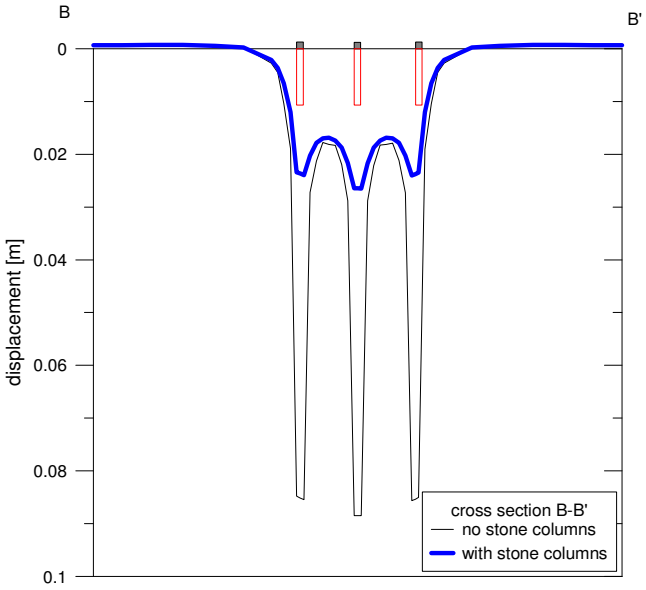

Figure 7.8: Settlement for raft footing case study after construction for cross-section: a) A-A’ and b) B-B’.

a)

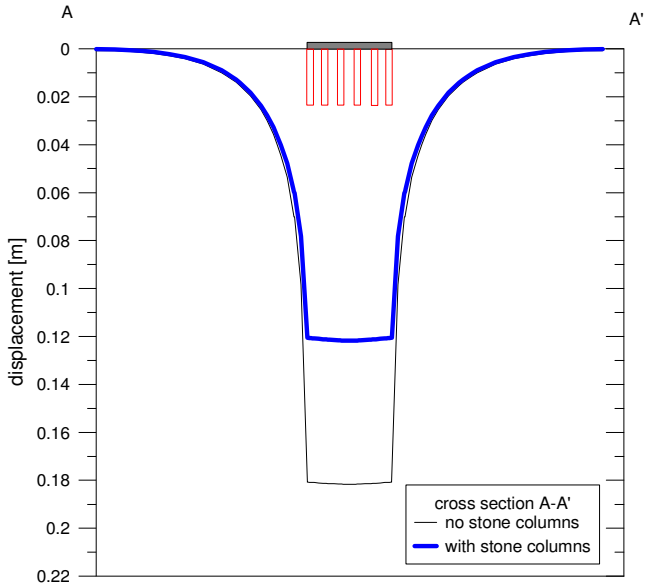

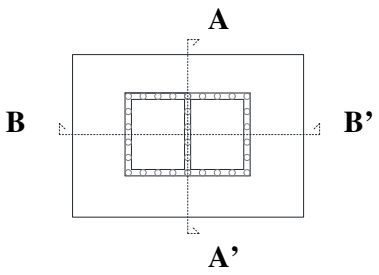

b)

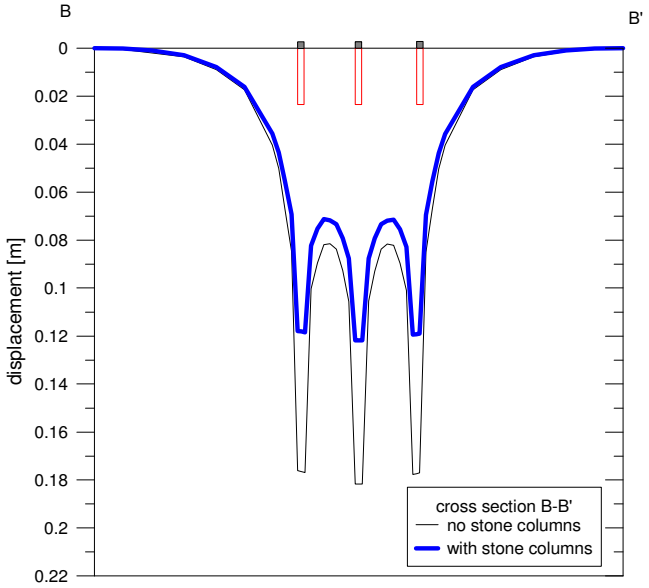

Figure 7.9: Settlement for raft footing case study at the end of consolidation for cross-section: a) A-A' and b) B-B'.

7.6.3 Vertical effective stresses

The plot of the vertical effective stresses along the depth profile at point 5 is presented in Figure 7.10. In the dry crust strata, simulated using the HS model, for both construction and consolidation, the effective vertical stress was found to be the same. Moreover, point 5 experiences during both phases almost the same vertical effective stress in the sandstone layer (from depth of 15 m downwards), which was also modelled with HS. Both the dry crust and sandstone strata were modelled as drained materials and hence during consolidation process no increase of the effective vertical stresses was predicted. As the clay layer is overlain by silty clay strata, and the stress distribution decreases with depth, in the silty clay layer the increase in the effective vertical stress value was found to be more pronounced than in the clay layer.

Vertical effective stress contours along the horizontal profile after construction for the cross-section A-A' are plotted in Figure 7.11, with and without the installation of stone columns. Detailed inspection of the improved zone reveals that the stress level maintained by the stone columns was much greater than that maintained by the surrounding soil. As floating stone columns are considered, the granular columns do not transfer the load into a rigid stratum but into the surrounding soil as part of a load transfer process. This process can be seen on each figure: in the upper part of the plot the granular material transfers more load than the surrounding soil. Then, at the column base level the load is transferred by the columns to the soil underneath. The 'neutral point', where the amount of load held

by the column and the surrounding soil is of the same value, and was found to be at a depth of approximately 4 m.

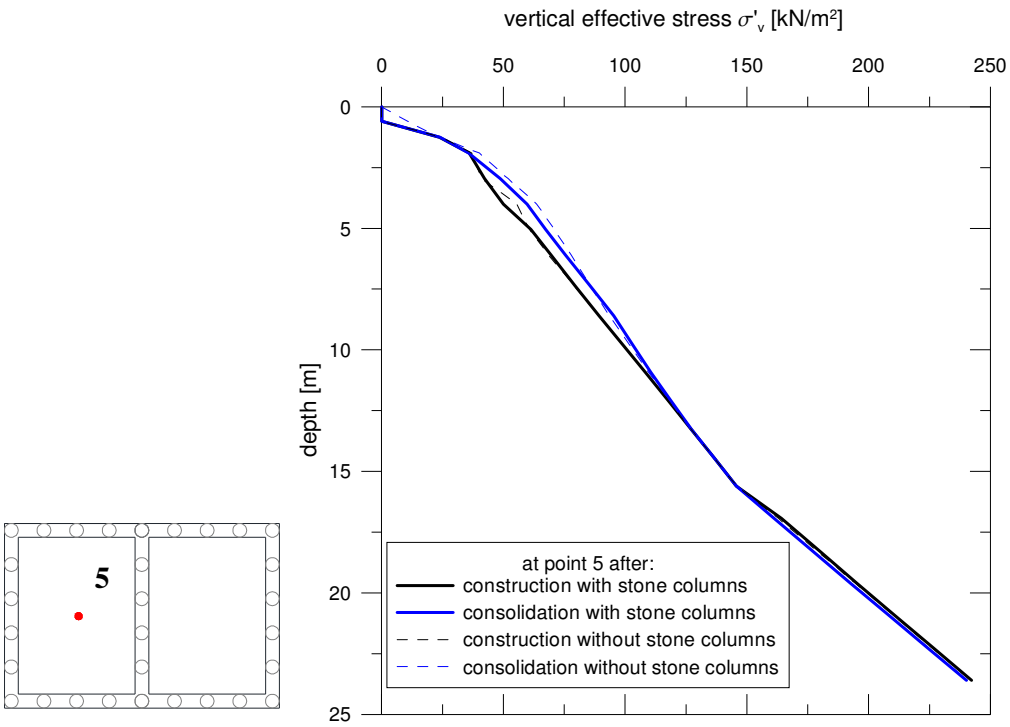

Figure 7.10: Vertical effective stress vs. depth at point 5: raft footing case study.

Vertical effective stress contours along the cross-section B-B' after construction are plotted in Figure 7.12. Again, general inspection indicates that the differential vertical stresses are similar for both case scenarios. As no stone columns are present in the B-B' cross-section, no higher effective stress is maintained as illustrated in Figure 7.12.

Figure 7.13 shows the vertical effective stress contours after the consolidation process for both case scenarios (with and without stone columns) for cross-section A-A'.

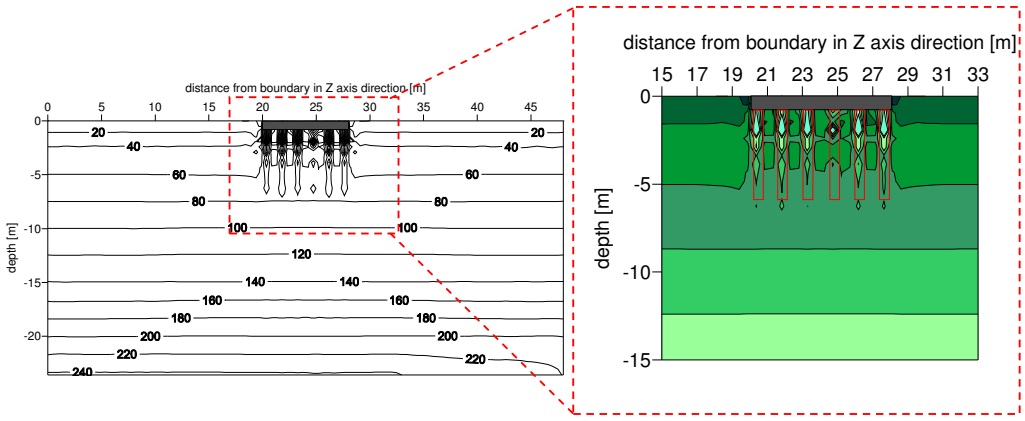

a)

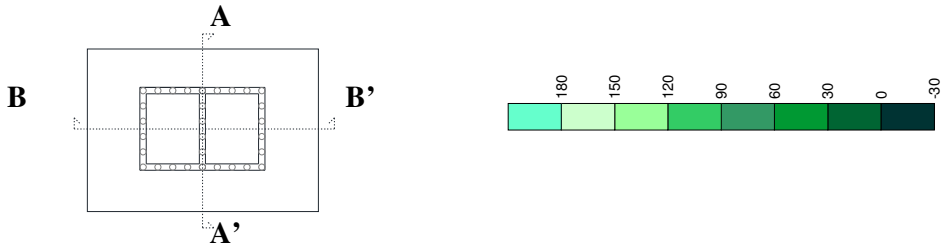

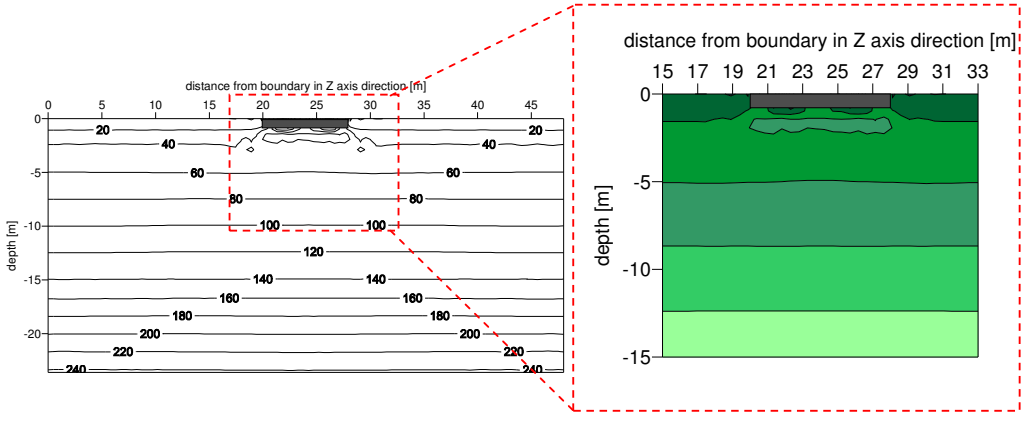

b)

Figure 7.11: Vertical effective stress contours (in kPa) for a raft footing case study after construction along cross-section A-A': a) with and b) without stone columns.

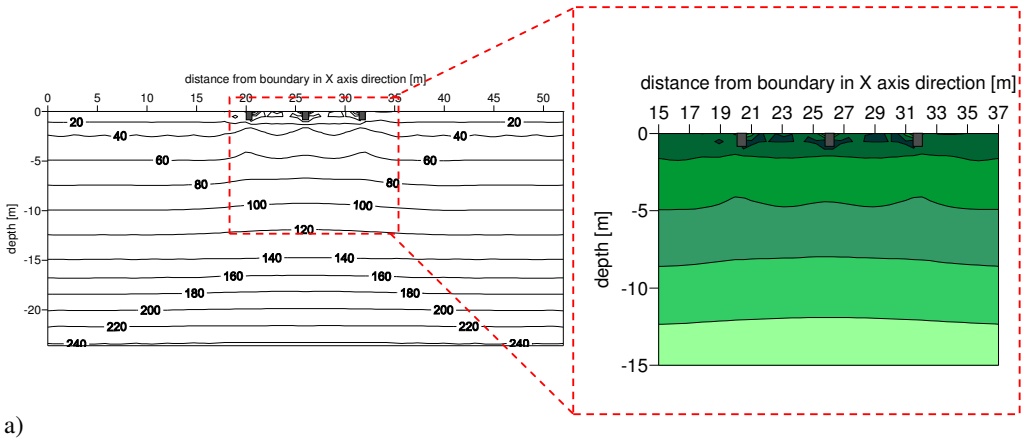

a)

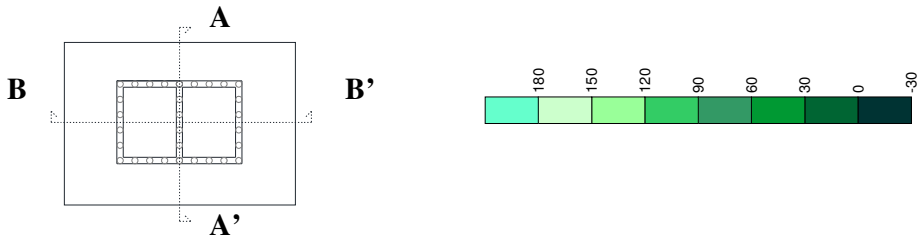

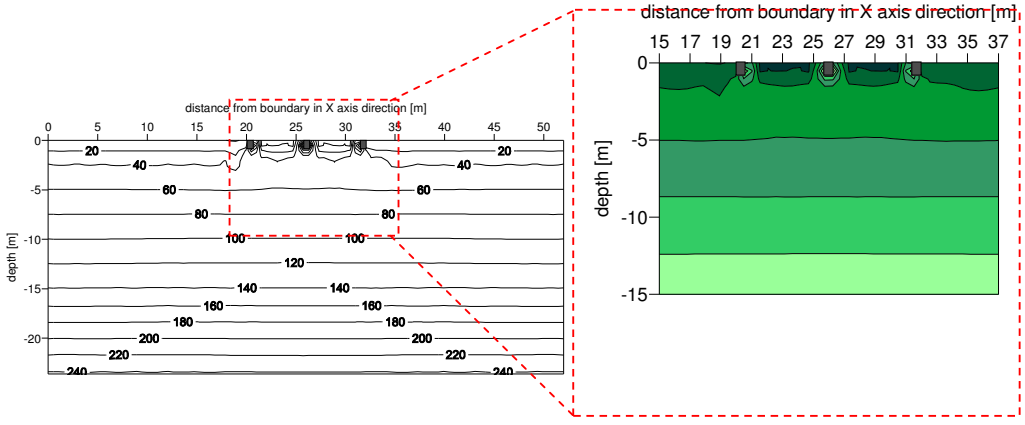

b)

Figure 7.12: Vertical effective stress contours (in kPa) for raft footing case study after construction in cross-section B-B': a) with and b) without stone columns.

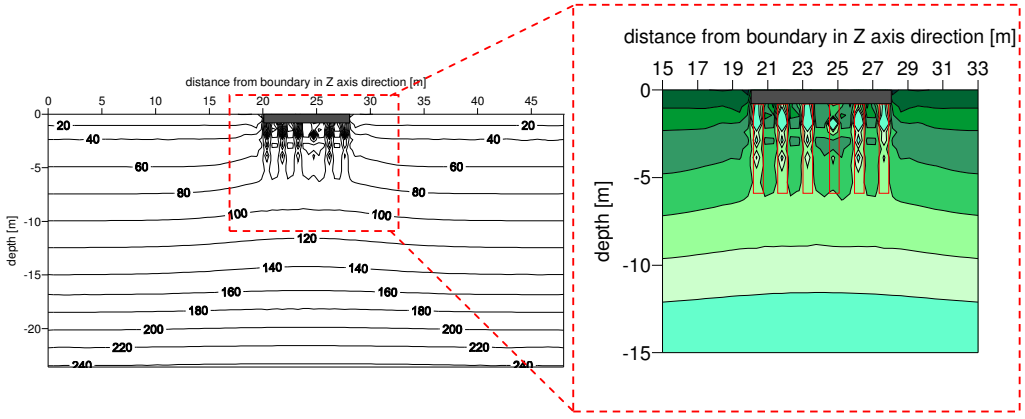

a)

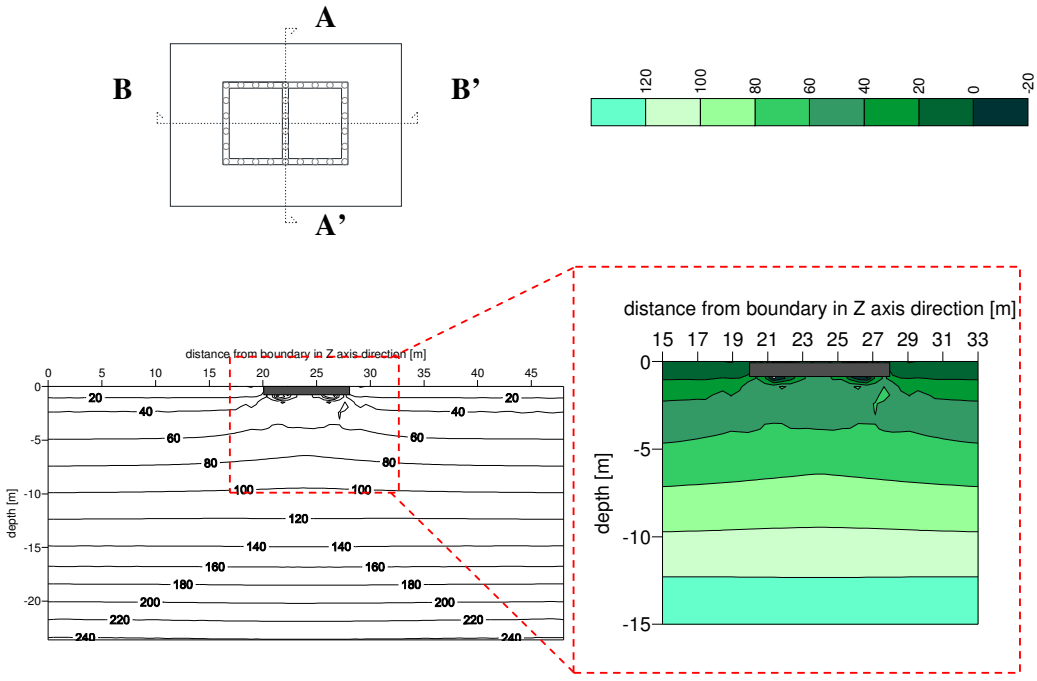

b)

Figure 7.13: Vertical effective stress contours (in kPa) for raft footing case study after consolidation in cross-section A-A': a) with and b) without stone columns.

One can see that the overall distribution of the vertical effective stress at this point is very similar to that presented in Figure 7.11 corresponding to the end of the construction phase. Only closer inspection of the improved zone indicates that the granular material of the stone columns support a smaller magnitude of the vertical effective stress at the end of consolidation than after construction. Again, the 'neutral point' at the end of consolidation was found to be at depth of approximately 4 m.

Contours of the vertical effective stresses along the cross-section B-B' after the consolidation process are plotted in Figure 7.14. Again, general inspection indicates that the differential vertical stresses are similar for both scenarios as no floating stone columns were present in the cross-section.

In order to fully investigate the influence of the stone column on the stress-strain behaviour of the soil deposit, the incremental vertical effective stresses are plotted along the horizontal profile. As project specification required investigation of the first 3 years of service, the incremental vertical effective stresses were defined as being the difference between the vertical effective stress at the end of the first consolidation stage (after 3 years) and the vertical effective stress during the initial phase of the FE calculations, see Figures 7.15 and 7.16.

As in previous sections, the incremental vertical effective stress contours were prepared for cross-sections A-A' and B-B' for cases with and without floating stone columns. A positive incremental stress value means that the vertical effective stress found in the soil mass was greater (after 3 years of consolidation) than the generated initial stresses, whereas a negative value indicates that after consolidation the vertical effective stresses are reduced with respect to the initial vertical stresses. Negative

values of the incremental vertical effective stresses are due to small rounding off errors and do not have any practical meaning.

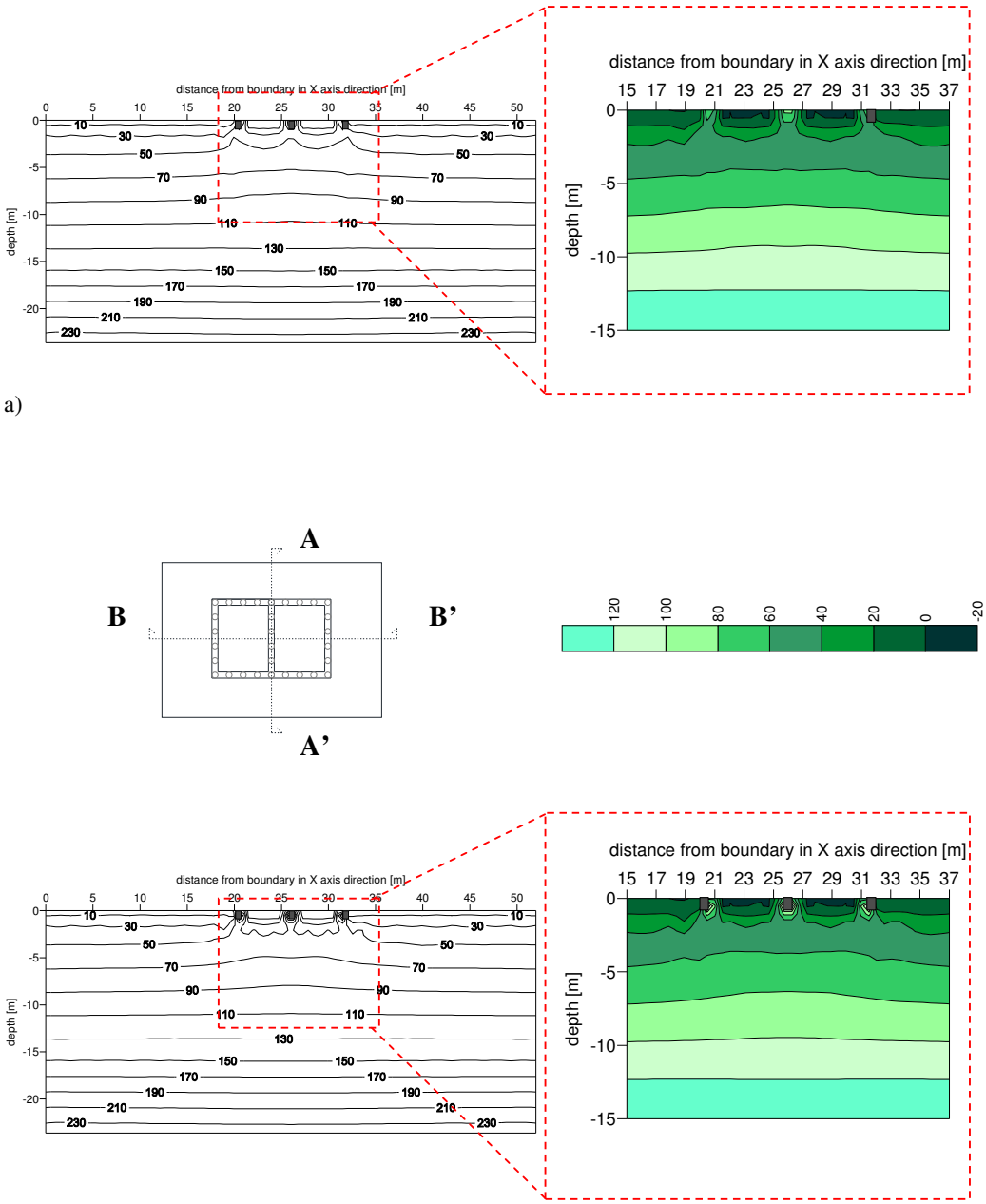

a)

b)

Figure 7.14: Vertical effective stress contours (in kPa) for raft footing case study after consolidation in cross-section B-B': a) with and b) without stone columns.

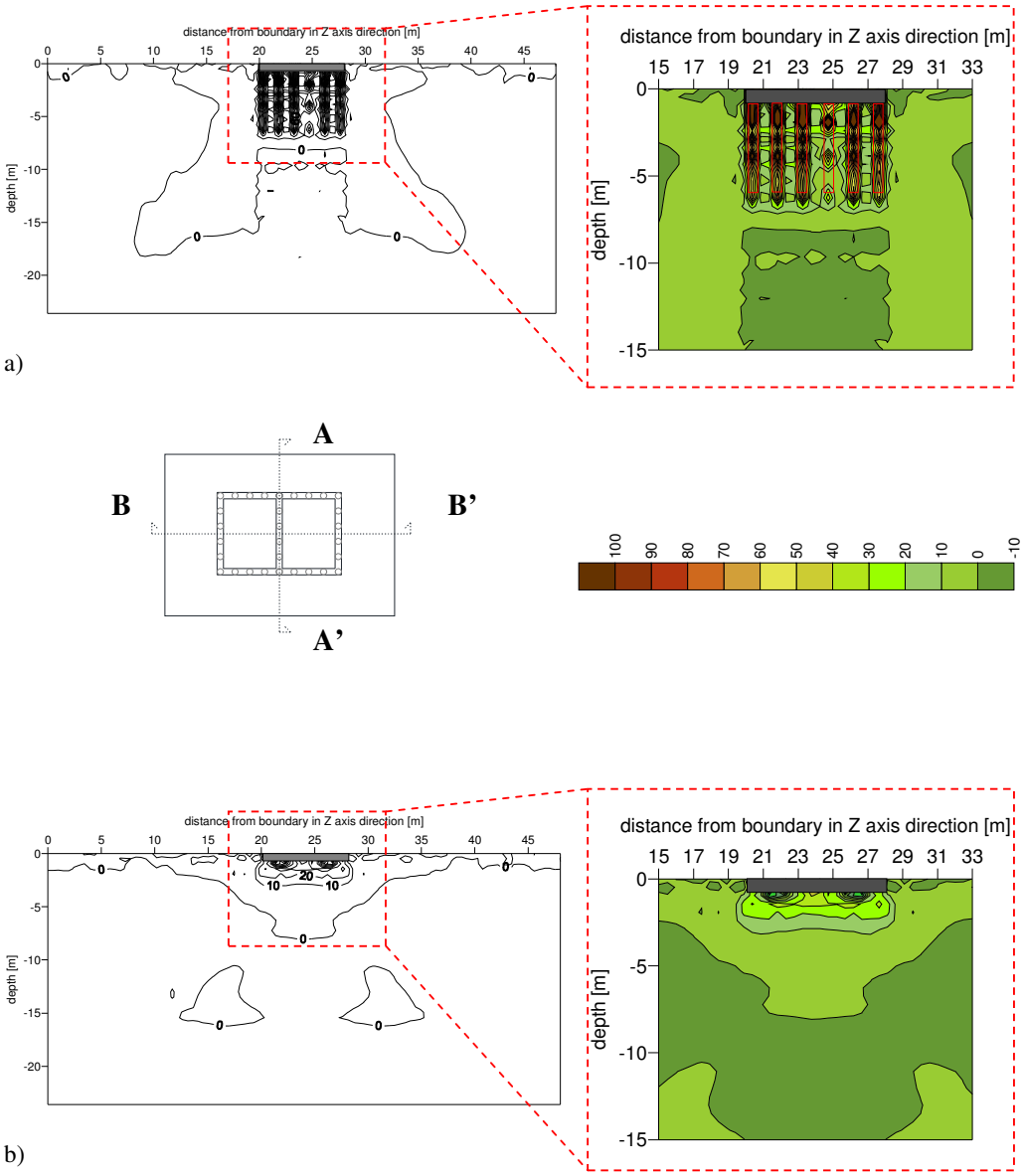

Figure 7.15: Incremental vertical effective stress contours (in kPa) for raft footing case study along cross-section A-A': a) with and b) without stone columns.

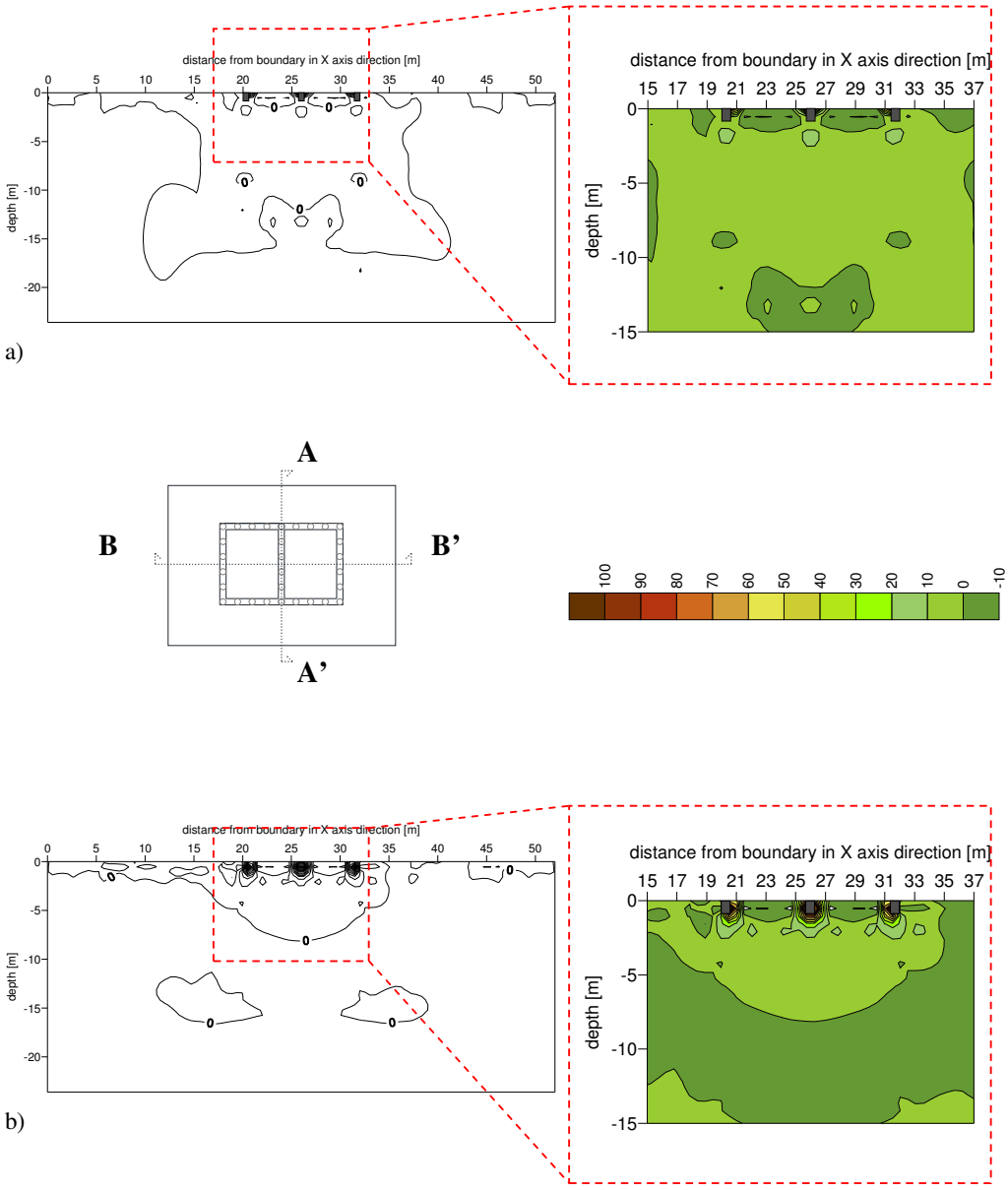

Figure 7.16: Incremental vertical effective stress contours (in kPa) for raft footing case study along cross-section B-B': a) with and b) without stone columns.

Figure 7.15 presents the incremental vertical effective stresses for the cross-section A-A'. Installation of the stone columns only affects the area directly underneath the footing. As expected, due to the high stiffness of the granular material the columns support more vertical effective stress than the surrounding soil. Construction of the stone columns leads to an increase of more than triple the incremental vertical effective stress values than in case of no ground improvement, which is a result of the columns transferring the load from the footing down to the deeper soil deposits.

Incremental vertical effective stress contours along the cross-section B-B' is presented in Figure 7.16. Installation of the stone columns supported some vertical stresses when compared with the case with no ground improvement, especially in the shallow deposits underneath the footing. One can see that the columns notably influence the incremental vertical effective stress contours, increasing the value of the stresses after the construction, loading and consolidation processes, see Figures 7.15 and 7.16.

7.6.4 Excess pore water pressures and time of consolidation

As the stone columns speed up consolidation, the prediction of the excess pore water pressures was inspected at chosen depths. Figure 7.17 illustrates the schematic sketch for point 5, which was chosen for inspection of the excess pore water pressure at various depths in the soft deposit. The evolution of the excess pore water pressures with time is plotted in Figures 7.18..7.21. The plot has been prepared for depths of

2.95 m (Figure 7.18), 6.1 m- column base level- (Figure 7.19), 8.6 m (Figure 7.20) and 9.77 m (Figure 7.21). The geotechnical sign convention for the pressure has been applied, where negative values refer to suction.

It can be observed that in the case with stone columns, the excess pore water pressures increase above their initial values and then dissipate with time to zero values. During coupled consolidation, due to the Mandel-Cryer effect (Mandel, 1950 and Cryer, 1963), time-dependent redistributions of total stresses take place within the soil.

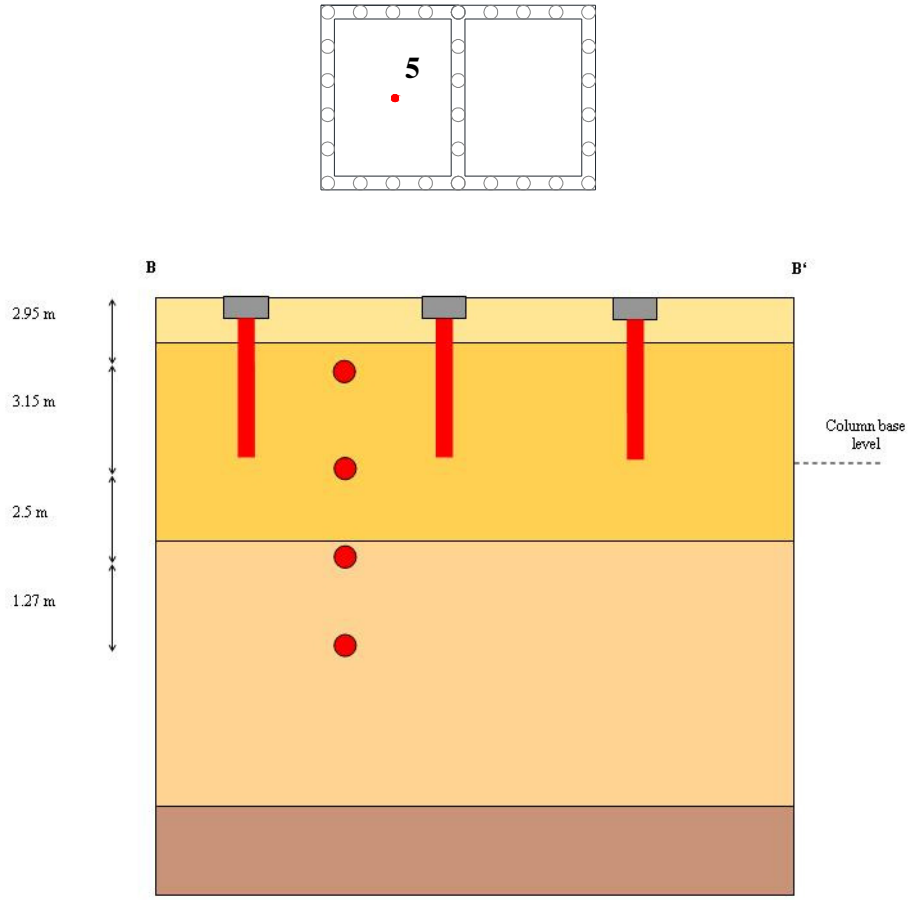

Figure 7.17: Sketch of the model geometry with chosen points for the excess pore water pressures predictions: raft footing case study.

This results in the increase of the excess pore water pressures in the zone beneath a footing at the start of consolidation, which is in contrast with Terzaghi's one-dimensional consolidation theory (1943). The Mandel-Cryer effect was observed for the first time in laboratory experiments on clay spheres by Gibson *et al.* (1963).

In the case study considered herein, this effect is predominant in the zone where the stone columns are installed (at depths of 2.95 m and 6.1 m), which is in agreement with the findings presented by Cui *et al.* (2009) for a piled raft constructed on soft soil. Small discontinuities in the excess pore water pressure results, which can be seen as sharp kinks in the pressure values, can be explained by numerical instabilities at the considered point of geometry.

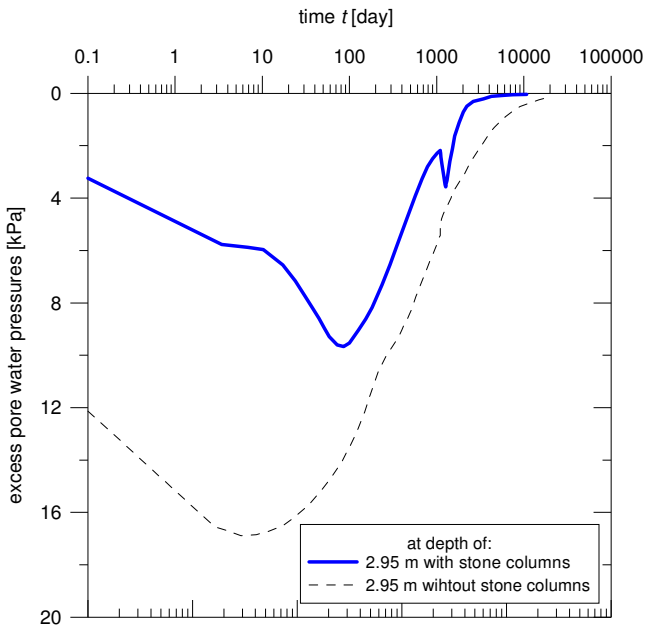

Figure 7.18: Excess pore water pressure evolution with time at a depth of 2.95 m: raft footing case study.

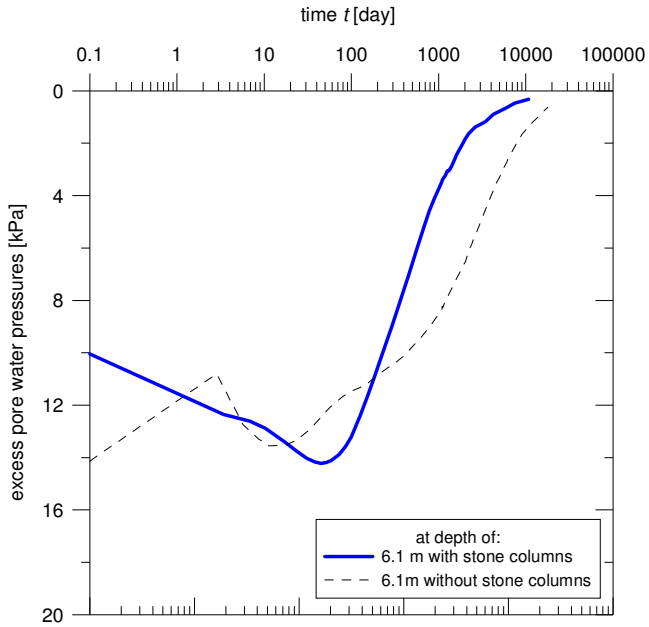

Figure 7.19: Excess pore water pressure evolution with time at a depth of 6.1 m: raft footing case study.

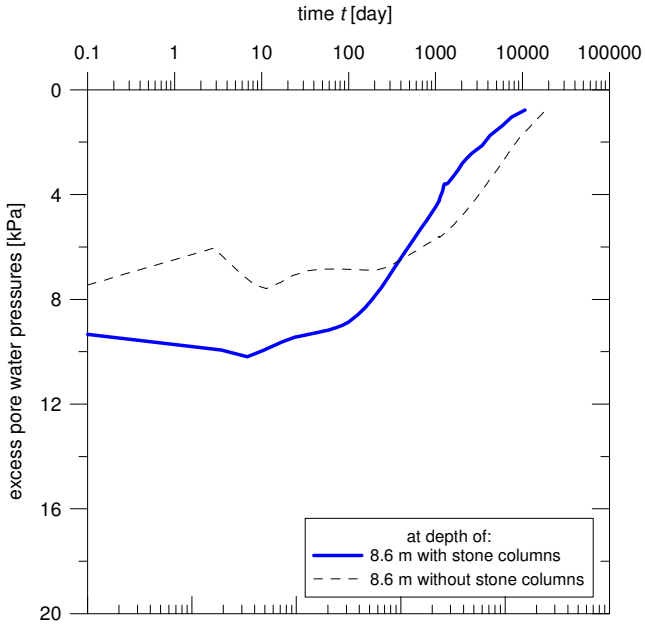

Figure 7.20: Excess pore water pressure evolution with time at a depth of 8.6 m: raft footing case study.

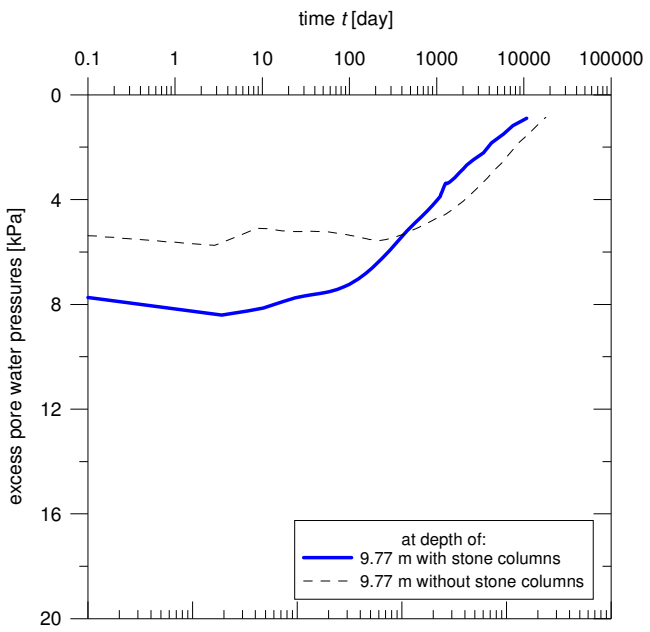

Figure 7.21: Excess pore water pressure evolution with time at a depth of 9.77 m: raft footing case study.

As consolidation progresses, the excess pore water pressures reduce. This phenomenon is particularly rapid at depths of 2.95 m and 6.1 m, where the stone columns are present in the soft deposit, as the dissipation of excess pore water pressures is speeded up by the good hydraulic conductivity of the columns. Points at a depth of 2.95 and at the column base level reached values of 1 kPa for the excess pore water pressures a lot earlier than points located in the deeper deposits, see Figures 7.18..7.21. When compared with the case where no stone columns were installed in the soil deposit, it is evident that the columns reduced the time required for excess pore water pressure dissipation by more than half.

The excess pore water pressure contours after construction along the cross-sections A-A' and B-B' are plotted in Figures 7.22 and 7.23. Again the geotechnical

sign convention has been applied for those plots and for the sake of completeness the improved zone has been magnified in an additional plot (with the outlines of the stone columns and the raft foundation indicated in red and grey, respectively). After construction the excess pore water pressures increased up to a value of approximately 50 kPa for the case with the floating stone columns. One can see that the granular material of the columns reduced the excess pore water pressure values in the close vicinity and below the column base level. The pore water pressure concentration between the columns underneath a raft footing is gradually erased by dissipation of the excess pore water pressures during the consolidation process.

The excess pore water pressure contours after the 1095^{th} day (3 years) in the consolidation process are plotted in Figures 7.24 and 7.25 for the A-A' and B-B' cross-sections. As the top consolidation boundary remained open during the consolidation phase, the lowest excess pore water pressure values were found at the top of the geometry model.

For the case with stone columns, a great concentration of excess pore water pressures in the untreated zones was evident, see Figures 7.24 and 7.25. Underneath the footing at a depth of 12 m the soil experienced an excess pore water pressure of approximately 4 kPa. Below the base level of the stone columns (and nearby) and in the improved area the excess pore water pressures decay so efficiently that a zero value was registered. Moreover, when comparing Figures 7.24a and 7.25a with the plots presenting the case with no ground improvement one can see that the effect of the stone columns in reduction of the excess pore water pressure values is significant. The excess pore water pressure value was approximately halved during the serviceability period in the area where the stone columns were installed.

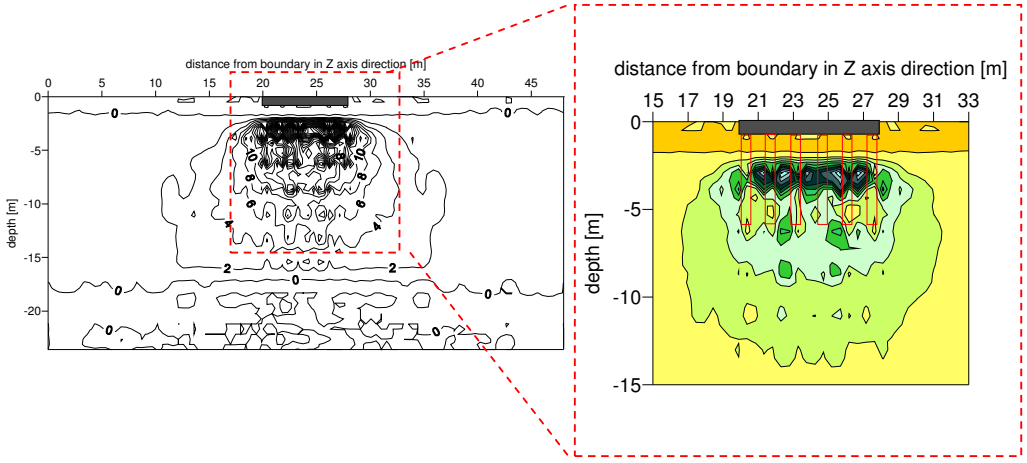

a)

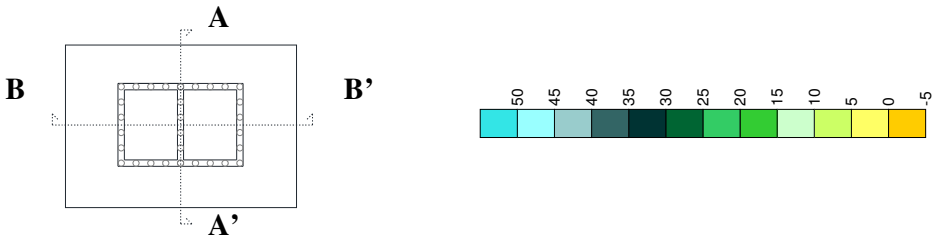

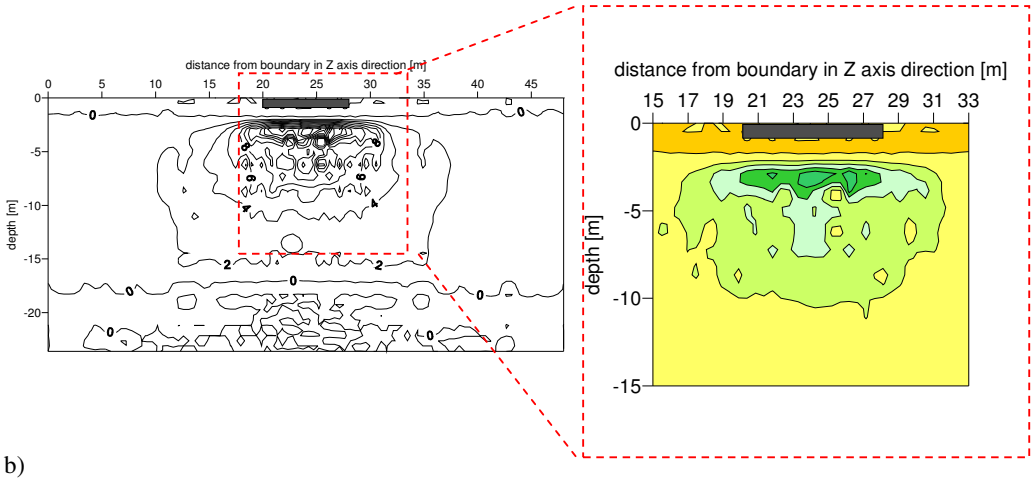

b)

Figure 7.22: Excess pore water pressures contours (in kPa) for raft footing case study after construction along cross-section A-A': a) with and b) without stone columns.

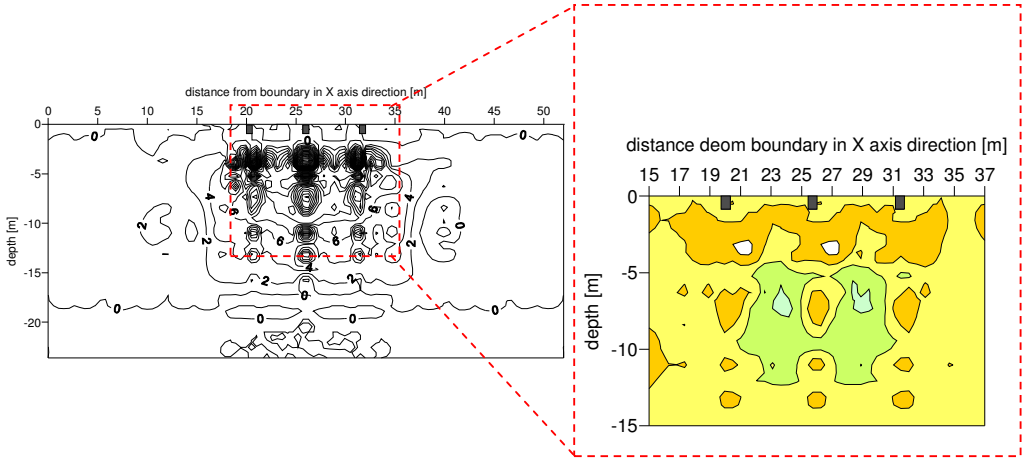

a)

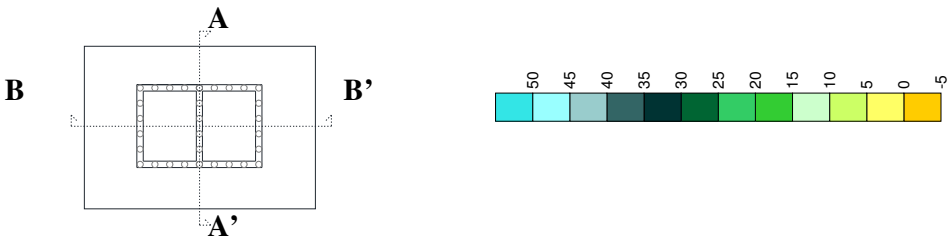

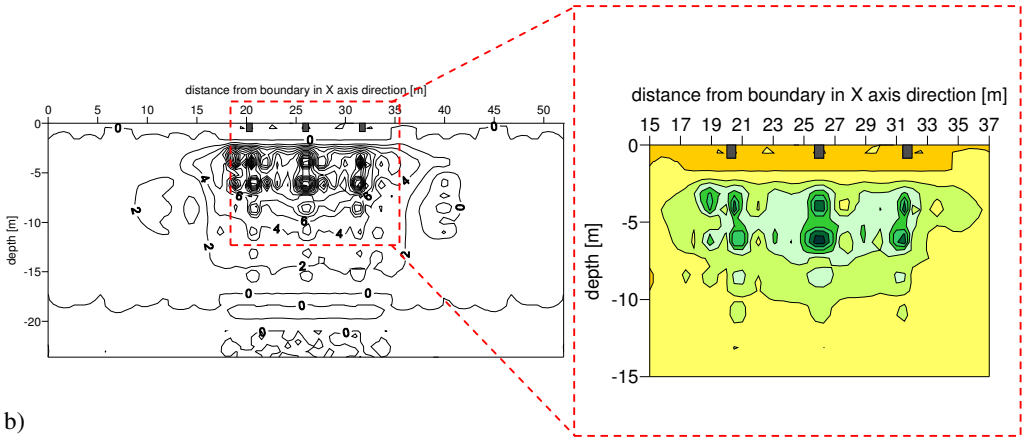

b)

Figure 7.23: Excess pore water pressures contours (in kPa) for raft footing case study after construction along cross-section B-B': a) with and b) without stone columns.

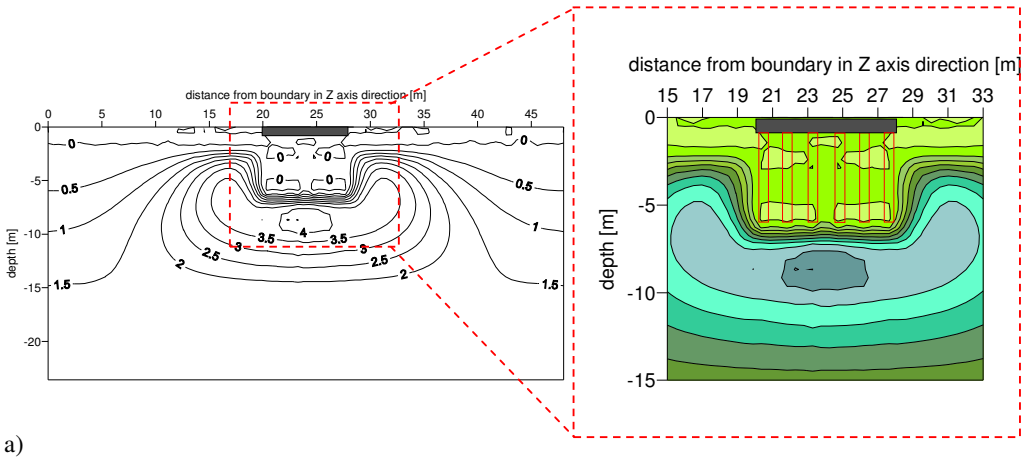

a)

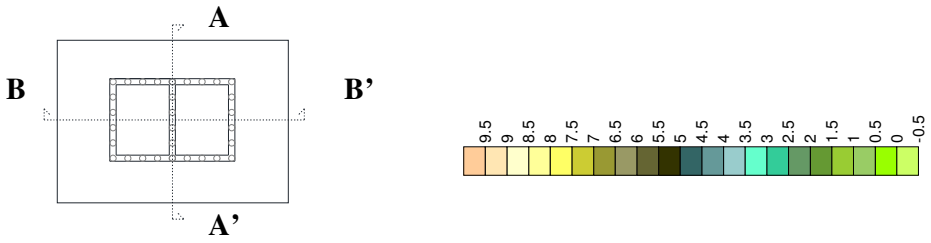

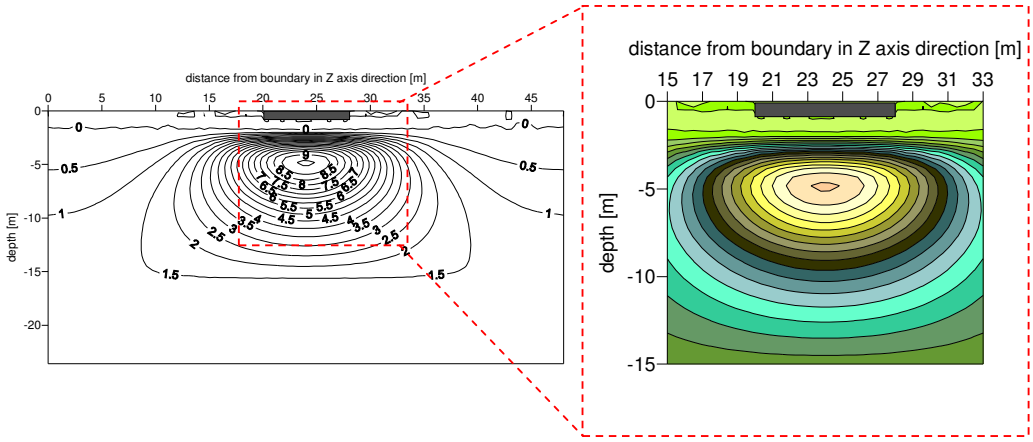

b)

Figure 7.24: Excess pore water pressures contours (in kPa) for raft footing case study after 3 years into consolidation along cross-section A-A': a) with and b) without stone columns.

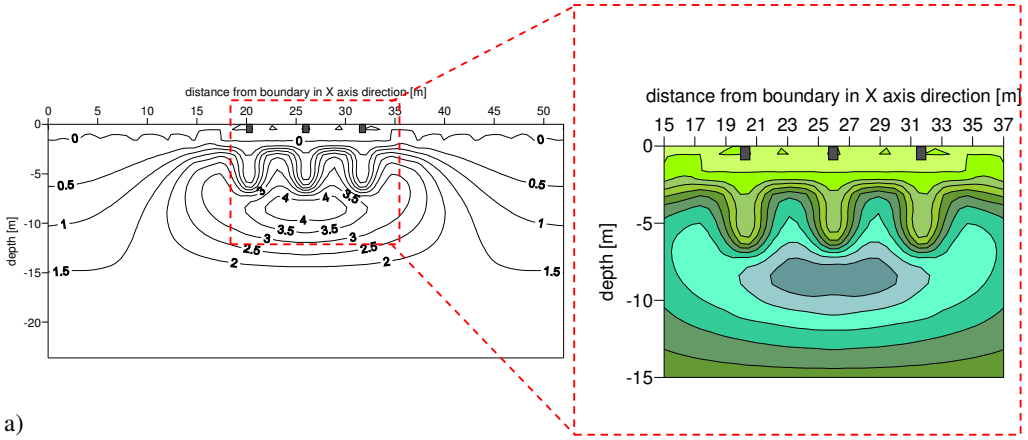

a)

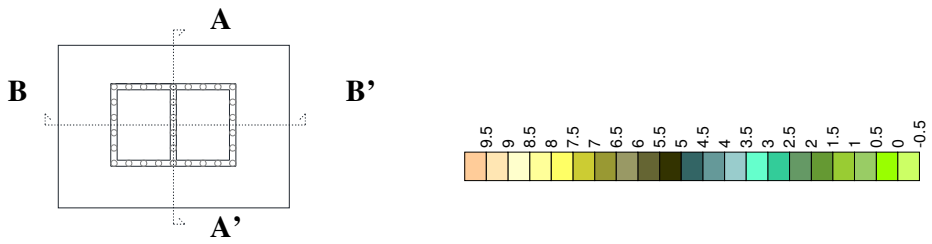

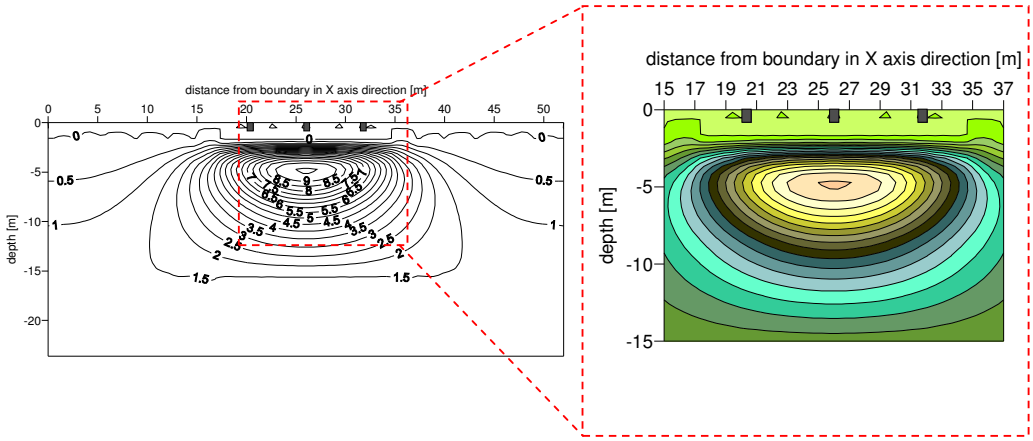

b)

Figure 7.25: Excess pore water pressures contours (in kPa) for raft footing case study after 3 years into consolidation along cross-section B-B': a) with and b) without stone columns.

7.6.5 Quality of soil sampling and its impact on the numerical results

Site investigation and laboratory testing should provide the necessary data for determination of the ground conditions and the geotechnical parameters required for all stages of the engineering work, such as tendering, design and construction. However, analysis of the current study indicated the poor quality and high disturbance of the soil samples, which raises concerns over the ability to reliably and correctly determine the engineering characteristics of the silty clay and clay layers.

As already mentioned in *Section 7.5.1*, the desk study indicated that the soft soil at Bishopton site is expected to be over-consolidated with compressibility parameters similar to that of the soft clay from Bothkennar. As a result of the poor quality of the soil samples, a conservative approach was chosen to model the soft soil deposits as a normally consolidated and fully reconstituted material. As the soil sampling quality is a matter of concern in this case study, a preliminary study on the impact of the over-consolidation ratio OCR on the settlement predictions was performed and is presented in this section.

In this study the compression of the silty clay and clay layers was defined by the apparent value of the slope of the compression curve λ in the $e - \ln p'$ and was determined to be equal to 0.3 for both layers. The over-consolidation ratio was assumed to vary from 1.0 to 1.5, as summarised in Table 7.9. Additionally, numerical results for the simulation analysed in *Sections 7.6.1..7.6.5* are indicated as Simulation G, see Table 7.9.

Table 7.9: Influence of the over-consolidation ratio on numerical predictions: raft footing case study.

Simulation	Over-consolidation ratio OCR [-]	Slope of compression curve λ [-]	
		Silty clay	Clay
A	1.0	0.3	0.3
B	1.1	0.3	0.3
C	1.2	0.3	0.3
D	1.3	0.3	0.3
E	1.4	0.3	0.3
F	1.5	0.3	0.3
G	1.0	0.125	0.133

Figure 7.26 presents the evolution of the surface settlement value with the value of the over-consolidation ratio for cases with and without stone columns. It is evident that as the value of the over-consolidation ratio increases, the predicted vertical displacement reduces (for both cases: with and without stone columns). Using data points for the case with stone columns installed underneath an embankment, the power function can be determined to define the relationship (indicated with dotted line in Figure 7.26):

$$\ln(\delta_y) = -3.47 \times \ln(OCR) - 1.88 \qquad (7.1)$$

where: δ_y is the maximum surface settlement and OCR is the over-consolidation ratio.

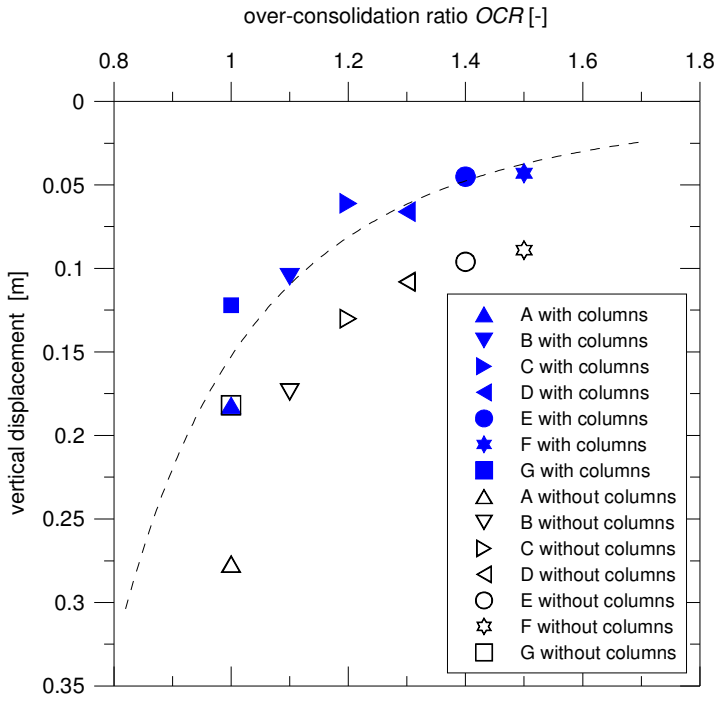

Figure 7.26: Evolution of the vertical displacement with the over-consolidation ratio: raft footing case study.

7.7 Summary and Conclusions

In this *Chapter* the total and differential settlement reduction of the stone column foundation constructed below a raft footing in a soft soil deposit during the construction, first 3 years of service and consolidation was studied. Floating stone columns have been proposed to be installed underneath a raft footing in a soft soil stratum on the Bishopton site (Scotland). The floating stone columns were simply 'wished-in-place'.

Given limited availability of the site investigation data and previous experience with soil material in this area, simulations were performed using the advanced

constitutive S-CLAY1 model (accounting for plastic anisotropy) implemented in the three-dimensional commercial finite element code, using the intrinsic value of the slope of the compression curve and an over-consolidation ratio equal to one. This results in conservative numerical predictions. It should be noted that this assumption has some implications on the numerical results, such as value of the in-situ coefficients of the earth pressure at rest and further reconstitution of the soil mass. Additionally, a preliminary study of the influence of the over-consolidation ratio OCR of the soft soil deposits on the numerical predictions of the settlement has been performed. As expected, an increase in the OCR value leads to a reduction in the predicted settlement value. It is concluded that the effect of the over-consolidation ratio on the numerical predictions is pronounced, resulting in a change in the surface settlement value by a factor of 4 in the considered range of the over-consolidation state (OCR =1.0..1.5). Therefore, for more detailed and less conservative numerical modelling of this case study, further site investigation is strongly recommended. It is essential to ensure high quality samples are obtained in order to minimise soil disturbance and to enable reliable determination of the geotechnical parameters and soil characteristics at the Bishopton site.

Application of stone columns in the Bishopton case study resulted in a predicted settlement reduction of approximately 50 %, and an increase in the excess pore water pressure dissipation by a factor of approximately 1.6. Unfortunately, recent news from the contractor suggests that development at the Bishopton site is unlikely to proceed in the short term due to the current global economic climate.

8

CONCLUSIONS AND RECOMMENDATIONS

The overall aim of this thesis was to use the state-of-the-art in advanced constitutive modelling applied to three-dimensional finite element (FE) analyses of soft soil improved with stone columns in order to gain an improved understanding of the stress-strain behaviour of the stone column foundation. In this thesis, stone columns were used as a support for two types of foundations: an embankment and a raft footing. These problems, as with many other engineering projects, are three-dimensional problems and as such, are modelled by conducting three-dimensional FE analyses. This chapter outlines the main conclusions based on the work done and gives recommendations for future research.

8.1 Parametric study on floating stone columns beneath an embankment

The majority of design methods for stone columns consider end-bearing columns, which is not necessary the most economical solution. Therefore, the aim of this thesis was to use three-dimensional finite element analyses, with an advanced constitutive model to represent the complexity of a soft soil material, to study the stress-strain behaviour of a floating stone column foundation constructed in a soft soil deposit. The soft soil was represented by the Bothkennar clay, a soft structured natural deposit. An embankment is a typical application of a large group of the floating stone columns.

First of all, the influence of the mechanical properties of the column material, such as the angle of friction and the stiffness was studied. Then, the effect of the physical properties of floating stone columns was investigated, considering factors such as the column diameter, spacing and length. Next, a study on the influence of the thickness of the soft soil layer was performed. These studies concluded that the predicted behaviour of the stone column foundation is controlled mainly by three factors: the column strength (expressed as the angle of friction), the column diameter and the column spacing. The value of the angle of friction of the granular column is limited by the material available, varying typically from 40º to 50º. The column diameter is restricted by the diameter of the poker inserted into the ground, therefore construction of excessive large or small columns is not practically feasible. The actual stiffness of the column material (selected on the basis of the stone material

available and those typically used in practice) was found to have little influence on the numerical settlement predictions of the column foundations considered.

The numerical studies suggest that within the range of column diameters commonly used, the column spacing/diameter ratio S_{SC} / D_{SC} is one of the key design parameters for floating columns with an optimum value of about 2.7..2.8. This value has been supported by field data collected from the literature. Following the 3D FE simulations, a simple bi-linear relationship between the S_{SC} / D_{SC} ratio and the settlement reduction ratio s_r was suggested, allowing the expected settlement reduction after stone column construction to be estimated.

The optimum column length for the benchmark problem considered appear to be $L_{SC} / D_{SC} \leq 17$ and $L_{SC} / S_{SC} \leq 5$, and is not notably influenced by the embankment height and the magnitude of load applied in the range of values studied. The numerical predictions suggest that in terms of settlement reduction, floating stone columns work as well as end-bearing columns. However, in order to achieve a desired rate of consolidation in deep deposits the length of the columns needs to be optimised.

The first set of parametric studies ignored the rate-dependent behaviour of soft soil. Given this is of vital importance in the response of a soft natural soil, a new-time dependent constitutive ACM-S model, which accounts for anisotropy and degradation of interparticle bonds, was developed. The proposed formulation is based on existing constitutive models for structured soft soils which are prone to creep and it was implemented in FE code (2D and 3D Foundation PLAXIS) using the dynamic link library as a user-defined soil model. The number of input parameters used for ACM-S was kept to a minimum, and all of them can be

determined directly via laboratory testing of structured soft soils. Thus, the soil parameters' determination is easy and straight-forward. As the proposed model has a hierarchical form, some of the soft soil features, such the anisotropy and the effect of bonding, can be simply switched off, which ensures the potential for wide application of the proposed model as an engineering tool.

The ACM-S model was used to simulate the behaviour of soft natural soils, including laboratory tests on various soft soils and a two-dimensional benchmark problem. Given the good agreement between the numerical simulations and the experimental results, the ACM-S model appears to be able to capture the essential features of soft soil behaviour, and also (to some extent) the creep rupture phenomenon. It was shown that the model can be easily applied for both simulations of laboratory testing and boundary value problems. A coupled consolidation analysis in FE code PLAXIS conducted in conjunction with ACM-S ensures that simulations of the boundary value problems can be carried out in both undrained and drained conditions. However, there were some concerns about the performance of the model at the boundary value level, and these were confirmed by additional parametric studies considering floating stone columns underneath an embankment.

In order to investigate the dependency of the stress-strain behaviour of an embankment constructed on floating stone columns on the constitutive soil model, the second part of the parametric studies used six different constitutive models: the Modified Cam Clay model (MCC), the Soft Soil Creep model (SSC), the S-CLAY1 model, the ACM model, the S-CLAY1S model and the ACM-S model. Additionally, the sensitivity of the predictions to the changes in the pre-consolidation stress on the soft soil was investigated.

It was found that in the case of the elasto-plastic models, accounting for anisotropy and destructuration of the soft soil deposit increased the predicted vertical displacement and reduced the predicted value of the horizontal movements. On the contrary, in the case of the creep models, taking account of anisotropy and destructuration reduced both the vertical and horizontal displacements. The isotropic Soft Soil Creep model, a standard model in the PLAXIS code, predicted the greatest (and unrealistic) vertical and horizontal movements, which is probably partly due to assumptions made for the creep part of the model and other issues (such as implementation of the formulation in PLAXIS). Generally, the predictions given by the creep models appeared to be unrealistic, showing significant self-weight surface settlements. In order to address this problem, a procedure of applying a consolidation phase with in-situ stresses only for a long period of time before the construction of the columns and embankment was studied. Nevertheless, the current study indicated that, although at a global level this procedure might lead to desired results, it leads to an incorrect over-consolidation state and therefore an incorrect amount of bonding in the soft soil at the start of the analysis, and is hence not satisfactory. The studies on the sensitivity of the predictions on the changes in the pre-consolidation stress demonstrated that the creep models are super-sensitive to the value of the over-consolidation ratio. Nonetheless, the settlement reduction ratio is not influenced as profoundly as the surface settlement predictions, but this might not be the case when higher magnitude of loads is considered. Moreover, the effect of the C_α / C_C ratio on the predictions of the surface settlement of the soft soil deposit was found to be pronounced. However, the effect of the over-consolidation ratio OCR was much more significant than the influence of the C_α / C_C ratio.

8.1.1 Limitations and recommendations for future work

A simple bi-linear relationship between the column spacing/diameter ratio and the settlement reduction ratio was determined after numerical studies were performed for the boundary value problem. However, this relationship was formulated for the case of an embankment involving a large number of floating stone columns and may not be valid for other types of foundations. Further research should be conducted in order to establish the applicability of this relationship for other structures and, if needed, the existence and possible form of similar relationships.

It is also recommended that further numerical studies on the optimum column length are conducted to account for other types of foundations used in engineering practice. It would be of benefit to study further the influence of a higher magnitude/different type of load applied on the optimum column length value and the over-consolidation ratio of the soft soil layer in order to establish and provide further support for the current findings.

Analyses with two standard constitutive soil models available in the finite element PLAXIS code (namely MCC and SSC), suggested unrealistic predictions for the SSC model. This is partly due to the assumptions made for the creep part of the model. But given the differences in the predictions by the SSC and ACM models, there might be some other causes as well, such as related to the numerical implementation. In order to investigate this problem further and to provide additional support for the current findings, it is recommended that additional numerical studies are conducted using the isotropic version of the ACM model. It would also be of

interest for future research to expand this study by using other advanced constitutive models, such as EVP-SCLAY1S (Karstunen & Yin, 2010).

Based on the boundary value simulations using the ACM-S model, some issues should be addressed and thoroughly studied in the future. First of all, the causes for the over-predictions of the vertical and horizontal displacements should be investigated. The simulations with ACM-S indicate that the subsoil under self-weight conditions (in the presence of in-situ stresses only) can exhibit significant (and unrealistic) creep settlements. This may be a result of the formulation of ACM-S (and ACM, Leoni *et al.,* 2008) itself, as it is assumed that the normal consolidation surface (NCS) is the contour of the constant volumetric creep strain rate. Following that, large volumetric creep strain increments between the K_0-line and the critical state line (CSL) may be calculated and greater than expected horizontal movements (and thus, greater vertical displacements) may be predicted. It should be pointed out that the experimental evidence suggesting contours of constant volumetric creep rate were based on assuming a fixed anisotropic yield surface. Moreover, in the ACM-S model the ratio between the secondary compression index C_α and the compression index C_c is assumed to be constant, and only components of this ratio are assumed to change due to destructuration. This assumption requires further experimental investigation.

The over-consolidation ratio is directly determined via laboratory tests results, thus it would be beneficial if its value is an input parameter for all constitutive soil models, both elasto-plastic and creep.

The proposed ACM-S model is applicable for normally and slightly over-consolidated natural soft soils. It may be of interest to adapt this model (and/or its

improved version) to account for heavily over-consolidated soils in order to ensure the wider application of this constitutive formulation. Additionally, as the stress-strain behaviour of soft soil under cyclic loading is different than under single (monotonic) loading, it is particularly essential to consider the cyclic material behaviour for fatigue analysis, strength and life calculations. Therefore, it may be of interest to expand the ACM-S model to take into account soft soil behaviour under cyclic loading, which will find its application in e.g. projects of windfarm foundations or structures constructed on seismic areas.

8.2 Feasibility of stone column foundation in settlement and consolidation time reduction

Finally, a case study considering the behaviour of a stone column foundation beneath a footing on a lightly over-consolidated soft soil deposit in Western Scotland was investigated for the following stages: (i) during construction, (ii) during the first three years of service and (iii) during consolidation. Due to the complex soil profile and heterogeneity of the ground conditions, both standard and advanced constitutive models were used to represent the soil and stone column material. The potential for reducing settlements and the consolidation time was demonstrated in this case using a detailed three-dimensional finite element analyses.

8.2.1 Limitations and recommendations for future work

Due to the limited site investigation and the poor quality of the soil samples retrieved, the work presented here is considered only as an initial numerical study of the feasibility of stone column foundations to reduce settlements and consolidation time. The limited site investigation and the unreliable laboratory test results led to a restricted soil characterisation of the soil deposits present at the Bishopton site. Therefore, in order to provide additional supporting information for the current study and for a more detailed numerical study, additional site investigation and laboratory tests are required. It is recommended that the sample disturbance be minimised to ensure good quality representative samples and as such, reliable laboratory tests results. A research proposal is currently under review submitted by the University of Strathclyde, in partnership with other universities, which will quantify the effects of sample disturbance on the creep of soft soils and investigate the possible means of reduction of sample disturbance.

It would also be of additional benefit to further expand the current study by conducting additional numerical studies with another constitutive model which is capable of accounting for the viscosity of the soft soil deposit, such as ACM-S, in order to ensure the most realistic stress-strain behaviour predictions.

8.3 Overall recommendations

In the current numerical studies, the stone columns were simply ‘wished-in-place’. It would benefit future research to expand the current studies to include column

installation effects; first, for a single column and then, to apply the procedure for groups of columns. Research is currently being carried out at the University of Strathclyde, in partnership with the University of Cantabria (Spain), which studies the changes in anisotropy, bonding and viscosity as a result of column installation in soft clays and these effects on the stress-strain behaviour of the structure. Column installation reduces the undrained shear strength of the soft soil and increases the lateral stresses, but the effects on the final structure are yet to be quantified. Therefore, it is recommend to upscale studies to well instrumented site tests to investigate the stress/excess pore water pressure distribution during stone column installation in soft soils and to study the effect of the column installation method (wet or dry method).

References

Adachi, T. & Okano, M. (1974). A constitutive equation for normally consolidated clay. *Soils & Foundations 14(4),* pp. 55-73.

Al-Tabbaa, A. & Muir Wood, D. (1989). An experimentally base 'bubble' model for clay. *Proc. Num. Models Geomech. NUMOG III* (eds Pietruszczak & Pande), Elsevier Applied Science, pp. 91-99.

Ambily, A. P. & Gandhi, S. R. (2007). Behavior of Stone Columns Based on Experimantal and FEM Analysis, *ASCE J. Geotech. & Geoenviromental Engng. 133(4),* pp. 405-415.

Anandarajah, A. , Kuganenthira, N. & Zhao, D. (1996). Variation of fabric anisotropy of kaolinite in triaxial loading. *J. Geotech. Engng. 122 (8),* pp. 633–640.

Andreou, P. & Papadopoulos, V. (2006). Modelling stone columns in soft clay. *Proc. Num. Meth. Geotech. Engng.*, Taylor & Francis Group, London, ISBN 0-415-40822-9.

Argyris, J. H. , Faust, G. , Szimmat, J. , Warnke, E. P. , Willam, K. J. (1974). Recent Development in the Finite Element Analysis of Pressure Container Reactor Vessel, *Nucl. Engng. Des. 28,* pp. 42-75.

Atkinson, J. H., Richardson, D. & Robinson, P. J. (1987). Compression and extension of K_0 normally consolidated kaolin clay. *ASCE J. Geotech. Engng. 113(12),* pp. 1468-1482.

Balaam, N. P. & Booker, J. R. (1981). Analysis of rigid raft supported by granular piles*, Int. J. Num. Anal. Meth. Geomech. 5(4)*, pp. 379-403.

Banerjee, P. K. & Yousif, N. B. (1986). A plasticity model for mechanical behaviour of anisotropically consolidated clay. *Int. J. Num. Anal. Meth. Geomech., Vol. 10*, pp. 521-541.

Barksdale, R. D. & Bachus, R. C. (1983). Design and Construction of Stone Columns. *Report FHWA/RD-83/026. Nat. Tech. Information Service*, Springfield, Virginia.

Baudet, B. A. & Stallebrass, S. E. (2004). A constitutive model for structured clays. *Géotechnique 54(4),* pp. 269-278.

Baumann, V. & Bauer, G. E. A. (1974). The performance of foundations on various soils stabilised by the vibro-compaction method. *Can. Geotech. J. 11(4),* pp.509-530.

BBC (2008). http://news.bbc.co.uk/go/pr/fr/-/1/hi/scotland/glasgow_and_west/7784474.stm, Published 15 December 2008, [Accessed 20 September 2010].

Bell, A. (2009). Private correspondence.

Benz, T. (2007). Small-strain stiffness of soils and its numerical consequences. PhD Thesis, Stuttgart University of Technology, Germany.

Bergado, D. T. & Long, P. V. (1994). Numeircal analysis of embankment on subsiding ground improved by vertical drains. *Proc. Int. Conf. Soil Mechanics & Foundation Engng.*, New Delhi, pp. 1361- 1366.

Bolton, M. D. & Sharma, J. S. (1994). Embankments with base reinforcement. *Proc. Centrifuge 94* (eds Leung *et al*.). Singapore. Balkema, Rotterdam: 587-592.

Borges, J. L. , Domnigues, T. S. & Cardoso A. S. (2009). Embankments on soft soil reinforced with stone columns: numerical analysis and proposal of a new design method. *Geotech. & Geological Engng. 27(6),* pp. 667-679.

Boulanger, R. W. & Duncan, J. M., *Geotechnical Engineering Photo Album* [Online] Available at: http://cee.engr.ucdavis.edu/faculty/boulanger/geo_photo_album/GeoPhoto.html [Accessed 7 April 2010].

BRE (2000). *Specifying vibro stone columns.* Construction research Communications Ltd. by permission of Building Research Establishment Ltd.

Brinkgreve, R. B. J. (1994). Geomaterial models and numerical analysis of softening. Doctoral Dissertation, Delft University of Technology.

Brinkgreve, R. B. J. (2001). The role of *OCR* in the SSC Model. *Plaxis Bulletin 10,* pp. 12-14.

Brinkgreve, R. B. J. (2002). PLAXIS Finite Element Code for Soil and Rock Analyses, 2D-Version 8. Balkema: Rotterdam.

British Standard Institution (2005). BS EN 14731:2005, *Execution of special geotechnical works- Ground treatment by deep vibration*.

Burland, J. B. (1990). On the compressibility and shear strength of natural clays. *Géotechnique 40(3),* pp. 327-370.

Casagrande, A. (1932). The structure of clay and its importance in foundation engineering. *J. Boston Soc. Civ. Engrs., 19(4),* pp. 168-209.

Casagrande, A. & Carrillo, N. (1944). Shear failure of anisotropic soils. *J. Boston Soc. Civ. Engrs., Contribution to Soil Mechanics*, pp. 1941-1953.

Castro, J. & Karstunen M. (2010). Numerical simulations of stone column installation. *Can. Geotech. J. 47(10),* pp. 1127-1138.

Castro, J. & Sagaseta, C. (2009). Consolidation around stone columns. Influence of column deformation. *Int. J. Num. Anal. Meth. Geomech. 33(7)*, pp. 851-877.

Castro, J. & Sagaseta, C. (2010). Disscusion of 'Simplified Plane-Strain Modelling of Stone-Column Reinforced Ground' by S.A Tan, S. Tjakyono, K. K., *ASCE J. Geotech. & Geoenvironmental Engng., June.*

Charles, J. A. (2002). Ground improvement: the interaction of engineering science and experienced-based technology. *Gèotechnique* 52 (7), pp. 527-532.

Clayton, C. R. I., Hight, D. W. & Hopper, R. J. (1992). Progressive destructuring of Bothkennar clay: implications for sampling and reconsolidation procedures. *Gèotechnique 42(2),* pp. 219-240.

Collins, K. & McGown, A. (1974). The form and function of microfabric features in a variety of natural soils. *Géotechnique 24 (3),* pp. 223-254.

Cotecchai, F. & Chandler, R. J. (1997). The influence of structure on the pre-failure behaviour of a natural clay. *Géotechnique 47 (3),* pp. 523-544.

Craig, W. H. & Al-Khafaji, Z. A. (1997). Reduction of soft clay settlement by compacted sand columns. *Proc. 3rd Int. Conf. Ground Improvement Geosystems*, *London*, pp. 218-231.

Cryer R. W. (1963). A comparison of three-dimensional theories of Biot and Terzaghi. *Q. J. Mech. Appl. Math. 16(4),* pp. 401–412.

Cudny, M. (2003). Simple multi-laminate model for soft soils incorporating structural anisotropy and destructuration. *Proc. Int. Workshop on Geotechnics of Soft Soils: Theory and Practice*, (eds Vermeer *et al.*)*,* Noordwijkerhout. VGE, pp. 181-188.

Cudny, M. & Neher, H.P. (2003). Numerical analysis of an embankment on soft grounds using an anisotropic model with destructuration., *Geotechnics of soft soils, theory and practice*, (eds Vermeer *et al.*)*,* Noordwijkerhout.

Cui Ch. Y. , Luan M. T. & Zhao Y. H. (2009). Time-dependent Behavior of Piled-raft on Soil foundation with Reference to Creep and Consolidation. *EJGE* vol. 14, Bundle A.

Dafalias, Y. F. (1986). An anisotropic critical state soil plasticity model. *Mechanics Research Communications, 13(6),* pp. 341-347.

Dafalias, Y. F. (1987). An anisotropic critical state clay plasticity model. *Proc. 2nd IC, Constitutive Laws for Engineering Materials: Theory and Applications, Vol. I,* (eds Desai *et al*) Elsevier, New York, pp. 513-521.

Davies, M. C. R. (1981). Centrifugal modelling of embankments on clay foundations. PhD Thesis, University of Cambridge, UK.

Davies, M. C. R. & Newson, T. A. A. (1993). Critical state constitutive model for anisotropic soils. *Proc. Predictive soil mechanics,* (eds Houlsby & Schofield), Oxford, UK, Telford, London, pp. 219-229.

Diaz-Rodriguez, J. A. , Leroueil, S. & Aleman, J. D. (1992). Yielding of Mexico City Clay and other natural clays. *ASCE J. Geotech. Engng. 118(7),* pp. 981-995.

Di Prisco, C. , Nova, R. & Lanier, J. (1993). A mixed isotropic-kinematic hardening constitutive law for sand. *Modern Approaches to Plasticity,* (eds Kolymbas). Elsevier, Amsterdam, pp. 83-124.

Elkasabgy M. A. (2005). Performance of stone columns reinforced grounds. MSc Thesis, University of Zagazig, Cairo.

Elshazly, H. A., Hafez, D. H. & Mossaad, M. E. (2006). Back calculating vibro-installation stresses in stone columns reinforced grounds. *Ground Improvement 10(2),* pp. 47-53.

Elshazly, H. A., Hafez, D. H. & Mossaad, M. E. (2008A). Reliability of Conventional Settlement Evaluation for Circular Foundations on Stone Columns, *Int. J. Geotech. & Geological Engng. 26(3),* pp. 323-334.

Elshazly, H. A. & Elkasabgy, M. (2008B). Effect of Inter-Column Spacing on Soil Stresses due to Vibro-Installed Stone Columns: Interesting Findings, *Int. J. Geotech. & Geological Engng. 26(2),* pp. 225-236.

Etezad, M., Hanna, A. M. & Ayadat, T. (2006). Bearing capacity of group of stone columns, *Proc. Num. Meth. Geotech. Engng. NUMGE 06*, Taylor & Francis Group, London, ISBN 0-415-40822-9.

Fang, H.–Y. (1991). Foundation engineering handbook. Kluwer Acadamic Publishers, Boston/Dordrecht/London, 2nd edition.

Fearon, R.E., Coop, M.R. (2000). Reconstitution - what makes an appropriate reference material?, *Géotechnique 50 (4),* pp. 471- 477.

Forschungsgesellschaft für das Straβenwesen (1979). *Merkblatt für die Untergrundverbesserung durch Tiefenrüttler***.**

Gajo, A. & Muir Wood, D. (2001). A new approach to anisotropic, bounding surface plasticity: General formulation and simulations of natural and reconstituted clay behaviour. *Int. J. Num. Anal. Meth. Geomech., 25(3),* pp. 207-241.

Galavi, V. (2007). A multilaminate Model for Structured Clay incorporating Inherent Anisotropy and Strain Softening. PhD Thesis, Gruppe Geotechnik Graz, Heft 32, Graz, University of Technology, Austria.

Gäb, M., Schweiger, H. F., Thurner, R. & Adam, D. (2007). Field trial to investigate the performance of a floating stone column foundation. *Proc. European Conf. Soil Mech. Geotech. Engng.*, Madrid, pp. 1311-1316.

Gäb, M., Schweiger, H. F., Kamrat-Pietraszewska, D. & Karstunen, M. (2008). Numerical analysis of a floating stone column foundation using different constitutive models. *Proc. 2nd Int. Workshop on Geotechnics of Soft Soil*, Glasgow, pp. 137-142.

Gens A. & Nova, R. (1993). Conceptual bases for a constitutive model for bonded soils and weak rocks. *Proc. Int. Symp. Hard Soils- Soft Rocks*, Athens, pp. 485-494.

Gens, A. & Potts, D. M. (1987). Critical state models in computational geomechanics. *Engng. Computation*, vol. 5, pp. 178- 197.

Gèotechnique (1992). Bothkennar soft clay test site: characterization and lessons learned, *Gèotechnique 42(2).*

Gibson R. E., Knight K. & Taylor P.W. (1963). A critical experiment to examine theories of three-dimensional consolidation. *Proc. European Conf. Soil Mech. Foundation Engng.,* vol. 1, pp. 69–76.

Goughnour, R. R. & Bayuk, A. A. (1979). Analysis of stone column- soil matrix interaction under vertical load*, Proc. Int. Conf. on Soil Reinforcements*, Paris, pp. 271-297.

Graham, J., Lew, K.V. & Noonan, M.L. (1983A). Yield states and stress-strain relationships in a natural plastic clay. *Can. Geotech. J. 20(3),* pp. 502-516.

Graham, J. & Houlsby, G.T. (1983B). Anisotropic elasticity of a natural clay. *Géotechnique 33,* pp. 165-180.

Graham, J. & Li, E. C. C. (1985). Comparision of natural remoulded plastic clay. *ASCE Journal of Geotechnical Engineering 111(7),* pp. 865-881.

Greenwood, D. A. (1990). Assurance of performance of stone columns. *In: Deep Foundation Improvements: Desing, Construction and Testing*. ASTM, (eds Bachus), Philadelphia.

Greenwood, D. A. (1991). Load tests on stone columns, *Proc. ASTM Specialty Conf. Deep Foundation Improvement: design, construction and testing*, ASTM Spec. Tech. Publ. 1089, pp. 148-171.

Grimstad, G. , Degago, S. A., Nordal, S. & Karstunen, M. (2010). Modeling creep and rate effects in structured anisotropic soft clays. *Acta Geotechnica 5(1),* pp. 69-81.

Guetif, Z. , Bouassida, M. & Debats, J. (2007). Improved soft clay characteristics due to stone column installation. *Computers and Geotechnics* 34, pp. 104-111.

Hayward Baker (2004). Vibro Systems. *Hayward Baker Inc. Pub. No. J83,* www.haywardbaker.com.

Herle, I. , Wehr, J. & Arnold, M. (2007). Influence of pressure level and relative density on friction angle of gravel in vibrated stone columns. *Mitteilung des Instituts für Grundbau und Bodenmechanik* , (eds Stahlmann), published in German, TU Braunschweig, Helft 84, pp. 81-93.

Huat, B. B. K. & Craig, W. H. (1994). Simulation of a sand column trial embankment. *Centrifuge 94*. (eds Leung *et al*.), Balkema, Rotterdam, pp. 561-566.

Hughes, J. M. & Withers, N. J. (1974). Reinforcing of soft cohesive soils with stone columns. *Ground Engineering* 7(3), pp. 47-49.

Husein, H. A., Flavigny, E. & Boulon, M. (2001). Long term behaviour finite element analysis of a dam with in situ measurements of the viscoplastic properties of its foundations. *Soft Soil Engineering,* (eds. Lee *et al*.), Swets & Zeillinger, ISBN90 265 1866 8.

Jaky J. (1948) Pressure in soils, *Proc. 2nd ICSMFE*, London, Vol. 1, pp. 103-107.

Janbu (1969). The resistance concept applied to deformations of soils. *Proc. 7th Int. Conf. Soil Mechanics Foundation Engng.,* Mexico City, pp. 191-196.

Kabbaj M. (1985). Aspects rhéologiques des argiles naturelles en consolidation. PhD Thesis, Laval University, Sainte-Foy, Québec.

Kabbaj M, Tavenas F, Leroueil S. (1988). In-situ and laboratory stress-strain relation*, Géotechnique 38(1),* pp. 83-100.

Kamrat-Pietraszewska, D, Krenn, H, Sivasithamparam, N, Karstunen, M. (2008). The influence of anisotropy and destructuration on a circular footing, *Proc. 2nd ICOF 2008*, Dundee, IHS BRE Press, pp. 1527-1536.

Karstunen, M. & Koskinen, M. (2008). Plastic anisotropy of soft reconstituted clays. *Can. Geotech. J. 45*, pp. 314-328.

Karstunen, M., Krenn, H., Wheeler, S. J., Koskinen, M. & Zentar, R. (2005). Effect of anisotropy and destructuration on the behaviour of Murro test embankment. *ASCE Int. J. Geomech. 5(2),* pp. 87-97.

Karstunen, M., Rezania, M., Sivasithamparam, N., Leoni, M. & Yin, Z.-Y. (2010). Recent developments on modelling time-dependent behaviour of soft natural clays. *25th Mexican Nat. Meeting Soil Mech. & Geotech. Engng.,* Acapulco, Mexico, vo. 3, pp. 931-938.

Karstunen, M. , Wiltafsky, C. , Krenn, H. , Scharinger, F. & Schweiger, H.F. (2006). Modelling the stress-strain behaviour of an embankment on soft clay with different constitutive models. *Int. J. Num. Anal. Meth. Geomech. 30(10),* pp. 953-982.

Karstunen, M. & Wheeler, S. J. (2002). Discussion on ‚Finite strain, anisotorpic Modified Cam Clay model with plastic spin, I: Theory', by G. Z. Voyiadjis & C. R. Song, *ASCE J. Engng. Mech. 128(4),* pp. 497-498.

Karstunen, M. & Yin, Z.-Y. (2010). Modelling time-dependent behaviour of Murro test embankment. *Géotechnique, 60(10),* pp. 735-749.

Kavvadas, M. & Amarosi, A. (2000). A constitutive model for structured soils. *Géotechnique 50(3),* pp. 263-273.

Kim Y. T. , Leroueil S. (2001). Modeling the viscoplastic behaviour of clays during consolidation: Application to Berthierville clay in both laboratory and field conditions, *Can. Geotech. J. 38(3),* pp. 484-497.

Kirsch, F. (2004). Experimentelle und numerische Untersuchungen zum Tragverhalten von Rüttelstopfsäulengruppen, PhD Thesis, (in German), University of Technology Braunschweig, Heft 75, Germany.

Kirsch, F. (2006). Vibro stone column instllation and its effects on ground improvement. *Proc. Num. Modelling of Construction Processes in Geotech. Engng. for Urban Environment*, (eds Triantafyllidis), Taylor and Francis, London.

Kirsch, F. & Sondermann, W. (2003). Field Measurements and Numerical Analysis of the Stress Distribution below Stone Column Supported Embankments and their Stability. *Proc. Int. Workshop on Geotechnics of Soft Soils- Theory and Practice,* (eds Karstunen & Cudny), pp. 598-600.

Korhonen, K.-H. & Lojander, M. (1987). Yielding of Perno clay. *Proc. 2nd Int. Conf. on Constitutive Laws for Engineering Materials: Theory and Application*, (eds Desai *et al.*), Tucson, Arizona, Elsevier, N. Y., Vol. 2, pp.1249-1255.

Koskinen, M. & Karstunen, M. (2004). The effect of structure on the compressibility of Finnish clays. *Proc. NGM 2004 XIV Nordic Geotechnical Meeting,* Ystad, Sweden.

Koskinen, M. & Karstunen, M. (2006). Numerical modelling of Murro test embankment with S-CLAY1S. *Proc. Conf. Num. Meth. Geotech. Engng. (NUMGE 2006),* Austria, pp. 455-461.

Koskinen, M., Karstunen, M. & Wheeler, S. J. (2002). Modelling destructuration and anisotropiy of a natural soft clay. *Proc. Conf. Num. Meth. Geotech. Engng. (NUMGE 2002),* (eds Mestat), Paris, Presses de l'ENPC, pp. 11-20.

Krenn, H. (2008). Numerical modelling of embankments on soft soils. PhD Thesis. University of Strathclyde, Glasgow, Scotland.

Lambe, T. W. & Whitman, R. V. (1969). Soil Mechanics. John Wiley and Sons Inc., New York.

Lee, J. (1993). Finite element analysis of structured media, PhD Thesis, University of Wales, Swansea, UK.

Lee, F.H., Ng, Y.W. & Young, K.Y. (2001). Effects of Installation Method on Sand Compaction Piles in Clay in the Centrifuge. *ASTM Geotech. Testing J.* 24(3), pp. 314-323.

Lee, J. & Pande, G. N. (1998). Analysis of stone-column reinforced foundations, *Int. J. Num. Anal. Meth. Geomech. 22(12),* pp. 1001-1020.

Leoni, M. , Karstunen, M. & Vermeer, P. A. (2008). Anisotropic creep model for soft soils. *Gèotechnique 58(3),* pp. 215-226.

Leoni, M. , Karstunen, M. & Vermeer, P. A. (2009). Validation of anisotropic creep model for soft soils. *Proc. Geotechnics of Soft Soils- Focus on Ground Improvement,* (eds Karstunen & M. Leoni), Taylor and Francis Group, pp. 165- 171.

Leroueil, S. & Hight, D. W. (2003). Behaviour and properties of natural soils and soft rocks. *Proc. Characterisation & Engng. Properties of Natural Soils,* (eds Tan *et al.),* Swets & Zeitlinger, Lisse.

Leroueil, S. , Kabbaj, M. , Tavenas, F. & Bouchard, R. (1985). Stress-strain rate relation for the compressibility of sensitive natural clays. *Géotechnique 35(2),* pp. 159-180.

Leroueil, S., Lerat, P., Hight, D. W. & Powell, J. J. M. (1992), Hydraulic conductivity of a recent estuarine silty clay at Bothkennar, *Gèotechnique 42(2),* pp. 275-288.

Leroueil, S. & Marques, M. E. S. (1996). Importance of strain rate and temperature effects in geotechnical engineering: state of the art. *Proc. ASCE Convention, Washington, D.C. ASCE Geotech. Spec. Publ. 61*, pp. 1–60.

Leroueil, S. , Tavenas, F. , Brucy, F. , La Rochelle, P. & Roy, M. (1979). Behaviour of destructured natural clays. *J. Geotech. Engng. 105(6*), pp. 759-778.

Leroueil, S. & Vaughan, P. R. (1990). The general and congruent effects of structure in natural soils and weak rocks. *Géotechnique 40(3*), pp. 452-467.

Liingaard, M. , Augustesen, A. & Lade, P.V. (2004). Characterization of Models for Time Dependent Behaviour of Soils. *Int. J. Geomech. 4(3),* pp. 157-177.

Liu, M. D. & Carter, J. P. (2000). Modelling the destructuring of soils during virgin compression, *Géotechnique 50(4*), pp. 479-483.

Liu M. D. & Carter J. P. (2002). Structured Cam Clay Model, *Can. Geotech. J. 39(6),* pp. 1313-1332.

Malvern, L. E. (1951). The propagation of longitudinal waves of plastic deformation in a bar of metal exhibition a strain rate effect. *J. App. Mech. 18*, pp. 203-208.

Mandel (1950). Etude de la consolidation des sols. *Actes du Collegie International de Méchanique, Poitiers* 4, pp. 9-19.

Mayne, P. W., Kulhawy, F. H., (1982). K_0-OCR relationship in soil*, ASCE J. Geotech. Engng. 108 (GT),* pp. 851–872.

Matsuoka H, Nakai T. (1982). A new failure condition for soils in three dimensional stresses, *Proc. IUTAM Sym. Deform. Failure Granular Mat.,* (eds Vermeer. & Luger), Delft, pp. 253-263.

McCabe, B. A., McNeill, J. A. & Black, J. A. (2007). Ground Improvement using the Vibro- Stone Column Technique, *Transactions of the Institution of Engineers of Ireland*.

McGinty, K. (2006). The stress-strain behaviour of Bothkennar clay. PhD Thesis, University of Glasgow, UK.

McKelvey, D. , Sivakumar, V. , Bell, A. & Graham, J. (2004). Modelling vibrated stone columns in soft clay, *Proc. ICE Geotech. Engng. 157(GE3),* pp.137-149.

McKenna, J. M., Eyre, W. A. & Wolstenholme, D. R. (1975). Performance of an embankment supported by stone columns in soft ground, *Gèotechnique 25 (1),* pp. 51-59.

Mesri, G. (2001). Primary compression and secondary compression. *Proc. Soil Behaviour & Soft Ground Construction*, Geotechnical Special Publication 199, ASCE Reston, pp. 122-166.

Mesri, G. , Feng, T. W. & Shahien, M. (1995). Compressibility parameters during primary consolidation. *Proc. Int. Symp. Compression & Consolidation of Clayey Soils,* Hiroshima, Japan, Lectures and Reports, pp. 201.217.

Mesri, G. & Godlewski, P. M. (1977). Time- and stress- compressibility interrelationship, *ASCE J. Geotech. Engng. 103 (5),* pp. 417-430.

Mesri, G. & Godlewski, P. M. (1979).Closure to time- and stress- compressibility interrelationship, *ASCE J. Geotech. Engng. 105 (1),* pp. 106.

Mesri, G. & Castro, A. (1987). C_α / C_c concept and K_0 during secondary compression, *J. Geotech. Engng. 113(3),* pp. 230-247.

Mesri, G. , Feng, T. W., Shahien, M. (1995). Compressibility parameters during primary consolidation. *Proc. Int. Symp. Compression & Consolidation of Clayey Soils,* Hiroshima, Japan, Lectures and Reports, pp. 201-217.

Mesri, G. , Lo, D. O. K. & Feng, T. W. (1994). Settlement of embankments on soft clays. *Keynote Lecture, Settlement'94*, Geotechnical Special Publication 40(1), Texas A & M University, College Station, pp. 8-56.

Mesri, G., Vardhanabhuti, B. (2005). Secondary compression, *J. Geotech. Geoenvironmental 131(3),* pp. 398-401.

Mitchell, J. K. (1976). Fundamentals of soil behaviour. John Wiley, New York.

Mitchell, J. K. & Huber, T. R. (1985). Performance of a stone column foundation, *ASCE J. Geotech. Engng. 11(2)*, pp.205-223.

Moreau, N. & Moreau, M. (1835). Foundations- Emploi du Sable. Annales des Ponts et Chaussees, *Memoires 224*, pp.171-214.

Mróz, Z., Norris, V. A. & Zienkiwicz, O. C. (1979). Application of an anisotropic hardening model in the analysis of elasto-plastic deformation of soil. *Gèotechnique 42(2),* pp. 163- 182.

Muir Wood, D., Hu, W. & Nash, D. F. T. (2000). Group effects in stone column foundations- model test, *Gèotechnique 50 (6),* pp. 689-698.

Murugesan, S. & Rajagopal, K. (2006). Geosynthetic-encased stone columns: Numerical evaluation*, Geotextiles & Geomembranes 24*, pp. 349-358.

Nash, D. F. T., Powell, J. J. M. & Lloyd, I. M. (1992A). Initial investigations of the soft clay test site at Bothkennar. *Gèotechnique 42(2),* pp. 1-34.

Nash, D. F. T., Sills, G. C. & Davison, R. L. (1992B). One-dimensional consolidation testing of soft clay from Bothkennar. *Gèotechnique 42(2),* pp. 241-256.

National House Building Council Standards NHBC (1988). *Vibratory ground improvement techniques,* Chapter 4.6.

National House Building Council Standards NHBC (2010). *Efficient design of piled foundations for low-rise housing. Design guide.* Building Research Establishment Ltd. Press.

Neher, H. P., Wehnert, M. & Bonnier, P. G. (2001). An evaluation of soft soil models based on trial embankments. *Proc. Computer Meth. Advances in Geomech.,* (eds Desai *et al.*), Balkema, pp. 373 - 378.

Näätänen, A. , Wheeler, S. J., Karstunen, M. & Lojander, M. (1999). Experimental investigation of an anisotropic hardening model for soft clays. *Proc. 2nd Int. Symp. on Pre-Failure Deformations Characteristic of Geomaterials,* (eds Jamiolkowski *et al*.), A. A. Balkema, Torino, vol. 1, pp. 541-548.

Nova, R. (1984). A model of soil behaviour in plastic and hysteretic ranges. Part I: monotonic loading. *Proc. Int. Workshop on Constitutive Modeling of Soil Behaviour* (eds. Gudehus *et al*.). Balkema, pp. 289–309.

Oliver, A. (2010). The new urban dream. *New Civil Engineering,* 15.07.10, pp. 16-20.

Pande, G. N. & Sharma, K.G. (1983). Multilaminate model of clays - numerical evaluation of the influence of rotation of principal stress axes. *Int. J. Num. Anal. Meth. Geomech. 7(4)*, pp. 397-418.

Perzyna, P. (1966). Fundamental problems in viscoplasticity. New York.

Pestana, J. M & Whittle, A. J. (1999). Formulation of a unified constitutive model for clays and sands. *Int. J. Num. Anal. Meth. Geomech. 23,* pp. 1215-1243.

Pietruszczak, S. & Pande. G. N. (1987). Multilaminate framework of soil models - plasticity formulation. *Int. J. Numer. Anal. Meth. Geomech. 11(6),* pp. 651-658.

Pooley, E. J., Springman, S. M. & Laue, J. (2009). Centrifuge modelling to compare ground improvement techniques on double porosity clay landfills. *Geotechnics of Soft Soils: Focus on Ground Improvement (eds Karstunen & Leoni), Proc. 2nd Int. Workshop on Geotechnics of Soft Soils*, Glasgow, UK, pp. 281-285.

Poorooshasb, H. B. & Meyerhof, G. G. (1997). Analysis of Behavior of Stone Columns and Lime Columns, *Computers & Geotechnics 20(1),* pp.47-70.

Priebe, H. J. (1995). The design of vibro-replacemen. *Ground Engng. 28,* Technical paper, pp. 12-61E.

Priebe, H. J. (2005). Design of vibro replacement. The application of Priebe's method to extremely soft soils, 'floating' foundations and proof against slope or embankment failure, *Ground Engng.,* January, pp. 25-27.

Raju, V. R. (1997). The Behaviour of Very Soft Soils Improved by Vibro Replacement, *Proc. Ground Improvement Geosystems: Densification and Reinforcement,* (eds Davis and Schlosser), Thomas Telford, London, pp. 12-64E.

Raju, V. R. , Hari Krishna R. & Wegue, R. (2004). Ground improvement using Vibro Replacement in Asia 1994 to 2004- a 10 year review, *Proc. 5th Int. Conf. Ground Improvement Techniques,* Kuala Lumpur, Malaysia.

Raju, V. R., Yee, Y. W., Tam, E. & Sreenivas, P. (2004). Vibro replacement for the construction of a 15 m high highway over a mining pond. *Proc. Malaysian Geotech. Conf.*, Kuala Lumpur, pp. 12-67E.

Rankka, K. , Andersson-Sköld, Y. , Hultén, C. , Larsson, R. , Leroux, V. & Dahlin, T. (2004). Quick clay in Sweden, *Swedish Geotech. Institute, Report No 64*.

Rocchi, G, Fontana, M. & Da Prat, M. (2003). Modelling of natural soft clay destruction processes using viscoplasticity theory. *Gèotechnique 53(8),* pp. 729-745.

Roscoe K. H. & Burland, J. B. (1968). On the generalised stress-strain behaviour of 'wet' clay. *Engng. Plasticity*, Cambridge University Press, pp. 553-609.

Roscoe, K. H., Schofield, A. N. (1963). Mechanical behaviour of an idealised 'wet' clay. *Proc. 2nd European Conf. Soil Mechanics and Foundation Engng.,* Wiesbaden, Germany, pp. 47-54.

Roscoe, K. H., Schofield, A. N & Wroth, C. P. (1958). On the yielding of soils. *Géotechnique 8(1)*, pp. 22-53.

Rouainia, M. & Muir Wood, D. (2000). A kinematic hardening constitutive model for natural clays with loss of structure. *Géotechnique 50(2)*, pp. 153-164.

Schweiger, H. F. (1989). Finite element analysis of stone column reinforced foundations. PhD Thesis, University of Swansea, UK.

Schweiger, H. , F. & Pande G. , N. (1988). Numerical analysis of a road embankment constructed on soft clay stabilised with stone columns, *Proc. Num. Meth. Geomech.*, Innsbruck, pp. 1329-1333.

Schweiger, H. F. & Pande G. , N. (1989). Modelling stone column reinforced soils- a modified Voigt approach, *Proc. 3rd Num. Models Geomech. (NUMOG),* pp. 204-214.

Schanz, T. (1998). Zur Modellierung des Mechanischen Verhaltens von Reibungsmaterialen, Habilitation, (in German), Univertity of Stuttgart, Germany.

Schanz, T. , Vermeer, P. A. & Bonnier, P. G. (1999). The hardening model: Formulation and verification. *Proc. PLAXIS Symp. Beyond 2000 in Computational Geotechnics,* Amsterdam, Balkema, Rotterdam, pp. 281-296.

Schweiger, H. F. , Wiltafsky, C. , Scharinger, F. & Galavi, V. (2009). A multilaminate framework for modelling induced and inherent anisotropy of soils. *Géotechnique 59(2)*, pp. 87-101.

Sekiguchi, H. & Ohta, H. (1977). Induced anisotropy and time dependency in clays. *Proc. 9th Int. Conf. Soil Mech. and Foundation Engng. (ICSMFE),* (eds Murayama & Schofield), Tokyo, Japan, Vol. 1, pp. 229-238.

Serridge, C. J. (2005). Achieving sustainability in vibro stone column techniques, *Proc. ICE Engineering Sustainability 158 (ES4),* pp. 211-222.

Shinsha, H. , Takata, K. & Kurumada, Y. (1991). Centrifuge model test on clay ground partly improved by sand compaction piles. *Proc. Centrifuge 91*. (eds Ko & McLean). Balkema, Rotterdam, pp. 311-318.

Sivakumar, V. , Boyd, J. L. , Black, J. A. & McNeil, J. A. (2010). Effects of granular columns in compacted fills. *Proc. ICE – Geotech. Engng.* 163 (4), pp. 189-196.

Slocombe, B. C. (2001). Deep compaction of problematic soils. *Problematic soils,* Thomas Telford (London), pp. 163-181.

Smith, P. R., Jardine, R. J. & Hight, D. W. (1992). The yielding of Bothkennar clay. *Gèotechnique 42(2),* pp. 257-274.

Springman, S. M. (1984). Lateral loading on piles due to embankment construction. MPhil. Thesis, University of Cambridge, UK.

Stallebrass, S. E & Taylor, R. N. (1997). The development and evaluation of a constitutive model for the prediction of ground movements in overconsolidated clay. *Gèotechnique 47(2),* pp. 235-253.

Suklje, L. (1957). The analysis of the consolidation process by the isotaches method. *Proc. 4th ICSMFE*, vol. 1, pp. 200-206.

Tavenas, F.& Leroueil, S. (1977). Effects of stresses and time on yielding of clays. Murayama & Schofield (eds.), *Proc. 9th Int. Conf. Soil Mech. & Foundation Engng. (ICSMFE),* Tokyo, Japan, Vol. 1, pp. 319-326.

Terzaghi K. (1943). *Theoretical Soil Mechanics*. New York, N Y: John Wiley and Sons Inc.

Yin Z.-Y., Karstunen M. (in press). Modelling strain-rate-dependency of natural soft clays combined with anisotropy and destructuration. Accepted by *Acta Mechanica Solida Sinica*.

Yin Z.-Y. , Karstunen M. , Chang C. S. , Koskinen M. & Lojander M. (in press). Modeling Time-dependent Behavior of Soft Sensitive Clay. Accepted by *ASCE J. Geotech. Geoenvironmental. Eng.*

Yu, Y. & Axelsson, K. (1994). Constitutive modelling of Swedish cohesive soils accounting for anisotropy", *Proc. Computer Meth. & Advances in Geomech.*, (eds Siriwardane & Zaman), Balkema, Rotterdam.

Van Impe, W. F. (2001). Recent advances in soil reinforcement and improvement. *Proc. 15th Int. Conf. Soil Mech. Geotech. Engng., Istanbul*, pp. 2755-2758.

Van Impe, W. F. & De Beer, E. (1983). Improvement of settlement behaviour of softy layers by means of stone columns. *8th Int. Conf. Soil Mech. & Foundation Engng.,* Helsinki, pp. 309-312.

Vermeer, P. A. (1978) A double hardening model for sand. *Gèotechnique28(4),* pp. 413-433.

Vogler, U. (2008). Numerical modelling of Deep Mixing with Volume Averaging Technique. PhD Thesis, University of Strathclyde, Glasgow, UK.

Watts, K. S. (2000). Specifying vibro stone columns. *Garston: Building Research Establishment.*

Weber, T. M. (2007). Modellierung der Baugrundverbesserung mit Schottersäulen, PhD Thesis, Swiss Federal Institute of Technology, ETH, Zürich, Switzerland

Weber, T. M. , Plötze, M. , Laue, J. , Peschke, G. & Springman, S. M. (2010). Smear zone identification and soil properties around stone columns constructed in-flight in centrifuge model tests. *Géotechnique 60(3)*, pp. 197-206.

Weber, T. M. , Springman, S. M. , Gäb, M. , Racansky, V. & Schweiger, H. F. (2009). Numerical modelling of stone columns in soft clay under an embankment. *Proc. 2nd Int. Workshop on Geotechnics of Soft Soil*, Glasgow, pp. 305-312.

Wehr, J. & Herle, I. (2006). Exercise on calculation of stone columns- Priebe method and FEM, *Proc. Num. Meth. Geotech. Engng.,* Taylor & Francis Group, London, ISBN 0-415-40822-9, pp. 773-776.

Wiltafsky, C. (2003). A multilaminate model for normally consolidated clay. PhD Thesis*,* Gruppe Geotechnik Graz, Heft 18, Graz, University of Technology, Austria.

Wiltafsky, C. , Scharinger, F. , Schweiger, H. F. , Krenn, H. & Zentar, R. (2003). Results from a geotechnical benchmark exercise of an embankment on soft clay. *Proc. Int. Workshop on Geotechnics of Soft Soils - Theory and Practice*, Noordwijkerhout, The Netherlands, VGE, Essen, Germany, pp. 381-390.

Wheeler, S. J. (1997). A rotational hardening elasto-plastic model for clays. *Proc. XIV ICSMFE*, Hamburg, A. A. Balkema, Rotterdam, Vol. 1, pp. 431-434.

Wheeler, S. J., Karstunen, M. & Näätänen, A. (1999). Anisotropic hardening model

for normally consolidated soft clay. *Proc. 7th Int. Symp. Num. Models Geomech. (NUMOG VII)*, (eds Pietruszczak & Schweiger) Graz, A. A. Balkema, pp. 33-40.

Wheeler, S. J. , Näätänen, A. , Karstunen, M. & Lojander, M. (2003). An anisotropic elastoplastic model for soft clays. *Can. Geotech. J. 40,* pp. 403-418.

Whittle, A. J & Kavvadas, M. J. (1994). Formulation of MIT-E3 constitutive model for overconsolidated clays. *J. Geotech. Engng. 120(1),* pp. 173-198.

Wlaź, P. (2009). Private correspondence.

Wroth, C. P. (1984). The interpretation of in situ soil tests. *Géotechnique 34(4)*, pp. 449-483.

Zdravkovic, L. & Potts, D. M. (1999). Advances in modelling soil anisotropy. *Proc. Constitutive Modelling of Granular Material*, (eds Kolymbas), Horton, Greece, Springer, Berlin, pp. 491-521.

Zdravkovic, L., Potts, D. M & Hight, D. W. (2002). The effect of anisotropy on the behaviour of embankments on soft ground. *Gèotechnique 52(6),* pp. 447-457.

Zentar, R. , Karstunen, M. , Wiltafafsky, C. , Schweiger, H. F. & Koskinen, M. (2002). Comparison of two approaches for modelling anisotropy of soft clays. *Proc.*

8th Int. Symp. Num. Models Geomech. (NUMOG VIII), (eds Pande & Pietruszczak), Rome, A. A. Balkema, pp. 115-121.

Zienkiewicz, O. C. & Pande, G. N. (1977). Time-dependent multilaminate model of rocks - A numerical study of deformation and failure of rock masses. *Int. J. Num. Anal. Meth. Geomech. 1(3),* pp. 219-247.